ASSESSMENT OF ABDOMINAL AORTIC ANEURYSM BIOLOGY USING MAGNETIC RESONANCE IMAGING AND POSITRON EMISSION TOMOGRAPHY-COMPUTED TOMOGRAPHY

By

RACHAEL OLIVIA FORSYTHE

APPENDICES

THESIS PRESENTED FOR THE DEGREE OF DOCTOR OF PHILOSOPHY

THE UNIVERSITY OF EDINBURGH

2017

APPENDIX i

Published Manuscript

10.1161/CIRCULATIONAHA.117.028433

Aortic Wall Inflammation Predicts Abdominal Aortic Aneurysm Expansion, Rupture and Need for Surgical Repair

Running Title: *The MA^{3}RS Study*

The MA^{3}RS Study Investigators

Address for Correspondence:
Professor David Newby
Centre for Cardiovascular Science
Room SU314, Chancellor's Building
49 Little France Crescent
Edinburgh, Scotland, EH16 4SA
Tel:+44 131 242 6515
Fax:+44 131 242 6379
Email: d.e.newby@ed.ac.uk

Abstract

***Background*—**Ultrasmall superparamagnetic particles of iron oxide (USPIO) detect cellular inflammation on magnetic resonance imaging (MRI). In patients with abdominal aortic aneurysm, we assessed whether USPIO-enhanced MRI can predict aneurysm growth rates and clinical outcomes.

***Methods*—**In a prospective multicentre open-label cohort study, 342 patients with abdominal aortic aneurysm (diameter ≥40 mm) were classified by the presence of USPIO enhancement and were monitored with serial ultrasound and clinical follow-up for at least 2 years. The primary endpoint was the composite of aneurysm rupture or repair.

***Results*—**Participants (85% male, 73·1±7·2 years) had baseline aneurysm diameter of 49·6±7·7 mm, and USPIO enhancement was identified in 146 (42·7%) participants, absent in 191 (55·8%) and indeterminate in 5 (1·5%). During follow-up (1005±280 days), there were 17 (5·0%) abdominal aortic aneurysm ruptures, 126 (36·8%) abdominal aortic aneurysm repairs, and 48 (14·0%) deaths. Compared to those without uptake, patients with USPIO enhancement have increased rates of aneurysm expansion (3·1±2·5 versus 2·5±2·4 mm/year, p=0·0424) although this was not independent of current smoking habit (p=0·1993). Patients with USPIO enhancement had higher rates of aneurysm rupture or repair (47·3% versus 35·6%; difference 11·7%, 95% confidence intervals 1·1 to 22·2%, p=0·0308): this was similar for each component of rupture (6.8% versus 3.7%, p=0·1857) or repair (41.8% versus 32.5%, p=0·0782). USPIO enhancement was associated with reduced event-free survival for aneurysm rupture or repair (p=0·0275), all-cause mortality (p=0·0635) and aneurysm-related mortality (p=0·0590). Baseline abdominal aortic aneurysm diameter (p<0·0001) and current smoking habit (p=0·0446) also predicted the primary outcome, and the addition of USPIO enhancement to the multivariate model did not improve event prediction (c-statistic, 0·7935 to 0·7936).

***Conclusions*—**USPIO-enhanced MRI is a novel approach to the identification of aortic wall cellular inflammation in patients with abdominal aortic aneurysms, and predicts the rate of aneurysm growth and clinical outcome. However, it does not provide independent prediction of aneurysm expansion or clinical outcomes in a model incorporating known clinical risk factors.

***Clinical Trial Registration*—**URL:http://www.isrctn.com/ Unique Identifier: ISRCTN76413758 EudraCT Number: 2012-002488-25

Key Words: abdominal aortic aneurysm; magnetic resonance imaging; clinical trial

Clinical Perspective

What is new?

- In this proof-of-concept phase 2 study, we demonstrate for the first time that functional imaging of abdominal aortic aneurysms can predict disease progression and clinical events.
- Aortic wall inflammation detected by ultrasmall superparamagnetic particles of iron oxide (USPIO)-enhanced magnetic resonance imaging (MRI) predicts the rate of aneurysm growth, and the risk of aneurysm rupture or repair as well as being associated with all-cause and aneurysm-related mortality.

What are the clinical implications?

- Multivariate analysis demonstrated that USPIO-enhanced MRI does not appear to improve risk stratification beyond current predictors of clinical outcome including ultrasound measures of aneurysm diameter.
- This technique may be a useful adjunctive imaging approach in those with high-risk or borderline aneurysm sizes, or those with larger aneurysms where the balance of risk and benefit is uncertain.
- This approach may also have utility in assessing candidate anti-inflammatory therapies targeted at reducing disease progression.

Abdominal aortic aneurysms have a prevalence of 5% in 65-74 year-old men and when ruptured, are associated with a mortality of up to 90%.[1] At a population level, ruptured aortic aneurysms are a major cause of death being the thirteenth commonest cause of death and accounting for over 150,000 deaths in 2013.[2] Pre-emptive elective open surgical or endovascular repair can be life-saving and is considered when the abdominal aortic aneurysm diameter exceeds 55 mm, is rapidly expanding (≥10 mm/year) or causes symptoms.[3-5]

Abdominal aortic aneurysms are usually associated with no symptoms and are often identified incidentally or as part of an ultrasound-based screening programme. Population screening has been established in some countries and is associated with a halving of the mortality associated with abdominal aortic aneurysms.[6,7] Continued surveillance of aneurysms is however challenging because of the non-linearity and unpredictability of expansion rates,[8] although the best current predictor of aneurysm expansion and rupture is the baseline aneurysm diameter.[1,9] Furthermore, the pathophysiological mechanisms underlying aneurysm expansion remain uncertain, and the role of cellular inflammation and macrophage infiltration has been debated. Finally, up to one fifth of ruptured abdominal aortic aneurysms are <55 mm in diameter and 40% of patients with aneurysm diameters between 70 and 100 mm do not experience aneurysm rupture.[10] There is therefore an unmet clinical need to identify more reliable methods of identifying those patients at risk of abdominal aortic aneurysm expansion and rupture,[11,12] and techniques that assess both the structure and biology of aneurysms hold considerable promise.

Ultrasmall superparamagnetic particles of iron oxide (USPIO) constitute a class of magnetic resonance imaging (MRI) contrast agent that are taken up by tissue-resident macrophages and can be used to identify cellular inflammation within tissues[13,14] including abdominal aortic aneurysms.[15,16] In a small pilot study of 29 patients with abdominal aortic

aneurysm,[15] we have previously demonstrated that USPIO enhancement on MRI is associated with macrophage infiltration of the abdominal aortic aneurysm wall and more rapid rates of abdominal aortic aneurysm expansion. We therefore aimed to validate these preliminary findings in a larger multicentre cohort of patients, and to determine whether USPIO-enhanced MRI could predict the rate of abdominal aortic aneurysm expansion, and subsequent rates of rupture or surgical repair.

Methods

Study Design

The Magnetic resonance imaging using ultrasmall superparamagnetic particles of iron oxide in patients under surveillance for Abdominal Aortic Aneurysm to predict Rupture or Surgical repair (MA^3RS) study was a prospective multi-centre observational open-label cohort study of patients under routine ultrasound surveillance for abdominal aortic aneurysm. The research design and protocol has been described previously (ISRCTN76413758).[17] The study was approved by the local research ethics committee (12/ES/0068) and the use of ferumoxytol was given Clinical Trial Authorisation by the Medicines and Healthcare products Regulatory Authority (MHRA) of the United Kingdom (EudraCT Number 2012-002488-25).

Study Population

Consecutive patients were recruited from three centres in Scotland, UK (Royal Infirmary of Edinburgh, Western Infirmary of Glasgow and Forth Valley Royal Hospital in Larbert) between 8th November 2012 and 5th December 2014. Inclusion criteria were age >40 years, maximum anteroposterior abdominal aortic aneurysm diameter ≥40 mm by abdominal ultrasound, and under ultrasound surveillance as part of routine clinical care. Exclusion criteria included patients

with planned repair of abdominal aortic aneurysm, known inflammatory aneurysm, aneurysm arising from a connective tissue disorder, women of child-bearing potential, renal failure (estimated glomerular filtration rate ≤30 mL/min/1.73 m^2) and contraindication to MRI or ferumoxytol. All participants gave written informed consent to participate in the study.

Study Protocol

Participants attended for a baseline assessment within 6 weeks of the screening abdominal ultrasound. Participant characterisation comprised of full clinical assessment, USPIO-enhanced MRI and computed tomography aortography. The scanning protocols and image analysis techniques have been described previously.[15,17] In brief, patients underwent a baseline 3T MRI (Magnetom Verio 3T, Siemens Healthcare, Erlangen, Germany) before receiving an intravenous infusion of a weight-adjusted dose of USPIO (4 mg/kg of ferumoxytol; Rienso®, Takeda Italia, Italy). A second MRI scan was performed 24-36 hours after USPIO administration. Two trained observers performed image analysis using bespoke software that compared pre- and post-contrast images using semi-automatic registration. To calculate the degree of USPIO enhancement, colour maps were generated to depict the percentage change in T2* which is the decay constant for the exponential decay of signal over time. Using the pre-defined threshold of ≥71% change in T2*, each colour map was independently classified by two trained observers into patients with or without USPIO enhancement (≥10 contiguous voxels[15]) within the wall of the abdominal aortic aneurysm (Figure 1). Discordant classifications were resolved by consensus.

Clinical Follow Up

Patients were reviewed every 6 months in the research clinic for a minimum of 24 months. Structured follow up data were collected on abdominal aortic aneurysm events, hospital admissions and other relevant clinical data. Clinical events were verified independently using

electronic health records and public registry data as described previously.[18,19] Serial maximum anteroposterior diameters were obtained by ultrasound in dedicated abdominal aortic aneurysm surveillance clinics performed by trained specialist vascular practitioners who were blinded to USPIO-enhanced MRI findings. We have previously reported interobserver coefficient of variation of aortic diameter measurements of 3.5%.[20] Participants unable to attend for subsequent research visits were followed-up through electronic health records as described previously.[18,19]

Clinical Endpoints and Adjudication

Clinical data from clinic visits, research database, electronic health records, primary care contacts and General Register Office were reviewed and clinical endpoints adjudicated by an independent Clinical Endpoint Committee. The committee members were blinded to the MRI findings. Follow-up was censored at 21st November 2016 or at the time of event.

Statistical Analysis

The primary endpoint was the composite of abdominal aortic aneurysm rupture or repair. We estimated that 130 events would be required to have adequate sensitivity to determine the added value of USPIO-enhanced MRI to predict the occurrence of the primary endpoint. Previous data from the United Kingdom have suggested a two-year event rate of 41% in patients under surveillance for abdominal aortic aneurysm.[21] We therefore aimed to recruit approximately 350 patients, with an expected drop-out rate of 10%, resulting in a minimum of 317 patients with 130 events to be included in the final analysis.

Categorical data are presented using counts and percentages, continuous variables presented using mean±standard deviation and absolute differences with 95% confidence intervals. Comparisons in baseline characteristics were made using either a binomial test for proportions in the case of categorical data or by two-sample *t*-test for continuous data. Aneurysm

growth rate was determined from serial ultrasound measurements using a linear regression model that was fitted to all available data and the slope used to determine the aneurysm growth rate per year. The primary and clinical event endpoints were assessed by log-rank test and are presented as Kaplan-Meier curves. Cox proportional hazards models were generated to include the baseline covariates of sex, smoking, systolic blood pressure and baseline aneurysm diameter determined by ultrasound. The additional value of USPIO enhancement was assessed by the c-statistic and net reclassification index.[22-24] Statistical significance was taken as two-sided p<0·05.

Role of the Funder

The funder played no role in developing the study design, the collection, analysis, and interpretation of data, in the writing of the report, or in the decision to submit the paper for publication.

Results

We screened approximately two thousand patients attending the out-patient vascular clinics of the study centres and identified 741 potentially eligible patients of whom ultimately 361 (48·7%) were recruited into the study (Figure 2). Nineteen patients were subsequently withdrawn predominantly because they were unable to undergo repeated magnetic resonance imaging due to claustrophobia. The final study population comprised of 342 participants who were predominantly elderly male current or ex-smokers with hypercholesterolaemia and hypertension (Table 1). There were no serious adverse events or reactions to intravenous ferumoxytol administration which was generally well tolerated by all participants. Mild asymptomatic hypotension that was possibly related to ferumoxytol was noted in one subject but required no action or intervention.

USPIO enhancement of the abdominal aortic aneurysm wall was identified in 146 (42·7%) participants, was absent in 191 (55·8%) and was indeterminate in 5 (1·5%). USPIO enhancement was strongly associated with current smoking status as well as baseline abdominal aortic aneurysm diameter and the presence of a common iliac aneurysm (Table 1).

Aneurysm Growth Rate

On ultrasound, baseline maximum abdominal aortic aneurysm diameter was 49·6±7·7 mm and was slightly larger in patients with USPIO enhancement (Table 1). The abdominal aortic aneurysm growth rate during the trial was 2·8±2·4 mm/year (n=279) and was greater in patients with USPIO enhancement (3·1±2·5 versus 2·5±2·4 mm/year; difference 0·6 [95% confidence intervals (CI), 0·02 to 1·2] mm/year, p=0·0424). Current smoking status (p=0·0305), but not aneurysm diameter (p=0·1853), baseline systolic blood pressure (p=0.6994) or USPIO enhancement (p=0·1993), was an independent predictor of aneurysm growth rate.

Clinical Follow-up

All participants were followed up for a mean of 1005±280 days. Overall, the primary endpoint occurred in 140 (40·9%) subjects with 17 abdominal aortic aneurysm ruptures and 126 abdominal aortic aneurysm repairs (Table 2): 3 subjects underwent repair after rupture. There were 48 (14·0%) deaths of which a third was abdominal aortic aneurysm related (17 [35·4%]) and a quarter was due to other cardiovascular causes (12 [25·0%]).

Rupture or Repair

The primary endpoint occurred more frequently in participants with USPIO enhancement of abdominal aortic aneurysm (69/146=47·3% versus 68/191=35·6%; difference 11·7%, 95% CI 1·1 to 22·2%, p=0·0308) and was associated with a reduced event-free survival (p=0·0275; Figure 3). This was consistent for both components of the endpoint (Table 2). In contrast to

female sex (hazards ratio 0·952, 95% confidence intervals 0·589 to 1·540; p=0·8413) and systolic blood pressure (hazards ratio 0·997, 95% confidence intervals 0·988 to 1·005; p=0·4492), baseline abdominal aortic aneurysm diameter (hazards ratio 1·077, 95% confidence intervals 1·061 to 1·094; p<0·0001) and current smoking habit (hazards ratio 1·464, 95% confidence intervals 1·001 to 2·120; p=0·0433) were the main predictors of the primary endpoint. The addition of USPIO enhancement to the model (hazards ratio 1·003, 95% confidence intervals 0·700 to 1·439; p=0·9849) did not improve the prediction of events (c-statistic, 0·7924 to 0·7926) or the unconditional net reclassification (-13·5%, 95% confidence intervals -36·4% to 9·3%). This was true for both components of the endpoint: (a) aneurysm rupture, c-statistic, 0·6317 to 0·6304 and net reclassification 29·9% (95% confidence intervals, -22·0% to 81·9%), and (b) aneurysm repair, c-statistic, 0·8000 to 0·7996 and net reclassification -9·9% (95% confidence intervals, -33·4% to 13·7%).

All-cause and abdominal aortic aneurysm-related death appeared to be more frequent in participants with USPIO enhancement of the abdominal aortic aneurysm (Table 2 and Figure 3) but fell short of statistical significance.

In post-hoc analysis, we explored whether USPIO enhancement varied according to aneurysm size. We dichotomised the population at the mean diameter into smaller (diameter 40-49 mm; n=187) and larger (diameter ≥50 mm; n=155) aneurysms. The rate of USPIO enhancement was lower in patients with smaller aneurysms: 65 (35·1%) versus 81 (53·3%) in those with larger aneurysms, difference 18·2% (95% confidence interval, 7·7 to 28·9; p=0·0008). However, in patients with smaller aneurysms, USPIO enhancement was associated with a doubling in the rate of repair or rupture without an effect on mortality (Table 3) whereas

in those with larger aneurysms, it was the reverse with a more than doubling of mortality but no effect on the primary endpoint (Table 4).

Discussion

In a prospective multicentre observational cohort study, we have demonstrated that USPIO-enhanced MRI not only predicts the rate of aneurysm expansion but also the future risk of abdominal aortic aneurysm rupture or repair. This is the largest prospective clinical study of magnetic resonance imaging in patients with abdominal aortic aneurysms, and is the first report of an imaging technique that not only identifies cellular inflammation, but also predicts disease progression and outcome. This suggests a central role of cellular inflammation in the pathophysiology, progression and outcome of abdominal aortic aneurysm disease.

Abdominal aortic aneurysm expansion is driven by several potential pathogenetic mechanisms that are associated with inflammation and tissue degradation.[1,11] Macrophages are central to many of these processes[25] and their depletion appears to prevent aneurysm formation or progression in preclinical models of abdominal aortic aneurysm.[26] Non-invasive *in vivo* imaging of tissue-resident macrophages would therefore seem an intuitive and promising approach in patients with abdominal aortic aneurysm but until now has not been prospectively tested in large clinical cohorts.[11,12,27] We here report the first study in a large clinical cohort to image tissue-resident macrophages with USPIO-enhanced MRI, and demonstrate that USPIO enhancement is associated with more rapid abdominal aortic aneurysm growth rates and adverse clinical outcomes. This provides strong support for the concept that imaging the biology of abdominal aortic aneurysm may be a promising new approach to risk stratify and manage patients with this disease.[11]

The rate of abdominal aortic aneurysm growth has previously been shown to be predicted by smoking status, aneurysm size and the presence of common iliac aneurysms.[9,28] Indeed, smoking habit is the principal modifiable risk factor for abdominal aortic aneurysm progression and rupture, and is the main focus of lifestyle modification in these patients. We here demonstrate that USPIO-enhanced MRI is associated with all of these three risk factors. In particular, current smoking was an independent risk factor for abdominal aortic aneurysm growth and intriguingly, USPIO enhancement was twice as frequent in current smokers. We know that smoking promotes inflammation, macrophage-mediated injury and vascular dysfunction.[29-31] This suggests a potential mechanistic link between smoking and macrophage-driven abdominal aortic aneurysm inflammation. Indeed, components of cigarette smoke, such as 3,4-benzopyrene, promote macrophage infiltration of abdominal aortic aneurysm leading to increased matrix metalloproteinase expression and vascular smooth muscle apoptosis.[32] Using adoptive transfer experiments, Jin and colleagues have further shown that *in vivo* exposure of leukocytes to smoke can accelerate the progression of aneurysm disease in smoke-free animals.[33] In this context, our USPIO data suggest that macrophage-mediated inflammation may be the mechanistic link to explain the association between smoking and disease progression in patients with abdominal aortic aneurysm.

The primary endpoint of the study was the rate of abdominal aortic aneurysm rupture or repair and although this was higher in patients with USPIO-enhancement on MRI, it was not independent of known predictors of outcome including baseline abdominal aortic aneurysm diameter and smoking habit. Indeed, incorporation of USPIO-enhanced MRI did not improve the discrimination of a model incorporating these known clinical risk factors. This likely reflects the mutual interdependence and potential causal association of these factors, namely that USPIO-

enhancement highlights areas of smoking induced cellular inflammation within the aneurysm which causes more rapid expansion and increase in the aneurysm diameter leading to aneurysm rupture or triggering of the threshold for repair.

Ultrasound measurements of abdominal aortic aneurysm diameter are the mainstay of clinical management and the principal determinant of the timing of elective surgical repair. Their dominant effect on the primary endpoint is therefore perhaps not surprising, especially as most events were due to elective surgical repair. Given that the clinicians were blind to the results of the USPIO-enhanced MRI, it would be challenging to demonstrate that it could lead to any changes in the rate of elective surgical repair. We therefore explored other measures of outcome that were independent of elective surgical repair. We found that USPIO enhancement appeared to be greater in those with emergent abdominal aortic aneurysm-related events including abdominal aortic aneurysm rupture and abdominal aortic aneurysm-related mortality although the absolute number of events was small and fell just short of achieving statistical significance. Given the small number of emergent events, our study did not have sufficient power to determine whether USPIO enhancement could provide clinically useful information that could independently predict emergent events. However, post-hoc analyses did suggest that USPIO-enhanced MRI did predict overall mortality in patients with larger aneurysms.

Although USPIO-enhanced MRI was not an independent predictor of outcome across the whole study population, it did identify aneurysm disease activity, correlate with rates of aneurysm expansion and appear to predict clinical outcome including rupture and death. If future studies confirm the utility of USPIO-enhanced MRI, how would it be applied in the clinic? For some patients, treatment decisions are not straight forward. For example, abdominal pain in a patient with an aortic aneurysm may be due to other abdominal pathology and not the aneurysm

itself. Urgent repair may be unhelpful in such circumstances and associated with considerable risk. Furthermore, decisions to undertake surgical repair can be challenging in those with high-risk or morphologically atypical aneurysms below 55 mm, those with borderline aneurysm sizes of 50-55 mm (especially in women), or those with larger aneurysms where the balance of risk and benefit is uncertain. Additional information regarding disease activity that is tied to disease progression and adverse clinical outcome may be helpful in guiding such decisions. The value of USPIO-enhanced MRI may also differ according to aneurysm size with the prediction of future aneurysm repair greater in patients with smaller aneurysms, and the future mortality risk more marked in those with larger aneurysms. Although not directly tested here, USPIO-enhanced MRI may assist the clinician in making these difficult management decisions that are associated with significant potential benefits and hazards. This requires further investigation.

There are no definitive medical treatments that can impact on disease progression in this serious and potentially fatal condition. Novel anti-inflammatory or other disease modifying therapies are potential interventions that could address this unmet clinical need. USPIO-enhanced MRI would provide a very useful surrogate biomarker of efficacy in such early proof-of-concept clinical trials. Reduction in USPIO enhancement would be predicted to correlate with reduced cellular inflammation within the aneurysm and consequently reduced rates of expansion. This merits further investigation.

Our study has a number of strengths. It was a multicentre prospective observational cohort study that ensured blinding of the USPIO-enhanced MRI findings from the patients, vascular technicians and attending clinicians, and was therefore independent of clinical decision making. It was an adequately sized phase 2 proof-of-concept trial that was ~10-fold larger than previous studies in this area.[15,34] The study also achieved its predicted event rates and met its

primary endpoint although not independent of known clinical predictors. However, the inclusion of elective surgical repair in the primary endpoint generates some challenges in interpretation because of the ultrasound and diameter-guided decision making for elective surgical repair. The prediction of emergent events appears promising but will require a much larger study with greater power to confirm these findings. Finally, USPIO-enhanced MRI is resource intensive and was not possible in a small number of patients due to contraindications or claustrophobia. However, it was a feasible, safe and deliverable clinical technique that was well tolerated in the vast majority of patients with no serious adverse effects of the MRI or contrast medium. Moreover, we have demonstrated its applicability across multiple sites, and have developed robust computer algorithms and image analysis techniques than enables automated reporting of USPIO enhancement, lending itself to immediate clinical application.

In conclusion, in a multicentre prospective observational cohort study, we have demonstrated that USPIO-enhanced MRI predicts the rate of aneurysm expansion, and the risk of abdominal aortic aneurysm rupture and repair. Although it does not provide independent prediction of aneurysm expansion or clinical outcomes in a model incorporating known clinical risk factors, this is the first demonstration of a cellular imaging technique that can predict clinical events in patients with abdominal aortic aneurysm. Whether clinical outcomes can be improved by treatment decisions based on this novel imaging approach remains to be established.

Sources of Funding

This study was funded by Medical Research Council (MRC) and managed by National Institute of Healthcare Research (NIHR) on behalf of the MRC-NIHR partnership (NIHR Efficacy and Mechanism Evaluation Programme: funding reference 11/20/03). The views expressed in this

publication are those of the authors and not necessarily those of the MRC, National Health Service (NHS), NIHR or the Department of Health. DEN is supported by the British Heart Foundation (CH/09/002, RE/13/3/30183, RM/13/2/30158) and is the recipient of a Wellcome Trust Senior Investigator Award (WT103782AIA). OMBM is supported by the Academic Department of Military Surgery and Trauma.

Acknowledgements

The Edinburgh Clinical Research Facility and Edinburgh Imaging Facility are supported by NHS Research Scotland. We would like to acknowledge the support of Karen Gallagher, Janice Taylor, Hayley Cuthbert, Annette Cooper and David Brian during the conduct of this study.

Declaration of interests

A patent (US 9275432 B2) held by the University of Edinburgh has been filed relating to the registration of medical images which were generated as part of this study.

Contribution to Manuscript

The MA^{3}RS Study Investigators contributed to the conception or design of the work, or the acquisition, analysis, or interpretation of data for the work. ROF and DEN wrote the first draft of the manuscript. The MA^{3}RS Study Investigators were involved in drafting the manuscript and revising it, and have given final approval of the version to be published. The MA^{3}RS Study Investigators are accountable for the work.

Sponsor

The University of Edinburgh and NHS Lothian Health Board were co-sponsors.

References

1. Kent KC. Clinical practice. Abdominal aortic aneurysms. *N Engl J Med*. 2014;371:2101-2108.
2. Global Burden of Disease 2013 Mortality Causes of Death Collaborators. Global, regional, and national age-sex specific all-cause and cause-specific mortality for 240 causes of death, 1990-2013: a systematic analysis for the Global Burden of Disease Study 2013. *Lancet*. 2015;385: 117–171.
3. Chaikof EL, Brewster DC, Dalman RL, Makaroun MS, Illig KA, Sicard GA, Timaran CH, Upchurch GR Jr, Veith FJ; Society for Vascular Surgery. The care of patients with an abdominal aortic aneurysm: the Society for Vascular Surgery practice guidelines. *J Vasc Surg*. 2009;50:S2-49.
4. Moll FL, Powell JT, Fraedrich G, Verzini F, Haulon S, Waltham M, van Herwaarden JA, Holt PJ, van Keulen JW, Rantner B, Schlösser FJ, Setacci F, Ricco JB; European Society for Vascular Surgery. Management of abdominal aortic aneurysms clinical practice guidelines of the European society for vascular surgery. *Eur J Vasc Endovasc Surg*. 2011;41:S1-S58.
5. Karthikesalingam A, Vidal-Diez A, Holt PJ, Loftus IM, Schermerhorn ML, Soden PA, Landon BE, Thompson MM. Thresholds for abdominal aortic aneurysm repair in England and the United States. *N Engl J Med.* 2016;375:2051-2059.
6. Multicentre Aneurysm Screening Study Group. Multicentre Aneurysm Screening Study (MASS) into the effect of abdominal aortic aneurysm screening on mortality in men: a randomised controlled trial. *Lancet* 2002;360:1531-1539.
7. Lindholt JS, Norman P. Screening for abdominal aortic aneurysm reduces overall mortality in men: a meta-analysis of the mid- and long-term effects of screening for abdominal aortic aneurysms. *Eur J Vasc Endovasc Surg* 2008;36:167-171.
8. Kurvers H, Veith FJ, Lipsitz EC, Ohki T, Gargiulo NJ, Cayne NS, Suggs WD, Timaran CH, Kwon GY, Rhee SJ, Santiago C. Discontinuous, staccato growth of abdominal aortic aneurysms. *J Am Coll Surg.* 2004;199:709-715.
9. Brady AR, Thompson SG, Fowkes FG, Greenhalgh RM, Powell JT. Abdominal aortic aneurysm expansion: risk factors and time intervals for surveillance. *Circulation* 2004;110:16-21.
10. Darling RC, Messina CR, Brewster DC, Ottinger LW. Autopsy study of unoperated abdominal aortic aneurysms: the case for early resection. *Circulation.* 1977;56:II161–II164.
11. Forsythe R, Newby DE, Robson JMJ. Monitoring the biological activity of abdominal aortic aneurysms: beyond ultrasound. *Heart.* 2016;102:817-824.
12. Wanhainen A, Mani K, Golledge J. Surrogate markers of abdominal aortic aneurysm progression. *Arterioscler Thromb Vasc Biol*. 2016;36:236-244.
13. Trivedi RA, Mallawarachi C, U-King-Im JM, Graves MJ, Horsley J, Goddard MJ, Brown A, Wang L, Kirkpatrick PJ, Brown J, Gillard JH. Identifying inflamed carotid plaques using in vivo USPIO-enhanced MR imaging to label plaque macrophages. *Arterioscler Thromb Vasc Biol.* 2006;26:1601-1606.
14. Alam SR, Shah ASV, Richards JR, Lang NN, Barnes G, Joshi N, MacGillivray T, McKillop G, Mirsadraee S, Payne J, Fox KAA, Henriksen PA, Newby DE, Semple SIK. Ultrasmall superparamagnetic particles of iron oxide in patients with acute myocardial infarction: early clinical experience. *Circ Cardiovasc Imaging* 2012;5:559-565.

15. Richards JMJ, Semple SI, MacGillivray TJ, Gray C, Langrish JP, Williams M, Dweck M, Wallace MD, McKillop G, Chalmers RTA, Garden OJ, Newby DE. Abdominal aortic aneurysm growth predicted by uptake of ultrasmall superparamagnetic particles of iron oxide. *Circ Cardiovasc Imaging* 2011;4:274-281.
16. Sadat U, Taviani V, Patterson AJ, Young VE, Graves MJ, Teng Z, Tang TY, Gillard JH. Ultrasmall superparamagnetic iron oxide-enhanced magnetic resonance imaging of abdominal aortic aneurysms–a feasibility study. *Eur J Vasc Endovasc Surg*. 2011;41:167-174
17. McBride OM, Berry C, Burns P, Chalmers RT, Doyle B, Forsythe R, Garden OJ, Goodman K, Graham C, Hoskins P, Holdsworth R, MacGillivray TJ, McKillop G, Murray G, Oatey K, Robson JM, Roditi G, Semple S, Stuart W, van Beek EJ, Vesey A, Newby DE. MRI using ultrasmall superparamagnetic particles of iron oxide in patients under surveillance for abdominal aortic aneurysms to predict rupture or surgical repair: MRI for abdominal aortic aneurysms to predict rupture or surgery-the MA(3)RS study. *Open Heart*. 2015;2:e000190.
18. Shah ASV Anand A, Sandoval Y, KK, Smith SW, Adamson PD, Chapman A, Langdon T, Sandeman D, Vaswani A, Strachan FE, Ferry A, Stirzaker A, Reid A, Gray AJ, Collinson PO, McAllister DA, Apple FS, Newby DE, Mills NL on behalf of the High STEACS Investigators. High-sensitivity cardiac troponin I at presentation in patients with suspected acute coronary syndrome. *Lancet* 2015;386:2481-2488.
19. The Scottish Computed Tomography of the HEART (SCOT-HEART) Trial Investigators. Computed tomography coronary angiography in patients with suspected angina due to coronary heart disease. *Lancet* 2015;385:2383-2391.
20. Wilson KA, Hoskins PR, Lee AJ, Fowkes FG, Ruckley CV, Bradbury AW. Ultrasonic measurement of abdominal aortic aneurysm wall compliance: a reproducibility study. *J Vasc Surg*. 2000;31:507–513.
21. Wilson KA, Lee AJ, Hoskins PR, Fowkes FG, Ruckley CV, Bradbury AW. The relationship between aortic wall distensibility and rupture of infrarenal abdominal aortic aneurysm. *J Vasc Surg*. 2003;37:112-117.
22. Polak JF, Pencina MJ, Pencina KM, O'Donnell CJ, Wolf PA, D'Agostino RB. Carotid-wall intima-media thickness and cardiovascular events. *N. Engl. J. Med*. 2011;365:213-221.
23. Pencina MJ, D'Agostino RB Sr, D'Agostino RB Jr, Vasan RS. Evaluating the added predictive ability of a new marker: from area under the ROC curve to reclassification and beyond. *Stat. Med.* 2008:27;157-172.
24. Pencina MJ, D'Agostino RB, Steyerberg EW. Extensions of net reclassification improvement calculations to measure usefulness of new biomarkers. *Stat. Med*. 2011:30;11-21.
25. Mallat Z. Macrophages. *Arterioscler Thromb Vasc Biol.* 2014;34:2509-2519.
26. Wang Y, Ait-Oufella H, Herbin O, Bonnin P, Ramkhelawon B, Taleb S, Huang J, Offenstadt G, Combadière C, Rénia L, Johnson JL, Tharaux PL, Tedgui A, Mallat Z. TGF-beta activity protects against inflammatory aortic aneurysm progression and complications in angiotensin II-infused mice. *J Clin Invest*. 2010;120:422-432.
27. Buijs RV, Willems TP, Tio RA, Boersma HH, Tielliu IF, Slart RH, Zeebregts CJ. Current state of experimental imaging modalities for risk assessment of abdominal aortic aneurysm. *J Vasc Surg.* 2013;57:851-859.
28. Sweeting MJ, Thompson SG, Brown LC, Powell JT, RESCAN collaborators. Meta-analysis of individual patient data to examine factors affecting growth and rupture of small abdominal aortic aneurysms. *Br J Surg*. 2012; 99:655-665.

29. Messner B, Bernhard D. Smoking and cardiovascular disease: mechanisms of endothelial dysfunction and early atherogenesis. *Arterioscler Thromb Vasc Biol.* 2014;34:509-15.
30. Newby DE, MacLeod AL, Uren NG, Flint LL, Ludlam CA, Webb DJ, Fox KAA, Boon NA. Impaired coronary tissue plasminigen activator release is associated with coronary atherosclerosis and cigarette smoking: direct link between endothelial dysfunction and atherothrombosis. *Circulation* 2001;103:1936-1941.
31. Harding SA, Josephs DH, Cruden NLM, Sarma J, Twomey PJ, Fox KAA, Newby DE. Upregulation of the CD40/CD40 ligand dyad and platelet-monocyte aggregation in cigarette smokers. *Circulation*. 2004;109;1926-1929.
32. Ji K, Zhang Y, Jiang F, Qian L, Guo H, Hu J, Liao L, Tang J. Exploration of the mechanisms by which 3,4-benzopyrene promotes angiotensin II-induced abdominal aortic aneurysm formation in mice. *J Vasc Surg.* 2014;59:492-499.
33. Jin J, Arif B, Garcia-Fernandez F, Ennis TL, Davis EC, Thompson RW, Curci JA. Novel mechanism of aortic aneurysm development in mice associated with smoking and leukocytes. *Arterioscler Thromb Vasc Biol*. 2012;32:2901-2909.
34. Jalalzadeh H, Indrakusuma R, Planken RN, Legemate DA, Koelemay MJ, Balm R. Inflammation as a predictor of abdominal aortic aneurysm growth and rupture: a systematic review of imaging biomarkers. *Eur J Vasc Endovasc Surg*. 2016;52:333-342.

10.1161/CIRCULATIONAHA.117.028433

Table 1. Baseline characteristics of participants

	All Participants n=342	Indeterminant USPIO Enhancement n=5	No USPIO Enhancement n=191	USPIO Enhancement n=146	Difference (95% CI)	P-value
Characteristic						
Age (years)	73·1±7·2	75·0±7·0	73·4±7·5	72·8±6·8	-0·6 (-2·2 to 0·9)	0·4330
Male	292 (85·4)	5 (100)	166 (86·9)	121 (82·9)	-4·0 (-11·8 to 3·7)	0·3019
Blood pressure - systolic (mmHg)	139·6±21·2	151·6±5·3	140·3±21·3	138·2±21·3	-2·1 (-6·8 to 2·5)	0·3610
Blood pressure - diastolic (mmHg)	81·4 ±10·8	87·0±10·7	80·5±10·3	82·3±11·3	1·9 (-0·4 to 4·2)	0·1101
Heart rate (/min)	70·7±10·1	71·6±12·1	70·0±10·1	71·5±10·0	1·5 (-0·7 to 3·7)	0·1779
Body-mass index (kg/m^2)	27·6±4·2	25·0±3·1	28·0±4·2	27·2±4·2	-0·8 (-1·7 to 0·1)	0·0729
Creatinine (µmol/L)	89·9±23·4	76·2±9·7	90·0±21·1	90·3±26·5	0·4 (-4·9 to 5·7)	0·8912
Cholesterol (mmol/L)	4·5±1·0	5·0±1·9	4·5±1·0	4·5±1·0	0·0 (-0·2 to 0·3)	0·7732
Smoking: Current smoker	101 (29·5)	4 (80)	40 (20·9)	57 (39·0)	18·1 (8·3 to 27·9)*	0·0003*
Ex-smoker	195 (57.0)	1 (20)	120 (62.8)	74 (50.7)		
Never smoker	46 (13.5)	0 (0)	31 (16.2)	15 (10.3)		
Aneurysm						
AAA diameter (mm)	49·6±7·7	54·4±12·3	48·2±6·6	51·4±8·4	3·2 (1·5 to 4·8)	0·0002
Concurrent iliac artery aneurysm	66 (19·3)	1 (20)	29 (15·2)	36 (24·7)	9·5 (0·8 to 18·1)	0·0289
Past Medical History						
Hypertension	246 (71·9)	3 (60)	143 (74·9)	100 (68·5)	-6·4 (-16·1 to 3·4)	0·1959
Hypercholesterolaemia	257 (75·1)	2 (40)	146 (76·4)	109 (74·7)	-1·8 (-11·1 to 7·5)	0·7056
Diabetes Mellitus	47 (13·7)	0 (0)	31 (16·2)	16 (11·0)	-5·3 (-12·6 to 2·0)	0·1663
Family history of AAA	61 (17·8)	0 (0)	32 (16·8)	29 (19·9)	3·1 (-5·3 to 11·5)	0·4626
Ischaemic heart disease	125 (36·5)	1 (20)	69 (36·1)	55 (37·7)	1·6 (-8·9 to 12·0)	0·7706
Peripheral vascular disease	66 (19·3)	1 (20)	34 (17·8)	31 (21·2)	3·4 (-5·1 to 12·0)	0·4288
Cerebrovascular disease	46 (13·5)	0 (0)	22 (11·5)	24 (16·4)	4·9 (-2·6 to 12·5)	0·1924
Baseline Medication						
Anti-platelet therapy	224 (65·5)	2 (40)	127 (66·5)	95 (65·1)	-1·4 (-11·7 to 8·8)	0·7847
Statin therapy	270 (78·9)	4 (80)	151 (79·1)	115 (78·8)	-0·3 (-9·1 to 8·5)	0·9483
Anti-coagulant therapy	25 (7·3)	0 (0)	16 (8·4)	9 (6·2)	-2·2 (-7·8 to 3·3)	0·4425
Beta blocker therapy	120 (35·1)	1 (20)	72 (37·7)	47 (32·2)	-5·5 (-15·7 to 4·7)	0·2948

Mean±SD or n (%).

*Current smoker versus combined ex-smoker and never smokers.

CI, confidence intervals; USPIO, ultrasmall superparagemagnetic particles of iron oxide; AAA, abdominal aortic aneurysm; ACE, angiotensin-converting enzyme.

Table 2. Clinical Outcome Events in All Patients

	All Participants n=342	Indeterminant USPIO Enhancement n=5	No USPIO Enhancement n=191	USPIO Enhancement n=146	Difference (95% CI)	P-value
Abdominal Aortic Aneurysm Event						
Rupture/repair	140 (40·9)	3 (60)	68 (35·6)	69 (47·3)	11·7 (1·1 to 22·2)	0·0308
Rupture	17 (5·0)	0 (0)	7 (3·7)	10 (6·8)	3·2 (-1·7 to 8·1)	0·1857
Repair	26 (36·8)	3 (60)	62 (32·5)	61 (41·8)	9·3 (-1·1 to 19·7)	0·0782
Type of repair: EVAR	53 (15·5)	1 (20)	29 (15·2)	23 (15·8)		
Open	73 (21·3)	2 (40)	33 (17·3)	38 (26·0)		
Type of surgery: Elective	120 (35·1)	3 (60)	58 (30·4)	59 (40·4)		
Emergency	6 (1·8)	0 (0)	4 (2·1)	2 (1·4)		
Death						
All cause	48 (14·0)	1 (20)	21 (11·0)	26 (17·8)	6·8 (-0·8 to 14·4)	0·0736
Cardiovascular - AAA related	17 (5·0)	0 (0)	6 (3·1)	11 (7·5)	4·4 (-0·6 to 9·3)	0·0679
Cardiovascular – non-AAA related	12 (3·5)	0 (0)	8 (4·2)	4 (2·7)		
Stroke	2 (0·6)	0 (0)	2 (1·0)	0 (0)		
Myocardial infarction	8 (2·3)	0 (0)	4 (2·1)	4 (2·7)		
Other cardiovascular	2 (0·6)	0 (0)	2 (1·0)	0 (0)		
Non-cardiovascular	19 (5·6)	1 (20)	7 (3·7)	11 (7·5)		
Malignancy	12 (3·5)	1 (20)	4 (2·1)	7 (4·8)		
Other	7 (2·0)	0 (0)	3 (1·6)	4 (2·7)		

n (%).

CI, confidence intervals; USPIO, ultrasmall superparamagnetic particles of iron oxide; AAA, abdominal aortic aneurysm; EVAR, endovascular aneurysm repair.

Table 3. Clinical Outcome Events in Patients with Small Aneurysms (diameter 40-49 mm).

	All Participants n=187	Indeterminant USPIO Enhancement n=2	No USPIO Enhancement n=120	USPIO Enhancement n=65	Difference (95% CI)	P-value
Abdominal Aortic Aneurysm Event						
Rupture/repair	42 (22·5)	0 (0)	20 (16·7)	22 (33·8)	17·2 (3·9 to 30·5)	0·0077
Rupture	4 (2·1)	0 (0)	2 (1·7)	2 (3·1)	1·4 (-3·4 to 6·2)	0·6136*
Repair	38 (20·3)	0 (0)	18 (15·0)	20 (30·8)	15·8 (2·9 to 28·7)	0·0113
Type of repair: EVAR	19 (10·2)	0 (0)	9 (7·5)	10 (15·4)		
Open	19 (10·2)	0 (0)	9 (7·5)	10 (15·4)		
Type of surgery: Elective	36 (19·3)	0 (0)	16 (13·3)	20 (30·8)		
Emergency	2 (1·1)	0 (0)	2 (1·7)	0 (0)		
Death						
All cause	20 (10·7)	1 (50)	14 (11·7)	5 (7·7)	-4·0 (-12·6 to 4·7)	0·3953
Cardiovascular - AAA related	4 (2·1)	0 (0)	2 (1·7)	2 (3·1)	1·4 (-3·4 to 6·2)	0·6136*
Cardiovascular – non-AAA related	8 (4·3)	0 (0)	7 (5·8)	1 (1·5)		
Stroke	1 (0·5)	0 (0)	1 (0·8)	0(0)		
Myocardial infarction	5 (2·7)	0 (0)	4 (3·3)	1 (1·5)		
Other cardiovascular	2 (1·1)	0 (0)	2 (1·7)	0 (0)		
Non-cardiovascular	8 (4·3)	1 (50)	5 (4·2)	2 (3·1)		
Malignancy	4 (2·1)	1 (50)	3 (2·5)	0 (0)		
Other	4 (2·1)	0 (0)	2 (1·7)	0 (0)		

n (%). CI, confidence intervals; USPIO, ultrasmall superparamagnetic particles of iron oxide; AAA, abdominal aortic aneurysm; EVAR, endovascular aneurysm repair. *Fisher's exact test due to small numbers.

Table 4. Clinical Outcome Events in Patients with Large Aneurysms (diameter ≥50 mm).

	All Participants n=155	Indeterminant USPIO Enhancement n=3	No USPIO Enhancement n=71	USPIO Enhancement n=81	Difference (95% CI)	P-value
Abdominal Aortic Aneurysm Event						
Rupture/repair						
Rupture	98 (63·2)	3 (100)	48 (67·6)	47 (58·0)	-9·6 (-24·9 to 5·7)	0·2235
Repair	13 (8·4)	0 (0)	5 (7·0)	8 (9·9)	2·8 (-6·0 to 11·7)	0·5330
Type of repair: EVAR	88 (56·8)	3 (100)	44 (62·0)	41 (50·6)	-11·4 (-27·0 to 4·3)	0·1595
Open	34 (21·9)	1 (33)	20 (28·2)	13 (16·0)		
Type of surgery: Elective	54 (34·8)	2 (67)	24 (33·8)	28 (34·6)		
Emergency	84 (54·2)	3 (100)	42 (59·2)	39 (48·1)		
Death	4 (2·6)	0 (0)	2 (2·8)	2 (2·5)		
All cause						
Cardiovascular - AAA related	28 (18·1)	0 (0)	7 (9·9)	21 (25·9)	16·1 (4·3 to 27·9)	0·0108
Cardiovascular – non-AAA related	13 (8·4)	0 (0)	4 (5·6)	9 (11·1)	5·5 (-3·2 to 14·2)	0·2283
Stroke	4 (2·6)	0 (0)	1 (1·4)	3 (3·7)		
Myocardial infarction	1 (0·6)	0 (0)	1 (1·4)	0 (0)		
Other cardiovascular	3 (1·9)	0 (0)	0 (0)	3 (3·7)		
Non-cardiovascular	0 (0)	0 (0)	0 (0)	0 (0)		
Malignancy	11 (7·1)	0 (0)	2 (2·8)	9 (11·1)		
Other	8 (5·2)	0 (0)	1 (1·4)	7 (8·6)		

n (%). CI, confidence intervals; USPIO, ultrasmall superparamagnetic particles of iron oxide; AAA, abdominal aortic aneurysm; EVAR, endovascular aneurysm repair.

Figure Legends

Figure 1. Magnetic resonance imaging of abdominal aortic aneurysm. **A** - T2-weighted HASTE sequence in the sagittal plane. **B** - Cross-sectional image (dashed line panel A) using a T2-weighted fat saturated sequence to highlight intraluminal thrombus (white) within the aneurysm. **C** - T2* map (blue) overlying the T2-weighted HASTE sequence of image B, demonstrating enhancement of the posterior aneurysm wall with ultrasmall superparamagnetic particles of iron oxide (red).

Figure 2. CONSORT diagram of participant recruitment.

Figure 3. Abdominal aortic aneurysm rupture or repair (primary endpoint; A), all-cause mortality (B) and aneurysm-related mortality (C) in participants with (red) and without (blue) ultrasmall superparamagnetic particles of iron oxide (USPIO) enhancement of the aneurysm wall. Cross-hairs represent individual censoring.

Figure 1

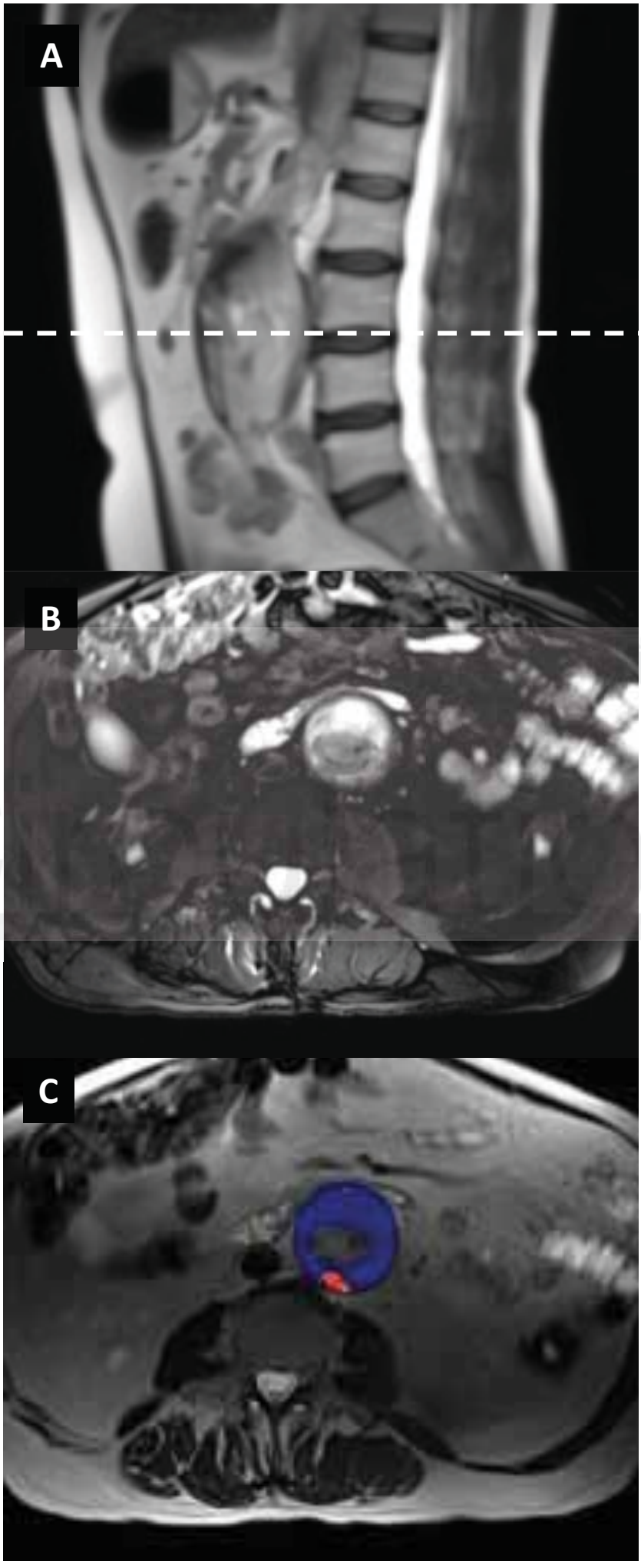

Figure 2

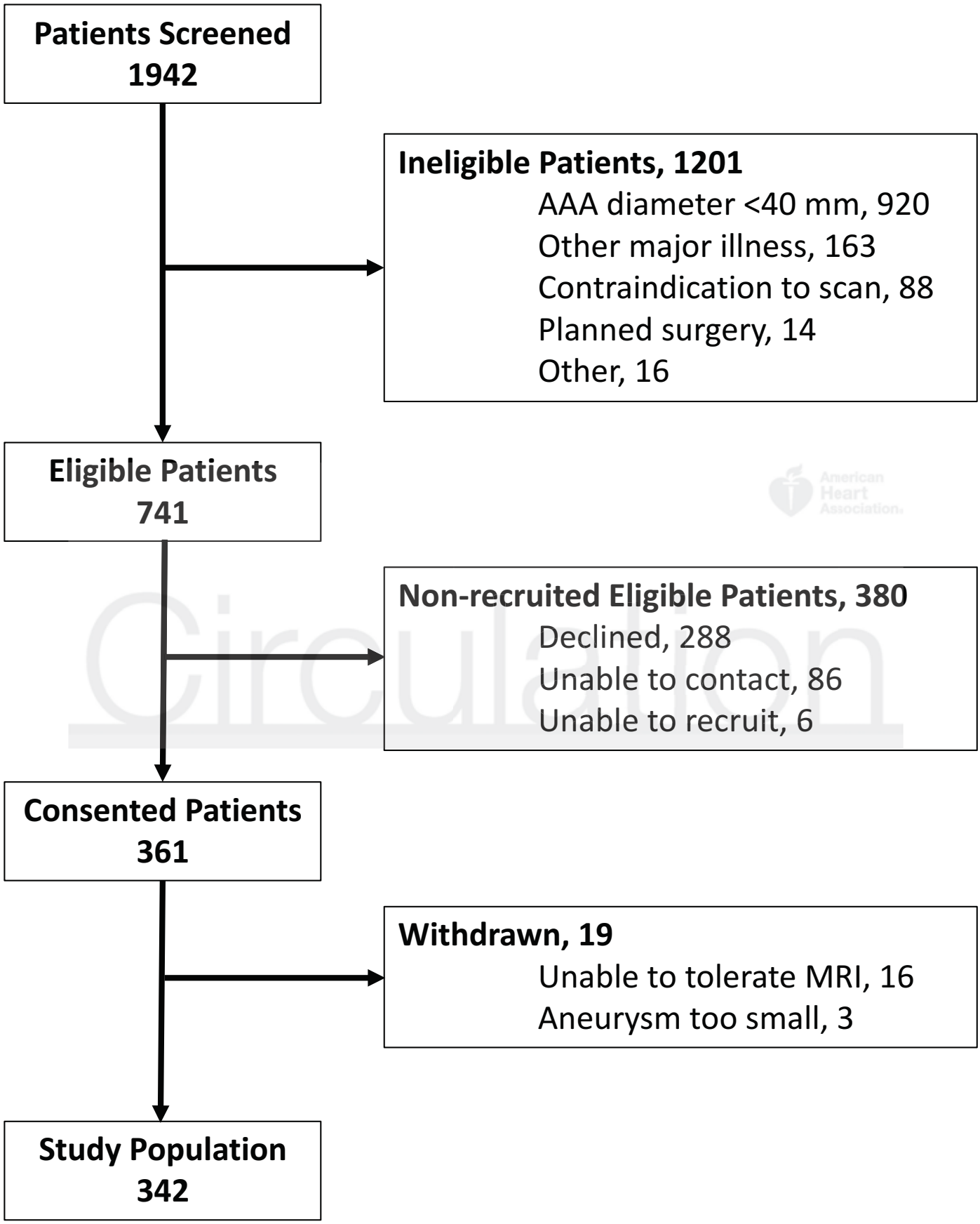

Figure 3

A

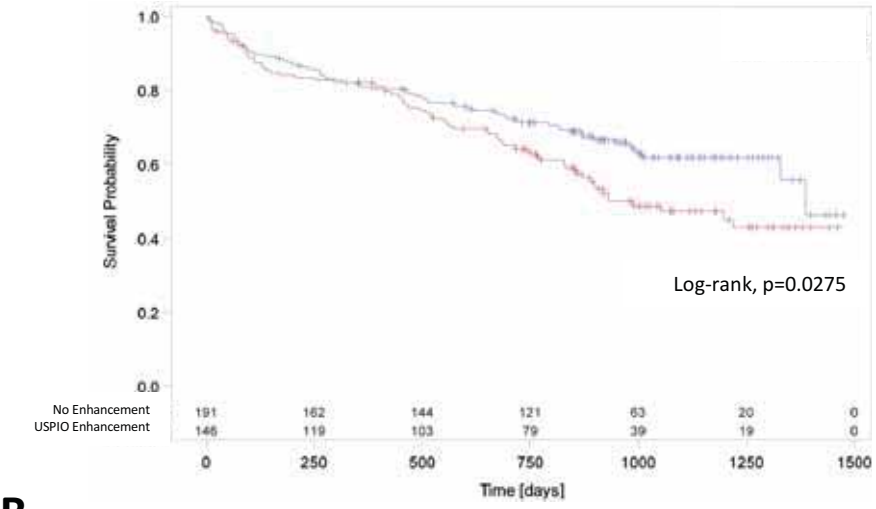

B

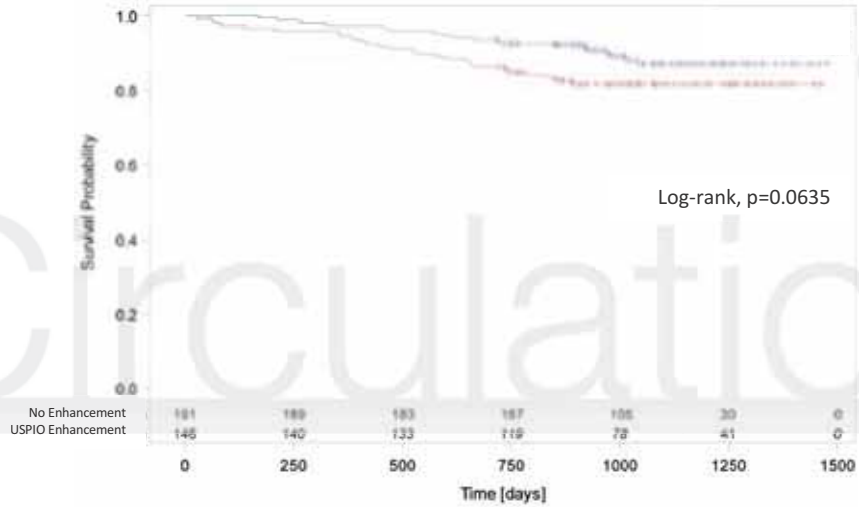

C

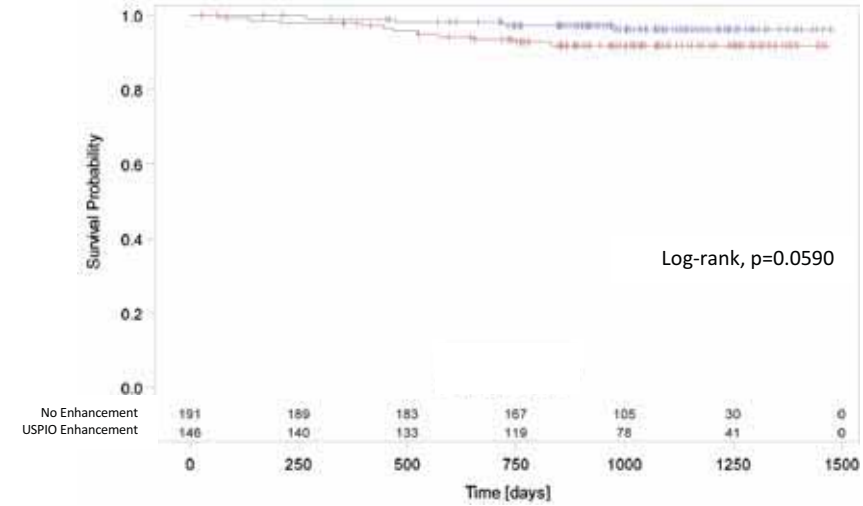

Aortic Wall Inflammation Predicts Abdominal Aortic Aneurysm Expansion, Rupture and Need for Surgical Repair

The MA³RS Study Investigators

Circulation. published online July 18, 2017;
Circulation is published by the American Heart Association, 7272 Greenville Avenue, Dallas, TX 75231

Print ISSN: 0009-7322. Online ISSN: 1524-4539

The MA^{3}RS Study Investigators

Chief Investigator: David Newby.

Trial Research Fellows: Rachael Forsythe, Olivia McBride, Jennifer Robson, Alex Vesey.

Study sites: Royal Infirmary of Edinburgh: Roderick Chalmers, Paul Burns, O James Garden, David Newby, Rachael Forsythe, Olivia McBride, Jennifer Robson, Scott Semple, Marc R. Dweck, Calum Gray, Tom MacGillivray, Chengjia Wang, Yolanda Georgia Koutraki, Neil Mitchard, Annette Cooper, Edwin van Beek, Graham McKillop, Weiyang Ho, Liz Fraser, Hayley Cuthbert, Peter Hoskins, Barry Doyle, Noel Conlisk. Western Infirmary, Glasgow: Wesley Stuart, Colin Berry, Alex Vesey, Giles Roditi, Laura Murdoch. Forth Valley Royal Hospital: Richard Holdsworth, Emma Scott.

Edinburgh Clinical Trials Unit: Lynsey Milne, Fiona Strachan, Fiona Wee, Katherine Oatey, Catriona Graham, Gordon Murray, Garry Milne, Marise Bucukoglu, Kirsteen Goodman.

Clinical Endpoint Committee: Jakub Kaczynski, Anoop Shah, Andrew Tambyraja.

The MA^{3}RS Study Steering Committee: Julie Brittenden (chair), Graeme Houston, Robert Lambie, John Norrie, Olivia McBride, Rachael Forsythe, David Newby, Graham McKillop, Scott Semple, Paul Burns, Colin Berry, Gordon Murray, Fiona Wee.

Exploring the biological and mechanical properties of abdominal aortic aneurysms using USPIO MRI and peak tissue stress: A combined clinical and finite element study

Conlisk: USPIO MRI and peak tissue stress in AAA

Authors:

Noel Conlisk[1,2,7], Rachael O. Forsythe[1,2,3], Lyam Hollis[1], Barry J. Doyle[1,5,6], Olivia M.B. McBride[1,2,3], Jennifer M.J. Robson[1,2], Chengjia Wang[1,3], Calum D. Gray[3], Scott I.K. Semple[1,3], Tom MacGillivray[1,4], Edwin J.R. van Beek[1,3], David E. Newby[1,3], Peter R. Hoskins[1,7]

[1]Centre for Cardiovascular Science, The University of Edinburgh, Edinburgh, UK
[2]School of Clinical Sciences, The University of Edinburgh, Edinburgh, UK
[3]Clinical Research Imaging Centre, The University of Edinburgh, Edinburgh, UK
[4]Centre for Clinical Brain Sciences, The University of Edinburgh, Edinburgh, UK
[5]Vascular Engineering Laboratory, Harry Perkins Institute of Medical Research, Perth, Australia
[6]School of Mechanical and Chemical Engineering, The University of Western Australia, Perth, Australia
[7]Institute for Bioengineering, The University of Edinburgh, Edinburgh, UK

Corresponding author:

Dr. Noel Conlisk
Institute for Bioengineering
The University of Edinburgh
Faraday Building
The King's Buildings
Mayfield Road
Edinburgh
EH9 3JL
Phone: +44 (0) 7775 332506
Fax: +44(0) 131 242 9101
Email: noel.conlisk@ed.ac.uk

Total word count: 5998

Abstract

Inflammation detected through the uptake of ultrasmall superparamagnetic particles of iron oxide (USPIO) on magnetic resonance imaging (MRI) and finite element (FE) modelling of tissue stress both hold potential in the assessment of abdominal aortic aneurysm (AAA) rupture risk. This study aimed to examine the spatial relationship between these two biomarkers.

Patients (n=50) > 40yrs with AAA maximum diameters >= 40 mm underwent USPIO-enhanced MRI and computed tomography angiogram (CTA). USPIO uptake was compared with wall stress predictions from CTA based patient-specific FE models of each aneurysm. Elevated stress was commonly observed in areas vulnerable to rupture (e.g. posterior wall, and shoulder). Only 16% of aneurysms exhibited co-localisation of elevated stress and mural USPIO enhancement. Globally, no correlation was observed between stress and other measures of USPIO uptake (i.e. mean or peak).

It is suggested that cellular inflammation and stress may represent different, but complimentary aspects of AAA disease progression.

Key words

Abdominal aortic aneurysms; finite element analysis; USPIO uptake; MRI; patient specific modelling.

Introduction

Each year over 10,000 deaths in the UK are attributed to rupture of abdominal aortic aneurysms (AAAs) [1]. It is thought that AAA rupture occurs when wall stress exceeds wall strength, and this is influenced by a number of biological and mechanical factors [2]. However, the exact mechanisms of AAA rupture are unknown. Various pathobiological processes contributing to AAA development and disease progression have been identified, including infiltration of inflammatory cells such as macrophages, proteolytic degradation of the extracellular matrix (ECM), and neovascularisation. All of these biological processes lead to changes in the mechanical properties of the artery wall including loss of elastin and deposition of collagen that compromises the strength and elasticity of the vessel [3,4].

It is clear that growth and ultimately rupture of AAAs over time occurs as a result of complex mechano-biological interactions within the diseased arterial wall [5]. However, it is unclear to what extent these biological and mechanical changes may co-exist and, indeed, contribute to the propagation of each other. Novel imaging studies have been undertaken in an attempt to understand the biological activity of AAA disease, such as the application of ^{18}F-fluoride to detect necrotic inflammation [6] and microcalcification [7], or the application of ultrasmall superparamagnetic particles of iron oxide (USPIO) to detect inflammation [8,9]. Also, we have previously demonstrated that ultrasmall superparamagnetic particles of iron oxide (USPIO) can identify areas of mural AAA inflammation, which is associated with more rapid aneurysm expansion [8]. Biomechanical studies can assess properties of AAA, such as wall stress and strength [10], and it has been shown that computational models based on the finite element (FE) method can identify rapidly expanding AAAs [11], assess rupture risk [12] and in some instances may even predict the location of rupture [13,14].

It has been suggested that focal areas of inflammation may be co-located with focal areas of increased mechanical stress [15]. The aim of this study was to explore the spatial relationship between areas of mural cellular inflammation measured by USPIO uptake on MRI, and regions of high tissue stress determined through patient-specific FE modelling, for a group of 50 patients under

surveillance for AAA disease.

Methods

Study design and setting

This is a sub-study of the MRI in AAA to predict Rupture or Surgery (MA^3RS) study (http://www.isrctn.com/ISRCTN76413758): a large multi-centre prospective observational cohort study aiming to determine the added value of USPIO-enhanced MRI in predicting AAA rupture or surgery in 342 patients with AAA under routine clinical surveillance. The MA^3RS study protocol has been described in full elsewhere [16] and the study is in the follow-up stages, due to report in 2017. In brief the MA^3RS study cohort, underwent USPIO MRI and CTA between November 2012 and December 2014 at the University of Edinburgh, Scotland. Patients were eligible for inclusion if they had an AAA ≥40 mm as measured on an ultrasound scan, if they were over 40 years of age, with no contraindications to USPIO MRI or CTA. Patients were excluded if the suspected aetiology of the aneurysm was inflammatory. An outline of the patient selection criteria is given in Fig. 1a.

For the present sub-study, we selected and analysed scans of consecutive patients recruited into the MA^3RS study using the process outlined in Figure 1b. During this phase 14 of the available consecutive scans were unable to be processed due to factors such as poor contrast on the CT scan (n = 6), segmentation difficulties (n = 4), and a lack of corresponding MRI-USPIO data (n = 4). These patients were therefore excluded from the final analysis. As per the selection algorithm (Fig. 1b) if a patient became ineligible, reconstruction and analysis moved on to the next consecutive patient until the predetermined target sample size of 50 eligible patients was reached. During the selection and reconstruction phase of the study, we were blinded to all demographic data, clinical outcomes and USPIO groupings for each patient.

USPIO magnetic resonance imaging and image analysis

The USPIO MRI and image analysis techniques used in the study have previously been described [16]. Briefly, participants underwent T2 and T2*-weighted MRI scanning at 3T (Siemens Magnetom Verio, Erlangen, Germany) both before and 24–36 hours after administration of a weight-adjusted dose of USPIO. Both

datasets (pre and post-USPIO) were then registered and analysed, using bespoke software. USPIO causes a rapid decline in T2*, which is the constant for the decay of MRI signal intensity over time, and as such, changes in T2* can be used to assess USPIO accumulation in the AAA [8]. Colour maps representing the percentage change in T2* (%ΔT2*) were generated using custom written scripts (MATLAB, The Mathworks Inc, Natick, MA). In order to minimise the effect of artefact, a threshold of ≥71% ΔT2* was used to identify areas of signal change attributable to true USPIO uptake, based on previous reproducibility data from our group [16].

Colour maps were classified according to a predefined criteria [8], into USPIO-negative (no mural USPIO uptake) or USPIO-positive (area(s) of significant mural USPIO enhancement indicative of macrophage-driven inflammation). Significant mural USPIO enhancement was defined as 10 or more contiguous USPIO-positive voxels adjacent to the aneurysm wall. Periluminal USPIO uptake is not considered to represent true inflammation and likely represents passive trapping of USPIOs in periluminal thrombus [17] although mural and periluminal uptake can be difficult to distinguish from posterior wall uptake due to their close proximity.

Computed tomography three-dimensional reconstruction and meshing

A standard high-resolution contrast-enhanced CTA was performed with a slice thickness of 1.0 mm and pixel size of 0.625 mm (Aquilion One, Toshiba Medical Systems Ltd, UK). These images were used to create patient-specific models of each aneurysm. Segmentation and 3D reconstruction was performed using commercial software (VASCOPS GmbH, Sweden). Early studies of AAA often assumed a uniform wall thickness [18], however, variable wall thickness has been shown to highly influence the predicted results [12,19-22]. Therefore, this package employs a specialist algorithm to calculate a more physiological aneurysm wall thickness distribution, which varies between 1.5 mm and 1.13 mm at the thrombus-free and covered sites respectively [19]. Finite element (FE) meshes were then created from the 3D aneurysm geometry using the A4 clinical research software (VASCOPS). After suitable refinement, each AAA volume mesh typically consisted of >160,000 (C3D8H) elements. These meshes

were then exported to Abaqus 6.10-1 (Dassault Systemes, Simulia, Providence, RI, USA) for analysis. Both the aortic wall and thrombus regions were modelled as hyperelastic, homogeneous, incompressible, and isotropic materials, using well established constitutive models [23,24] with material constants based on population data. Loading representative of peak systolic blood pressure was applied as an outward facing uniformly distributed pressure load acting on the luminal surface of the aneurysm. To remove any variability due to loading, and to allow for comparison across patient cases, a peak systolic blood pressure of 120 mm Hg (0.016 MPa) was chosen, as in many previous studies [25,26]. In the present study, the effect of wall shear stress due to blood flow was not considered due to its negligible magnitude. Residual stresses in the aortic wall itself, and the interaction of the aorta with the surrounding structures of the body (e.g. organs and spine), were also not considered. However, displacements at the distal and proximal most regions of each aneurysm were restrained, in all degrees of freedom, to model attachment of the AAA to the rest of the aorta.
For efficiency, a custom script was developed in Python (Python Software Foundation. Python Language Reference, version 2.7. Available at http://www.python.org) to automate the definition of the model parameters and batch process all 50 patients. All simulations were computed on a Dell Precision T7600 workstation with 16 cores and 64GB of ram. Contour plots of von Mises stress were output for all aneurysms, and their locations were manually aligned to USPIO uptake colour maps. Maximum AAA diameter, as measured orthogonal to the AAA centreline, was also extracted from each CT reconstruction.

Comparison of two-dimensional contour plots and USPIO uptake on colour maps
In order to compare the spatial relationship between elevated stress and areas of inflammation represented by USPIO uptake, the two-dimensional (2D) contour maps of von Mises stress were manually co-aligned with the USPIO colour maps. The MRI slice with the largest area of USPIO uptake (i.e. most-diseased segment) was chosen for analysis, ensuring that the corresponding cross-sectional slice was analysed from the 2D contour map (Fig. 2a). Co-location of elevated PS and areas of mural USPIO enhancement was examined for visual overlap on the chosen slice.

Global comparisons: whole AAA analysis

Global comparisons between peak wall stress (PWS) predicted for each patient (from FE) and maximum and peak USPIO uptake (%ΔT2*) per patient were also investigated, using values derived from the entire aneurysm. Maximum AAA diameter was also included in the analysis, as this is the most widely used predictor of aneurysm rupture. To test if correlations varied with classification of USPIO uptake (ie USPIO-negative or USPIO-positive), comparisons by group were also investigated.

Mural USPIO enhancement

To examine the trends with respect to the focal mural inflammation observed in USPIO-positive aneurysms more closely, the correlation of diameter and whole-vessel PWS with mural USPIO uptake values (mean and peak USPIO values identified on the most-diseased segment) was investigated. Non-focal areas of USPIO uptake (ie those which did not meet the definition of mural USPIO enhancement) were removed prior to this analysis.

Statistical analysis

Linear dependence between variables was investigated using the Pearson correlation coefficient. Unpaired two sample t-tests were used to assess differences in mean values between AAA groups. Statistical significance was determined using a two-tailed $p<0.05$. All statistical analyses were performed using Minitab® 17 (Minitab Ltd., Coventry CV 2TE UK).

Results

Fifty patients were included in this study who were predominantly elderly (mean age of 72 (65-87) years) men (90%), with a mean CT AAA diameter of 52.96 (40.60-69.40) mm. Mural USPIO enhancement was seen in 21 (42%) patients who had a significantly greater mean AAA diameter (55.19 vs 51.34 mm without mural enhancement, p=0.0255). There was no difference between groups in terms of other relevant characteristics (Table 1).

2D contour plot and USPIO colour map comparison

The maximum areas of PWS were most commonly (n=28; 56%) found in the posterior wall and regions of high curvature such as the shoulder region. When analysing the most-diseased segment, 40 aneurysms (80%) demonstrated some degree of visual overlap between regions of elevated stress and USPIO enhancement anywhere (e.g. adjacent to lumen and/or wall) in the vessel, in the remaining 10 cases no visual overlap was observed (e.g. Fig. 2b). Of the 40 aneurysms which did exhibit overlap, only 19 (38%) demonstrated spatial co-location of increased stress and USPIO enhancement adjacent to the aneurysm wall, the remaining aneurysms exhibited overlap of elevated stress at areas of peri-luminal USPIO uptake where classification is challenging (e.g. Fig. 2c). Overall, only 8 aneurysms (16%) demonstrated co-location of elevated stress with an area meeting the definition of mural USPIO enhancement (e.g. Fig. 2d). Details of inter- and intra-observer variability for stress and USPIO comparisons, as well as additional contour plot comparisons for the full 50 patients can be found in the supplementary text (supplement A).

Global comparisons: whole AAA analysis

The average PWS for all aneurysms was 0.1980 MPa. There was no difference between the average PWS for USPIO-negative aneurysms (0.1999±0.1326 MPa) and USPIO-positive aneurysms (0.1955±0.1495 MPa; p = 0.83, 95% CI -0.0920 to 0.0740).

Maximum diameter was not associated with PWS (r = 0.13, p = 0.36) or maximum USPIO uptake (r = 0.05, p = 0.74). There was no correlation between PWS and maximum USPIO enhancement over the entire aneurysm (r = 0.17, p =

0.23), as shown in Fig. 3.

When comparing between groups, diameter was not correlated with PWS in either group (USPIO-negative: r = 0.17, p = 0.39; USPIO-positive: r = 0.13, p = 0.61), nor was diameter and peak USPIO uptake (USPIO-negative: r = 0.04, p = 0.85; USPIO-positive: r = -0.15, p = 0.52), as shown in Fig. 4. There was no difference in correlation between PWS and mural USPIO enhancement between groups (r = 0.23 vs. r = 0.09; p = 0.22).

Focal mural USPIO enhancement

There were no associations between PWS and mean or peak USPIO uptake within the individual areas of mural USPIO enhancement on the most-diseased segment (r = 0.37, p = 0.10; r = 0.32, 0.16), as shown in Fig. 5.

Similarly, mean USPIO uptake within the identified regions of mural USPIO enhancement did not correlate with diameter (r = -0.05, p = 0.61), as shown in Fig. 6a. However, a significant weak inverse correlation was observed between peak USPIO uptake and diameter (r = -0.45, p = 0.04), as shown in Fig. 6b.

Discussion

In the present study, we analysed the spatial relationship between two biomarkers of abdominal aortic aneurysm (AAA) rupture risk; namely, inflammation detected through the uptake of ultrasmall superparamagnetic particles of iron oxide (USPIO) and wall stress calculated using patient-specific finite element (FE) models. Elevated stress was commonly observed in areas vulnerable to rupture (e.g. the posterior wall and shoulder), while regions of USPIO enhancement typically occurred near the wall behind thick thrombus. Only 16% of aneurysms exhibited co-localisation of elevated stress and mural USPIO enhancement. Globally, no correlation was observed between peak stress and other measures of USPIO uptake, e.g. mean or peak uptake.

The maximal area of PWS (as demonstrated using FE modelling) is most commonly found in the posterior aneurysm wall, where thrombus is typically thin or absent and the blood pool is in close proximity. Up to 82% of AAA ruptures occur on the posterior wall [27], yet most aneurysms bulge anteriorly. This may be explained by the restriction in radial expansion of the posterior wall due to the spinal column, with increasing anterior asymmetry resulting in an increase in posterior wall peak stress [28]. In addition, PWS was also frequently observed in regions of high curvature, including the shoulder region. These findings have been reported in many previous FE studies [29,30], some of which have demonstrated that increased stress at the aneurysm shoulder is associated with AAA expansion [11], possibly due to stress-induced changes in vessel wall stiffness [3].

Despite there being general visual overlap between stress and USPIO uptake, only 16% of all aneurysms in our study demonstrated co-location of elevated stress with mural USPIO enhancement. The finding of co-location of elevated stress and USPIO uptake in the posterior wall is challenging because this is a very thin structure and we cannot resolve whether this represents mural or periluminal uptake of USPIOs. Periluminal USPIO uptake is non-specific and reflects the passive trapping of USPIOs within the gelatinous thrombus immediately adjacent to the lumen. Histological analysis of aneurysm tissue has demonstrated that the immediate luminal aspect consists of freshly deposited thrombus that is highly cellular (including macrophages) with progressive

organisation towards the abluminal surface, which is acellular and consists largely of fibrin [31]. Therefore, the presence of USPIO uptake in the fibrinous thrombus adjacent to the aneurysm wall can be considered to represent true inflammation, whereas periluminal uptake of USPIO does not represent true cellular inflammation. Gadolinium-based MRI studies appear to reiterate this – the luminal surface of thrombus enhances with gadolinium, in contrast to the organized part of the thrombus and the aortic wall, which typically do not [8]. With regards to co-location of PWS and mean, maximum or peak USPIO uptake, no significant associations were demonstrated. These findings suggest that areas of elevated stress and objective measures of focal inflammation (as demonstrated on USPIO-enhanced MRI) do not commonly co-locate in AAA disease. Whilst we know that focal mechanical and biological processes do contribute towards AAA disease progression and rupture, it appears that stress and inflammation represent two distinct processes that are not necessarily connected spatially or causally. Our previous pilot study of USPIO MRI demonstrated a link between regions of focal cellular inflammation and future AAA expansion. Indeed histological analysis of tissue obtained during AAA repair provided evidence of the accumulation of USPIO within macrophages and USPIO-positive aneurysms were found to expand three times more rapidly than USPIO-negative aneurysms [8].

Other molecular imaging studies of AAA wall inflammation using positron emission tomography (PET) have demonstrated the ability of ^{18}F-FDG to identify regions of inflammation, confirmed by histological analysis [32]. However there is no definite consensus as to whether increased ^{18}F-FDG uptake correlates with clinical outcomes such as expansion or rupture [33,34]. In addition, we recently examined vascular inflammation in a small population of AAAs (n = 15) and found some but not a close correlation between ^{18}F-FDG uptake on PET/CT and USPIO uptake on MRI [17]. This may reflect the different elements of macrophage activity that these imaging techniques detect: glycolysis and phagocytosis, respectively.

Some other studies have also attempted to quantify the interaction between inflammation and peak stress, using a combined mechanical and biological approach to assess the overall stability of individual AAAs. In a pilot study (n=5),

Xu *et al* reported a tentative link between ^{18}F-FDG metabolic activity and high wall stress [30]. Later work by Maier *et al* confirmed that wall stress predicted by FE and ^{18}F-FDG uptake evaluated by PET/CT correlated both quantitatively and spatially in the cases examined (n=18) [29]. Interestingly, our study has observed that high stress often occurs in regions of high curvature or inflection points, such as the aneurysm shoulder and posterior luminal surface, which have been reported to have high ^{18}F-FDG uptake [29,17,6,30]. However, more recent work by Nchimi and colleagues [6] on a larger sample size (n=53) concluded that the relationship between ^{18}F-FDG uptake and peak stress was not directly correlated, instead pointing to a complex multi-factorial relationship between increased ^{18}F-FDG uptake and patient specific factors such as aneurysm location (thoracic or abdominal), wall stress, and family history/patient lifestyle. The present study also suggests that the relationship between inflammation and peak stress is complex and potentially independent.

Translational impact and clinical implications

While each marker (e.g. USPIO uptake or stress) provides and independent indicator of aneurysm rupture risk, neither presents the full picture in isolation. However, when a combined approach such as presented in this study is taken, then added insight into the mechanical and biological condition of the wall can be provided where indicators from these two independent markers coincide. Such insights may potentially lead to new methods for patient risk stratification, in particular in patients below the standard 55mm intervention threshold or in larger aneurysms where the benefit/risk of intervention is less certain.

Limitations and future direction

Our study has some technical limitations. We employed a continuum modelling strategy for the intraluminal thrombus, which is thought to act as a mechanical buffer [35], meaning that stress behind thick thrombus may be under-represented. Improvements in thrombus modelling may improve this [36], however our strategy is in keeping with most previous studies. In addition, our regions of mural USPIO enhancement were identified on axial slices in the 2D plane – this is based on the techniques used in our previous pilot study and is

considered a reasonable, pragmatic approach to image analysis. However, our group is also exploring 3D mural USPIO enhancement detection [37], that may provide additional data with which to compare wall stress in the future. Furthermore, as in many previous studies, we have assumed population-mean parameters for the AAA material properties, which may influence the resulting wall stress. Ongoing work aims to eliminate the potential uncertainty surrounding material properties [38], it is hoped that this step in combination with a more comprehensive comparison of USPIO-uptake and PWS in 3D may provide some further insight into the complex interplay of these two factors in AAA disease progression. One final limitation is the lack of longitudinal data with which to verify our hypothesis that overlapping regions of stress and USPIO may potentially identify patients at greater risk of rupture. Recent findings from the main MA^{3}RS study [39] have already demonstrated that USPIO uptake predicts expansion, but that this is not independent of diameter. Final follow-up data from the trial has been collected and we have recently started to explore other secondary analyses, including how baseline stress/USPIO uptake predictions relate to the evolution of the aneurysm over time. However, given the non-trivial nature of this work it will take many months before the data is fully analysed and interpreted. Once analysed, it is anticipated that these findings will provide a greater level of insight into disease progression and the significance of the overlapping regions of stress and inflammation.

Conclusions

In this combined clinical and FE study of 50 aneurysms, poor correlations between USPIO uptake and stress suggest that these biological and mechanical factors address different aspects of the aberrant pathway towards disease progression in AAA. We observed that peak stress most commonly occurs in regions of increased curvature (such as the posterior wall and inflection points), and further correlation with peak stress and different markers of inflammation is warranted. Whilst both macrophage-mediated inflammation and peak wall stress play a part in AAA expansion and rupture, they do not spatially co-locate and this only serves to reinforce the complex multi-factorial elements in

aneurysm disease progression. However, it remains a possibility that although PWS and mural USPIO enhancement are independent processes, when they co-localise, this could be a trigger for aneurysm rupture. To address this hypothesis requires long term follow up of clinical cohorts. Additional clinical and biomechanical studies are therefore required to further investigate the synergy between biological and biomechanical aspects of AAA disease.

Acknowledgements

The authors would like to gratefully acknowledge the staff at the Clinical Research Imaging Centre (CRIC), University of Edinburgh, for facilitating access to the imaging data.

Funding

Funding for this work was provided through the National Institute of Health Research (NIHR) Efficacy and Mechanism Evaluation (EME) Programme as part of the MA^{3}RS clinical trial (NIHR EME 11/20/03).

Conflict of Interest

One of the authors (CW) was in part supported by funding from Toshiba Medical Visualization Systems (Europe) Ltd.

Ethical Approval

The study was approved by a local research ethics committee (East of Scotland Ethics Research Service, ref 12/ES/0068) and performed in accordance with the Declaration of Helsinki.

Informed Consent

Informed written consent was obtained for all patients prior to participation in the study.

References

1. Mitchell, D., Hindley, H., Naylor, R., Wyatt, M., & Loftus, I. (2012). The Abdominal Aortic Aneurysm Quality Improvement Programme The Vascular Society of Great Britian & Ireland.
2. Choke, E., Cockerill, G., Wilson, W. R., Sayed, S., Dawson, J., & Loftus, I. (2005). A review of biological factors implicated in abdominal aortic aneurysm rupture. *Eur J Vasc Endovasc Surg, 30*, doi:10.1016/j.ejvs.2005.03.009.
3. Helderman, F., Manoch, I. J., Breeuwer, M., Kose, U., Schouten, O., Sambeek, M. R. M., et al. (2008). A numerical model to predict abdominal aortic aneurysm expansion based on local wall stress and stiffness. *Medical & Biological Engineering & Computing, 46*(11), 1121-1127, doi:10.1007/s11517-008-0358-3.
4. O'Leary, S. A., Mulvihill, J. J., Barrett, H. E., Kavanagh, E. G., Walsh, M. T., McGloughlin, T. M., et al. (2015). Determining the influence of calcification on the failure properties of abdominal aortic aneurysm (AAA) tissue. *J Mech Behav Biomed Mater, 42*(0), 154-167, doi:http://dx.doi.org/10.1016/j.jmbbm.2014.11.005.
5. Humphrey, J. D., & Holzapfel, G. A. (2012). Mechanics, mechanobiology, and modeling of human abdominal aorta and aneurysms. *Journal of Biomechanics, 45*(5), 805-814, doi:http://dx.doi.org/10.1016/j.jbiomech.2011.11.021.
6. Nchimi, A., Cheramy-Bien, J. P., Gasser, T. C., Namur, G., Gomez, P., & Seidel, L. (2014). Multifactorial relationship between 18F-fluoro-deoxy-glucose positron emission tomography signaling and biomechanical properties in unruptured aortic aneurysms. *Circulation: Cardiovascular Imaging, 7*, doi:10.1161/circimaging.112.000415.
7. Forsythe, R. O., Newby, D. E., & Robson, J. M. J. (2016). Monitoring the biological activity of abdominal aortic aneurysms Beyond Ultrasound. *Heart*, doi:10.1136/heartjnl-2015-308779.
8. Richards, J. M., Semple, S. I., MacGillivray, T. J., Gray, C., Langrish, J. P., Williams, M., et al. (2011). Abdominal aortic aneurysm growth predicted by uptake of ultrasmall superparamagnetic particles of iron oxide: a pilot study. *Circ Cardiovasc Imaging, 4*(3), 274-281, doi:10.1161/circimaging.110.959866.
9. Sadat, U., Taviani, V., Patterson, A. J., Young, V. E., Graves, M. J., Teng, Z., et al. (2011). Ultrasmall Superparamagnetic Iron Oxide-enhanced Magnetic Resonance Imaging of Abdominal Aortic Aneurysms–A Feasibility Study. *European Journal of Vascular and Endovascular Surgery, 41*(2), 167-174, doi:http://dx.doi.org/10.1016/j.ejvs.2010.08.022.
10. Malkawi, A. H., Hinchliffe, R. J., Xu, Y., Holt, P. J., Loftus, I. M., & Thompson, M. M. (2010). Patient-specific biomechanical profiling in abdominal aortic aneurysm development and rupture. *Journal of Vascular Surgery, 52*(2), 480-488, doi:http://dx.doi.org/10.1016/j.jvs.2010.01.029.
11. Li, Z.-Y., Sadat, U., U-King-Im, J., Tang, T. Y., Bowden, D. J., Hayes, P. D., et al. (2010). Association Between Aneurysm Shoulder Stress and Abdominal Aortic Aneurysm Expansion: A Longitudinal Follow-Up Study. *Circulation, 122*(18), 1815-1822, doi:10.1161/circulationaha.110.939819.
12. Conlisk, N., Geers, A. J., McBride, O. M. B., Newby, D. E., & Hoskins, P. R. (2016). Patient-specific modelling of abdominal aortic aneurysms: The

influence of wall thickness on predicted clinical outcomes. *Medical Engineering & Physics, 38*(6), 526-537, doi:http://dx.doi.org/10.1016/j.medengphy.2016.03.003.

13. Xenos, M., Rambhia, S. H., Alemu, Y., Einav, S., Labropoulos, N., Tassiopoulos, A., et al. (2010). Patient-Based Abdominal Aortic Aneurysm Rupture Risk Prediction with Fluid Structure Interaction Modeling. [journal article]. *Annals of Biomedical Engineering, 38*(11), 3323-3337, doi:10.1007/s10439-010-0094-3.
14. Doyle, B. J., McGloughlin, T. M., Miller, K., Powell, J. T., & Norman, P. E. (2014). Regions of High Wall Stress Can Predict the Future Location of Rupture of Abdominal Aortic Aneurysm. [journal article]. *CardioVascular and Interventional Radiology, 37*(3), 815-818, doi:10.1007/s00270-014-0864-7.
15. Vallabhaneni, S. R., Gilling-Smith, G. L., How, T. V., Carter, S. D., Brennan, J. A., & Harris, P. L. (2004). Heterogeneity of Tensile Strength and Matrix Metalloproteinase Activity in the Wall of Abdominal Aortic Aneurysms. *Journal of Endovascular Therapy, 11*(4), 494-502, doi:10.1583/04-1239.1.
16. McBride, O. M. B., Berry, C., Burns, P., Chalmers, R. T. A., Doyle, B., Forsythe, R., et al. (2015). MRI using ultrasmall superparamagnetic particles of iron oxide in patients under surveillance for abdominal aortic aneurysms to predict rupture or surgical repair: MRI for abdominal aortic aneurysms to predict rupture or surgery—the MA3RS study. *Open Heart, 2*(1), doi:10.1136/openhrt-2014-000190.
17. McBride, O. M. B., Joshi, N. V., Robson, J. M. J., MacGillivray, T. J., Gray, C. D., Fletcher, A. M., et al. (2016). Positron Emission Tomography and Magnetic Resonance Imaging of Cellular Inflammation in Patients with Abdominal Aortic Aneurysms. *European Journal of Vascular and Endovascular Surgery, 51*(4), 518-526, doi:http://dx.doi.org/10.1016/j.ejvs.2015.12.018.
18. Raghavan, M. L., Vorp, D. A., Federle, M. P., Makaroun, M. S., & Webster, M. W. (2000). Wall stress distribution on three-dimensionally reconstructed models of human abdominal aortic aneurysm. *Journal of Vascular Surgery, 31*(4), 760-769, doi:http://dx.doi.org/10.1067/mva.2000.103971.
19. Gasser, T. C., Auer, M., Labruto, F., Swedenborg, J., & Roy, J. (2010). Biomechanical Rupture Risk Assessment of Abdominal Aortic Aneurysms: Model Complexity versus Predictability of Finite Element Simulations. *European Journal of Vascular and Endovascular Surgery, 40*(2), 176-185, doi:http://dx.doi.org/10.1016/j.ejvs.2010.04.003.
20. Martufi, G., Satriano, A., Moore, R. D., Vorp, D. A., & Di Martino, E. S. (2015). Local Quantification of Wall Thickness and Intraluminal Thrombus Offer Insight into the Mechanical Properties of the Aneurysmal Aorta. [journal article]. *Annals of Biomedical Engineering, 43*(8), 1759-1771, doi:10.1007/s10439-014-1222-2.
21. Shang, E. K., Nathan, D. P., Woo, E. Y., Fairman, R. M., Wang, G. J., Gorman, R. C., et al. (2013). Local wall thickness in finite element models improves prediction of abdominal aortic aneurysm growth. *Journal of Vascular Surgery*(0), doi:http://dx.doi.org/10.1016/j.jvs.2013.08.032.
22. Shum, J., DiMartino, E. S., Goldhamme, A., Goldman, D. H., Acker, L. C., Patel, G., et al. (2010). Semiautomatic vessel wall detection and quantification of wall thickness in computed tomography images of human abdominal aortic

aneurysms. *Medical Physics, 37*(2), 638-648.
23. Raghavan, M. L., & Vorp, D. A. (2000). Toward a biomechanical tool to evaluate rupture potential of abdominal aortic aneurysm: identification of a finite strain constitutive model and evaluation of its applicability. *Journal of Biomechanics, 33*(4), 475-482, doi:http://dx.doi.org/10.1016/S0021-9290(99)00201-8.
24. Wang, D. H. J., Makaroun, M., Webster, M. W., & Vorp, D. A. (2001). Mechanical properties and microstructure of intraluminal thrombus from abdominal aortic aneurysm. [Article]. *J Biomech Eng, 123*(6), 536-539, doi:10.1115/1.1411971.
25. Doyle, B. J., Callanan, A., Walsh, M., Grace, P., & McGloughlin, T. (2009). A finite element analysis rupture index (FEARI) as an additional tool for abdominal aortic aneurysm rupture prediction. *Vascular Disease Prevention, 6*, 114 - 121.
26. Vorp, D. A., Raghavan, M. L., & Webster, M. W. (1998). Mechanical wall stress in abdominal aortic aneurysm: Influence of diameter and asymmetry. *Journal of Vascular Surgery, 27*(4), 632-639, doi:http://dx.doi.org/10.1016/S0741-5214(98)70227-7.
27. Fillinger, M. F., Racusin, J., Baker, R. K., Cronenwett, J. L., Teutelink, A., & Schermerhorn, M. L. (2004). Anatomic characteristics of ruptured abdominal aortic aneurysm on conventional CT scans: Implications for rupture risk. *J Vasc Surg, 39*, doi:10.1016/j.jvs.2004.02.025.
28. Doyle, B. J., Callanan, A., Burke, P. E., Grace, P. A., Walsh, M. T., Vorp, D. A., et al. (2009). Vessel asymmetry as an additional diagnostic tool in the assessment of abdominal aortic aneurysms. *Journal of Vascular Surgery, 49*(2), 443-454, doi:http://dx.doi.org/10.1016/j.jvs.2008.08.064.
29. Maier, A., Essler, M., Gee, M. W., Eckstein, H.-H., Wall, W. A., & Reeps, C. (2012). Correlation of biomechanics to tissue reaction in aortic aneurysms assessed by finite elements and [18F]–fluorodeoxyglucose–PET/CT. *Int. J. Numer. Method. Biomed. Eng., 28*(4), 456-471, doi:10.1002/cnm.1477.
30. Xu, X. Y., Borghi, A., Nchimi, A., Leung, J., Gomez, P., & Cheng, Z. (2010). High levels of 18F-FDG uptake in aortic aneurysm wall are associated with high wall stress. *Eur J Vasc Endovasc Surg, 39*, doi:10.1016/j.ejvs.2009.10.016.
31. Gasser, T. C., Martufi, G., Auer, M., Folkesson, M., & Swedenborg, J. (2010). Micromechanical Characterization of Intra-luminal Thrombus Tissue from Abdominal Aortic Aneurysms. [journal article]. *Annals of Biomedical Engineering, 38*(2), 371-379, doi:10.1007/s10439-009-9837-4.
32. Courtois, A., Nusgens, B. V., Hustinx, R., Namur, G., Gomez, P., & Somja, J. (2013). 18F-FDG uptake assessed by PET/CT in abdominal aortic aneurysms is associated with cellular and molecular alterations prefacing wall deterioration and rupture. *J Nucl Med, 54*, doi:10.2967/jnumed.112.115873.
33. Kotze, C. W., Groves, A. M., Menezes, L. J., Harvey, R., Endozo, R., & Kayani, I. A. (2011). What is the relationship between (1)(8)F-FDG aortic aneurysm uptake on PET/CT and future growth rate? *Eur J Nucl Med Mol Imaging, 38*, doi:10.1007/s00259-011-1799-8.
34. Reeps, C., Essler, M., Pelisek, J., Seidl, S., Eckstein, H. H., & Krause, B. J. (2008). Increased 18F-fluorodeoxyglucose uptake in abdominal aortic aneurysms in positron emission/computed tomography is associated with inflammation, aortic wall instability, and acute symptoms. *J Vasc Surg, 48*,

doi:10.1016/j.jvs.2008.03.059.
35. Doyle, B., & McGloughlin, T. (2011). Computer-Aided Diagnosis of Abdominal Aortic Aneurysms. In T. McGloughlin (Ed.), *Biomechanics and Mechanobiology of Aneurysms* (Vol. 7, pp. 119-138, Studies in Mechanobiology, Tissue Engineering and Biomaterials): Springer Berlin Heidelberg.
36. Ayyalasomayajula, A., Vande Geest, J. P., & Simon, B. R. (2010). Porohyperelastic finite element modeling of abdominal aortic aneurysms. *J Biomech Eng, 132*(10), 104502, doi:10.1115/1.4002370.
37. Koutraki, Y. G., Forsythe, R. O., McBride, O. M. B., Wang, C., Robson, J. M. J., MacGillivray, T. J., et al. (2016). *Automatic Classification and 3D Visualisation of Abdominal Aortic Aneurysms to Predict Aneurysm Expansion and Rupture.* Paper presented at the ISMRM 24th Annual Meeting & Exhibition, Singapore, 07 - 13 May 2016
38. Joldes, G. R., Miller, K., Wittek, A., & Doyle, B. (2016). A simple, effective and clinically applicable method to compute abdominal aortic aneurysm wall stress. *J Mech Behav Biomed Mater, 58*, 139-148, doi:http://dx.doi.org/10.1016/j.jmbbm.2015.07.029.
39. Study Investigators, T. M. R. (2017). Aortic Wall Inflammation Predicts Abdominal Aortic Aneurysm Expansion, Rupture and Need for Surgical Repair. *Circulation*, doi:10.1161/circulationaha.117.028433.

Figure legends

Fig. 1 Flowcharts detailing a) patient inclusion/exclusion criteria, and b) the patient selection algorithm.

Fig. 2 a) the slice with the largest mural USPIO enhancement (most-diseased segment) is selected from MRI. The corresponding slice is then extracted from the CT based FE model using relevant anatomical landmarks (e.g. Z-distance from the iliac bifurcation). The contours are then visually compared to determine if co-location occurs. Examples of aneurysms with no co-location, some periluminal co-location (which does not represent inflammation), and true co-location of elevated stress with significant mural USPIO enhancement can be seen in panels b), c), and d) respectively. Note: black arrows point to approximate regions of co-location

Fig. 3 Global comparisons (n=50) of aneurysm diameter, peak stress predicted by finite element analysis and % ΔT2* USPIO, using data from the entire aneurysm. There are no significant correlations between any of the measured parameters.

Fig. 4 Comparisons of diameter, peak stress and % ΔT2* USPIO uptake per group; USPIO-negative (n=29) vs USPIO-positive (n=21), using data from the entire aneurysm. No significant correlations demonstrated.

Fig. 5 Mural USPIO enhancement analysis. Correlation between peak stress (derived from the entire aneurysm) with mean and peak USPIO uptake on the most-diseased segment (n=21). No significant correlations identified.

Fig. 6 Mural USPIO enhancement analysis. Correlation between aneurysm diameter with mean and peak USPIO uptake in the identified areas of significant mural USPIO enhancement on the most-diseased segment (n=21).

Tables

Table 1 Summary demographics of patients, per USPIO classification group, using comparisons of proportion or chi-squared test, where appropriate.

Variable	All patients (n=50)	USPIO-negative (n=29)	USPIO-positive (n=21)	Difference between groups - p value
Age in years (SD)	72.34 (6.32)	71.96 (6.37)	72.86 (6.37)	0.6372
Male sex (%)	45 (90)	25 (86)	20 (95)	0.383
Mean AAA diameter in mm (SD)	52.96 (6.08)	51.34 (5.19)	55.19 (6.62)	0.0255
Past medical history				
Family history of AAA (%)	12 (24)	6 (20.69)	6 (28.57)	0.738
Coronary artery disease (%)	16 (32)	9 (31.03)	7 (33.33)	1
Stroke or transient ischemic attack (%)	3 (6)	2 (6.90)	1 (4.76)	1
Peripheral vascular disease (%)	3 (6)	3 (10.34)	0 (0)	0.254
Cerebrovascular disease (%)	2 (4)	2 (6.90)	0 (0)	0.503
Risk factors				
Current smoking habit (%)	12 (24)	5 (17.24)	7 (33.33)	0.314
Previous smoking habit (%)	32 (64)	20 (68.97)	12 (57.14)	0.551
Hypertension (%)	40 (80)	24 (82.76)	16 (76.20)	0.7232
Hypercholesterolaemia (%)	44 (88)	25 (86.21)	19 (90.48)	1
Diabetes (%)	7 (14)	4 (13.79)	3 (14.29)	1
Medication				
Anti-Diabetes medication (%)	6 (12)	5 (17.24)	1 (4.76)	0.38
Statin therapy (%)	2 (4)	2 (6.90)	0 (0)	0.503
Anti-coagulant therapy (%)	1 (2)	0 (0)	1 (4.76)	0.42

Figure_1

Click here to download Figure Figure_1.tif

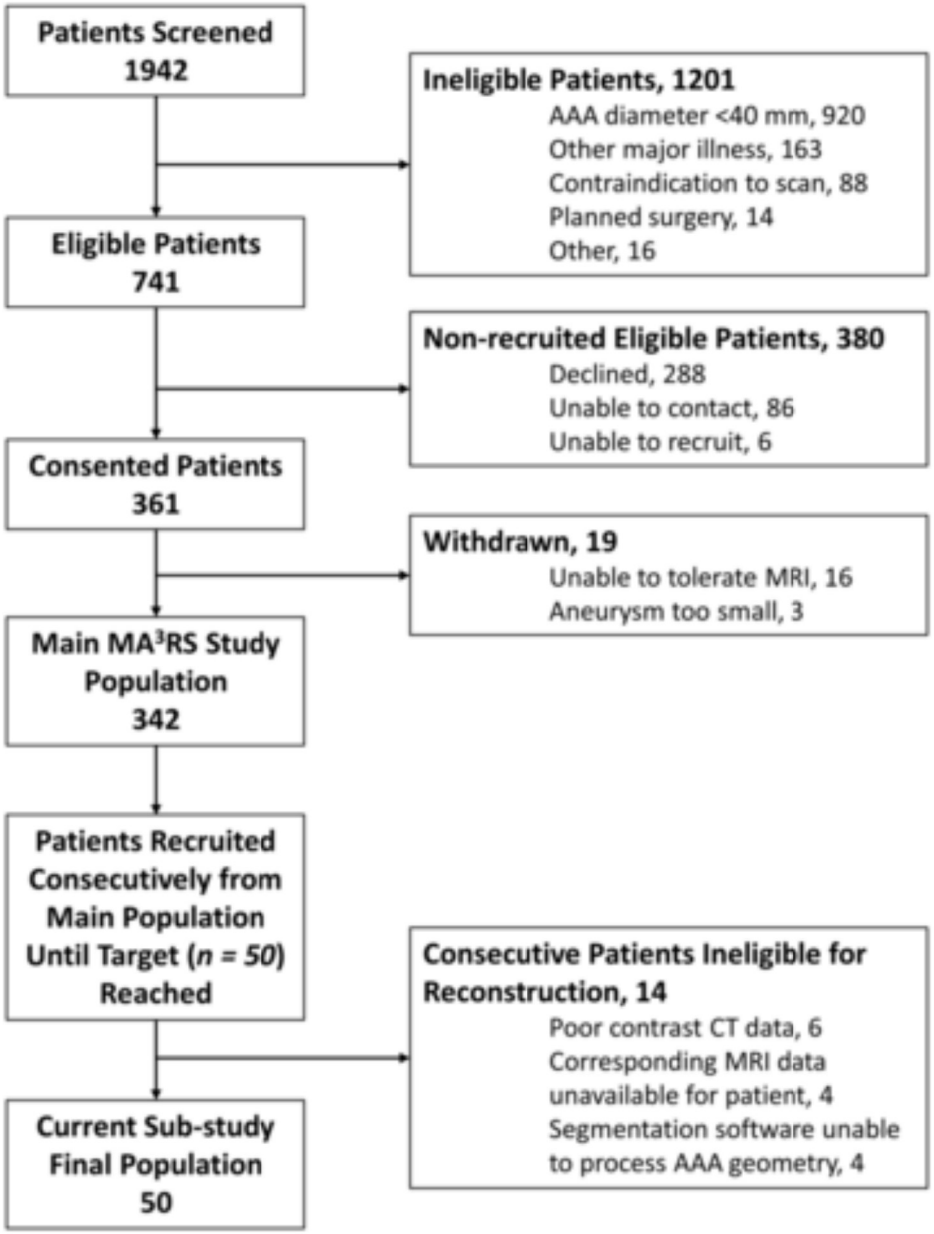

a)

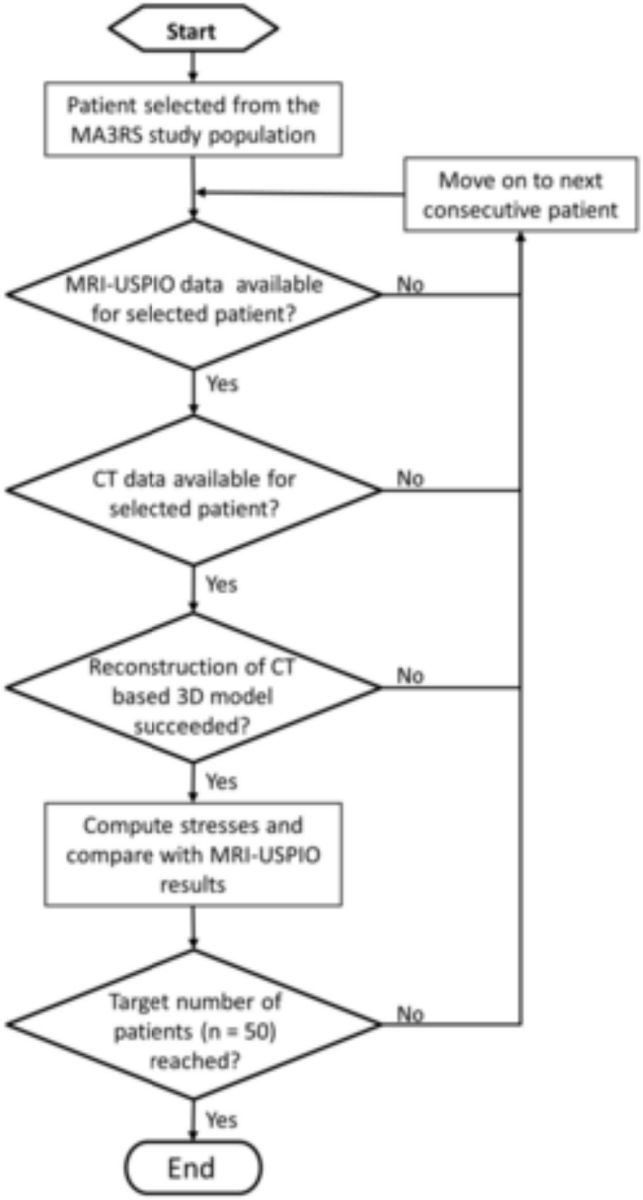

b)

Figure_2

Click here to download Figure Figure_2.tif

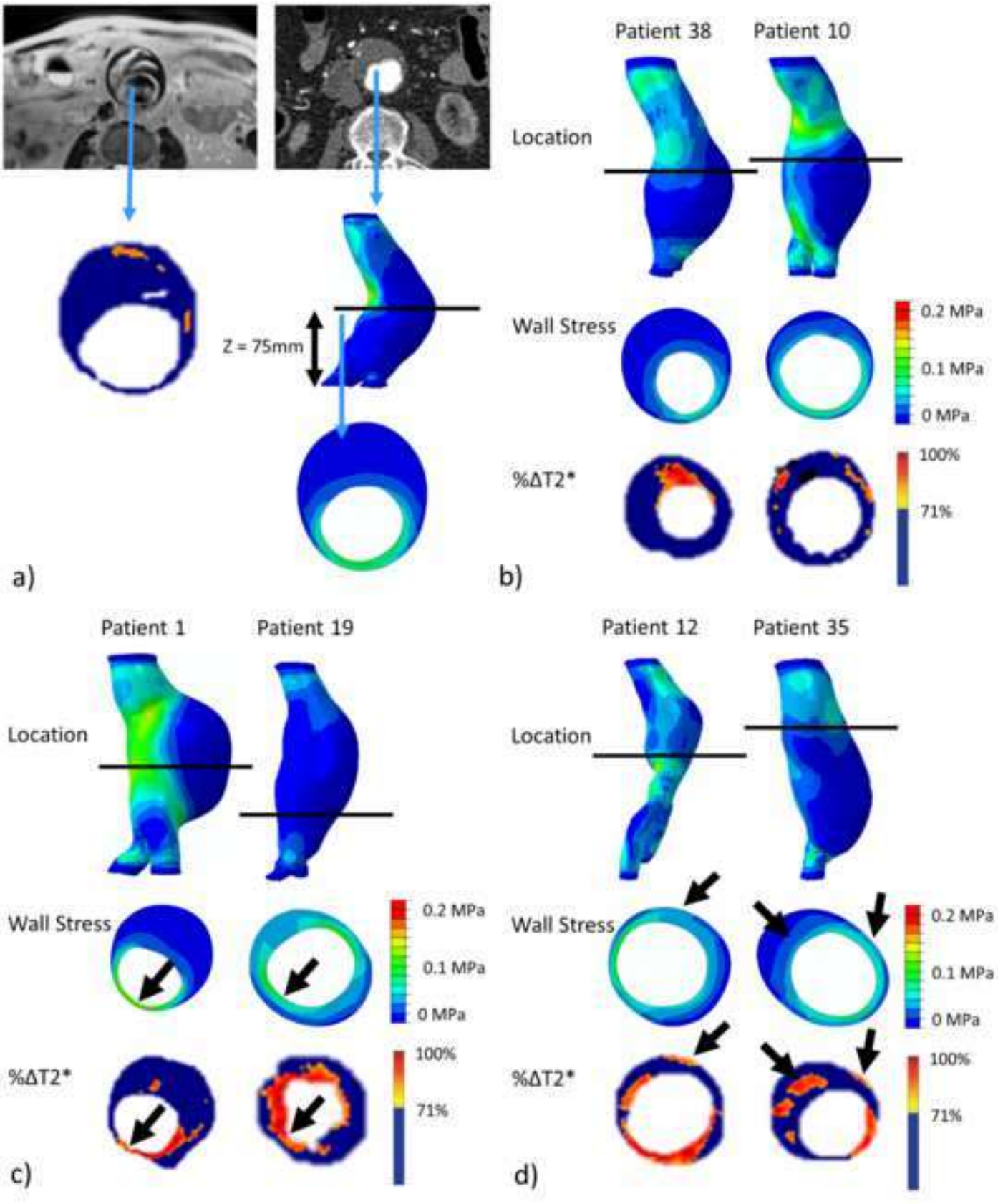

Figure_3

Click here to download Figure Figure_3.tif

a)

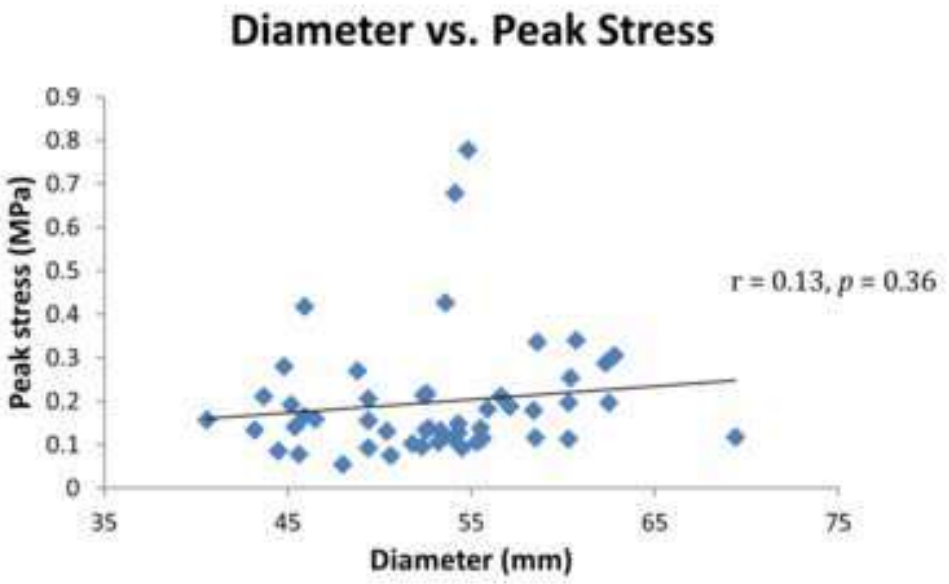

b)

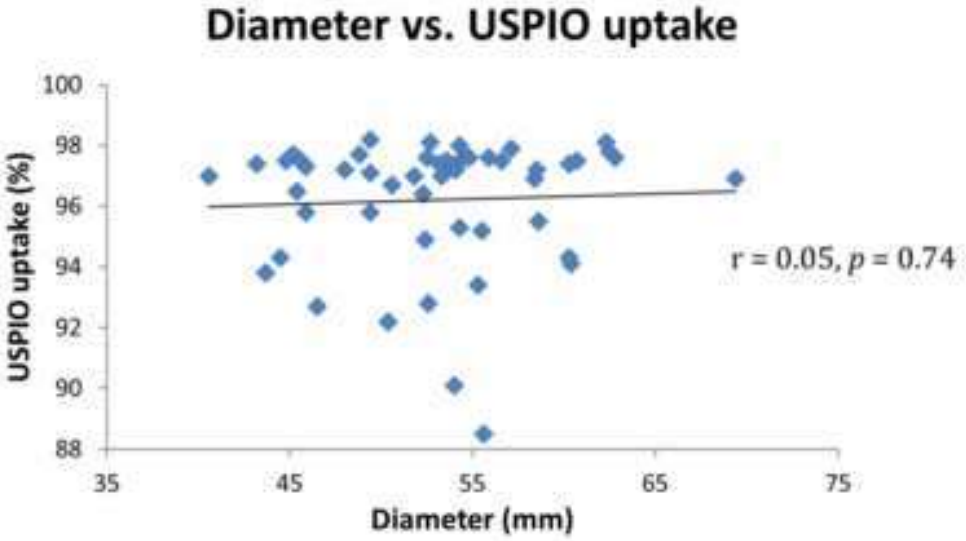

c)

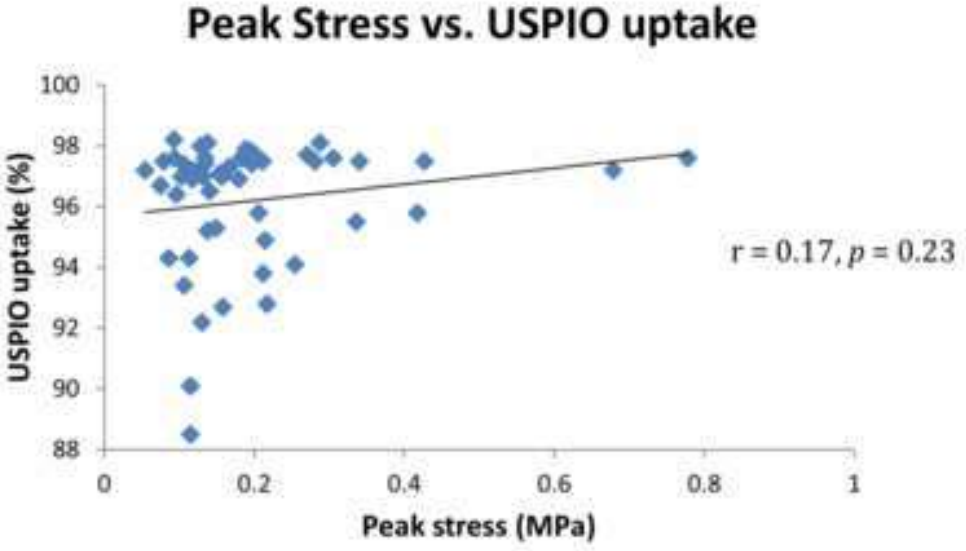

Figure_4

Click here to download Figure Figure_4.tif

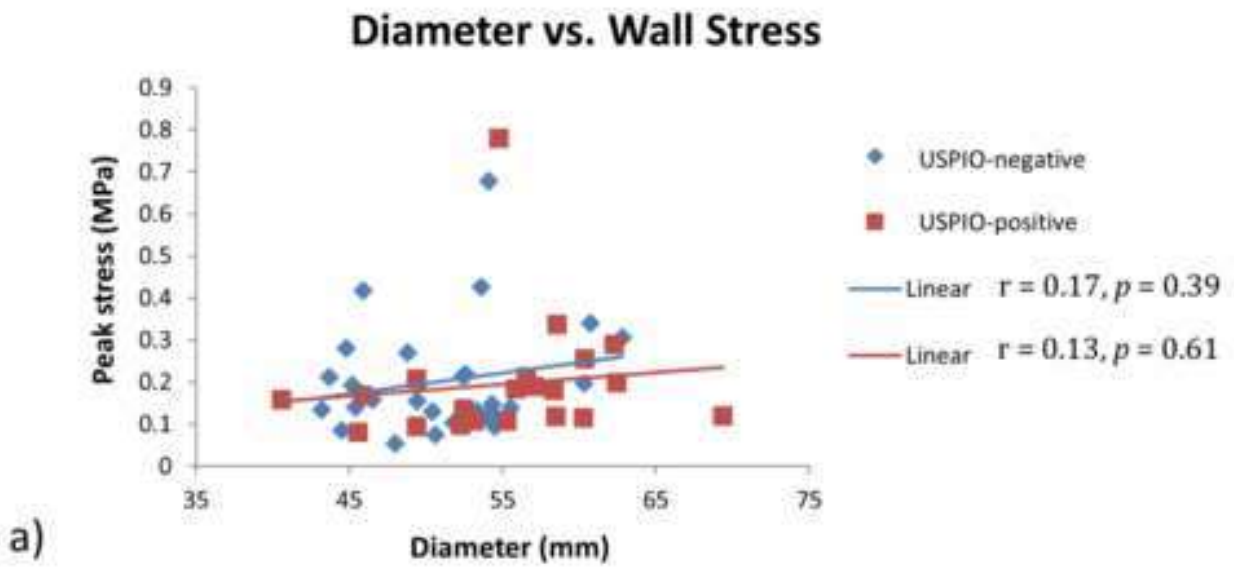

a)

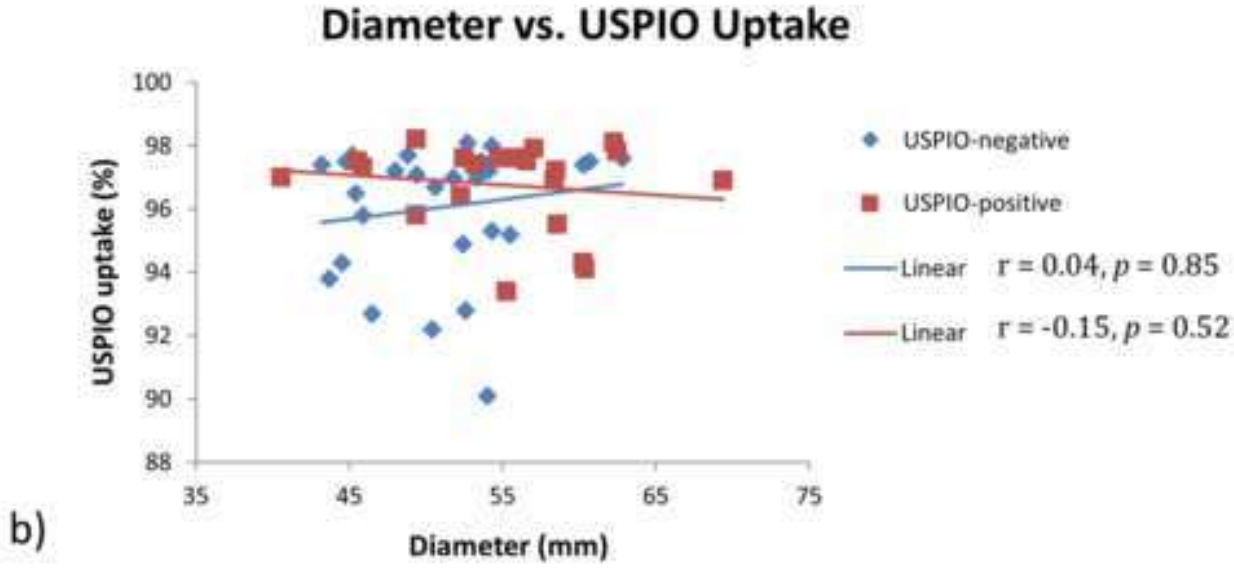

b)

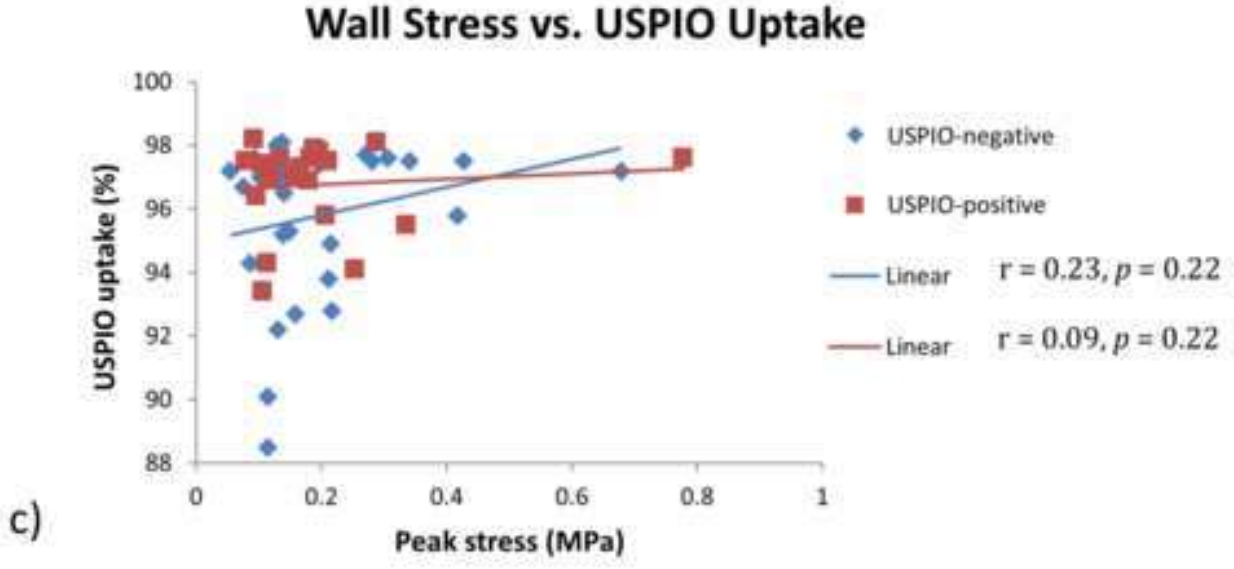

c)

Figure_5

Click here to download Figure Figure_5.tif

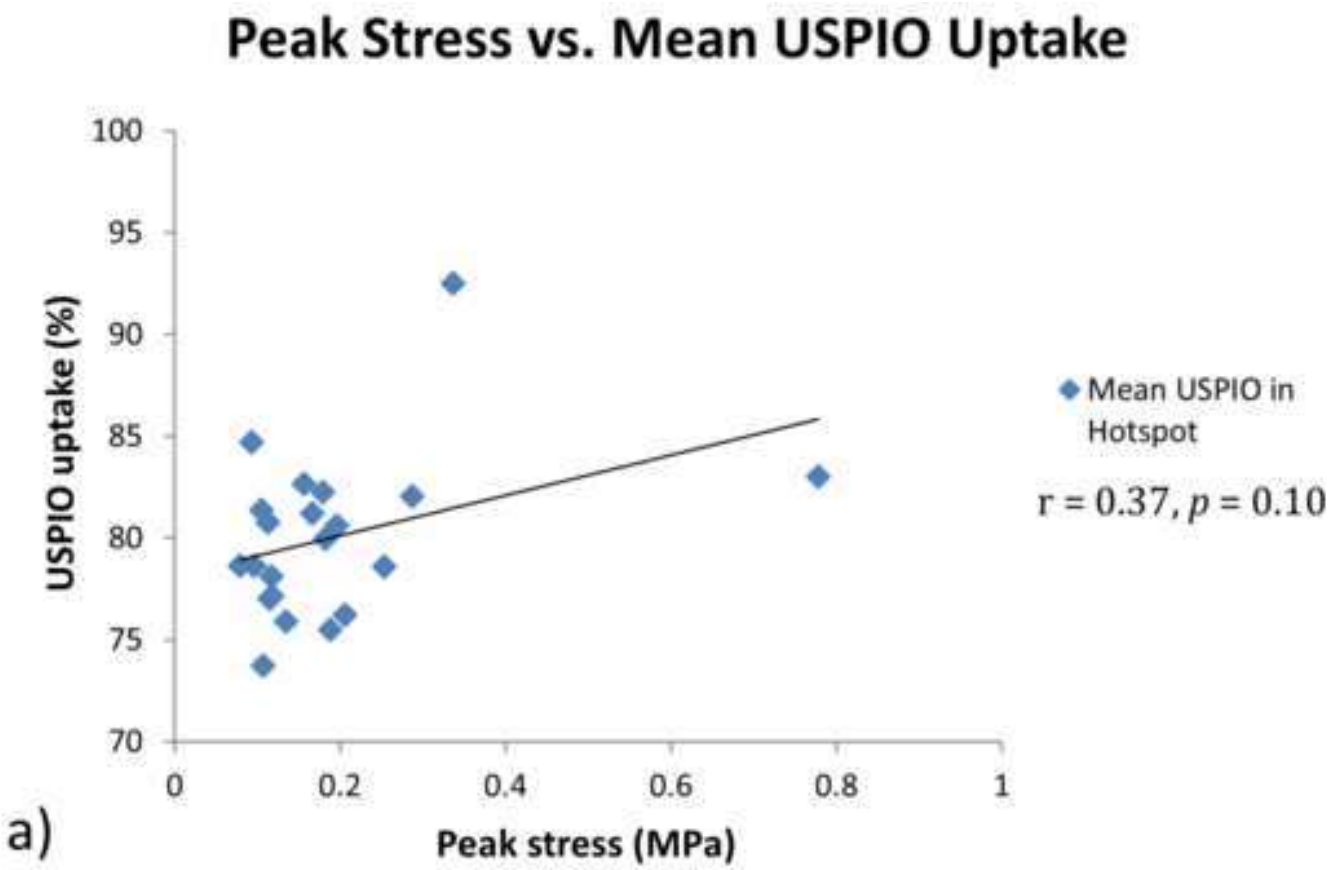

a)

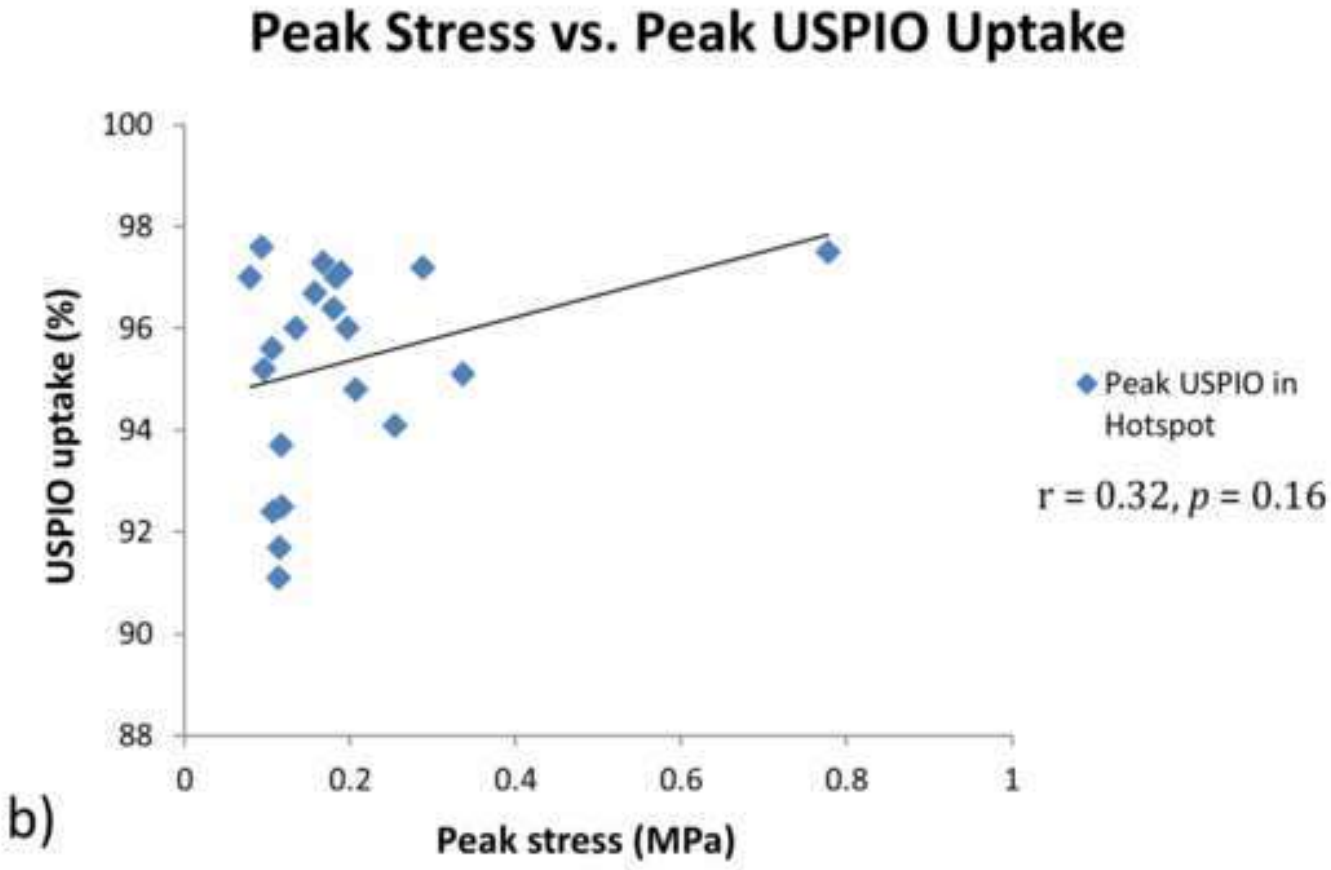

b)

Figure_6

Click here to download Figure Figure_6.tif

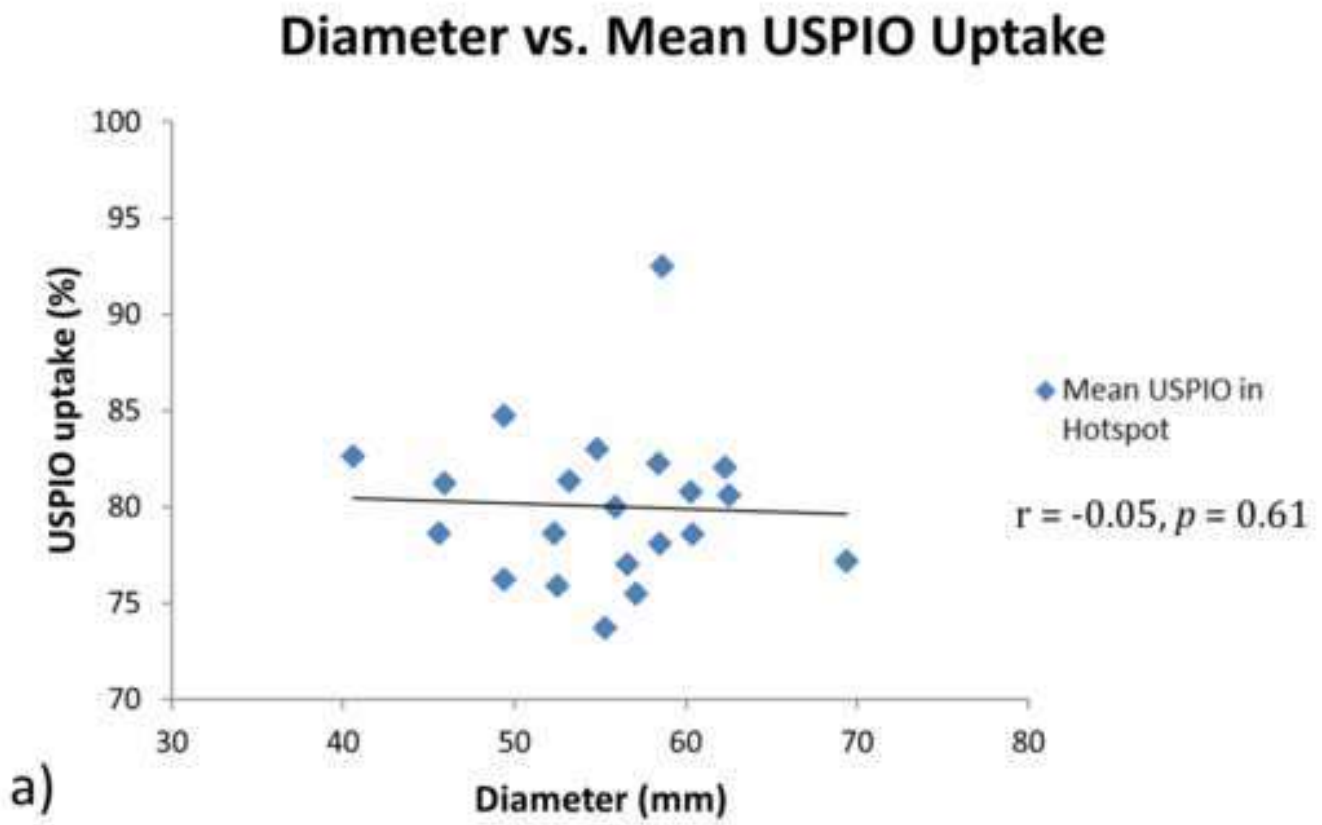

a)

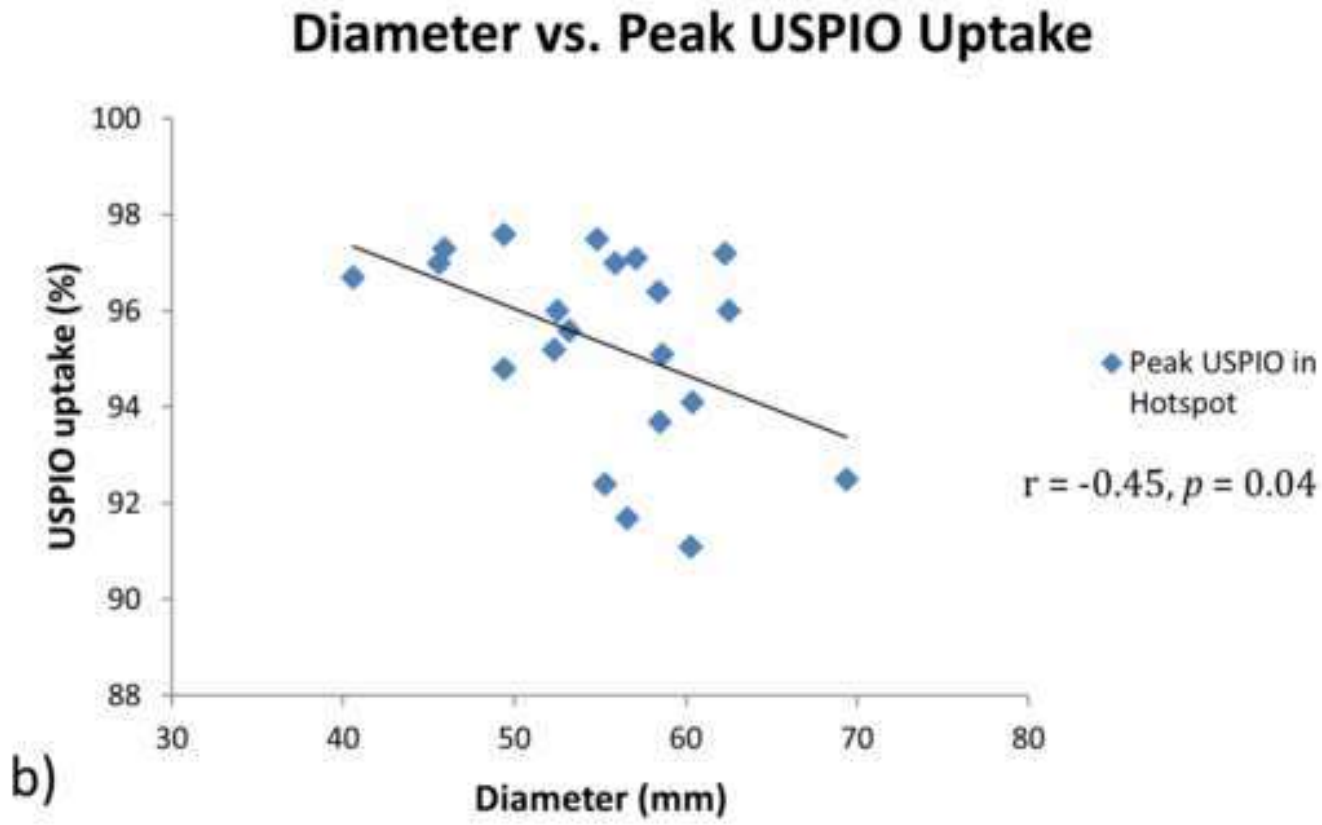

b)

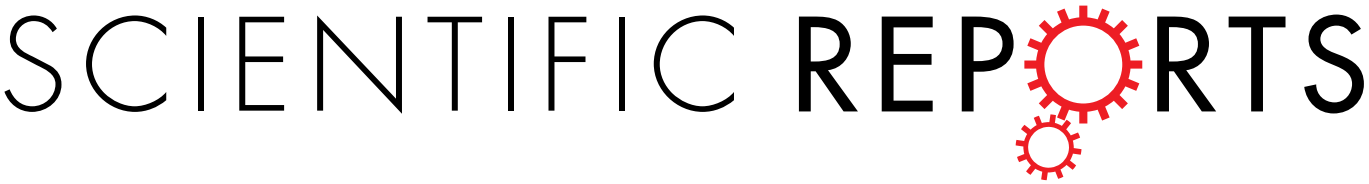

OPEN

BioPARR: A software system for estimating the rupture potential index for abdominal aortic aneurysms

Received: 5 May 2016
Accepted: 19 May 2017
Published online: 05 July 2017

Grand Roman Joldes[1,2,3], Karol Miller[1,2,4], Adam Wittek[1,2], Rachael O. Forsythe[5], David E. Newby[5] & Barry J. Doyle[2,5,6]

An abdominal aortic aneurysm (AAA) is a permanent and irreversible dilation of the lower region of the aorta. It is a symptomless condition that, if left untreated, can expand until rupture. Despite ongoing efforts, an efficient tool for accurate estimation of AAA rupture risk is still not available. Furthermore, a lack of standardisation across current approaches and specific obstacles within computational workflows limit the translation of existing methods to the clinic. This paper presents BioPARR (Biomechanics based Prediction of Aneurysm Rupture Risk), a software system to facilitate the analysis of AAA using a finite element analysis based approach. Except semi-automatic segmentation of the AAA and intraluminal thrombus (ILT) from medical images, the entire analysis is performed automatically. The system is modular and easily expandable, allows the extraction of information from images of different modalities (e.g. CT and MRI) and the simulation of different modelling scenarios (e.g. with/without thrombus). The software uses contemporary methods that eliminate the need for patient-specific material properties, overcoming perhaps the key limitation to all previous patient-specific analysis methods. The software system is robust, free, and will allow researchers to perform comparative evaluation of AAA using a standardised approach. We report preliminary data from 48 cases.

There are many limitations to the current clinical definition of 'high-risk' of rupture for AAA, based mainly on the maximum diameter of the AAA. Many researchers across both engineering and medical disciplines believe that biomechanics based patient-specific modelling (PSM) could have major clinical potential to provide more accurate patient-specific rupture risk assessment[1–4].

With the advances in medical imaging technology and medical image analysis software, it became possible to create anatomically-correct reconstructions of the AAA, which were then used for computer simulations that have steadily increased in complexity[3,5–7]. These simulations can compute the stress in the AAA wall due to the internal blood pressure. Mechanically-speaking, rupture of an artery occurs when the local wall stress exceeds the local wall strength. Vande Geest *et al.* proposed a useful statistical model for the non-invasive estimation of AAA wall strength[8] and also introduced the rupture potential index (RPI)[2]. The RPI combines the estimated patient-specific AAA wall strength with the AAA wall stress computed using the finite element method. The RPI has since been implemented in several AAA rupture risk assessment studies[3,4,9–11] and also in a commercial software for AAA analysis (VASCOPS)[12].

The current approach to RPI computation, including that implemented in the VASCOPS software, uses routinely acquired computed tomography (CT) data of the AAA to create three-dimensional (3D) reconstructions

[1]Intelligent Systems for Medicine Laboratory, The University of Western Australia, 35 Stirling Highway, Perth, WA, 6009, Australia. [2]School of Mechanical and Chemical Engineering, The University of Western Australia, 35 Stirling Highway, Perth, WA, 6009, Australia. [3]School of Engineering and Information Technology, Murdoch University, 90 South St, Murdoch, WA, 6150, Australia. [4]School of Engineering, Cardiff University, The Parade, CF24 3AA, Cardiff, UK. [5]BHF Centre for Cardiovascular Science, The University of Edinburgh, Edinburgh, UK. [6]Vascular Engineering Laboratory, Harry Perkins Institute of Medical Research, QEII Medical Centre, and Centre for Medical Research, The University of Western Australia, Perth, WA, 6009, Australia. Correspondence and requests for materials should be addressed to G.R.J. (email: grand.joldes@uwa.edu.au)

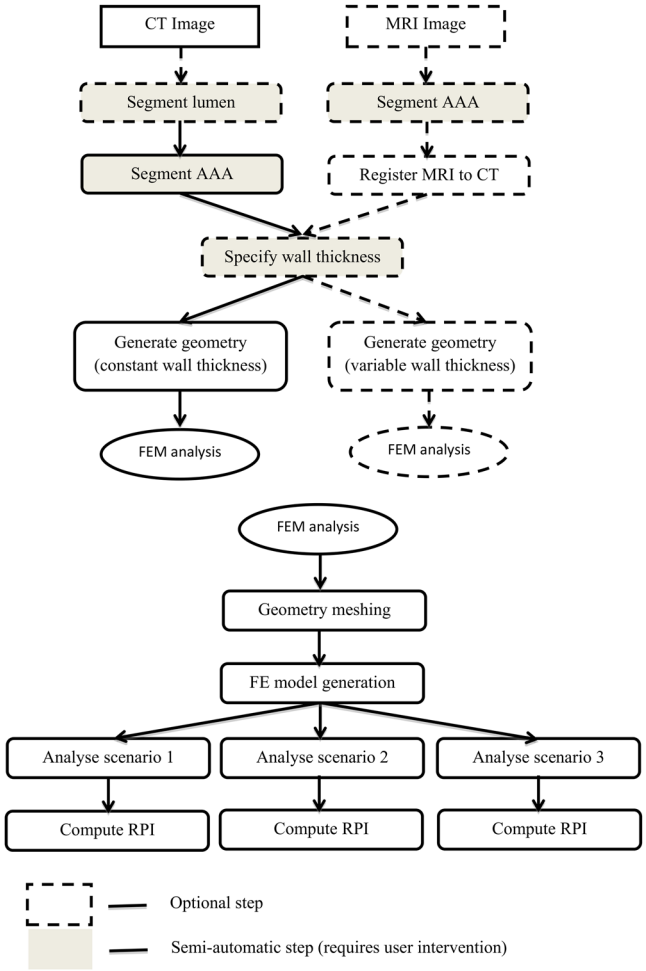

Figure 1. Diagram of the workflow. Only segmentation and wall thickness specification require user intervention; all other steps are automated. Multiple modelling scenarios are analysed (Scenario 1: pressure load on internal ILT wall; Scenario 2: no ILT included; scenario 3: ILT included and pressure load on internal AAA wall). MRI = magnetic resonance imaging, CT = computed tomography, FEM = finite element method.

of the aneurysm. Despite some researchers developing algorithms and methods to measure AAA wall thickness from CT[7, 13, 14], the poor soft tissue contrast of CT data compared to magnetic resonance imaging (MRI) limits the visibility of the AAA wall. Therefore, the vast majority of previous computational studies on AAA rupture risk assume a uniform wall thickness. A uniform wall is anatomically incorrect and results in inaccurate wall stress distributions, and thus RPI estimates. Therefore, RPI data based on uniform aortic wall thickness could be misleading in a clinical setting. Irrespective of uniform or variable wall thickness methods, the 3D reconstructed geometry is converted into a computational mesh of elements, typically tetrahedral elements due to the ease of automated mesh generation. Material properties must then be assigned to the model and are typically based on population-mean mechanical test data for the AAA wall tissue and the intraluminal thrombus (ILT)[15, 16]. A key obstacle in the translation of RPI to the clinic is the use of average material data, as in doing so, the model deviates away from a patient-specific simulation.

However, in some problems of biomechanics (and mechanics in general), material properties have negligible impact on wall stress[17, 18]. This occurs when the geometry to be analysed is already deformed, as is the case when examining arteries reconstructed from medical images. The medical image data represents the geometry under pressurisation from blood. Much effort has focussed on determining the pressure-free geometry using inverse procedures[17, 19]; however, what was observed when using the inverse method is that wall stress is almost independent of material properties. Building on from this, we have reformulated the mechanics of the AAA problem and demonstrated that AAA wall stress can be computed without knowledge of material properties and through a direct linear analysis[19].

In this paper, we present our framework and describe the key algorithms and techniques that we have implemented. An important aspect of our software is automation. Besides the semi-automatic 3D reconstruction of the AAA, the analysis is completely 'push button', thus eliminating potential inter-user variation and creating a standardised approach.

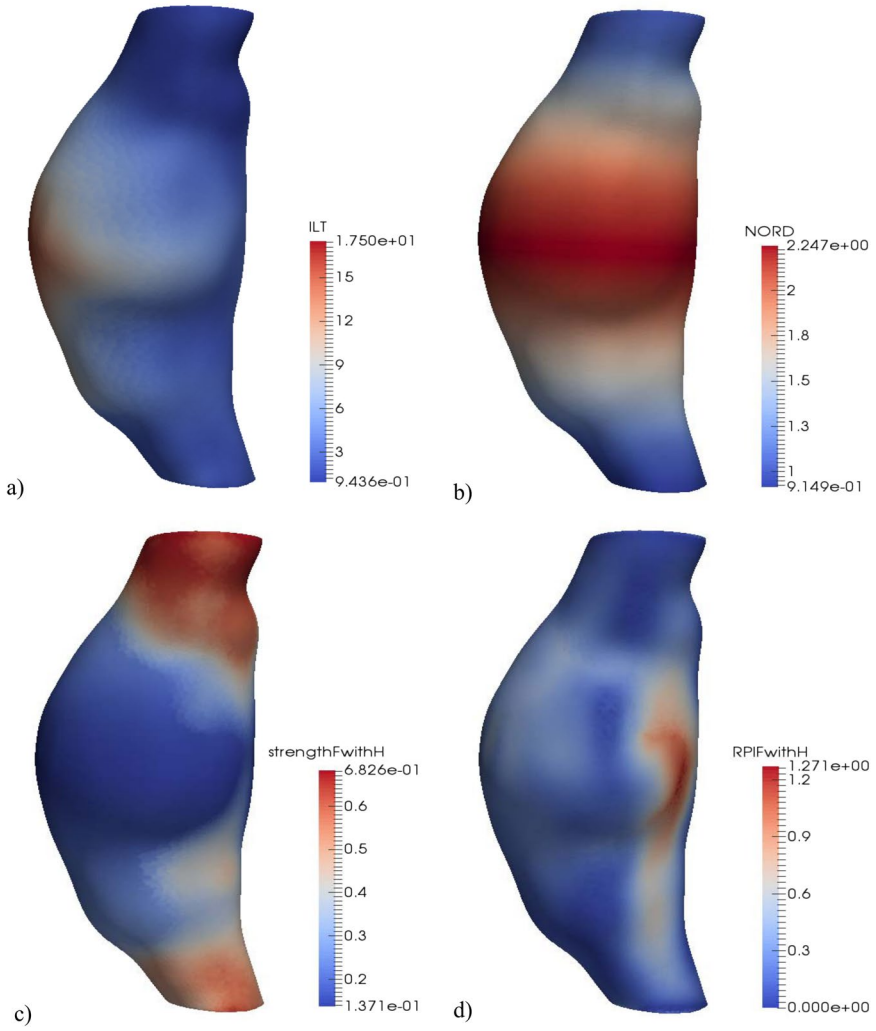

Figure 2. Example of RPI computation results. (**a**) ILT thickness [mm]. (**b**) Normalized diameter (NORD). (**c**) Wall strength for a female with family history of AAA [MPa]. (**d**) RPI for a female with family history of AAA.

Results and Discussion

We have developed a semi-automatic, modular and easily extendable software system for analyzing the rupture potential of an AAA using a finite element analysis based rupture index. The software system, available for free download and usage[20], consists of a collection of programs and scripts which perform the required steps in the AAA workflow, from image segmentation to geometry creation, meshing, finite element analysis and rupture potential index (RPI) computation (Fig. 1). The software is divided into several modules which perform specific tasks and are being run in sequence from a master script (batch) file. Data communication between these modules is performed using files in standard formats; this allows the user flexibility in changing or extending the functionality of the software, by replacing or adding additional modules.

To guarantee the accuracy of the results, the analysis by the finite element method (FEM) is conducted using the commercial finite element software Abaqus[21]. All the other modules consist of free or open source software programs. The software runs on 64Bit Windows operating systems and has been tested on Windows 7 and 8. We have created a series of tutorial training videos for each step of the analysis; the access link for these resources is included with the software.

Figure 1 shows the developed workflow. The software system allows the analyst to extract and combine data from images of different modality (such as CT and MRI), by using an inter-modality image registration algorithm. The analyst has control over many parameters influencing the analysis results: the thickness of the AAA wall, inclusion of thrombus, geometry meshing, finite element type selection, and finite element simulation scenarios. The software can be used in the case when both CT and MRI data are available for a patient or, the more typical situation, when only CT is acquired.

We have automated the finite element analysis and so have removed the need for technical expertise in computational mechanics. There is still the need to semi-automatically reconstruct the geometry, as this part of the workflow cannot be fully automated. However, this step takes approximately 45 minutes per case and, as with most manual tasks, the required time reduces with increasing familiarity. This segmentation time is comparable

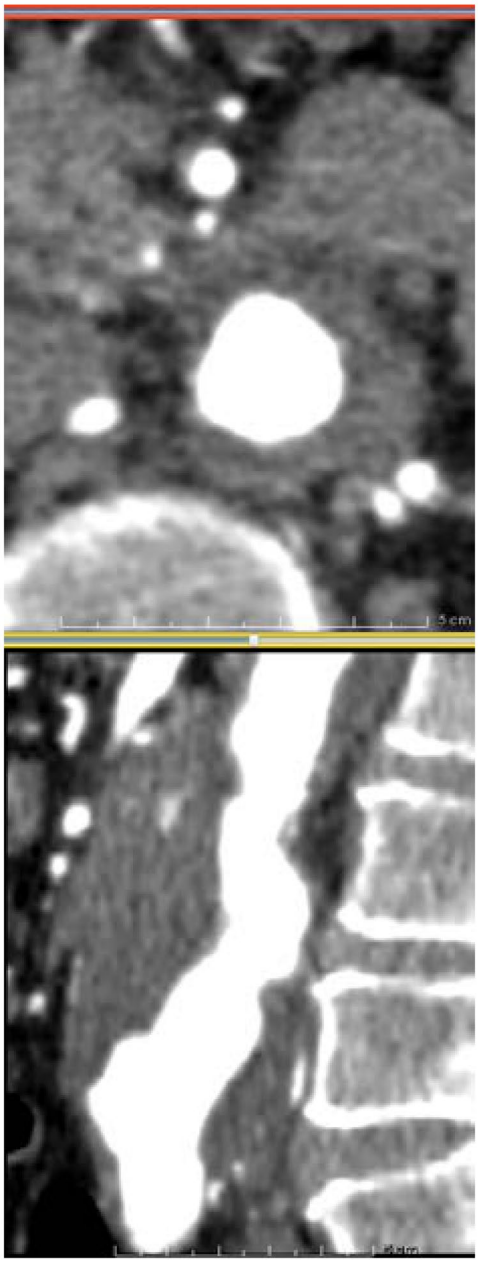

Figure 3. Case 2 used in reproducibility analysis. Axial (top) and sagittal (bottom) CT slices of the AAA. The poor contrast between the AAA and surrounding organs makes segmentation very challenging.

with that needed to segment AAA using the commercial VASCOPS software (~40 minutes)[22]. In the future, the segmentation time may be reduced by using better quality images (having enhanced contrast between AAA and the surrounding structures) or through the adoption of emerging image analysis techniques, such as those relying on machine learning[23]. An important aspect of our software is the fast return of data. Our computational approach removes non-linearities (both material and geometric) from the model. As such, the computation time is dramatically reduced and can fit into the clinical workflow.

Example results generated by our software are presented in Fig. 2. The program automatically generates 3D color-contoured visualizations of the key patient-specific components of the analysis, namely, ILT thickness (ILT), the normalized ratio of the maximum AAA diameter and the diameter in the proximal neck of the aneurysm (NORD), the estimated wall strength, and the final RPI. In this particular example, the patient was female with a family history of AAA; both gender and family history of the disease significantly affect the wall strength estimation. Excluding the 3D geometry reconstruction time, the entire analysis of this scenario took approx. 6 minutes on an Intel(R) Core(TM) i7-5930K CPU @ 3.50 GHz with 64 GB of RAM running Windows 8 OS. The analysis time greatly depends on the problem size (i.e. size of the computational grid, in this case just under 200 k nodes and 740 k elements, and the type of elements used, in this case linear tetrahedrons) and the number of scenarios considered.

Case	Max. diameter [mm]	User	AAA DSC	Lumen DSC	Max. ILT thickness [mm]	Max. NORD	Max. principal stress [MPa]
1	48	A	1	1	19.8	2.2	0.69
		B	0.982	0.997	20.3 (3%)	2.3 (5%)	0.62 (10%)
		C	0.953	0.981	19.3 (3%)	2.5 (14%)	0.52 (24%)
2	54	A	1	1	19.6	1.8	1.05
		B	0.952	0.983	19.6 (0%)	2.1 (17%)	1.0 (5%)
		C	0.896	0.969	21 (7%)	1.6 (11%)	1.1 (5%)
3	48	A	1	1	16.4	1.8	0.62
		B	0.955	0.961	16.1 (2%)	1.8 (0%)	0.58 (6%)
		C	0.899	0.908	17.3 (5%)	1.7 (6%)	0.75 (21%)

Table 1. Reproducibility of analysis results. The relative differences between the results of users B and C and user A are shown in parenthesis. NORD = normalized diameter.

In addition to its clinical potential, our software system can be used to answer research questions related to the evaluation of AAA rupture potential index, such as:

- What is the influence of wall thickness and boundary conditions on the computed stress and RPI?
- How many layers of finite elements and what type of elements should be used in the discretization to obtain convergence for the finite element analysis results?
- What simulation scenario leads to the most accurate prediction of stress distribution?
- What combination of simulation parameters leads to the most efficient and accurate RPI?

Finally, a major hurdle to translation of computational biomechanics methods to a clinical setting is robust statistical evidence. Until now, computational methods required intensive analyst time and expertise, and generally resulted in studies that lack statistical power. This problem is further compounded by the lack of standardization of computational methods[24], which makes meta-analyses of studies difficult[25]. Without statistical evidence that the RPI closely correlates with the rupture risk, clinical uptake is unlikely. Therefore, we have made our software freely available to all[20], easily expandable and modifiable, and we hope this will enable multi-centre studies of large cohorts to generate statistical evidence.

In conclusion, we have created and offered a free software system for estimating the risk of rupture in abdominal aortic aneurysms. All analysis steps have been automated, except image segmentation, which is impossible to perform automatically given the current image acquisition techniques and image processing algorithms. Therefore, once the software system has been configured, it can be run automatically for different segmented AAA cases and by different analysts without any user intervention; this reduces the analysis time, does not require technical knowledge from the user and generates reproducible results. Having a modular structure with data transfer between modules using standard file formats, the software system is easy to modify and expand.

We used our software system to analyse 48 cases acquired in the initial phase of the MRI in AAA to predict Rupture or Surgery (MA^3RS) study[26] – a multicentre observational cohort study of patients under surveillance for AAA with maximum diameter greater than 4 cm (EudraCT 2012-002488-25). It proved reliable and able to handle all cases, which included a large range of AAA sizes and shapes. Once follow-up data of the entire MA3RS cohort is available, we plan to analyse that data and collect the much needed statistical evidence regarding the accuracy of this AAA rupture risk analysis method. Some preliminary results from this analysis are presented in the following subsections, using the assumption of constant AAA wall thickness and a standard blood pressure of 120 mmHg. We used second order tetrahedral elements, for accurate stress computation. The stresses computed near the top and bottom AAA boundaries (which are constrained) were excluded when extracting the maximum stresses or RPI, as stress concentrations occur in these areas.

Reproducibility of analysis results. Because the entire workflow after image segmentation is automated, the analysis following image segmentation is completely reproducible. Image segmentation involves manual user intervention and its reproducibility depends on the experience of the user and the quality of the images. We have performed the following study to quantify the effect of image segmentation on the computation results:

- Three users with different levels of experience in AAA segmentation have each segmented the AAA and lumen from three CT datasets;
- The segmentations were compared using the Dice Similarity Coefficient (DSC);
- The segmentations were used as input to the analysis framework and the results compared;

The three users are marked as user A (experienced, with many hours of AAA segmentation and usage of 3D Slicer), user B (less experienced, with only a couple of AAA segmentations done using 3D Slicer) and user C (novice, no previous AAA segmentations). Users B and C were instructed by user A in the application of the software and given access to several online tutorials. The results obtained by user A were considered as the best and the results from the other users were compared against them.

The results of the experiment are presented in Table 1. From the data we can draw the following conclusions:

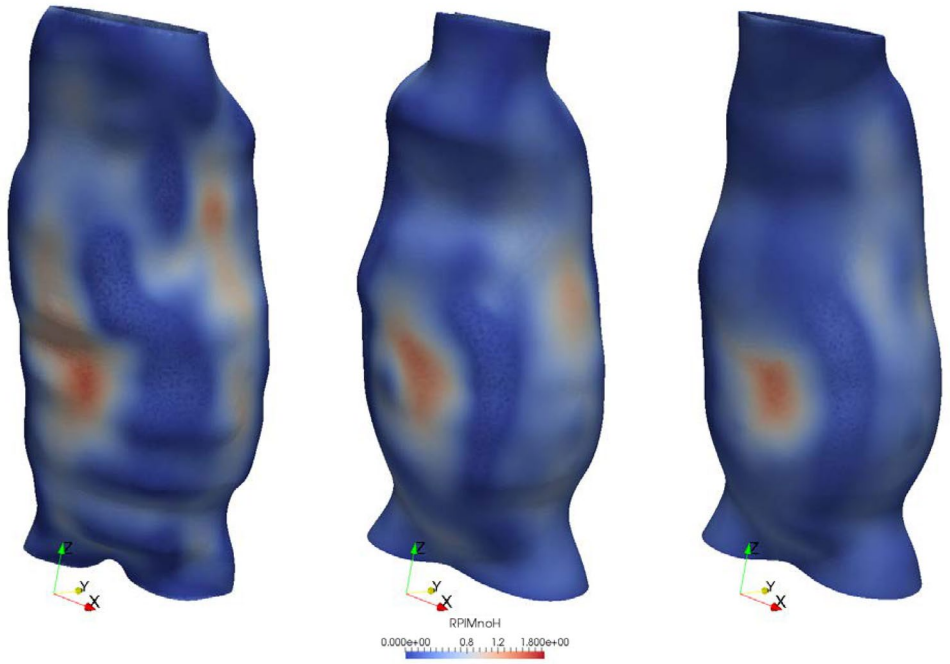

Figure 4. RPI distribution for case 2 used in reproducibility analysis. The results are obtained based on the segmentations performed by user A (right), B (center) and C (left). Despite the visual differences in geometry from user to user, the difference between the maximum RPI is ~5%.

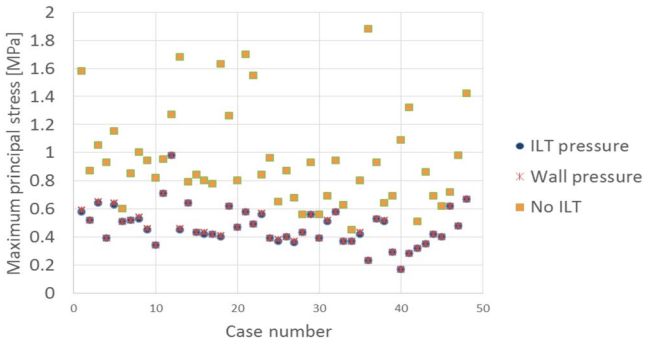

Figure 5. Influence of modelling scenario on the computed stress. Three scenarios are compared. There is little difference between the stresses computed using the "ILT pressure" and "Wall pressure" scenarios. The inclusion of ILT results in a significant reduction in the computed stress.

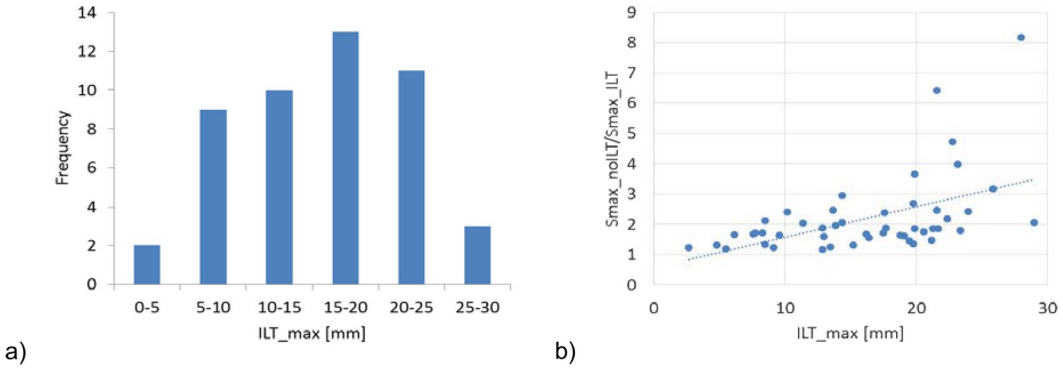

Figure 6. Influence of ILT thickness. (**a**) The distribution of maximum ILT thickness for the analysed cases. (**b**) Influence of maximum ILT thickness on the ratio between the maximum principal stresses computed in the "No ILT" and "ILT pressure" modelling scenarios.

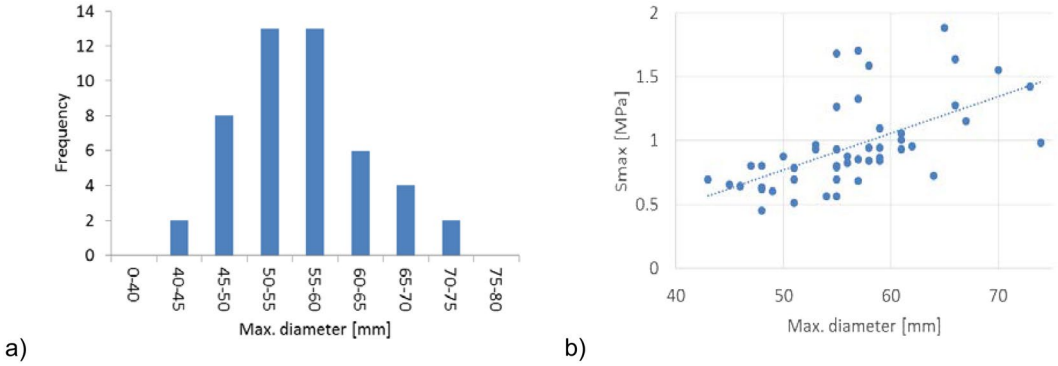

Figure 7. Influence of AAA diameter. (**a**) The distribution of maximum AAA diameter for the analysed cases. (**b**) Variation of computed maximum principal stress with the maximum AAA diameter ($R^2 = 0.34$). The "No ILT" scenario results are presented, to eliminate the influence of ILT thickness on the results.

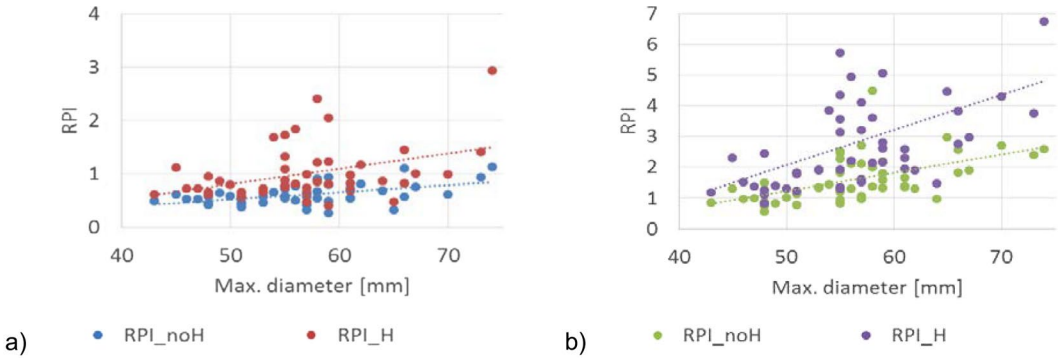

Figure 8. Influence of AAA diameter, ILT, and family history of AAA on the computed RPI. (**a**) RPI computed in the "ILT pressure" scenario, with ($R^2 = 0.16$) and without ($R^2 = 0.25$) considering a family history of AAA for each case. (**b**) RPI computed in the "No ILT" scenario, with ($R^2 = 0.18$) and without ($R^2 = 0.3$) considering a family history of AAA for each case.

- The accuracy of segmentation increases with the user experience, as indicated by the DSC coefficients;
- Parts of the image with good contrast were easily segmented by all users (there is much smaller difference in the lumen DSC and maximum ILT thickness between users);
- For the novice user, the differences in the computed maximum principal stress were less than 25%.

The differences between segmentations must be considered by taking into account the resolution of the CT images, of 0.625 mm × 0.625 mm × 2 mm (therefore, a one voxel segmentation error results in a 2.5% AAA radius error) and the lack of contrast in parts of the image, as illustrated in Fig. 3. However, despite the relatively large difference in peak wall stress calculated between users, the difference between the maximum computed RPI for this case is approximately 5%. This is due to the RPI calculation including information specific to the 3D reconstruction (i.e. NORD and ILT thickness). The computed RPI for this case is presented in Fig. 4.

A more detailed study of inter-user and intra-user reproducibility of CT segmentation and its effect on the computation of wall stress is presented in Hyhlik-Durr *et al.*[22]. In that study the commercial VASCOPS software was used to perform semi-automatic segmentation of CT images having much higher resolution (in plane resolution 0.33 mm, slice thickness 0.7–1.0 mm). The authors reported a high reproducibility of volume and maximum diameter measurements in infrarenal AAAs. We note the fact that segmentations obtained using the VASCOPS software can also be used as inputs for our software system.

Comparison between different modelling scenarios. We used three different modelling scenarios and assumed the AAA wall was of uniform thickness (1.5 mm) and the ILT was a homogeneous material:

- AAA with ILT and the blood pressure load applied on the ILT surface (ILT pressure);
- AAA with ILT and blood pressure load applied on the internal wall surface, bypassing the ILT (Wall pressure);
- AAA without ILT and blood pressure load applied on the internal AAA wall surface (No ILT).

A comparison between the maximum principal stresses obtained for each case is presented in Fig. 5. While the inclusion of ILT results in a significant reduction in the computed maximum principal stress, there is little

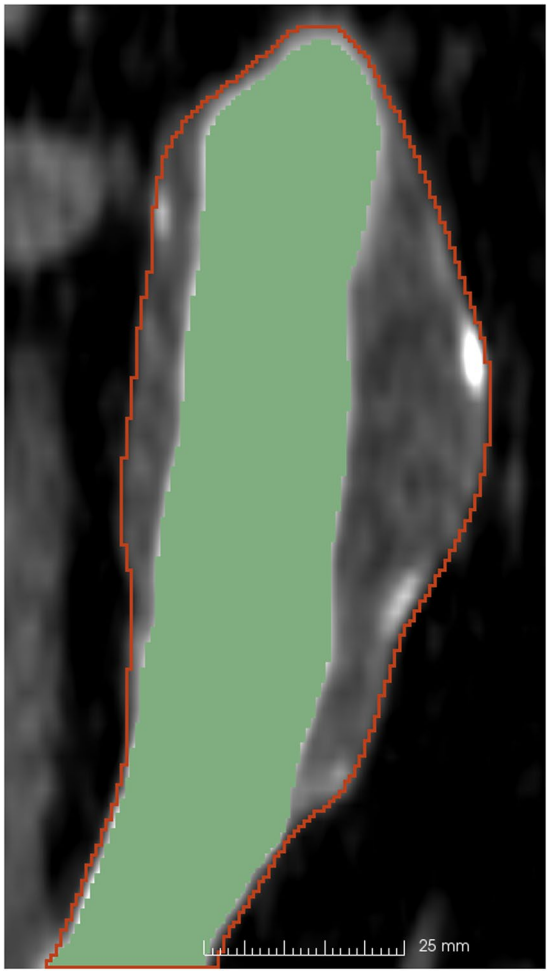

Figure 9. Example segmentation of an AAA from CT (one CT slice in the coronal view). The contour of the AAA segmentation is shown in red and the lumen segmentation is in green. The region of interest has been extracted from an abdominal CT with a resolution of 0.625 mm × 0.625 mm × 2 mm and segmented using the FastGrowCut algorithm for the AAA and intensity thresholding for lumen (with manual seed creation and segmentation corrections).

difference between the stresses computed using the "ILT pressure" and "Wall pressure" scenarios, as previously reported[27]. The stresses computed using the "Wall pressure" scenario are slightly higher than those computed using the "ILT pressure" scenario, but the maximum difference across all cases is less than 3%. Therefore, there is no need to analyse these two scenarios separately, and only the "ILT pressure" scenario results will be considered in the following analysis.

To better understand the influence of ILT on the computed stress, we plotted the reduction in stress between the "No ILT" and "ILT pressure" modelling scenarios against the maximum ILT thickness in Fig. 6. We find that a larger ILT thickness leads to a larger reduction in the maximum principal stress (up to 8 times higher wall stress without ILT). Clearly, the decision on whether or not to include the ILT in the analysis has a major influence on the computation results, especially for cases with large ILT thickness.

Influence of AAA diameter on stress. The relation between the maximum AAA diameter and maximum principal stress for all the analysed cases is presented in Fig. 7. Only the "No ILT" scenario results are presented, to eliminate the influence of ILT thickness and only capture the influence of AAA diameter on the computed stress. There is a trend of increased maximum principal stress with increased AAA diameter, although there are other factors influencing the stress value (such as the shape of the AAA) which lead to a relatively large dispersion of the results ($R^2 = 0.34$).

Relation between AAA diameter, ILT, family history of AAA and RPI. The variation of computed maximum RPI against the maximum AAA diameter for the "ILT pressure" and "No ILT" scenarios, with and without considering the family history of AAA for each case, is presented in Fig. 8. In each modelling scenario there is a trend of increased RPI with increased AAA diameter, especially when ILT is omitted from the model. Furthermore, without ILT, most RPI exceed the theoretical rupture value of 1.0, yet all AAAs were intact when

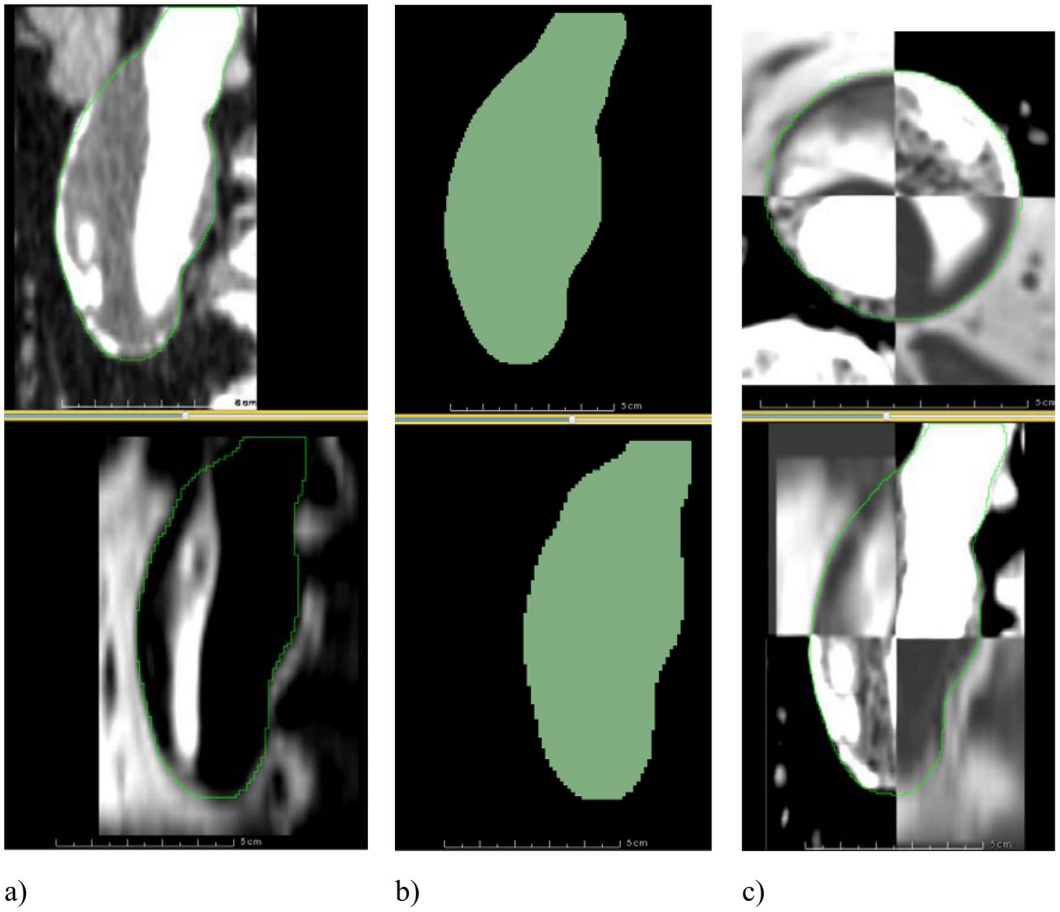

Figure 10. MRI to CT registration. (**a**) A sagittal slice of an AAA in a contrast-enhanced CT image (top) and the corresponding slice in the MR image (bottom). The contours of the AAA segmentations are shown in green. The two images occupy different positions in space and need to be registered. (**b**) The segmentations of the CT (top) and MR (bottom) images. The two label maps are registered and the resulting transform is saved. (**c**) The transform obtained from the label map registration is used to register the MRI dataset to the CT dataset. A checkerboard display of the two images is used to verify the registration result in axial (top) and sagittal (bottom) views, with the contour of the AAA segmentation shown in green.

images were acquired. This further supports the necessity to include ILT into the risk assessment models. We also found that the parameters influencing the wall strength, such as family history of AAA, have a major impact on the RPI computation (the wall strength is computed based on a statistical model[8], as described in the section "Rupture Potential Index Computation"), reducing the correlation between RPI and maximum diameter, as indicated by the smaller R^2 values.

In all the presented results, although some trends can be identified, there is a large dispersion of the data. Due to the influence of multiple parameters on the computed stress/RPI, simplistic conclusions such as "larger ILT thickness leads to a smaller stress" or "larger AAA diameter leads to larger stress" cannot be drawn. The obtained results suggest that patient-specific analysis is needed in each case.

Methods

Image segmentation. The high variability in AAA geometry, as well as low discrimination between the AAA and the surrounding tissue in parts of the image, make automatic AAA segmentation practically impossible. Therefore, we have used the segmentation tools available in the free, open source image analysis software 3D Slicer[28]. Any other segmentation software can be used. We have found that using the 3D Slicer extension FastGrowCut for segmentation[29] can help reduce the segmentation time. Manual intervention is still required in defining the region of interest in the image, cropping, defining the seeds for the FastGrowCut algorithm and performing corrections and smoothing of the resulting label maps. Using this method, we can easily extract the AAA from CT or MRI (Fig. 9). In the preliminary data presented in this work, we have segmented the AAA from immediately below the renal arteries to the iliac bifurcation.

Inter-modality image registration. Registering inter-modality images allows the user to extract geometrical information, such as the AAA wall thickness, from medical images from different imaging

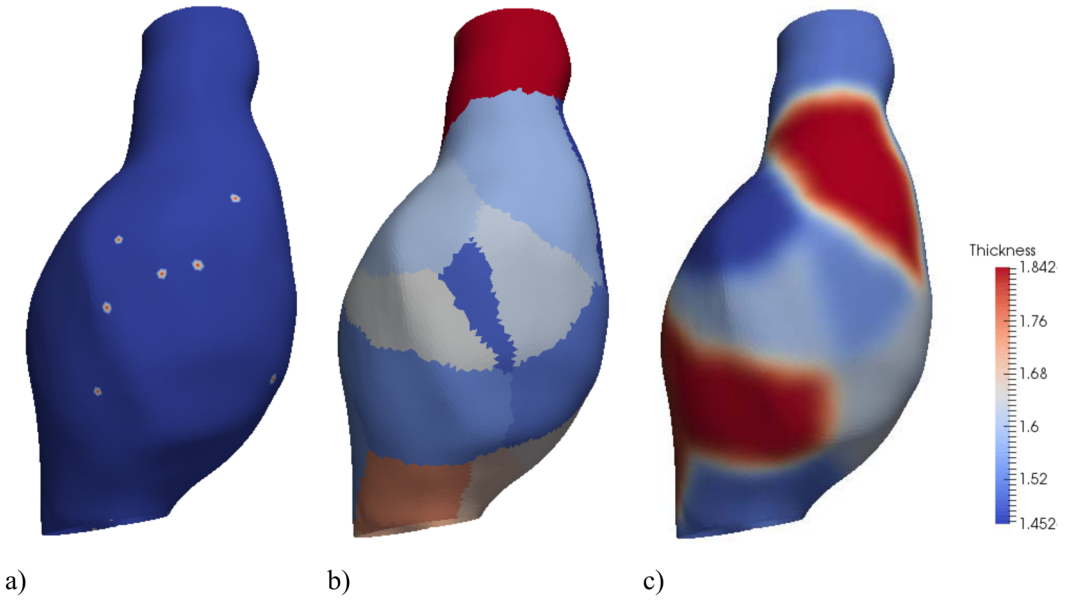

Figure 11. Example of thickness interpolation for an AAA. (**a**) Thickness measurements points. (**b**) Areas of the surface discretization associated with each measurement point (similar to a Voronoi diagram in plane) – the thickness at the measurement point will be extended to these areas. In this image the colors are determined by the measurement point id – for illustration purposes, only a limited number of measurement points are defined in order to have a clear separation of these areas. (**c**) Thickness values (using 10 smoothing iterations) [mm].

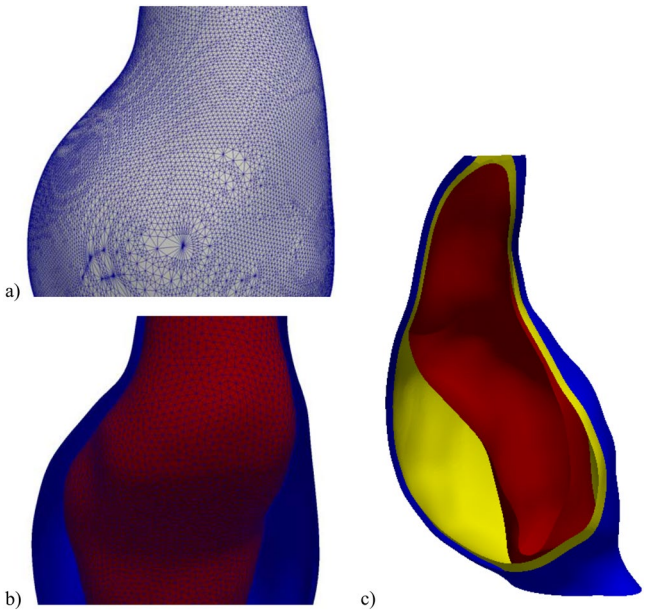

Figure 12. Example of geometry creation. (**a**) Geometry extracted from label map. (**b**) Re-meshed geometry. (**c**) Final geometry (AAA exterior surface in blue, interior surface in yellow and ILT surface in red).

systems. Registration involves aligning different images into the same coordinate system. Automatic registration of inter-modality images is practically impossible most of the time, because different image modalities can reveal and represent very different information about an organ. In order to overcome this difficulty, we implemented a label map based registration algorithm and used it to register MRI to CT images. The basic principle of the algorithm is to register the AAA label maps extracted from MRI and CT and then use the obtained transform to bring the MRI image in the same coordinate system as the CT image (Fig. 10), using the following steps:

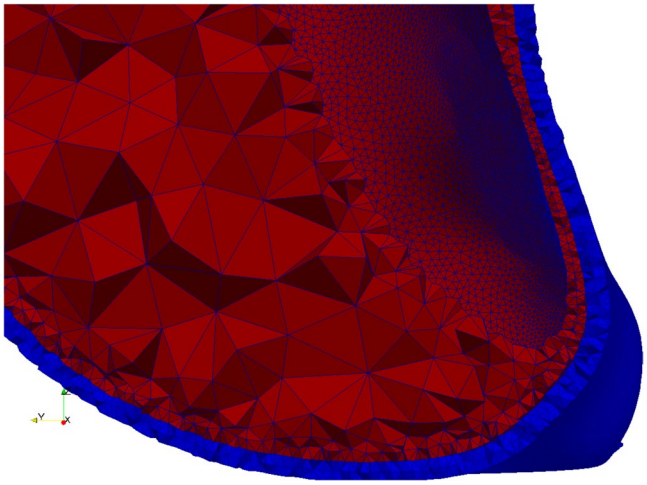

Figure 13. Example of meshing. The AAA wall is meshed using 2 layers of elements (configurable). The ILT is meshed using a minimum of 2 layers of elements (configurable); the element size is increased in the middle of the ILT layer to reduce the number of elements in the mesh.

- Segment the AAA from both CT and MRI (Fig. 10a), resulting in 2 binary images defining the label maps (Fig. 10b);
- Register the MRI label map to the CT label map and extract the resulting transform;
- Use the transform to register the MRI image to the CT image (Fig. 10c).

These steps are performed using the general registration and resampling algorithms (BRAINSFit and BRAINSResample) available in 3D Slicer. The registration algorithm has been implemented in a Python script so it can be run without user intervention. One disadvantage of this registration method is that it cannot take into consideration local deformations; therefore only rigid registration is implemented.

Wall thickness specification. Although wall thickness has a great influence on the stress distribution within the AAA wall[19], accurate extraction from medical images remains problematic due to the low image resolution and soft tissue contrast. This uncertainty is why many authors have used constant wall thickness in their analyses. It is nevertheless important to understand the effect of such an assumption on the computed rupture potential index (RPI). Therefore, we offer the possibility of specifying wall thickness at multiple points on the AAA surface.

Measuring surface thickness from medical images or excised tissue samples is difficult and usually results in measurements only at sparse locations on the AAA surface. Therefore, we devised a new method of generating the thickness information for all points of the AAA surface using interpolation and smoothing of the sparse measurements (Fig. 11).

Thickness information can be specified in different ways. One possibility is to measure the wall thickness at different locations with the ruler tool available in 3D Slicer on the registered images (i.e. CT and MRI), and then save the measurements as 3D Slicer annotation files. The software can read the thickness from these files. Another option is to generate the annotation files (which are simple text files) containing thickness information using some other method. For example, *ex vivo* measurements of excised tissue can be performed[30] or wall thickness can be estimated from CT[13] and the thickness data entered into the annotation files. If only one file containing thickness information exists, a constant thickness AAA wall will be created. In the preliminary data presented in this study, we used a constant thickness of 1.5 mm.

Geometry creation. The label maps segmented from the images and the wall thickness information are used to create the AAA geometry. The following surfaces are automatically created: the external AAA wall surface, the internal AAA wall surface and the internal intraluminal thrombus (ILT) surface. The ILT surface is only created if the lumen label map is available. In few cases of AAA (~5%), there is no ILT present[31].

The AAA geometry is created in three stages. The first stage is performed using 3D Slicer and consists of label map manipulation (to make sure the lumen label map is contained within the AAA label map), subtraction of the lumen label map from the AAA label map, and surface extraction using the 3D Slicer module Model Maker[32]. Because the resulting tessellated surface discretisation is only intended for visualization, it has many triangles of different sizes and bad aspect ratios (Fig. 12a). This leads to problems in creating the internal AAA wall surface in the third stage. Therefore, in the second stage, the surface is automatically re-meshed using the surface mesh resampling software ACVDQ[33–35] (Fig. 12b).

In the third stage, a custom command line interface (CLI) 3D Slicer module is used to generate the discretised surfaces. The module uses the re-meshed AAA surface from the previous stage to separate the exterior AAA wall surface from the ILT surface (if it exists), interpolates the thickness measurements over the external AAA wall surface, creates the internal AAA wall surface by displacing the nodes of the external AAA wall surface along the

Figure 14. Example of Abaqus model, showing constraints applied on the top and bottom surfaces of the AAA. Definitions of the important surfaces in the model (where loads and boundary conditions are applied) are created by the software and available to the user in the generated input files.

surface normal, modifies the internal ILT surface to make sure that the ILT has a configured minimum thickness (to simplify ILT meshing, the default value is 1 mm), computes the ILT surface thickness, and outputs the created surfaces (in standard STereoLithography. STL file format) and element size information to be used for meshing.

The element size is computed based on the local wall and ILT thickness, so that a configured number (default value of 2) of element layers are generated over the thickness of the wall. The element size information is generated for all the points of a 1 mm spaced structured grid which covers the entire AAA geometry and saved in a format readable by the meshing software.

Meshing. Meshing of the AAA wall and ILT, based on the surfaces and element size configuration from the previous step, is performed in three stages using custom command files for the free, open source meshing software Gmsh[36, 37]. In the first stage, the surfaces are meshed using the generated element size information. Additional constraints on the element size can be included by modifying the command files, such as curvature dependent element sizing. In the second stage, the volumes of the AAA wall and ILT are created by generating end surfaces between the external and internal AAA wall surfaces, and between the internal AAA wall surface and the ILT surface. We perform this necessary step to ensure the geometry consists of watertight closed surfaces, as this is not guaranteed by the VTK toolkit[38] used to create surfaces in the previous step. In the third and final stage, a tetrahedral volumetric mesh is created using the element size information generated in the previous step (Fig. 13). This process ensures a conforming mesh between the ILT and AAA wall. The generated meshes are saved as standard.vtk files.

This new meshing approach maintains the geometric accuracy of the meshed surfaces by using very small elements on these surfaces. At the same time, by increasing the element size inside the ILT volume and in the thicker areas of the AAA wall, it reduces the mesh size and, therefore, the computational cost of the finite element analysis.

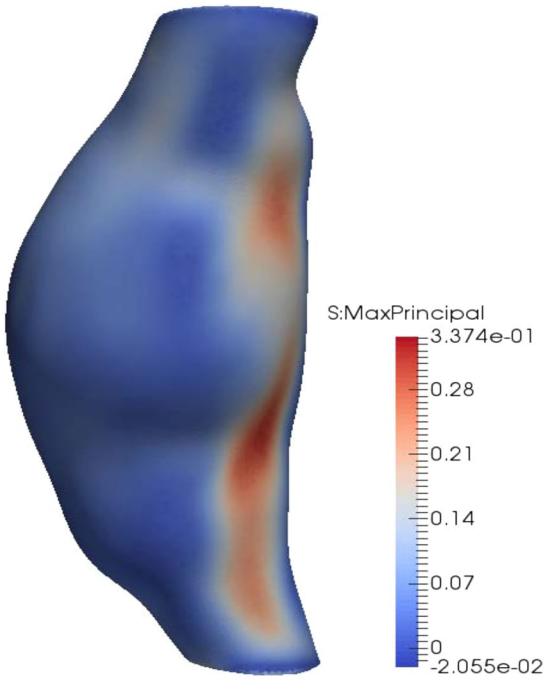

Figure 15. Example of stress computation results. The maximum principal stress [MPa] is computed at each node of the finite element mesh.

Finite Element Model Creation. A custom CLI 3D Slicer module reads the volumetric mesh files created in the previous step and generates input (.inp) files for the finite element software Abaqus[21] containing the AAA wall and the ILT meshes as parts. The surfaces necessary for defining loads and boundary conditions are automatically detected and included in the generated files and the element type can be configured as linear or quadratic, displacement only or hybrid displacement-pressure formulation. The generated files are then copied into separate folders for each simulation scenario that needs to be analysed.

Three analysis scenarios are currently included: (i) AAA with ILT and the blood pressure load applied on the ILT surface; (ii) AAA with ILT and blood pressure load applied on the internal wall surface, bypassing the ILT; and (iii) AAA without ILT and blood pressure load applied on the internal AAA wall surface. These scenarios are a result of uncertainty in the role of ILT. The ILT is believed to buffer the blood pressure being applied to the wall[16], thus reducing wall stress. However, *in vivo* measurements with a pressure probe placed directly into the ILT showed no reduction in pressure[39]. Therefore, the ILT is thought to act similar to a series of ropes, anchoring the AAA wall but enabling pressure transmission[27,40]. For each scenario, an Abaqus input file defines the simulation parameters and includes the generated AAA wall and ILT mesh files in order to define the geometry, loading and boundary conditions (Fig. 14). Therefore, the user has complete control over each simulation scenario by simply editing the Abaqus input file corresponding to that scenario. More information on how to edit, add or remove a simulation scenario is included in the configuration instructions accompanying the software.

Finite Element Analysis. The finite element analysis is performed using the commercial finite element software Abaqus, for each configured simulation scenario. The simulations are carried out using the procedure described in Joldes *et al.*[19], which allows the computation of stress in the AAA wall without exact knowledge of the material properties. The approach exploits the fact that the geometry of an AAA extracted from medical images represents the deformed geometry (under internal blood pressure). The AAA in the deformed configuration is a statically determined structure. Therefore, the internal stress has to balance the externally applied forces; the stress is determined by the applied load and the AAA geometry and is very weakly dependent on the material properties. This is of great practical significance, as patient-specific material properties for the AAA wall and ILT are difficult to obtain *in vivo*. Removing the dependency on material properties is a major innovation in AAA biomechanics research. For a detailed discussion of the problem of obtaining solutions without knowing mechanical properties of tissues please see also Miller *et al.* and Wittek *et al.*[18,41].

The results of the finite element simulation (maximum principal stresses in the AAA wall) are extracted using the Abaqus scripting interface and saved in a.vtk file (Fig. 15).

Rupture Potential Index Computation. We used the statistical model for AAA wall strength proposed by Vande Geest *et al.*[8], which has subsequently been used in several AAA rupture risk assessment studies[3,4,9–11]. The wall strength at any point of the AAA surface is determined based on the following variables: local ILT thickness (ILT), normalized AAA diameter (NORD), sex of the patient and whether or not the patient has family history

of AAA. NORD is the ratio of the maximum AAA diameter to the diameter at the proximal aorta distal to the renal arteries.

By combining the computed wall stress with the wall strength information, the rupture potential index (RPI) can be computed at any point of the AAA surface as the ratio between wall stress and wall strength[2]. A RPI of one is the theoretical point of rupture as the local stress higher has exceeded the local strength; therefore, values above one imply a high likelihood of rupture.

The RPI is computed using a custom CLI 3D Slicer module, and the results (including intermediate variables used for wall strength computation, such as ILT thickness and normalized diameter) are saved in a Visualisation Toolkit Polygonal data (.vtp) file for visualization and assessment (see Fig. 2).

References

1. McGloughlin, T. M. & Doyle, B. J. New approaches to abdominal aortic aneurysm rupture risk assessment: engineering insights with clinical gain. *Arterioscler. Thromb. Vasc. Biol.* **30**, 1687–1694, doi:10.1161/atvbaha.110.204529 (2010).
2. Vande Geest, J. P., Di Martino, E. S., Bohra, A., Makaroun, M. S. & Vorp, D. A. A biomechanics-based rupture potential index for abdominal aortic aneurysm risk assessment: demonstrative application. *Ann. N. Y. Acad. Sci.* **1085**, 11–21, doi:10.1196/annals.1383.046 (2006).
3. Gasser, T. C., Auer, M., Labruto, F., Swedenborg, J. & Roy, J. Biomechanical rupture risk assessment of abdominal aortic aneurysms: model complexity versus predictability of finite element simulations. *Eur. J. Vasc. Endovasc. Surg.* **40**, 176–185, doi:10.1016/j.ejvs.2010.04.003 (2010).
4. Gasser, T. C. *et al.* A novel strategy to translate the biomechanical rupture risk of abdominal aortic aneurysms to their equivalent diameter risk: method and retrospective validation. *Eur. J. Vasc. Endovasc. Surg.* **47**, 288–295, doi:10.1016/j.ejvs.2013.12.018 (2014).
5. Raghavan, M., Vorp, D., Federle, M., Makaroun, M. & Webster, M. Wall stress distribution on three-dimensionally reconstructed models of human abdominal aortic aneurysm. *J. Vasc. Surg.* **31**, 760–769 (2000).
6. Doyle, B., Callanan, A. & McGloughlin, T. A comparison of modelling techniques for computing wall stress in abdominal aortic aneurysms. *Biomed. Eng. Online* **6**, 38 (2007).
7. Li, Z.-Y. *et al.* Association between aneurysm shoulder stress and abdominal aortic aneurysm expansion: a longitudinal follow-up study. *Circulation* **122**, 1815–1822, doi:10.1161/circulationaha.110.939819 (2010).
8. Vande Geest, J., Wang, D., Wisniewski, S., Makaroun, M. & Vorp, D. Towards a non-invasive method for determination of patient-specific wall strength distribution in abdominal aortic aneurysms. *Ann. Biomed. Eng.* **34**, 1098–1106 (2006).
9. Maier, A. *et al.* A comparison of diameter, wall stress, and rupture potential index for abdominal aortic aneurysm rupture risk prediction. *Ann. Biomed. Eng.* **38**, 3124–3134, doi:10.1007/s10439-010-0067-6 (2010).
10. Erhart, P. *et al.* Finite element analysis in asymptomatic, symptomatic, and ruptured abdominal aortic aneurysms: in search of new rupture risk predictors. *Eur. J. Vasc. Endovasc. Surg*, doi:10.1016/j.ejvs.2014.11.010 (2014).
11. Hyhlik-Durr, A. *et al.* Reproducibility of deriving parameters of AAA rupture risk from patient-specific 3D finite element models. *J. Endovasc. Ther.* **18**, 289–298, doi:10.1583/10-3384mr.1 (2011).
12. VASCOPS. *AAA Analyser - A4clinics*™. Available at: http://www.vascops.com/en/vascops-A4clinics.html (Accessed: 18 March 2016) (2007).
13. Martufi, G., Di Martino, E. S., Amon, C. H., Muluk, S. C. & Finol, E. A. Three-dimensional geometrical characterization of abdominal aortic aneurysms: image-based wall thickness distribution. *J. Biomech. Eng.* **131**, 061015, doi:10.1115/1.3127256 (2009).
14. Shang, E. K. *et al.* Validation of semiautomated and locally resolved aortic wall thickness measurements from computed tomography. *J. Vasc. Surg.* **61**, 1034–1040, doi:10.1016/j.jvs.2013.11.065 (2015).
15. Raghavan, M. L. & Vorp, D. A. Toward a biomechanical tool to evaluate rupture potential of abdominal aortic aneurysm: identification of a finite strain constitutive model and evaluation of its applicability. *J. Biomech.* **33**, 475–482 (2000).
16. Wang, D. H., Makaroun, M., Webster, M. W. & Vorp, D. A. Mechanical properties and microstructure of intraluminal thrombus from abdominal aortic aneurysm. *J. Biomech. Eng.* **123**, 536–539 (2001).
17. Lu, J., Zhou, X. & Raghavan, M. L. Inverse elastostatic stress analysis in pre-deformed biological structures: Demonstration using abdominal aortic aneurysms. *J. Biomech.* **40**, 693–696 (2007).
18. Miller, K. & Lu, J. On the prospect of patient-specific biomechanics without patient-specific properties of tissues. *J. Mech. Behav. Biomed. Mater.* **27**, 154–166, doi:10.1016/j.jmbbm.2013.01.013 (2013).
19. Joldes, G. R., Miller, K., Wittek, A. & Doyle, B. A simple, effective and clinically applicable method to compute abdominal aortic aneurysm wall stress. *J. Mech. Behav. Biomed. Mater.* **58**, 139–148, doi:10.1016/j.jmbbm.2015.1007.1029 (2016).
20. Joldes, G. R. *BioPARR - biomechanics based prediction of aneurysm rupture risk*. (2016) Available at: http://bioparr.mech.uwa.edu.au/ (Accessed: 20 April 2016).
21. ABAQUS. *ABAQUS Theory Manual Version 6.9*. (Dassault Systèmes Simulia Corp., 2009).
22. Hyhlik-Durr, A. *et al.* Reproducibility of deriving parameters of AAA rupture risk from patient-specific 3D finite element models. *J. Endovasc. Ther.* **18**, 289–298, doi:10.1583/10-3384MR.1 (2011).
23. Hong, H. A. & Sheikh, U. U. Automatic detection, segmentation and classification of abdominal aortic aneurysm using deep learning. In *2016 IEEE 12th International Colloquium on Signal Processing & Its Applications (CSPA)*. 242–246.
24. Doyle, B. J., Hoskins, P. R. & McGloughlin, T. M. Computational rupture prediction of AAAs: what needs to be done next? *J. Endovasc. Ther.* **18**, 226–229, doi:10.1583/10-3244C.1 (2011).
25. Khosla, S. *et al.* Meta-analysis of peak wall stress in ruptured, symptomatic and intact abdominal aortic aneurysms. *Br. J. Surg.* 101, 1350–1357; discussion 1357, doi:10.1002/bjs.9578 (2014).
26. McBride, O. M. B. *et al.* MRI using ultrasmall superparamagnetic particles of iron oxide in patients under surveillance for abdominal aortic aneurysms to predict rupture or surgical repair: MRI for abdominal aortic aneurysms to predict rupture or surgery—the MA3RS study. *Open Heart* 2, doi:10.1136/openhrt-2014-000190 (2015).
27. Meyer, C. A., Guivier-Curien, C. & Moore, J. E. Jr. Trans-thrombus blood pressure effects in abdominal aortic aneurysms. *J. Biomech. Eng.* **132**, 071005, doi:10.1115/1.4001253 (2010).
28. Fedorov, A. *et al.* 3D Slicer as an image computing platform for the Quantitative Imaging Network. *Magn. Reson. Imaging* **30**, 1323–1341 (2012).
29. Zhu, L., Kolesov, I., Gao, Y., Kikinis, R. & Tannenbaum, A. An effective interactive medical image segmentation method using Fast GrowCut in *International Conference on Medical Image Computing and Computer Assisted Intervention (MICCAI), Interactive Medical Image Computing Workshop* (2014).
30. O'Leary, S. A., Doyle, B. J. & McGloughlin, T. M. Comparison of methods used to measure the thickness of soft tissues and their influence on the evaluation of tensile stress. *J. Biomech.* **46**, 1955–1960, doi:10.1016/j.jbiomech.2013.05.003 (2013).
31. Hans, S. S., Jareunpoon, O., Balasubramaniam, M. & Zelenock, G. B. Size and location of thrombus in intact and ruptured abdominal aortic aneurysms. *J. Vasc. Surg.* **41**, 584–588, doi:10.1016/j.jvs.2005.01.004 (2005).
32. Lorensen, W. E. & Cline, H. E. Marching cubes: A high resolution 3D surface construction algorithm. in *SIGGRAPH '87 Proceedings of the 14th annual conference on Computer graphics and interactive techniques*. 163–169 (ACM) (1987).

33. Valette, S. & Chassery, J.-M. Approximated centroidal voronoi diagrams for uniform polygonal mesh coarsening. In *Computer Graphics Forum (Eurographics 2004 proceedings)* 381–389 (2004).
34. Valette, S., Chassery, J.-M. & Prost, R. Generic remeshing of 3D triangular meshes with metric-dependent discrete Voronoi Diagrams. *IEEE Transactions on Visualization and Computer Graphics* **14**, 369–381 (2008).
35. Valette, S., Chassery, J.-M. & Prost, R. *ACVD: Surface mesh coarsening and resampling*. Available at: http://www.creatis.insa-lyon.fr/site/en/acvd (Accessed: 02 March 2016).
36. Geuzaine, C. & Remacle, J.-F. *Gmsh - A three-dimensional finite element mesh generator with built-in pre- and post-processing facilities*. Available at: http://gmsh.info/ (Accessed: 03 March 2016).
37. Geuzaine, C. & Remacle, J.-F. Gmsh: a three-dimensional finite element mesh generator with built-in pre- and post-processing facilities. *Int. J. Numer. Meth. Eng.* **79**, 1309–1331 (2009).
38. Kitware. *VTK - The visualisation toolkit*. Available at: http://www.vtk.org/ (Accessed: 03 March 2016).
39. Schurink, G. W., van Baalen, J. M., Visser, M. J. & van Bockel, J. H. Thrombus within an aortic aneurysm does not reduce pressure on the aneurysmal wall. *J. Vasc. Surg.* **31**, 501–506 (2000).
40. Thubrikar, M. J., al-Soudi, J. & Robicsek, F. Wall stress studies of abdominal aortic aneurysm in a clinical model. *Ann. Vasc. Surg.* **15**, 355–366, doi:10.1007/s100160010080 (2001).
41. Wittek, A., Hawkins, T. & Miller, K. On the unimportance of constitutive models in computing brain deformation for image-guided surgery. *Biomech. Model. Mechanobiol.* **8**, 77–84 (2009).

Acknowledgements

The financial support of the Australian Research Council (Discovery Grant No. DP120100402) and the National Health and Medical Research Council (Grant No. APP1063986 and APP1083572) is gratefully acknowledged. We wish to acknowledge the Raine Medical Research Foundation for funding G. R. Joldes through a Raine Priming Grant. D. E. Newby is supported by the British Heart Foundation (CH/09/002 and RG/16/10/32375) and the Wellcome Trust (WT103782AIA). The MA3RS study was funded by grant (20/11/03) from the Medical Research Council National Institute for Health Research Efficacy and Mechanism Evaluation (NIHR EME) programme. The Clinical Research Imaging Centre and Wellcome Trust Clinical Research Facility (Edinburgh), and the Clinical Research Facility Glasgow, are supported by National Health Service Research Scotland (NRS).

Author Contributions

G.R.J. implemented the software, performed the numerical simulations and analysed the results. G.R.J. and B.D. wrote the main manuscript text. B.D., R.O.F. and D.E.N. provided AAA data. G.R.J., K.M. and A.W. have contributed ideas related to the finite element analysis of AAA All authors have reviewed the manuscript.

Additional Information

Competing Interests: The authors declare that they have no competing interests.

Publisher's note: Springer Nature remains neutral with regard to jurisdictional claims in published maps and institutional affiliations.

Multidimensional assessments of abdominal aortic aneurysms by magnetic resonance against ultrasound diameter measurements

Papanastasiou G[1], González-Castro V.[2], Gray C.D.[1], Forsythe RO[1,3], Sourgia-Koutraki Y[1,3], Mitchard N[4], Newby D.E.[1,3], Semple S.I.K.[1,3]

[1] Clinical Research Imaging Centre, University of Edinburgh, Edinburgh, UK
[2] Department of Electric, Systems and Automatics Engineering, University of León, León, Spain
[3] Centre for Cardiovascular Science, University of Edinburgh, Edinburgh, UK
[4] Department of Radiology, Royal Infirmary of Edinburgh, Edinburgh, UK
g.papanas@ed.ac.uk

Abstract. Volumetric and 3D tortuosity, curvature and asymmetry measurements were assessed for the first time from magnetic resonance (MR) data against ultrasound (US)-derived diameters, in a pilot cohort of 26 patients with abdominal aortic aneurysm (AAA) disease. We demonstrated that MR multidimensional analysis can better detect morphologic aneurysmal differences over time compared to diameters extracted from US imaging, which is the current clinical standard method for assessing AAA progression. Our 3D descriptors correlated more strongly with MR volumes, compared to US diameters at baseline and over time. Following further assessments in a larger patient cohort, this multidimensional analysis may enhance rupture risk prediction and improve clinical decision making.

Keywords: Abdominal aortic aneurysm, Magnetic Resonance Imaging, Ultrasound, Multidimensional assessments.

1 Introduction

Abdominal aortic aneurysm (AAA) disease is an important cause of morbidity that affects up to 5% of men aged 65-74 years in Western Europe, with a mortality rate that can be greater than 80% when rupture occurs [1]. In the clinical setting, decision making must take into account significant risks associated with elective AAA repair, with a 30-day mortality rate of up to 5% [2]. It is therefore important, that for the clinical management of a patient with AAA, the risks of elective repair must be weighed against the risk of rupture [1, 2].

The current guidelines suggest that the risk of rupture in an AAA increases with its size [3]. Elective repair should be considered when the AAA exceeds 5.5 cm in anteroposterior diameter, or expansion exceeds 0.7 cm per six months, or 1 cm per year [4]. Despite these guidelines, up to 1 in 5 ruptured AAAs occur in small aneurysms

(<5.5 cm), whilst there are many patients under surveillance with aneurysms far exceeding 5.5 cm in diameter that do not rupture [2, 4].

Ultrasound (US) is the reference standard technique for assessing AAA diameter growth rates accurately, with no radiation exposure and at low cost. However, other than visual morphological assessments, it is not possible to provide additional quantitative information about AAA volume and morphology [5]. Computed tomography (CT) data analysis has recently showed that AAA volume may better predict aneurysm growth rate [6], whilst correlated more strongly with increasing estimated biomechanical rupture risk, than maximum diameter [3]. These data suggest that aneurysms exhibit non-linear, discontinuous growth patterns and hence, morphological changes beyond US-derived diameter growth rates must be assessed [3, 5, 6].

Magnetic resonance (MR) imaging is widely accepted as a diagnostic imaging tool for cardiovascular diseases but its utility in monitoring volumetric as well as asymmetry AAA changes has not been rigorously examined [7]. Furthermore, although some AAA diameter and volume [3, 6], 2D tortuosity indices [8, 9] and asymmetry [10] have been assessed (using CT imaging), more advanced multidimensional AAA morphological changes such as 3D tortuosity and curvature have not been extensively investigated.

We assessed growth rates and correlations between AAA volumes derived from MR images versus US-derived diameters in a pilot cohort of patients. We also assessed for the first time multidimensional 3D tortuosity, curvature and asymmetry estimated from MR imaging versus US-derived diameters and MR-derived volumes in this pilot cohort.

2 Methods

2.1 Study population

26 patients with asymptomatic AAA (diameter 38-56 mm on ultrasound examination) and with aneurysmal expansions <1 cm per year (24 males, 2 females), were retrospectively selected from the MA3RS study database (full cohort N=350) [11]. After informed consent, MR imaging was acquired in all patients. AAA volumes and multidimensional 3D geometrical descriptors (3D tortuosity, curvature, asymmetry) were extracted from the MR images and comparisons as well as correlations with clinical standard US-derived diameters were assessed.

2.2 Ultrasound and MR acquisition

Standard US imaging was carried out in an accredited clinical vascular science laboratory. Participants underwent US evaluation of the maximum anteroposterior diameter of the abdominal aorta by an expert ultrasonographer using a 3.5 MHz linear array transducer.

MRI scans were performed on a 3T Magnetom Verio scanner (Siemens, Erlangen, Germany), as previously described [11]. T2-weighted multi-slice Half Fourier Acquisition Single Shot Turbo Spin Echo (HASTE) sequences were used to identify the

extent of the aneurysm and anatomical data were obtained using a respiratory-gated T2-weighted turbo spin echo sequence. US and MR protocols were implemented for baseline and 1-year follow up imaging.

2.3 Image and 3D geometrical analysis

Maximum anteroposterior diameters (US_Diam) were extracted from the US images by an expert clinician. AAAs from MR images were manually segmented by an experienced user, using dedicated segmentation software (SliceOmatic, TomoVision, Canada). Regions or interest (ROIs) for the lumen, thrombus and aortic wall were manually defined across all slices for which abdominal aortas were MR visible (Fig. 1a, 11-25 slices depending on the length of abdominal aortas). MR data were anatomically landmarked by an expert clinician and matching slices from the same anatomical areas for both baseline and 1-year follow up data were analysed for each subject.

AAA volumes and 3D geometrical descriptors were calculated using in-house software developed in Matlab (Mathworks, USA). From the SliceOmatic data, the centroids for the lumen ROIs (Lum) and the combined ROIs (Com=lumen + thrombus + aortic wall) were derived for all MR slices across all subjects (Fig. 1b) and were then used to derive 3D tortuosity, curvature and asymmetry measurements. AAA volumes and 3D geometrical descriptors were calculated for Lum and Com ROIs and centrelines (Fig 1b, each centreline connects consecutive centroids) respectively. AAA volumes for Lum and Com ROIs are described as Vol_Lum, Vol_Com respectively.

For 3D tortuosity measurements, the distance measure (DM) algorithm was originally developed for retinal 2D data analysis, as previously described [12]. To adapt the DM algorithm for 3D tortuosity measurements, the lengths of the 3D vectors (3D Euclidean distances) connecting consecutive centroids were calculated and summed across both the Lum and Com centrelines (Fig 1c, Lc=Lc1+Lc2+…Lcn). Furthermore, the length of the 3D vector connecting the two end points of each Lum and Com centreline was measured (Lx). DM tortuosity algorithm was finally calculated in the 3D space for both Lum and Com centrelines (abbreviated as Tor_Lum, Tor_Com respectively) by using:

$$DM = \frac{L_c}{L_x} \tag{1}$$

The curvature was measured for both Lum and Com centrelines (Cur_Lum, Cur_Com respectively). To devise 3D curvature measurements, singular value decomposition was used to fit osculating circles at each centroid in 3D space (see equation 2 and Fig. 1d). For the singular value decomposition, the following factorisation was used:

$$A = U\Sigma V^T \tag{2}$$

where A is an 3 x 3 matrix, in which each column represents a 3D centroid point across the Lum and Com centrelines. In matrix A, the second column corresponds to

the local 3D centroid point in which the osculating circle was fitted, whilst the first and third columns describe the 3D centroid points before and after the local 3D centroid point, across each centreline. *U* and *V* represent orthogonal matrices describing the left and right singular vectors respectively, with V^T denoting the transpose of *V*. Σ denotes the diagonal matrix in decreasing order. Following singular value decomposition, the first and second unit orthogonal vectors in *U* were extracted and multiplied by the matrix A. The product of this multiplication defined two 3D unit vectors which were subsequently used to fit an osculating circle for each local 3D centroid point.
The radius of each osculating circle (r) is also the radius of the curvature (κ), whilst curvature equals the reciprocal of radius r (see also equation 3) [13]. The smaller the radius r of the circle, the higher the curvature is and vice versa. (note: curvature is 0 for a straight line because the radius tends to infinity).

$$\kappa = \frac{1}{r} \tag{3}$$

Two types of asymmetry measurements were derived. The first type has been previously described by Doyle et al [14] and is based on calculating the perpendicular distance from each centroid to the straight line connecting the AAA end points (Fig.1e). This asymmetry type was calculated for both the Lum and Com centrelines (Ass_Lum, Ass_Com respectively). The second type of asymmetry is introduced by the authors, defined as centroid asymmetry (Ass_Cen). The lengths of the 3D vectors connecting paired (corresponding to the same slice) Lum and Com centroids were calculated, summed across all centroids and normalised to the Com centreline length for each AAA (Fig. 1f). In a vessel with no aneurysmal expansion, the lumen and outer wall are approaching concentricity and Ass_Cen tends to 0.

2.4 Statistical analysis

Statistical analysis was performed using R software (R Foundation for statistical computing, Vienna, Austria). A non-linear growth model (NLGM) was used to assess growth (for AAA expansion measurements: diameter, volumes, asymmetry) and change rates (for 3D tortuosity, curvature), between baseline and 1-year follow-up data [3, 6]:

$$NLGM = (e^{12 \cdot L} - 1) \cdot 100 \frac{\%}{year} \tag{4}$$

with L being a logarithmic growth factor:

$$L = \frac{1}{t} \cdot \ln\left(\frac{M_{follow-up}}{M_{baseline}}\right) \tag{5}$$

in which M is an US or MR estimate and t is the time (in months) between baseline and follow-up measurements. The Shapiro-Wilk test was used to assess normality of

the data and comparisons were assessed using paired and unpaired Student's t-tests as appropriate. Box and whisker plots investigated growth/change rates across all US and MR measurements. Linear regression and Pearson's correlation coefficients were used to investigate correlations between MR AAA volumes versus US-derived diameters, and between MR 3D geometrical descriptors versus diameters and volumes (two-sided P value <0.05 were considered significant).

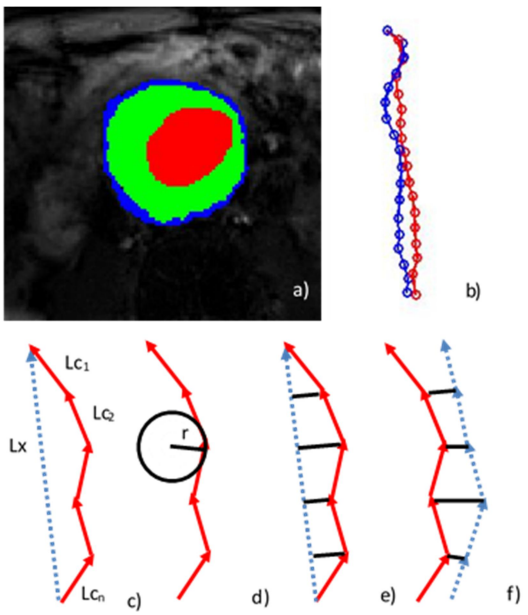

Fig. 1. (a) Lumen (red), thrombus (green) and outer wall (blue) segments shown from a patient with AAA disease at baseline. (b) Centrelines for Lum (lumen, with red) and Com (combined=lumen + thrombus + outer wall, with blue) regions of interest, from the same patient data set. (c) Tortuosity DM algorithm applied across 6 example centroids, where $Lc_{1\text{-}n}$ and Lx (dot blue line) are the 3D vectors connecting consecutive centroids and end points in centrelines, respectively. (d) Curvature measured by fitting osculating circles in 3D space. (e) and (f) two different types of vessel asymmetry metrics (in c-f. the solid red centrelines represent the Lum centreline, in f. the dot blue line shows the Com centreline).

3 Results

26 patients (2 females, 24 males) with AAA were included in the analysis. The median time between baseline and follow up US and MR imaging was 12 months (interquartile range (IQR), 11-13 months). MR imaging was acquired within 1-week from the day of US imaging. The mean(SD) US-derived AAA diameter was 45(4) mm and 47(5) mm, at baseline and follow up respectively.

3.1 Growth and change rates

Increased growth rates were observed for all parameters describing AAA expansion (Fig. 2). For US_Diam, median diameter growth rate was 3.32 %/year (IQR were 0.00 to 8.56 %/year). For Vol_Lum and Vol_Com, median volume growth rates were 7.18 and 8.23 %/year (IQRs were 0.38 to 18.54, 4.59 to 13.67) respectively. The growth rates for Vol_Com showed a significant difference versus US_Diam ($P<0.05$). For 10 patients who showed no diameter increases, Vol_Com showed a significant growth rate increase ($P<0.001$).

Median growth rates for Ass_Lum and Ass_Com were 9.52 and 5.71 %/year (IQRs were -8.60 to 33.90, -9.92 to 24.90 %/year) respectively. Ass_Cen demonstrated the largest growth rate (median was 12.74 % /year; IQR was -0.40 to 34.52 %/year, Fig. 2). The growth rate for Ass_Cen showed a significant difference versus US_Diam ($P<0.05$). For 10 patients who showed no diameter increases, Ass_Cen showed a significant growth rate increase ($P<0.01$). No other significant differences were observed between growth rates.

Change rates for 3D tortuosity and curvature were not significantly increased (all median values<US_Diam median).

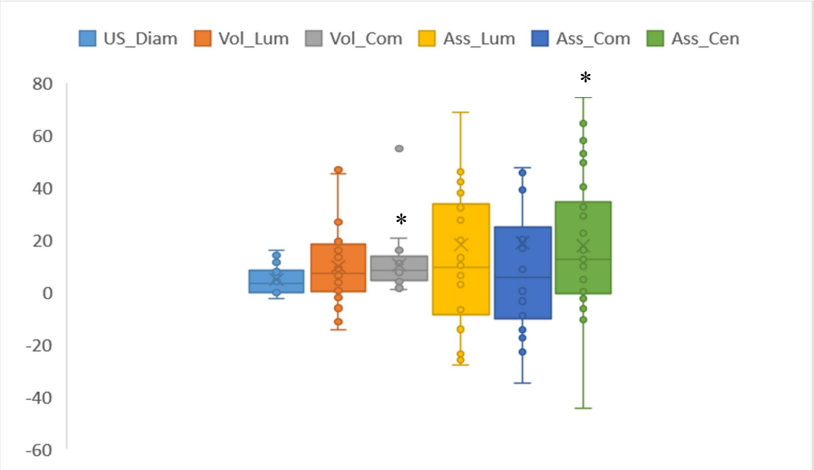

Fig. 2. Growth rates for US and MR measurements demonstrating aneurysmal expansions across all subjects (US_Diam: ultrasound-derived diameters, Vol_Lum: MR-derived volumes of the lumen, Vol_Com: volumes of the combined regions of interest, Ass_Lum: asymmetry for the lumen centreline, Ass_Com: asymmetry for the combined centreline, Ass_Cen: centroid asymmetry). Significant growth rate increases in patients with no diameter changes are indicated with *.

3.2 Correlations at baseline

Initially, correlations across all measurements were examined at baseline. Vol_Lum and Vol_Com showed significant, strong correlations with US_Diam (Fig. 3a-b). A significant, strong correlation was also observed between Vol_Com and Ass_Cen (Fig. 3c, all P<0.001). There was also a moderate but significant correlation between US_Diam and Ass_Cen (r=0.46, P<0.05).

All 3D geometrical descriptors (tortuosity, curvature, asymmetry) for both Lum and Com centrelines correlated positively (r=0.51-0.59, P<0.001), with Tor_Com versus Ass_Com reaching the highest correlation (r=0.83, P<0.001).

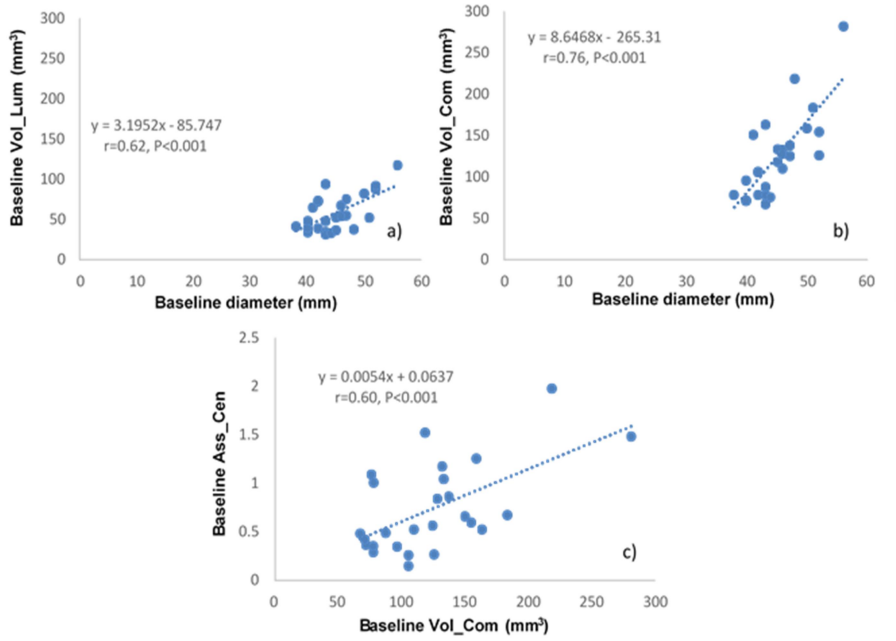

Fig. 3. Significant, strong correlations shown at baseline (Vol_Lum: MR-derived volumes of the lumen, Vol_Com: volumes of the combined regions of interest, Ass_Cen: centroid asymmetry).

3.3 Correlations between growth and change rates

Subsequently, correlation coefficients were investigated between growth rates for US derived diameters and MR derived volumes versus change rates for all 3D geometrical descriptors. The strongest correlation was observed between Vol_Com and Cur_Com (r=0.63, P<0.001, Fig.3). There were also moderate but significant correlations between US_Diam and Cur_Lum and between Vol_Com and Tor_Com (r=0.45, 0.50 respectively, P<0.05).

Significant, strong correlations were finally observed between change rates of 3D geometrical descriptors. Specifically, between Tor_Lum and Cur_Lum (r=0.60), Tor_Com and Cur_Com (r=0.60), Tor_Com and Ass_Com (r=0.71, all P<0.01). All other correlations at both baseline and 1-year follow-up growth/change rates demonstrated weaker non-significant relationships.

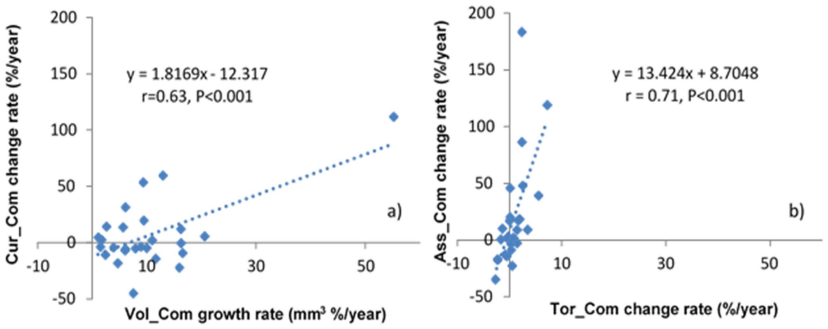

Fig. 4. Significant, strong correlations for growth/change rates. Vol_Com: volume, Cur_Com: curvature, Tor_Com: tortuosity, Ass_Com: asymmetry, of the combined regions of interest (Com).

4 Discussion

We investigated growth rates for US diameters as well as MR volumes and asymmetries derived from a pilot cohort of AAA patients. MR-derived volumes and centroid asymmetries demonstrated significant growth rate increases in patients with small asymptomatic aneurysms and low US diameter increases. We also assessed all 3D geometrical descriptors versus US diameters and MR volumes and demonstrated significant correlations both at baseline and over time (between baseline and 1-year).

4.1 Growth rates of AAA expansion measures

This is the first study assessing MR derived volumes and asymmetries against US reference standard diameter measurements. The AAA structural integrity can be compromised by fast AAA growth and may increase the risk of AAA rupture [6, 15, 16]. Monitoring the growth rate of small AAAs can therefore be crucial for decision making in surveillance programs. In our analysis, we showed that MR-derived volumes may better detect morphologic aneurysmal differences over time compared to US diameters, the current clinical standard method for monitoring AAA changes. This is in agreement with a previous CT study suggesting that volume can better predict AAA growth rate than diameter [3].

Similarly, we demonstrated that centroid asymmetry, our novel 3D asymmetry descriptor, can better represent morphologic aneurysmal changes compared to US diam-

eters. Centroid asymmetry can identify morphological differences beyond diameter and longitudinal growths across the AAA (accounted for by volumetric analysis), describing both areas of thrombus increases and aortic lumen dislocations inside the AAA over time. Moreover, centroid asymmetry demonstrated increased growth rate compared to asymmetry of the combined centreline (Fig. 2), which has previously been suggested as a potentially useful adjunct to diameter using CT data analysis [10].

In our pilot cohort, we also showed for the first time significant, strong correlations between MR-derived volumes and US diameters at baseline (Fig. 3a-b), whilst demonstrated that baseline centroid asymmetry correlated with both US diameters and MR volume. The above correlations at baseline were not observed when the respective growth rates were assessed, which can suggest that volume and centroid asymmetry may follow different growth patterns compared to maximum US diameters (Fig. 2). These results can suggest that MR volume and centroid asymmetry estimates may be able to detect morphological abnormalities at baseline as well as changes over time, and improve decision making in surveillance programs.

4.2 Further assessment of 3D geometrical descriptors

Our analysis demonstrated that changes in the curvature and tortuosity are associated with diameter and volume increases. The strongest correlation was observed between MR volume and curvature of the combined ROIs. Although there was a significant correlation between US diameters and curvature of the lumen, curvature and tortuosity correlated more strongly with MR volume of the combined ROIs. Significant, strong correlations were also shown between change rates of 3D geometrical descriptors (tortuosity and curvature of the lumen, tortuosity and curvature, tortuosity and asymmetry of the combined ROIs). To our knowledge, this is the first study assessing 3D tortuosity and curvature algorithms in AAAs using medical imaging data. Previous studies have mainly assessed 2D tortuosity indices [8, 9], or have focused in biomechanical analysis using peak wall stress [3, 10, 17, 18]. In the context of biomechanical analysis, studies have suggested that AAAs predominantly dilate (thrombotic expansion) in the anterior plane due to spinal cord constraints in the posterior direction and thus, peak wall stress is frequently increased in areas of the posterior wall [3, 17, 18]. Molacek et al. investigated the elastic properties of AAAs by performing a distensibility study using CT data and suggested that thrombotic morphologies may in some cases act protectively against the risk of rupture [19]. Further investigation of our 3D descriptors may provide additional quantitative information to biomechanical analysis, for which cases thrombus morphologies may act as risk [17, 18] or protective factors [19] of rupture.

In conclusion, we showed that MR multidimensional analysis can better detect morphologic aneurysmal differences over time compared to US diameters. In addition, our 3D descriptors correlated more strongly with MR volumes, compared to US diameters at baseline and over time. Further evaluation is underway in our larger patient cohort (N=350) to further assess our 3D geometrical descriptors and evaluate their ability in predicting rupture risk and disease progression.

References

1. Ashton HA, Buxton MJ, Day NE, et al. Multicentre Aneurysm Screening Study Group. The Multicentre Aneurysm Screening Study (MASS) into the effect of abdominal aortic aneurysm screening on mortality in men: a randomised controlled trial. Lancet 2002; 360:1531-9.
2. Forsythe RO, Newby DE, Robson JMJ, et al. Monitoring the biological activity of abdominal aortic aneurysms Beyond Ultrasound. Heart 2016; 102(11):817-824.
3. Liljeqvist ML, Hultgren R, Gasser TC, et al. Volume growth of abdominal aortic aneurysms correlates with baseline volume and increasing finite element analysis-derived rupture risk. J Vasc Surg 2016; 63:1434-42.
4. Nicholls SC, Gardner JB, Meissner MH, et al. Rupture in small abdominal aortic aneurysms. J Vasc Surg 1998; 28: 884-8.
5. Chaikof EL, Brewster DC, Dalman RL, et al. The care of patients with an abdominal aortic aneurysm: the Society for Vascular Surgery practice guidelines. J Vasc Surg 2009; 50: S2-49.
6. Martufi G, Auer M, Roy J, et al. Multidimensional growth measurements of abdominal aortic aneurysms. J Vasc Surg 2013; 58(3): 748-755.
7. Buijs RVC, Willems TP, Tio RA, et al. Current state of experimental imaging modalities for risk assessment of abdominal aortic aneurysm. J Vasc Surg 2013; 57:851-9.
8. Pappu S, Dardik A, Tagare H, et al. Beyond fusiform and saccular: A novel quantitative tortuosity index may help classify aneurysm shape and predict aneurysm rupture potential. Ann Vasc Surg 2008; 22(1): 88-97.
9. Fillinger MF, Racusin J, Baker RK, et al. Anatomic characteristics of ruptured abdominal aortic aneurysm on conventional CT scans: implications for rupture risk. J Vasc Surg 2004; 39(6): 1243-1252.
10. Doyle BJ, Callanan A, Burke PE, et al. Vessel asymmetry as an additional diagnostic tool in the assessment of abdominal aortic aneurysms. J Vasc Surg 2009; 49(2): 443-454.
11. McBride, OMB, Berry C, Burns P, et al. MRI using ultrasmall superparamagnetic particles of iron oxide in patients under surveillance for abdominal aortic aneurysms to predict rupture or surgical repair: MRI for abdominal aortic aneurysms to predict rupture or surgery-the MA^3RS study. Open Heart 2015; 2.
12. Lisowska A, Annunziata R, Loh GK, et al. An Experimental Assessment of Five Indices of Retinal Vessel Tortuosity with the RET-TORT Public Dataset. Proc 36th Annu Int Conf IEEE Eng Med Biol Soc 2014; 5414-5417.
13. Lewiner T, Gomes JD Jr, Lopes H, et al. Curvature and torsion estimators based on parametric curve fitting. Comput Graph 2005; 29: 641-55.
14. Doyle BJ, Callanan A, Burke PE, et al. Vessel asymmetry as an additional diagnostic tool in the assessment of abdominal aortic aneurysms. J Vasc Surg 2009; 49(2): 443-454.
15. Freestone T, Turner RJ, Coady A, et al. Inflammation and matrix metalloproteinases in the enlarging abdominal aortic aneurysm. Arterioscler Thromb Vasc Biol 1995;15: 1145-51.
16. Anidjar S, Dobrin PB, Eichorst M, et al. Correlation of inflammatory infiltrate with the enlargement of experimental aortic aneurysm. J Vasc Surg 1992; 16:139-47.
17. Venkatasubramaniam AK, Mehta T, Fagan MJ, et al. A comparative study of aortic wall stress using finite element analysis for ruptured and non-ruptured abdominal aortic aneurysm. Eur J Vasc Endovasc Surg 2004; 28:168-76.
18. Fillinger MF, Marra SP, Raghavan ML, et al. Prediction of rupture risk in abdominal aortic aneurysm during observation: wall stress versus diameter. J Vasc Surg 2003; 37:724-32.

19. Molacek Baxa J, Houdek K, Treska V, et al. Assessment of abdominal aortic aneurysm wall distensibility with electrocardiography-gated computed tomography. Ann Vasc Surg 2011; 25: 1036–1042.

OPEN

^{18}F-Fluoride and ^{18}F-Fluorodeoxyglucose Positron Emission Tomography After Transient Ischemic Attack or Minor Ischemic Stroke

Case–Control Study

Alex T. Vesey, MD; William S. A. Jenkins, MD; Agnese Irkle, PhD; Alastair Moss, MD; Greg Sng, MD; Rachael O. Forsythe, MD; Tim Clark, MSc; Gemma Roberts, MSc; Alison Fletcher, PhD; Christophe Lucatelli, PhD; James H. F. Rudd, MD, PhD; Anthony P. Davenport, PhD; Nicholas L. Mills, MD, PhD; Rustam Al-Shahi Salman, MA, PhD; Martin Dennis, MD, PhD; William N. Whiteley, MD, PhD; Edwin J. R. van Beek, MD, PhD; Marc R. Dweck, MD PhD; David E. Newby, MD, PhD, DSc

Background—Combined positron emission tomography (PET) and computed tomography (CT) can assess both anatomy and biology of carotid atherosclerosis. We sought to assess whether ^{18}F-fluoride or ^{18}F-fluorodeoxyglucose can identify culprit and high-risk carotid plaque.

Methods and Results—We performed ^{18}F-fluoride and ^{18}F-fluorodeoxyglucose PET/CT in 26 patients after recent transient ischemic attack or minor ischemic stroke: 18 patients with culprit carotid stenosis awaiting carotid endarterectomy and 8 controls without culprit carotid atheroma. We compared standardized uptake values in the clinically adjudicated culprit to the contralateral asymptomatic artery, and assessed the relationship between radiotracer uptake and plaque phenotype or predicted cardiovascular risk (ASSIGN score [Assessing Cardiovascular Risk Using SIGN Guidelines to Assign Preventive Treatment]). We also performed micro PET/CT and histological analysis of excised plaque. On histological and micro PET/CT analysis, ^{18}F-fluoride selectively highlighted microcalcification. Carotid ^{18}F-fluoride uptake was increased in clinically adjudicated culprit plaques compared with asymptomatic contralateral plaques ($\log_{10}$standardized uptake value$_{mean}$ 0.29±0.10 versus 0.23±0.11, P=0.001) and compared with control patients ($\log_{10}$standardized uptake value$_{mean}$ 0.29±0.10 versus 0.12±0.11, P=0.001). ^{18}F-Fluoride uptake correlated with high-risk plaque features (remodeling index [r=0.53, P=0.003], plaque burden [r=0.51, P=0.004]), and predicted cardiovascular risk [r=0.65, P=0.002]). Carotid ^{18}F-fluorodeoxyglucose uptake appeared to be increased in 7 of 16 culprit plaques, but no overall differences in uptake were observed in culprit versus contralateral plaques or control patients. However, ^{18}F-fluorodeoxyglucose did correlate with predicted cardiovascular risk (r=0.53, P=0.019), but not with plaque phenotype.

Conclusions—^{18}F-Fluoride PET/CT highlights culprit and phenotypically high-risk carotid plaque. This has the potential to improve risk stratification and selection of patients who may benefit from intervention. **(*Circ Cardiovasc Imaging*. 2017;10:e004976. DOI: 10.1161/CIRCIMAGING.116.004976.)**

Key Words: carotid stenosis ■ fluorides ■ inflammation ■ nuclear medicine ■ phenotype ■ stroke

Although carotid endarterectomy reduces risk of ipsilateral stroke in people with symptomatic carotid artery stenosis, the number needed to treat to prevent one stroke is large,[1,2] especially in asymptomatic stenosis.[3] Furthermore, the pathological event that leads to cerebral thromboembolism (atherosclerotic plaque rupture) is not necessarily correlated with luminal stenosis severity.[4] Other pathological features, such as inflammation, cell death, and microcalcification, are important in driving both plaque formation and instability.[5–7] New imaging biomarkers of these processes are therefore needed to improve risk stratification and clinical

See Editorial by Tawakol et al
See Clinical Perspective

Received May 2, 2016; accepted January 12, 2017.

From the BHF Centre for Cardiovascular Science, University of Edinburgh, United Kingdom (A.T.V., W.S.A.J., A.M., G.S., R.O.F., N.L.M., E.J.R.v.B., M.R.D., D.E.N.); Division of Experimental Medicine and Immunotherapeutics, University of Cambridge, United Kingdom (A.I., J.R., A.P.D.); and Clinical Research Imaging Centre (T.C., G.R., A.F., C.L., E.J.R.v.B., M.R.D., D.E.N.) and Centre for Clinical Brain Sciences (R.A.-S.S., M.D., W.W.), University of Edinburgh, United Kingdom.

The Data Supplement is available at http://circimaging.ahajournals.org/lookup/suppl/doi:10.1161/CIRCIMAGING.116.004976/-/DC1.

Correspondence to Alex T. Vesey, MD, Centre for Cardiovascular Science, University of Edinburgh, Room SU 305, Chancellor's Bldg., 49 Little France Crescent, Edinburgh, EH16 4SB, United Kingdom. E-mail: avesey@staffmail.ed.ac.uk

decision-making. Such biomarkers could also assess the response of plaque biology to novel pharmacological interventions and provide a way of identifying culprit lesions in patients with multiple plaques.

Hybrid positron emission tomography and computed tomography (PET/CT) is a molecular imaging modality that has high sensitivity for noninvasive in vivo detection of radiolabeled biomolecules tuned to a variety of pathophysiological processes. In carotid atherosclerosis imaging, the most widely used tracer has been ^{18}F-fluorodeoxyglucose (^{18}F-FDG)[8–14]: Recently, we have described another radiotracer, ^{18}F-fluoride, in atherosclerosis imaging.[15,16] We[15–18] and others[19–23] have shown that this tracer has major potential in cardiovascular disease. ^{18}F-Fluoride can highlight culprit plaque in patients after myocardial infarction and high-risk plaques in patients with apparently stable coronary heart disease.[16] We have shown that this is because ^{18}F-fluoride can highlight areas of microcalcification indicative of necrotic atheroma.[24] The ability to identify high risk or culprit plaque in the cephalic circulation has the potential to improve risk stratification in patients at high risk of stroke with a view to more targeted interventions. Our study aims were to compare and contrast the identification of clinically adjudicated culprit and high-risk plaque at the carotid bifurcation using ^{18}F-fluoride and ^{18}F-FDG PET/CT.

Methods

Patient Population

Two cohorts of people with a recent transient ischemic attack (TIA) or minor ischemic stroke were recruited: a case cohort with a high-grade internal carotid artery stenosis (≥50% by North American Symptomatic Carotid Endarterectomy Trial[25] criteria for men, ≥70% for women) scheduled to undergo carotid endarterectomy and a control cohort in whom the cause of stroke was not attributed to carotid atheroma. Participants were recruited from outpatient clinics in National Health Service Lothian between January 2013 and June 2014 (for exclusion criteria, see Appendix in the Data Supplement). Research ethics committee approval (National Health Service West of Scotland Research Ethics Committee: 12/WS/0227) and the written and informed consent of all participants were obtained.

Baseline Assessment

Participants underwent clinical assessment at baseline including standard hematologic and biochemical indices. Serum C-reactive protein concentration was measured using the MULTIGENT CRP Vario assay on the high-throughput ARCHITECT system (Abbott Laboratories, Abbott Park, IL). Predicted cardiovascular risk was estimated using the ASSIGN score: a validated Scottish cardiovascular risk score that is similar to the Framingham risk score but includes additional factors, such as social deprivation and family history.[26]

PET/CT Protocol

Static ^{18}F-FDG PET/CT was acquired using a hybrid scanner (Biograph mCT, Siemens Medical Systems, Erlangen, Germany) 90 minutes after the intravenous administration of a target dose of 200 MBq. A rigid neck collar was fitted to minimize movement and standardize position. An attenuation-correction CT scan (nonenhanced, low dose 120 kV, 50 mAs) was then performed followed by PET acquisition covering 2 bed positions with the first upper bed centered over the carotid bifurcation in 3-dimensional mode for 20 minutes per bed. Patients were fasted for 6 hours before scanning.

^{18}F-Fluoride PET/CT was undertaken the subsequent day 60 minutes after administering 250 MBq ^{18}F-fluoride. A neck collar was

Table 1. Baseline Clinical Characteristics

	Stenosis Symptomatic	No Stenosis Symptomatic	*P* Value
n	18	8	
Age, y	71.7±12.3	66.1±12.5	0.30
Men, n (%)	12 (66.7)	4 (50)	0.67
BMI, kg·m^{-2}	26.2±5	27.3 (23.38–36)	0.40
Systolic blood pressure (mm Hg)	137±25	154±16	0.08
Diastolic blood pressure (mm Hg)	78±18	85±3.4	0.34
ASSIGN score	31±15.5	21.1±13.1	0.13
Presenting syndrome, n (%)			0.22
Stroke	8 (44)	6 (75)	
TIA/amaurosis fugax	10 (56)	2 (25)	
CEA side, right (%)	8 (44)		
Cardiovascular history, n (%)			
Coronary artery disease	10 (56)	2 (25)	0.22
Myocardial infarction	5 (28)	1 (13)	0.63
Risk factors, n (%)			
Hypertension	11 (61)	7 (88)	0.36
Diabetes	1 (6)	0	1
Hypercholesterolemia	13 (72)	5 (63)	0.67
Current smoker	6 (33)	2 (25)	0.67
Medication, n (%)			
Single antiplatelet therapy	14 (78)	6 (88)	1
Dual antiplatelet therapy	3 (17)	0	0.53
Anticoagulant	1 (6)	2 (25)	0.22
Statin	17 (94)	6 (75)	0.22
ACEi/AIIRB	7 (39)	2 (25)	0.20
Beta-antagonist	7 (39)	(131)	0.36
Calcium antagonist	7 (39)	2 (25)	0.67
Other antihypertensive	6 (39)	3 (38)	1
Hematology			
Hemoglobin, g/L	139.8±19	142.6±12.3	0.71
White cell count, ×10^9/L	8±1.4	6.4 (3.8–7.9)	0.06
Platelet count, ×10^9/L	259±64	273±63	0.60
Biochemistry			
Creatinine, mmol/L	88.5 (78–97.5)	76.8±13.5	0.07
Total cholesterol, mg/dL	117.9±34.8	181.7±54.1	0.81
C-reactive protein, mg/L*	3.1±2.6	2.4±3.5	0.66

Parametric data presented as mean±SD. Nonparametric data presented as median (IQR). Categorical data presented as number (%). ACE indicates angiotensin converting enzyme; AIIRB, angiotensin 2 receptor antagonists; BMI, body mass index; CAD, coronary artery disease; CEA, carotid endarterectomy; IQR, interquartile range; and transient ischemic attack.

*C-reactive protein values > 10 excluded as per AHA guidelines.

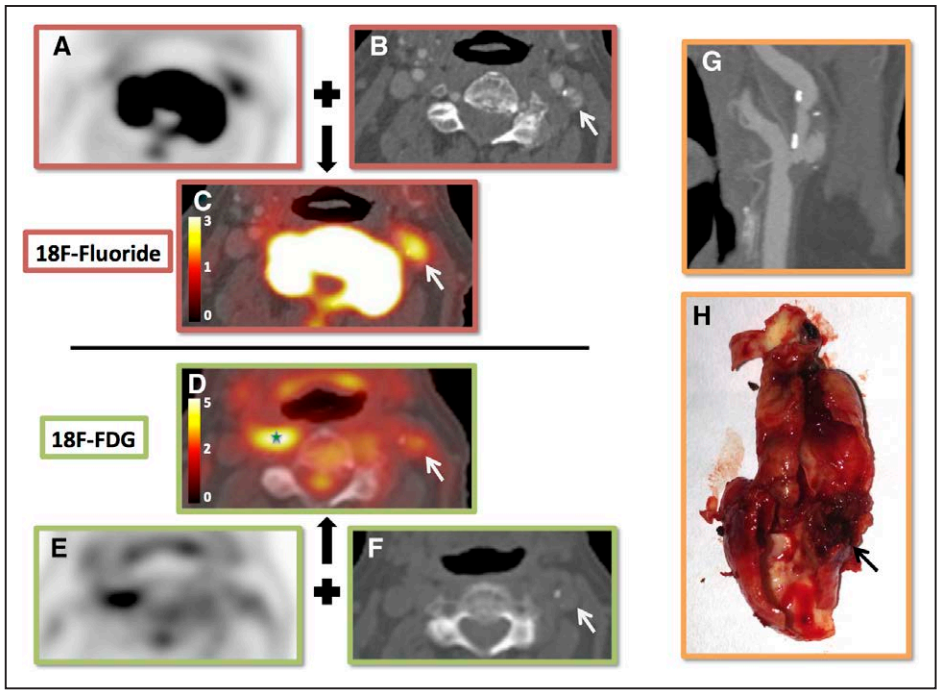

Figure 1. ^{18}F-Fluoride and ^{18}F-fluorodeoxyglucose (FDG) positron emission tomography of carotid arteries. Example of ^{18}F-fluoride (**A**, **B**, **C**) and ^{18}F-FDG (**D**, **E**, **F**) positron emission tomography (PET)/computed tomography (CT) of 1 patient before surgery for symptomatic carotid stenosis. **A**, ^{18}F-Fluoride PET axial slice. **B**, Registered CT angiogram axial slice. **C**, Fused PET/CT image. White arrow, Ruptured plaque showing ^{18}F-fluoride uptake. **D**–**F**, Same slice but with ^{18}F-FDG. Culprit shows uptake, but the contralateral side is obscured by uptake in the right longus colli (green star). An oblique computed tomography carotid angiogram reformat of the culprit (**G**). The operative specimen (**H**).

fitted and an attenuation-correction CT scan was performed. This was followed by PET acquisition covering 2 similar bed positions to the ^{18}F-FDG scan allowing 15 minutes per bed. A subset of 5 patients underwent fully dynamic ^{18}F-fluoride PET/CT with pharmacokinetic analysis as described previously.[24] Dynamic PET provides a quantitative assessment of uptake and these data were used to validate the semiquantitative static imaging data.

After PET acquisition, a CT carotid angiogram was performed without moving the subject (Care Dose 4D, 120 kV, 145 mA, rotation time 0.5 seconds, pitch 0.8. Contrast: 50 mL Niopam 370).

Static PET data were reconstructed using the Siemens UltraHD algorithm: ordered subset expectation maximization+point spread function modeling+time-of-flight; 2 iterations and 21 subsets; matrix size 200×200; 5 mm full-width half-maximum Gaussian smoothing. Dynamic PET data were similarly reconstructed but only using coincident events from the 60- to 75-minute time-bin. Dynamic data were analyzed as reported previously[24] and a K_i value was calculated using Patlak analysis.[27,28]

Tissue Collection, Micro PET/CT, and Histology

At the time of endarterectomy, plaques were collected immediately after excision, photographed, and snap frozen. A random selection (n=8) of specimens was analyzed by micro PET/CT and histology to explore ^{18}F-fluoride binding patterns (see Appendix in the Data Supplement for detailed methods).

Image Analysis

Positron Emission Tomography/Computed Tomography

Static analysis of ^{18}F-FDG and ^{18}F-fluoride uptake was performed on an OsiriX workstation (OsiriX version 3.5.1 64-bit; OsiriX Imaging Software, Geneva, Switzerland). PET/CT data were reviewed alongside the CT angiogram. Scans were qualitatively assessed for registration, image quality, patient movement, and visual evidence of radiotracer uptake. PET and CT data were individually and carefully manually coregistered by lining up fiducial markers apparent on both modalities (eg, cervical spine, mandible and hyoid on ^{18}F-fluoride imaging; skin, spinal cord, and brain on ^{18}F-FDG imaging). No formal inter-PET registration was performed. Three regions of interests (ROIs) were drawn on the carotid of interest on adjacent 3-mm axial slices. If a plaque was present, the ROIs were centered on the area of highest uptake. If there was no plaque, the uptake in the proximal 1 cm of internal carotid artery, just distal to the bifurcation was quantified. From these, standardized uptake values (SUVs; maximum, mean maximum, and mean) were recorded. Blood pool activity was determined from the average of 5 ROIs within the lumen of the superior vena cava to calculate target to background ratios.

Uptake in the proximal left common carotid artery was quantified to explore the relationships between arterial ^{18}F-FDG and ^{18}F-fluoride uptake in a site unaffected by an acute plaque event. Three ROIs were placed around this vessel and uptake was recorded.

Inter- and intraobserver reproducibility of ^{18}F-fluoride uptake measurements were determined using a random selection of 12 patients (24 carotids) by 2 experienced observers (A.T.V., G.S.) who were blinded to the clinical data during analysis.

Computed Tomography

The CT angiogram was assessed for image quality, plaque presence, location, and characteristics. Analysis was undertaken on a cardiovascular workstation (Vital Images, Minnetonka, MN). A blinded and experienced observer (A.V.) performed the semiautomated CT plaque analysis.

Statistical Analysis

Radiotracer uptake, expressed as mean and maximum SUV, was compared between the clinically adjudicated culprit carotid plaque and the contralateral side. Continuous variables are expressed as mean±standard deviation for normally distributed data and median (interquartile range) for skewed distributions. Skewed datasets underwent logarithmic transformation to normalize their distribution. Parametric (unpaired and paired *t*-tests) and nonparametric (Mann–Whitney *U* or Wilcoxon matched-pairs signed rank) tests were used for normally distributed and skewed data, respectively. Categorical

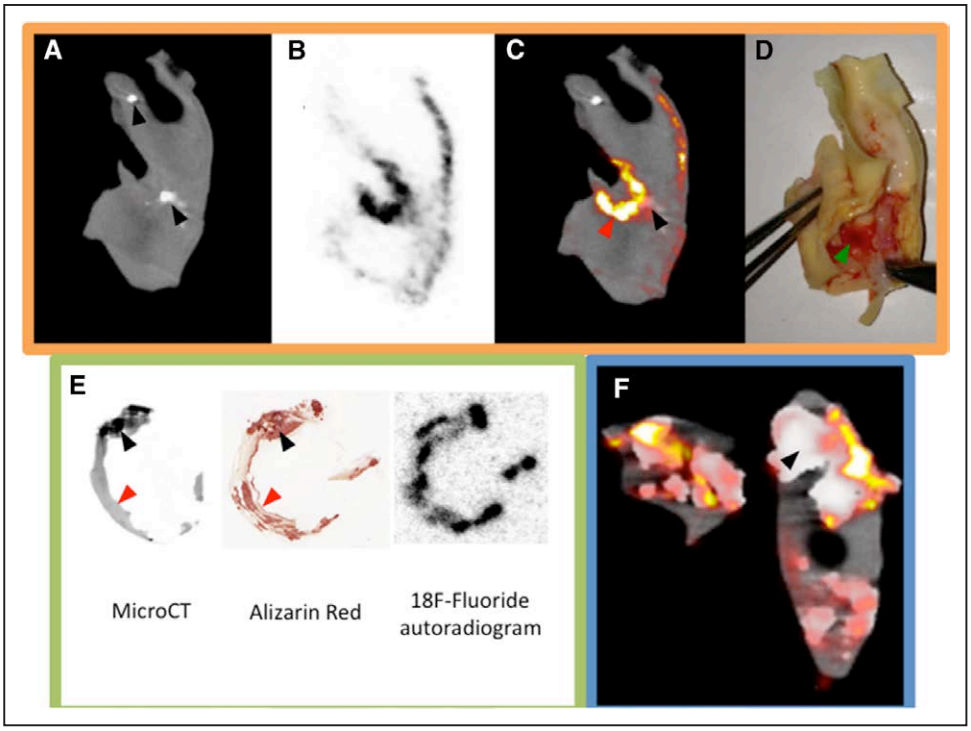

Figure 2. ^{18}F-Fluoride micro positron emission tomography (PET)/computed tomography (CT), autoradiography, and alizarin red staining. Two examples of ex vivo ^{18}F-fluoride micro PET/CT are shown (**A**–**D**, **F**). **A**, Coronal micro CT slice; **B**, corresponding micro PET; **C**, fused image; **D**, the plaque. Green arrow, Adherent thrombus over plaque rupture. Red arrow, Associated area of ^{18}F-fluoride uptake (microcalcification). Black arrows, Areas of macrocalcification showing comparatively little uptake (**A**, **C**, **F**). These examples show that ^{18}F-fluoride provides information of the presence of microcalcification and does not simply highlight all calcification. **E**, An example of micro CT slice registered to an alizarin red-stained section and the corresponding autoradiogram from a specimen that had been incubated whole in ^{18}F-fluoride. It can be seen that the tracer is unable to penetrate the deeper layers of macrocalcification (black arrow), but is able to highlight microcalcification beyond the resolution of even micro CT (red arrow), thus explaining the findings in the micro PET/CT images.

data are presented as n (%) and were compared using Fisher's exact or Chi-squared tests. Correlation was undertaken with either Pearson's r or Spearman's ρ subject to the normality of the variables tested. To quantify inter- and intraobserver reproducibility of ^{18}F-fluoride uptake measurement, the intraclass correlation coefficient was calculated and Bland-Altman analysis was undertaken.

Statistical analyses were performed with the use of SPSS version 18 (SPSS Inc, Chicago, IL) and Graph Pad Prism version 6.0 (GraphPad Software Inc, San Diego, CA). Statistical significance was defined as a 2-sided $P<0.05$.

Results

Study Population

We recruited 26 patients: 18 in the carotid endarterectomy cohort and 8 in the control cohort (Figure I in the Data Supplement). Baseline characteristics (Table 1) were similar in both cohorts. Twenty patients completed all the imaging techniques (Figure 1). A minority did not receive all scans because of the technical and feasibility challenges of completing our multimodality imaging protocol in the very short time frame before surgery. Actual doses and uptake times are specified in Table I in the Data Supplement. There were no adverse events during the study. There were 3 withdrawals.

Micro PET/CT and Histology

^{18}F-Fluoride was observed to selectively highlight areas of pathologically high-risk microcalcification (Figure 2 and Supplementary Movie I in the Data Supplement). Both on autoradiography and micro PET/CT, ^{18}F-fluoride was observed to bind avidly to areas of microcalcification but only to the surface of large volume stable macrocalcifications. Our previous studies[24] would suggest that this was because of the inability of the fluoride ion to penetrate to the deeper layers of a large crystalline mass (with a low surface-area-to-volume ratio). In contradistinction, the powdery deposits of microcalcification (not visible on CT) provide a large area (high surface-area-to-volume ratio) for the fluoride ion to bind.

Imaging

When comparing the ^{18}F-fluoride uptake on static imaging with full dynamic modeling, K_i was most strongly correlated with the SUV_{mean} (r=0.93 [95% confidence interval 0.64–0.99], P=0.001; Figure 3). There were no fixed or proportional biases in the SUV measurements within and between observers (Table II in the Data Supplement). These assessments also demonstrated high intraclass correlation coefficients (all >0.90).

Assessment of Uptake: Culprit Compared With Contralateral and Controls

^{18}F-Fluoride uptake was variably present in most plaques with all culprits showing uptake on visual assessment. In the large majority of patients undergoing carotid endarterectomy who were scanned (87%; 13/15), there was more visual uptake of ^{18}F-fluoride in the culprit compared with the contralateral

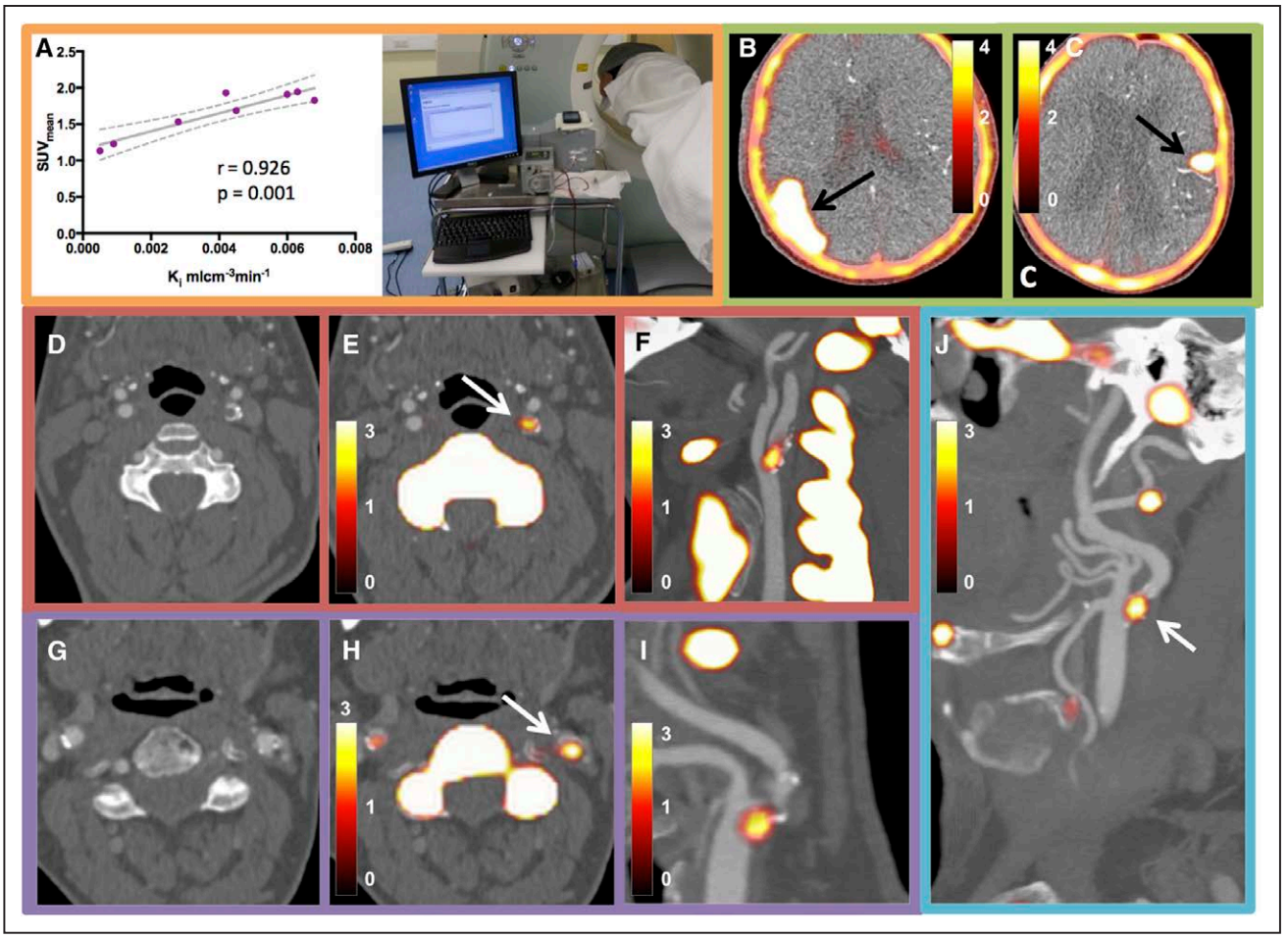

Figure 3. Dynamic positron emission tomography (PET) acquisition and examples of ^{18}F-fluoride uptake. **A**, Correlation between statically derived standardized uptake value (SUV)$_{mean}$ and dynamically measured K_i (dotted line is 95% confidence interval). Photograph shows a dynamic PET study in process. **B**, **C**, ^{18}F-Fluoride uptake into areas of cerebral infarction. **D**–**F**, From 1 patient. **D**, Axial image from computed tomography carotid angiogram; **E**, Fused axial ^{18}F-fluoride PET/computed tomography (CT; white arrow, culprit plaque); **F**, Oblique reconstruction. **G**–**I**, Similar reconstructions from a different patient. **J**, Obliquely reformatted PET/CT image from a patient who developed a fatal stroke (ipsilateral to the lesion marked by a white arrow) 2 weeks after this scan. The contralateral side, which had shown minimal uptake, had been deemed the culprit based on duplex assessment.

side. In the 2 patients without discriminatory uptake, there was heavy uptake bilaterally but more ^{18}F-fluoride uptake on the contralateral side. One patient had grossly ossified carotids and the second, at the time of surgery, was found to have a fibrous stenosis (low signal side) and was subsequently admitted with a fatal ischemic stroke on the contralateral side (high signal side, Figure 3J). ^{18}F-Fluoride uptake was focal and readily identifiable with excellent signal to background discrimination. Spillover from the hyoid bone, thyroid cartilage and cervical vertebrae occasionally made drawing ROI difficult, but only 1 vessel was rendered uninterpretable. On SUV analysis, the clinically adjudicated culprit showed higher uptake than either the paired contralateral ($\log_{10}$SUV$_{mean}$ 0.29±0.10 versus 0.23±0.11, P=0.001) or an unpaired control ($\log_{10}$SUV$_{mean}$ 0.29±0.10 versus 0.12±0.11, P=0.001) irrespective of the method of quantification (Table 2 and Figures 3 and 4).

Of note, in patients with a stroke in whom the imaging extended to encompass the affected territory of the brain (n=3), intense ^{18}F-fluoride uptake was noted in regions of cerebral infarction (SUV$_{mean}$ 4.8±1.98 versus SUV$_{mean}$ of 0.07±0.02 for contralateral noninfarcted brain, P<0.001; Figure 3B and 3C, Movie II in the Data Supplement).

Seven of the 16 culprit carotid plaques demonstrated clear and discernible increased ^{18}F-FDG uptake. However, this uptake was generally more diffuse than ^{18}F-fluoride and analysis was more frequently hampered by overspill from sternocleidomastoid, longus colli, tonsillar tissue, and the submandibular salivary glands (Figure 1). This rendered 5 vessels noninterpretable. In the remaining 4 culprit vessels, no increase in ^{18}F-FDG uptake could be observed. Overall on semiquantitative analysis, ^{18}F-FDG uptake was not higher in the clinically adjudicated culprit compared with either the paired contralateral (SUV$_{mean}$ 1.83±0.55 versus 1.81±0.46, P=0.269) or control vessels (SUV$_{mean}$ 1.83±0.55 versus 2.08±0.33, P=0.269) irrespective of the method of quantification (Table 2 and Figure 4).

Uptake Compared With Plaque Features and Baseline Characteristics

^{18}F-Fluoride uptake was correlated with several plaque characteristics on CT plaque analysis (Table 3). The strongest

Table 2. Radiotracer Uptake: Comparative Data

	Culprit Vessel	Contralateral Vessel	*P* Value for Culprit vs Contralateral	Control	*P* Value for Culprit vs Control
^{18}F-Fluoride					
SUV_{max}	2.56 (2.35–3.54)	2.18 (1.94–3.01)	*	1.78 (1.55–2.22)	*
$SUV_{meanmax}$	2.42 (2.24–3.24)	1.97 (1.78–2.74)	*	1.67 (1.41–2.08)	*
SUV_{mean}	1.92 (1.71–2.46)	1.64 (1.39–1.98)	*	1.41 (1.10–1.53)	*
TBR_{max}	2.75 (2.39–3.21)	2.42 (2.02–2.82)	*	2.44 (1.715–2.48)	*
$TBR_{meanmax}$	2.61 (2.24–2.90)	2.32 (1.74–2.58)	*	2.29 (1.61–2.37)	*
TBR_{mean}	1.96 (1.62–2.22)	1.71 (1.38–1.86)	*	1.67 (1.28–1.95)	*
$Log_{10}SUV_{max}$	0.44±0.14	0.38±0.16	0.013	0.25±0.09	<0.001
$Log_{10}SUV_{meanmax}$	0.42±0.13	0.34±0.15	0.005	0.22±0.10	<0.001
$Log_{10}SUV_{mean}$	0.29±0.10	0.23±0.11	0.001	0.12±0.11	<0.001
$Log_{10}TBR_{max}$	0.45±0.13	0.39±0.13	0.014	0.31±0.15	0.016
$Log_{10}TBR_{meanmax}$	0.43±0.13	0.35±0.12	0.005	0.28±0.15	0.014
$Log_{10}TBR_{mean}$	0.30±0.12	0.24±0.11	0.001	0.18±0.13	0.029
^{18}F-FDG					
SUV_{max}	2.32±0.78	2.32±0.77	0.675	2.61±0.53	0.375
$SUV_{meanmax}$	2.21±0.72	2.24±0.74	0.755	2.51±0.46	0.317
SUV_{mean}	1.83±0.55	1.81±0.46	0.346	2.08±0.33	0.269
TBR_{max}	1.88±0.31	1.81±0.31	0.496	1.86±0.27	0.848
$TBR_{meanmax}$	1.80±0.29	1.74±0.29	0.554	1.79±0.20	0.925
TBR_{mean}	1.49±0.19	1.44±0.19	0.358	1.48±0.10	0.922

Parametric data presented as mean±SD. Nonparametric data presented as median (IQR). FDG indicates fluorodeoxyglucose; SUV, standardized uptake value; TBR, target to background ratio; and IQR, interquartile range.
*Statistical testing performed on the normalized log_{10} transformed data.

correlation was with the Agatston score (SUV_{mean} r=0.72, P<0.001), although there were also strong correlations with high-risk features such as plaque burden (SUV_{mean} r=0.51, P=0.003) and positive remodeling (wall-distal internal carotid artery lumen ratio, with SUV_{mean} r=0.53, P=0.003).

In terms of baseline cardiovascular risk indices, uptake of both tracers in the vasculature correlated with age (^{18}F-FDG $SUV_{meanmax}$ r=0.48, P=0.037; ^{18}F-fluoride SUV_{mean} r=0.59, P=0.007) and the cardiovascular risk score (^{18}F-FDG $SUV_{meanmax}$ r=0.53, P=0.019; ^{18}F-fluoride SUV_{mean} r=0.65, P=0.002) but neither was associated with serum C-reactive protein concentration.

Discussion

We have shown that the culprit plaques of patients with recent TIA or minor ischemic strokes enhance with ^{18}F-fluoride on PET/CT. Uptake was focal, readily identifiable, and discriminated between culprit and nonculprit. ^{18}F-Fluoride uptake was associated with high-risk plaque phenotype and predicted cardiovascular risk. In contrast, while ^{18}F-FDG uptake was present in plaque and correlated with cardiovascular risk, it was more diffuse and prone to spillover and therefore less discriminatory. ^{18}F-FDG also failed to correlate with established high-risk plaque morphological features.

We have previously shown that ^{18}F-fluoride uptake is associated with increased intraplaque markers of cell death, procalcific proteins, inflammation, and high-risk features in the coronary circulation in vivo and the carotid system ex vivo.[16] Here, we confirm our previous observations[24] (which we have also recently reviewed[29]) that this is explained by the ability of ^{18}F-fluoride to report microcalcification. Why is this the case? Far from a passive and degenerative process, vessel mineralization is a controlled response to a variety of insults, particularly oxidized inflammatory lipid (as in the calcific response to tuberculosis infection where lipid-rich bacterial cell walls become oxidized through leukocyte action). It is therefore perhaps no surprise that direct links between atherosclerosis and the induction of extraskeletal osteogenesis have been identified.[30,31] The presence of cellular necrosis and apoptosis[32] is also likely to potentiate this relationship further. Hydroxyapatite nanocrystals themselves may also further drive the inflammatory cycle by setting up a positive feedback loop of increasing calcification, increasing inflammation, and increasing cell death.[30] Furthermore, by accumulating in the surface of thin fibrous caps, microcalcifications may focally increase mechanical stress and thus promote structural cap failure and plaque rupture.[7,33,34] ^{18}F-Fluoride can demonstrate this pathologically important microscopic calcific response.

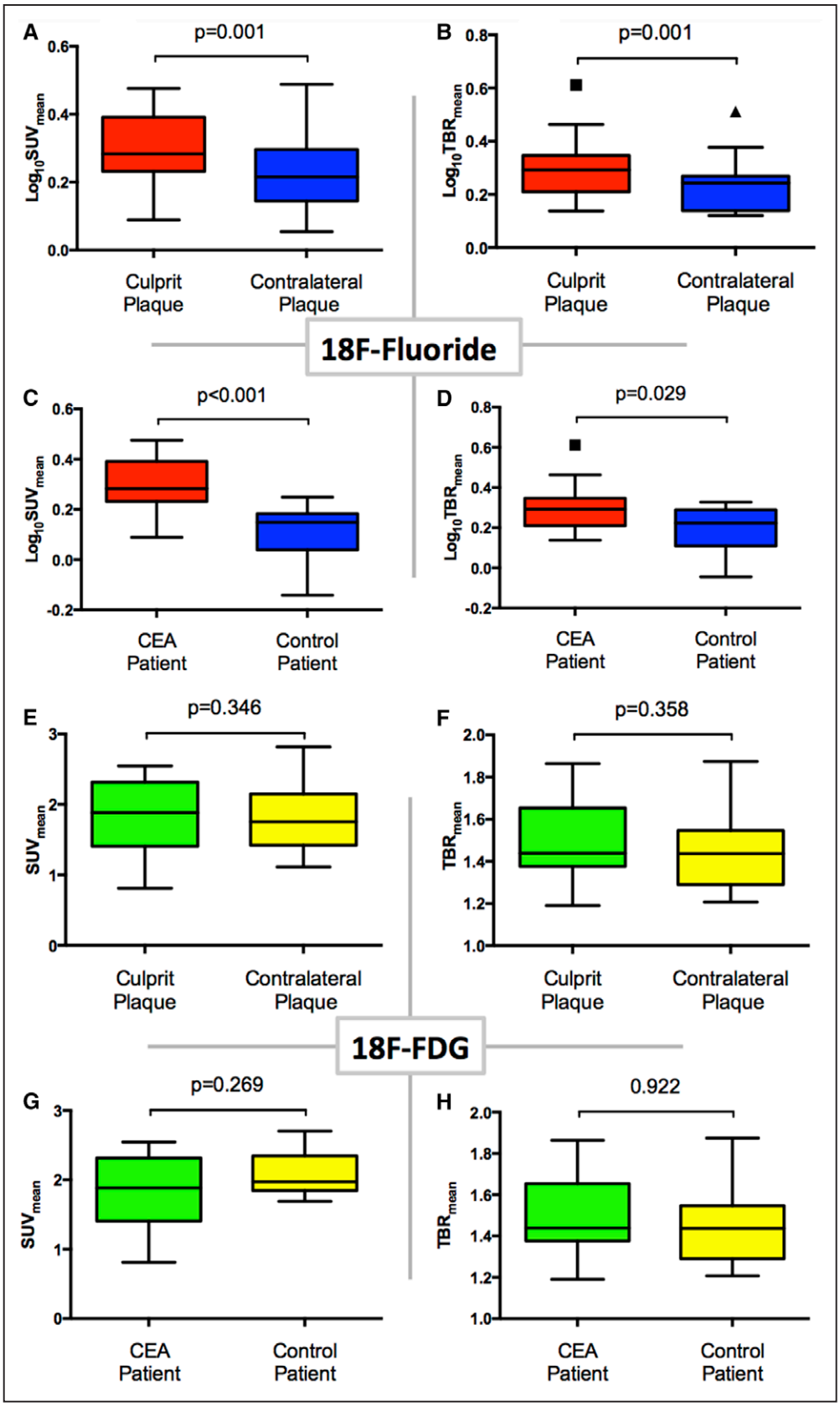

Figure 4. ^{18}F-Fluoride and ^{18}F-fluorodeoxyglucose (FDG) positron emission tomography (PET)/computed tomography uptake. Dynamic PET acquisition and examples of ^{18}F-fluoride uptake. Uptake in clinically adjudicated culprit vs contralateral and vs controls. Tukey box and whisker plots. **A**, **B**, ^{18}F-Fluoride uptake into culprit (red) and contralateral (blue) plaque using the standardized uptake value $(SUV)_{mean}$ and target to background ratio $(TBR)_{mean}$ measurements, respectively. **C**, **D**, Each demonstrate comparison in ^{18}F-fluoride uptake between carotid endarterectomy (CEA) patients (red) and controls (blue); uptake is reported by SUV_{mean} in **C** and TBR_{mean} in **D**. **E**–**H**, The same comparisons but using ^{18}F-FDG.

This is the first observation of ^{18}F-fluoride uptake in necrotic brain tissue and merits consideration. Uptake of this and other bone metabolism markers has previously been observed in tissue necrosis.[33,35] This is likely to be because of cell membrane disruption with influx of calcium and formation of nanoscale calcium phosphate complexes. These offer a substrate to which ^{18}F-fluoride can adsorb, allowing us to visualize the microcalcification associated with necrosis. We have also observed the same process in myocardial tissue postinfarction (Figure II in the Data Supplement).

We confirmed identification of culprit plaque in 2 ways. First, we compared the culprit to the ideal internal control, the contralateral carotid artery (which is almost invariably diseased). Second, we compared the culprit against a valid external control; patients with a TIA or minor ischemic stroke not attributed to carotid plaque. This shows that ^{18}F-fluoride may have real potential in helping to identify culprit plaque thus helping decision-making. This is exemplified by the case where a plaque with high uptake deemed nonculprit subsequently caused a fatal ischemic stroke.

We compared uptake of ^{18}F-fluoride with ^{18}F-FDG. Unlike ^{18}F-fluoride, overall, ^{18}F-FDG uptake was not significantly higher in culprit lesions. Moreover, on a per-lesion basis, ^{18}F-FDG failed to correlate with high-risk plaque morphological features, whereas ^{18}F-fluoride uptake correlated with plaque burden, positive remodeling, and luminal stenosis: all established markers of plaque risk. Other studies have explored the utility of ^{18}F-FDG alone in carotid atherosclerosis[9–11,14,36–39] and a few have directly compared clinical culprit with nonculprit plaques.[8,12,13] Our results are consistent with these previous findings with significant uptake noted in some but not all culprit plaques, in part because of spillover from adjacent muscle. Our observations are also influenced by the ubiquity of statin therapy, potentially blunting ^{18}F-FDG uptake. We did, however, note that proximal carotid uptake correlated with cardiovascular risk indicating that ^{18}F-FDG does reflect a major aspect of vessel pathobiology. As others suggest,[38,40] it may be that ^{18}F-FDG better reflects generalized vascular inflammation and that the relationship between the tracer and a single advanced and acute plaque is more complicated. There are increasing data available concerning other more specific markers of inflammation, such as those targeting the macrophage-specific somatostatin receptor.[41] These will theoretically be less hampered by overspill.

Our findings confirm those of a smaller study of 9 patients by Quirce et al[23] that explored ^{18}F-fluoride and ^{18}F-FDG uptake in symptomatic patients. They showed that ^{18}F-fluoride uptake appeared to be higher in the symptomatic carotid and that 18-FDG uptake was nondiscriminatory. Taken together with our current larger series, this suggests that ^{18}F-fluoride has the potential to be a useful and robust clinical tool to identify culprit atherosclerotic plaque. Vascular ^{18}F-fluoride imaging could therefore guide clinical management better than the current standard of care, and lead to trials of plaque-specific interventions that go beyond simple assessments of anatomic luminal stenosis severity.

Table 3. Plaque Analysis by CT and PET

	All Patients	
Calcium score		
Patients with AC CT usable for calcium score	24	
Carotid bifurcations analyzed for calcium score	48	
Agaston score, AU	164 (5–494)	
Log_{10}Agaston score	1.76±1.13	
Calcium volume, mm^3	150 (15.75–404)	
CT plaque analysis		
Patients with analyzable CT angiogram	17	
Internal carotid artery plaques analyzed	33	
CT diameter stenosis, %	50 (0–77)	
Wall-distal ICA lumen ratio, %	90 (54–173)	
Plaque burden, %	49.4±16.4	
Lipid/necrosis volume, mm^3	37.5 (8.6–79.5)	
Lipid/necrosis % volume	6.7 (2.4–15.8)	
Fibrofatty volume, mm^3	201 (96–313)	
Fibrofatty % volume	42.8±15.6	
Calcium volume, mm^3	211 (124–358)	
Calcium % volume	47.4±20.8	
^{18}F-Fluoride PET SUV_{mean}	1.69 (1.40–2.04)	
	r	*P* Value
vs CT Agatson score	0.79	<0.001
vs CT diameter stenosis	0.54	0.002
vs plaque burden	0.51	0.004
vs wall-distal ICA lumen ratio	0.53	0.003
vs lipid/necrosis volume	0.32	0.080
vs fibrofatty volume	0.29	0.126
vs calcium volume	0.72	<0.001
^{18}F-FDG PET SUV_{mean}	1.92±0.46	
	r	*P* Value
vs CT Agatson score	−0.14	0.469
vs CT diameter stenosis	−0.10	0.620
vs plaque burden	−0.03	0.873
vs wall-distal ICA lumen ratio	0.00	0.996
vs lipid/necrosis volume	−0.19	0.315
vs fibrofatty volume	−0.15	0.457
vs calcium volume	0.01	0.918

Parametric data presented as mean±SD. Nonparametric data presented as median (IQR). AC indicates attenuation correction; AU; arbitrary units; CT, computed tomography; FDG, fluorodeoxyglucose; ICA, internal carotid artery; IQR, interquartile range; PET, positron emission tomography; and SUV, standardized uptake value.

Limitations

This was a small pilot observational study (recruitment is very challenging given the time pressure to intervene) and findings should be regarded as preliminary. The true utility of ^{18}F-fluoride PET/CT will need to be evaluated by prospective studies with patients randomized to intervention based on imaging. ^{18}F-Fluoride PET/CT will need to be

compared with other techniques[42] (in particular MR or PET/MR) which have the advantages of improved soft tissue definition, reduced radiation, and lack of iodinated contrast. We did not perform prolonged-delayed ^{18}F-FDG imaging which some authors have suggested is advantageous.[43] We also acknowledge that quantitative vascular PET has some potential limitations because of the partial volume effects of small vascular structures. Finally, as vascular ^{18}F-fluoride imaging is developed, consideration must be given to harmonizing acquisition and reconstruction protocols,[44] as well as achieving consensus on the uptake parameter of choice (SUV versus target to background ratio versus volumetric parameters[45]) and whether to use manual or automated methods to define ROI. This will reduce variation between scanners and research groups and permit meaningful multicenter studies.

Conclusion

We have shown that ^{18}F-fluoride PET/CT is able to identify culprit or high-risk carotid plaque. In comparison, ^{18}F-FDG, the most widely used tracer in cardiovascular PET imaging, did not reliably identify culprit plaque and did not correlate with high-risk morphological features. ^{18}F-Fluoride PET has major potential to improve how we assess and manage the risk of stroke in patients with atherosclerosis.

Acknowledgments

We acknowledge the help and support of the vascular surgical staff at the Royal Infirmary of Edinburgh and the radiography and radiochemistry staff of the Clinical Research Imaging Centre.

Sources of Funding

Dr Vesey and the study were funded by program grants from the British Heart Foundation (PG12/8/29371) and Chest Heart and Stroke Scotland (R13/A147). Dr Jenkins, Vesey, Dweck, and Newby are supported by the British Heart Foundation (FS/14/78/31020, CH/09/002) and the Wellcome Trust (WT103782AIA). Dr Dweck is the recipient of the Sir Jules Thorn Biomedical Research Award 2015. The Wellcome Trust Clinical Research Facility and the Clinical Research Imaging Centre are supported by National Health Service (NHS) Research Scotland (NRS) through NHS Lothian. Dr Beek is supported by the Scottish Imaging Network—a Platform of Scientific Excellence (SINAPSE). Dr Rudd is part-supported by the National Institute for Health Research Cambridge Biomedical Research Centre, the British Heart Foundation, and the Wellcome Trust.

Disclosures

None.

References

1. Rothwell PM, Eliasziw M, Gutnikov SA, Fox AJ, Taylor DW, Mayberg MR, Warlow CP, Barnett HJ; Carotid Endarterectomy Trialists' Collaboration. Analysis of pooled data from the randomised controlled trials of endarterectomy for symptomatic carotid stenosis. *Lancet*. 2003;361:107–116.
2. Rerkasem K, Rothwell PM. Carotid endarterectomy for symptomatic carotid stenosis. *Cochrane Database Syst Rev* 2011; CD001081.
3. Chambers BR, Donnan GA. Carotid endarterectomy for asymptomatic carotid stenosis. *Cochrane Database Syst Rev* 2005; CD001923.
4. Stone GW, Maehara A, Lansky AJ, de Bruyne B, Cristea E, Mintz GS, Mehran R, McPherson J, Farhat N, Marso SP, Parise H, Templin B, White R, Zhang Z, Serruys PW; PROSPECT Investigators. A prospective natural-history study of coronary atherosclerosis. *N Engl J Med*. 2011;364:226–235. doi: 10.1056/NEJMoa1002358.
5. Libby P. Inflammation in atherosclerosis. *Arterioscler Thromb Vasc Biol*. 2012;32:2045–2051. doi: 10.1161/ATVBAHA.108.179705.
6. Libby P. Mechanisms of acute coronary syndromes and their implications for therapy. *N Engl J Med*. 2013;368:2004–2013. doi: 10.1056/NEJMra1216063.
7. Ewence AE, Bootman M, Roderick HL, Skepper JN, McCarthy G, Epple M, Neumann M, Shanahan CM, Proudfoot D. Calcium phosphate crystals induce cell death in human vascular smooth muscle cells: a potential mechanism in atherosclerotic plaque destabilization. *Circ Res*. 2008;103:e28–e34. doi: 10.1161/CIRCRESAHA.108.181305.
8. Rudd JH, Warburton EA, Fryer TD, Jones HA, Clark JC, Antoun N, Johnström P, Davenport AP, Kirkpatrick PJ, Arch BN, Pickard JD, Weissberg PL. Imaging atherosclerotic plaque inflammation with [18F]-fluorodeoxyglucose positron emission tomography. *Circulation*. 2002;105:2708–2711.
9. Tawakol A, Migrino RQ, Bashian GG, Bedri S, Vermylen D, Cury RC, Yates D, LaMuraglia GM, Furie K, Houser S, Gewirtz H, Muller JE, Brady TJ, Fischman AJ. *In vivo* 18F-fluorodeoxyglucose positron emission tomography imaging provides a noninvasive measure of carotid plaque inflammation in patients. *J Am Coll Cardiol*. 2006;48:1818–1824. doi: 10.1016/j.jacc.2006.05.076.
10. Tawakol A, Migrino RQ, Hoffmann U, Abbara S, Houser S, Gewirtz H, Muller JE, Brady TJ, Fischman AJ. Noninvasive *in vivo* measurement of vascular inflammation with F-18 fluorodeoxyglucose positron emission tomography. *J Nucl Cardiol*. 2005;12:294–301.
11. Fayad ZA, Mani V, Woodward M, Kallend D, Bansilal S, Pozza J, Burgess T, Fuster V, Rudd JH, Tawakol A, Farkouh ME. Rationale and design of dal-PLAQUE: a study assessing efficacy and safety of dalcetrapib on progression or regression of atherosclerosis using magnetic resonance imaging and 18F-fluorodeoxyglucose positron emission tomography/computed tomography. *Am Heart J*. 2011;162:214–221.e2. doi: 10.1016/j.ahj.2011.05.006.
12. Davies JR, Rudd JH, Fryer TD, Graves MJ, Clark JC, Kirkpatrick PJ, Gillard JH, Warburton EA, Weissberg PL. Identification of culprit lesions after transient ischemic attack by combined 18F fluorodeoxyglucose positron-emission tomography and high-resolution magnetic resonance imaging. *Stroke*. 2005;36:2642–2647. doi: 10.1161/01.STR.0000190896.67743.b1.
13. Marnane M, Merwick A, Sheehan OC, Hannon N, Foran P, Grant T, Dolan E, Moroney J, Murphy S, O'Rourke K, O'Malley K, O'Donohoe M, McDonnell C, Noone I, Barry M, Crowe M, Kavanagh E, O'Connell M, Kelly PJ. Carotid plaque inflammation on 18F-fluorodeoxyglucose positron emission tomography predicts early stroke recurrence. *Ann Neurol*. 2012;71:709–718. doi: 10.1002/ana.23553.
14. Tahara N, Kai H, Ishibashi M, Nakaura H, Kaida H, Baba K, Hayabuchi N, Imaizumi T. Simvastatin attenuates plaque inflammation: evaluation by fluorodeoxyglucose positron emission tomography. *J Am Coll Cardiol*. 2006;48:1825–1831. doi: 10.1016/j.jacc.2006.03.069.
15. Dweck MR, Chow MW, Joshi NV, Williams MC, Jones C, Fletcher AM, Richardson H, White A, McKillop G, van Beek EJ, Boon NA, Rudd JH, Newby DE. Coronary arterial 18F-sodium fluoride uptake: a novel marker of plaque biology. *J Am Coll Cardiol*. 2012;59:1539–1548. doi: 10.1016/j.jacc.2011.12.037.
16. Joshi NV, Vesey AT, Williams MC, Shah AS, Calvert PA, Craighead FH, Yeoh SE, Wallace W, Salter D, Fletcher AM, van Beek EJ, Flapan AD, Uren NG, Behan MW, Cruden NL, Mills NL, Fox KA, Rudd JH, Dweck MR, Newby DE. 18F-fluoride positron emission tomography for identification of ruptured and high-risk coronary atherosclerotic plaques: a prospective clinical trial. *Lancet*. 2014;383:705–713. doi: 10.1016/S0140-6736(13)61754-7.
17. Dweck MR, Jones C, Joshi NV, Fletcher AM, Richardson H, White A, Marsden M, Pessotto R, Clark JC, Wallace WA, Salter DM, McKillop G, van Beek EJ, Boon NA, Rudd JH, Newby DE. Assessment of valvular calcification and inflammation by positron emission tomography in patients with aortic stenosis. *Circulation*. 2012;125:76–86. doi: 10.1161/CIRCULATIONAHA.111.051052.
18. Dweck MR, Jenkins WS, Vesey AT, Pringle MA, Chin CW, Malley TS, Cowie WJ, Tsampasian V, Richardson H, Fletcher A, Wallace WA, Pessotto R, van Beek EJ, Boon NA, Rudd JH, Newby DE. 18F-sodium fluoride uptake is a marker of active calcification and disease progression in patients with aortic stenosis. *Circ Cardiovasc Imaging*. 2014;7:371–378. doi: 10.1161/CIRCIMAGING.113.001508.
19. Beheshti M, Saboury B, Mehta NN, Torigian DA, Werner T, Mohler E, Wilensky R, Newberg AB, Basu S, Langsteger W, Alavi A. Detection and global quantification of cardiovascular molecular calcification by fluoro18-fluoride positron emission tomography/computed tomography–a novel concept. *Hell J Nucl Med*. 2011;14:114–120.
20. Hyafil F, Messika-Zeitoun D, Burg S, Rouzet F, Benali K, Iung B, Vahanian A, Le Guludec D. Detection of 18fluoride sodium accumulation

by positron emission tomography in calcified stenotic aortic valves. *Am J Cardiol*. 2012;109:1194–1196. doi: 10.1016/j.amjcard.2011.11.060.
21. Li Y, Berenji GR, Shaba WF, Tafti B, Yevdayev E, Dadparvar S. Association of vascular fluoride uptake with vascular calcification and coronary artery disease. *Nucl Med Commun*. 2012;33:14–20. doi: 10.1097/MNM.0b013e32834c187e.
22. Quirce R, Martínez-Rodríguez I, De Arcocha Torres M, Jiménez-Bonilla JF, Banzo I, Rebollo M, Revilla MA, Palacio E, Rubio-Vassallo A, Ortega-Nava F, Del Castillo-Matos R, Carril JM. Contribution of 18F-sodium fluoride PET/CT to the study of the carotid atheroma calcification. *Rev Esp Med Nucl Imagen Mol*. 2013;32:22–25. doi: 10.1016/j.remn.2012.08.003.
23. Quirce R, Martínez-Rodríguez I, Banzo I, Jiménez-Bonilla J, Martínez-Amador N, Ibáñez-Bravo S, López-Defilló J, Jiménez-Alonso M, Revilla MA, Carril JM. New insight of functional molecular imaging into the atheroma biology: 18F-NaF and 18F-FDG in symptomatic and asymptomatic carotid plaques after recent CVA. Preliminary results. *Clin Physiol Funct Imaging*. 2016;36:499–503. doi: 10.1111/cpf.12254.
24. Irkle A, Vesey AT, Lewis DY, Skepper JN, Bird JL, Dweck MR, Joshi FR, Gallagher FA, Warburton EA, Bennett MR, Brindle KM, Newby DE, Rudd JH, Davenport AP. Identifying active vascular microcalcification by (18)F-sodium fluoride positron emission tomography. *Nat Commun*. 2015;6:7495. doi: 10.1038/ncomms8495.
25. North American Symptomatic Carotid Endarterectomy Trial Collaborators. Beneficial effect of carotid endarterectomy in symptomatic patients with high-grade carotid stenosis. *N Engl J Med*. 1991;325:445–453.
26. de la Iglesia B, Potter JF, Poulter NR, Robins MM, Skinner J. Performance of the ASSIGN cardiovascular disease risk score on a UK cohort of patients from general practice. *Heart*. 2011;97:491–499. doi: 10.1136/hrt.2010.203364.
27. Patlak CS, Blasberg RG, Fenstermacher JD. Graphical evaluation of blood-to-brain transfer constants from multiple-time uptake data. *J Cereb Blood Flow Metab*. 1983;3:1–7. doi: 10.1038/jcbfm.1983.1.
28. Patlak CS, Blasberg RG. Graphical evaluation of blood-to-brain transfer constants from multiple-time uptake data. Generalizations. *J Cereb Blood Flow Metab*. 1985;5:584–590. doi: 10.1038/jcbfm.1985.87.
29. Dweck MR, Aikawa E, Newby DE, Tarkin JM, Rudd JH, Narula J, Fayad ZA. Noninvasive molecular imaging of disease activity in atherosclerosis. *Circ Res*. 2016;119:330–340. doi: 10.1161/CIRCRESAHA.116.307971.
30. Sage AP, Tintut Y, Demer LL. Regulatory mechanisms in vascular calcification. *Nat Rev Cardiol*. 2010;7:528–536. doi: 10.1038/nrcardio.2010.115.
31. Aikawa E, Nahrendorf M, Figueiredo JL, Swirski FK, Shtatland T, Kohler RH, Jaffer FA, Aikawa M, Weissleder R. Osteogenesis associates with inflammation in early-stage atherosclerosis evaluated by molecular imaging in vivo. *Circulation*. 2007;116:2841–2850. doi: 10.1161/CIRCULATIONAHA.107.732867.
32. Proudfoot D, Skepper JN, Hegyi L, Bennett MR, Shanahan CM, Weissberg PL. Apoptosis regulates human vascular calcification *in vitro*: evidence for initiation of vascular calcification by apoptotic bodies. *Circ Res*. 2000;87:1055–1062.
33. Maldonado N, Kelly-Arnold A, Vengrenyuk Y, Laudier D, Fallon JT, Virmani R, Cardoso L, Weinbaum S. A mechanistic analysis of the role of microcalcifications in atherosclerotic plaque stability: potential implications for plaque rupture. *Am J Physiol Heart Circ Physiol*. 2012;303:H619–H628. doi: 10.1152/ajpheart.00036.2012.
34. Bobryshev YV, Killingsworth MC, Lord RS, Grabs AJ. Matrix vesicles in the fibrous cap of atherosclerotic plaque: possible contribution to plaque rupture. *J Cell Mol Med*. 2008;12:2073–2082. doi: 10.1111/j.1582-4934.2008.00230.x.
35. Wang Y-F, Lin T-K, Chuang M-H. Myocardial infarction: an incidental finding on bone scintigraphy. *Tzu Chi Med J*. 2002;14:49–53.
36. Graebe M, Pedersen SF, Borgwardt L, Højgaard L, Sillesen H, Kjaer A. Molecular pathology in vulnerable carotid plaques: correlation with [18]-fluorodeoxyglucose positron emission tomography (FDG-PET). *Eur J Vasc Endovasc Surg*. 2009;37:714–721. doi: 10.1016/j.ejvs.2008.11.018.
37. Pedersen SF, Graebe M, Fisker Hag AM, Højgaard L, Sillesen H, Kjaer A. Gene expression and 18FDG uptake in atherosclerotic carotid plaques. *Nucl Med Commun*. 2010;31:423–429. doi: 10.1097/MNM.0b013e32833767e0.
38. Moustafa RR, Izquierdo-Garcia D, Fryer TD, Graves MJ, Rudd JH, Gillard JH, Weissberg PL, Baron JC, Warburton EA. Carotid plaque inflammation is associated with cerebral microembolism in patients with recent transient ischemic attack or stroke: a pilot study. *Circ Cardiovasc Imaging*. 2010;3:536–541. doi: 10.1161/CIRCIMAGING.110.938225.
39. Figueroa AL, Subramanian SS, Cury RC, Truong QA, Gardecki JA, Tearney GJ, Hoffmann U, Brady TJ, Tawakol A. Distribution of inflammation within carotid atherosclerotic plaques with high-risk morphological features: a comparison between positron emission tomography activity, plaque morphology, and histopathology. *Circ Cardiovasc Imaging*. 2012;5:69–77. doi: 10.1161/CIRCIMAGING.110.959478.
40. Joshi F, Rosenbaum D, Bordes S, Rudd JH. Vascular imaging with positron emission tomography. *J Intern Med*. 2011;270:99–109. doi: 10.1111/j.1365-2796.2011.02392.x.
41. Pedersen SF, Sandholt BV, Keller SH, Hansen AE, Clemmensen AE, Sillesen H, Højgaard L, Ripa RS, Kjær A. 64Cu-DOTATATE PET/MRI for detection of activated macrophages in carotid atherosclerotic plaques: studies in patients undergoing endarterectomy. *Arterioscler Thromb Vasc Biol*. 2015;35:1696–1703. doi: 10.1161/ATVBAHA.114.305067.
42. Naylor AR, Sillesen H, Schroeder TV. Clinical and imaging features associated with an increased risk of early and late stroke in patients with symptomatic carotid disease. *Eur J Vasc Endovasc Surg*. 2015;1–11.
43. Blomberg BA, Akers SR, Saboury B, Mehta NN, Cheng G, Torigian DA, Lim E, Del Bello C, Werner TJ, Alavi A. Delayed time-point 18F-FDG PET CT imaging enhances assessment of atherosclerotic plaque inflammation. *Nucl Med Commun*. 2013;34:860–867. doi: 10.1097/MNM.0b013e3283637512.
44. Huet P, Burg S, Le Guludec D, Hyafil F, Buvat I. Variability and uncertainty of 18F-FDG PET imaging protocols for assessing inflammation in atherosclerosis: suggestions for improvement. *J Nucl Med*. 2015;56:552–559. doi: 10.2967/jnumed.114.142596.
45. Mehta NN, Torigian DA, Gelfand JM, Saboury B, Alavi A. Quantification of atherosclerotic plaque activity and vascular inflammation using [18-F] fluorodeoxyglucose positron emission tomography/computed tomography (FDG-PET/CT). *J Vis Exp*. 2012:e3777–e3777.

CLINICAL PERSPECTIVE

Stroke remains the leading global cause of disability and is responsible for huge healthcare costs. It is commonly caused by thromboembolism from extracranial atherosclerotic plaque. In addition to medical therapy, invasive carotid artery intervention (by endarterectomy or stenting) has a role in reducing the chances of subsequent stroke. However, intervention itself is associated with significant risk and the decision to proceed with surgery is still based principally on stenosis severity, an outdated parameter. This report shows that by selectively demonstrating intraplaque microcalcification, a pathologically high-risk process that reflects ongoing inflammation and cell death, ^{18}F-fluoride PET/CT may be able to identify plaque at particular risk of causing future stroke. The technique, as part of a multimodal risk stratification strategy, may help to ensure the appropriate planning of surgical intervention. This would potentially avoid unnecessary surgery on quiescent yet tightly stenosed plaques and conversely permit the identification and removal of high-risk plaques that currently do not meet criteria for intervention. ^{18}F-Fluoride PET/CT also offers the possibility of noninvasively assessing the response to existing or novel pharmacological agents permitting the personalization of therapy to maximize benefit and minimize risk of complications.

Circulation
Cardiovascular Imaging

^{18}F-Fluoride and ^{18}F-Fluorodeoxyglucose Positron Emission Tomography After Transient Ischemic Attack or Minor Ischemic Stroke: Case–Control Study

Alex T. Vesey, William S. A. Jenkins, Agnese Irkle,, Alastair Moss, Greg Sng,, Rachael O. Forsythe, Tim Clark, Gemma Roberts, Alison Fletcher, Christophe Lucatelli, James H. F. Rudd, Anthony P. Davenport,, Nicholas L. Mills, Rustam Al-Shahi Salman, Martin Dennis, William N. Whiteley, Edwin J. R. van Beek, Marc R. Dweck and David E. Newby

Circ Cardiovasc Imaging. 2017;10:
doi: 10.1161/CIRCIMAGING.116.004976
Circulation: Cardiovascular Imaging is published by the American Heart Association, 7272 Greenville Avenue, Dallas, TX 75231

Print ISSN: 1941-9651. Online ISSN: 1942-0080

Supplemental Material

Supplemental Methods

Exclusion criteria

A modified Rankin score >3 (due to the burden of participation in those with limited mobility), insulin-dependent diabetes mellitus (due to the variability of 18F-FDG uptake), women of child-bearing potential, severe chronic kidney disease (estimated glomerular filtration rate <30 mL/min/1.73 m^2), known allergy to iodine-based contrast media, prior ipsilateral internal carotid artery intervention, prior neck irradiation, or those unable to provide informed consent.

MicroPET/CT

Carotid artery specimens were stored at -80 degree Celsius following removal during carotid endarterectomy. Thawed non-decalcified carotid artery specimens were incubated for 60 minutes in 18F-sodium fluoride 104.89kBq/mL solution (10.5MBq 18F-NaF in 99.5mLs 0.9% NaCl). Samples were twice washed in 100mLs 0.9% NaCl for 2 minutes to remove unbound 18F-Fluoride. Carotid artery specimens were scanned using high-resolution micro-positron emission tomography and non-contrast computed tomography [50kVp tube voltage, 300msec exposure time] (Mediso nanoScan PET/CT, Mediso Medical Imaging Systems, Hungary). PET-CT images were analysed on an OsiriX workstation (OsiriX version 7.5.1, 64-bit, OsiriX Imaging Software, Geneva, Switzerland).

Autoradiography and Histology

To perform 18F-fluoride autoradiography, 18F-fluoride was diluted to 1 x 10-11 M. Whole carotid plaque specimens were thawed in 5 mL PBS for 1 h, and then placed in 5 mL of the diluted 18F-fluoride solution for 1 h at room temperature. They were then washed in PBS three time and dipped in distilled water. Specimens was then embedded in the OCT Compound (CellPath, Powys, UK) and 20 µm thick, serial sections were cut on a Bright (Huntingdon, UK) cryostat and placed on Superfrost Plus slides (VWR, Lutterworth, UK). After drying, sections were placed on a charged phosphor screen (Perkin Elmer, Waltham, Massachusetts) and left overnight. The next day screens were read using PerkinElmer's Cyclone Plus Phosphor Imager (Waltham, Massachusetts) and data analysed with OptiQuantTM software (Packard Instrument, Meriden, Connecticut).

Alizarin Red (Alfa Aesar, Heysham, UK) was employed to stain calcium. Sections were fixed in acetone (4 °C) for ten minutes then washed in PBS at room temperature. After washing, 300 µL Alizarin Red was applied to each section for one minute. Samples were then transferred to acetone for 1 min, before being washed, in acetone:xylene (50:50) for 1 min. Sections were then incubated in xylene for at least 1 h. Tissue was then mounted using DePeX mounting medium Gurr (VWR, Lutterworth, UK) and glass coverslips (Menzel-Gläser, Braunschweig, Germany) were applied. Slides were imaged using Wild Heerbrugg M3Z microscope (Leica, Heerbrugg, Switzerland).

Supplemental Figures

Supplementary Figure 1: Study Flow Chart

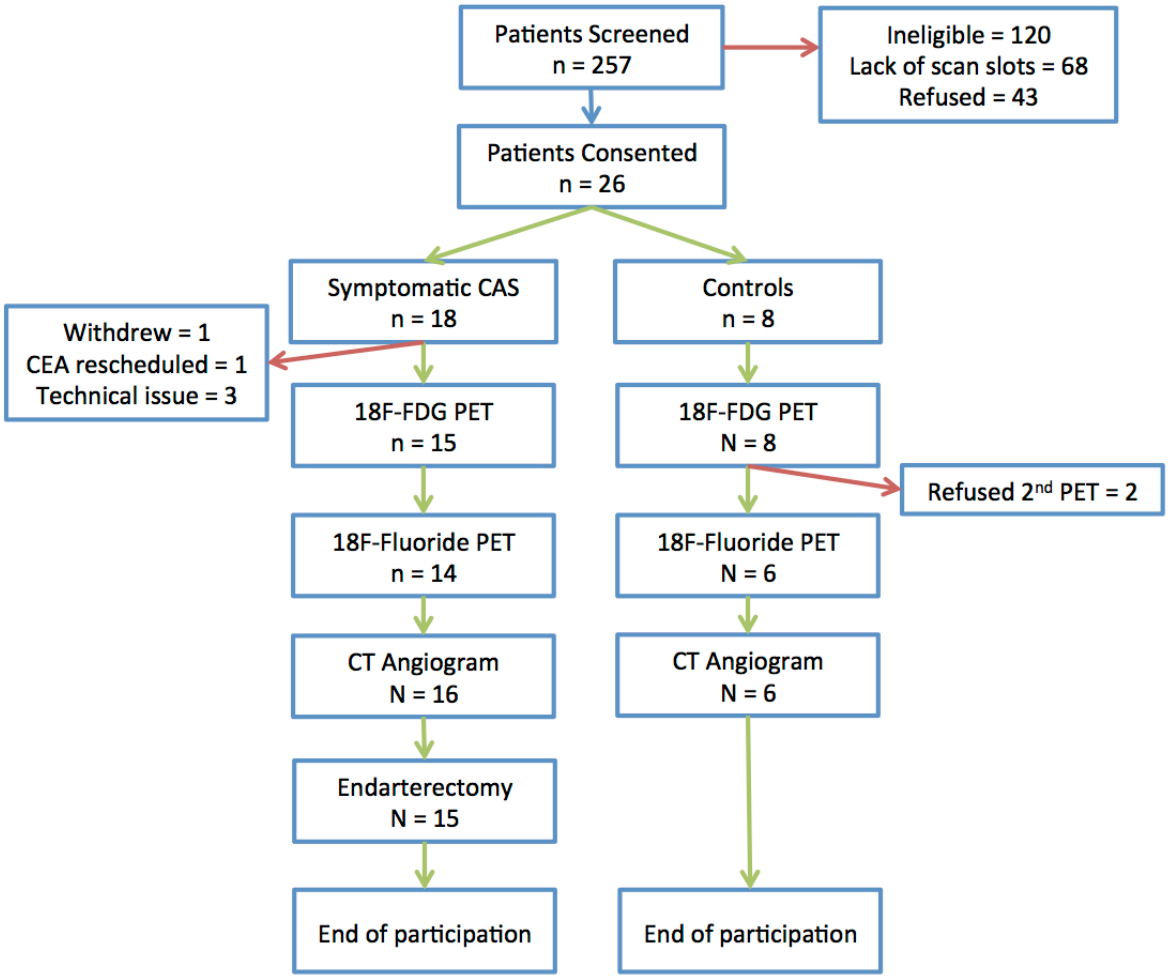

Abbreviations: CAS, carotid artery stenosis, CEA, carotid endarterectomy; CT, computed tomography; FDG, fluorodeoxylucose; PET, positron emission tomography.

Supplementary Figure 2: 18F-Fluoride Uptake in a Patient with a Large Anterior ST-elevation Myocardial Infarction

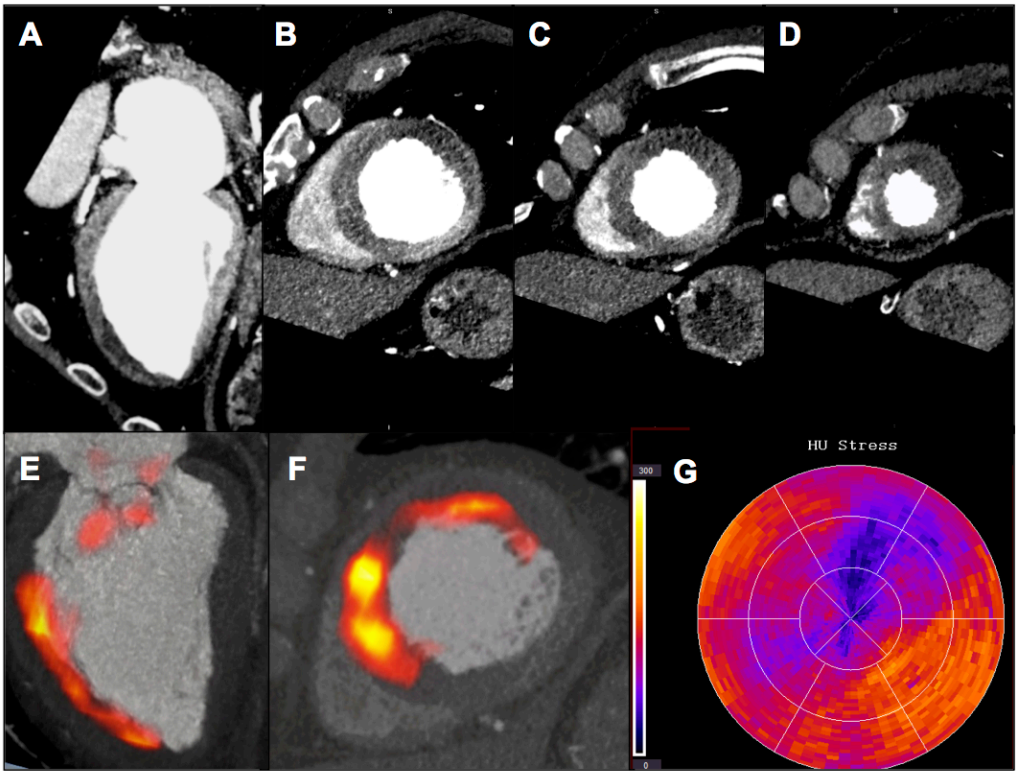

Panels A-D: CT coronary angiogram in long axis (A) and short axis (B-D) reformats. Panels E and F: Fused 18F-fluoride PET CT image in long (E) and short (F) axis reformats. Panel G: 16 segment map of myocardial perfusion during stress. The hypoattenutating, hypoperfused infarcted areas visible on the CT angiogram and perfusion map can be seen to co-localise with intense 18F-fluoride uptake.

Supplementary Tables

Supplementary Table 1: Baseline Scanning Protocol and Radiation Dose Data

	All Patients
Target 18F-FDG Dose (MBq)	200
Actual 18F-FDG Dose (MBq)	199.8 (194.7-203.7)
Actual 18F-FDG Dose range	184-206
Target 18F-Fluoride Dose (MBq)	250
Actual 18F-Fluoride Dose (MBq)	244.5±12.66
Actual 18F-Fluoride Dose range	218 – 266
Target 18F-FDG Uptake Time (min)	90
Actual 18F-FDG Uptake Time	94.1±5.5
Actual 18F-FDG Uptake Time range	84.9-109.8
Target 18F-Fluoride Uptake Time (min)	60
Actual 18F-Fluoride Uptake Time (min)	64.6±5.6
Actual 18F-Fluoride Uptake Time range	56.0 -80.5
Interval between 18F-FDG and 18F-Fluoride (days)	1 (1-2)
Effective Radiation Dose	
Average CT dose (mSv)	4.1
Average dose from 18F-Fluoride (mSv)	5.8
Average dose from 18F-FDG (mSv)	4
Average total dose (mSv)	12.9

Parametric data are presented as mean±SD. Non-parametric data are presented as median(IQR). Categorical data are presented as number (percentage). Abbreviations: FDG, fluorodeoxyglucose; MBq, megabecquerels; MSv, millisieverts. *One patient was accidentally given an oncologic dose (368.9MBq) so the actual 18F-FDG dose data are skewed (this patient has been excluded from the range)

Supplementary Table 2: Interobserver And Intraobserver Reproducibility Studies For 18F-Fluoride Uptake At The Internal Carotid Artery And The Blood Pool

Interobserver	Bias	SD of bias	95% LoA	ICC (95%CI)
ICA SUV_{max}	0.04	0.22	-0.39 – 0.47	0.98 (0.96 – 0.99, p<0.001)
ICA $SUV_{meanmax}$	0.04	0.28	-0.50 – 0.59	0.97 (0.93 – 0.99, p<0.001)
ICA SUV_{mean}	-0.002	0.26	-0.51 – 0.51	0.93 (0.84 – 0.97, p<0.001)
Blood pool SUV_{mean}	0.004	0.18	-0.35 – 0.36	0.85 (0.54 – 0.96, p = 0.001)

Intraobserver	Bias	SD of bias	95% LoA	ICC (95%CI)
ICA SUV_{max}	0.04	0.25	-0.44 – 0.53	0.97 (0.93 – 0.99, p<0.001
ICA $SUV_{meanmax}$	0.01	0.22	-0.41 – 0.44	0.97 (0.94 – 0.99, p<0.001
ICA SUV_{mean}	-0.10	0.15	-0.39 – 0.19	0.97 (0.92 – 0.99, p<0.001
Blood pool SUV_{mean}	0.04	0.12	-0.19 – 0.27	0.96 (0.86 – 0.99, p<0.001

ICC – intra-class correlation co-efficient (calculated used a 2-way random effects model to assess absolute agreement)

Supplementary Movie Titles and Legends

Supplementary Movie 1: Explanted Culprit Carotid Plaques As Seen On 18F-Fluoride MicroPET/CT

Two examples of carotid plaques scanned using 18F-Fluoride microPET/CT. The relationship between calcium deposits visible on microCT and the areas of tracer uptake is clearly complex. The tracer is clearly not merely highlighting areas of calcium, but rather micocalcification not resolved by even microCT.

Supplementary Movie 2: Examples Of 18F-Fluoride Uptake Into Areas Of Cerebral Infarction

Three sequential examples of patients with established cerebral infarction showing intense uptake of 18F-Fluoride. Each patient has a run of 2-dimensional axial fused PET/CT images followed by a 3-dimensional render of the ^{18}F-fluoride uptake. The uptake is remarkably high; greater indeed than the adjacent skull.

Benefits of local anaesthesia for ruptured abdominal aortic aneurysm repair

RO Forsythe and RJ Hinchliffe

Introduction

Ruptured abdominal aortic aneurysms represent the 13th commonest cause of death in the UK, with an overall mortality of over 80%.[1] If untreated, a ruptured abdominal aortic aneurysm is almost always fatal and of those patients who survive long enough to reach hospital, 41.6% are too unwell to undergo attempted repair.[2] Moreover, even if a patient reaches the operating theatre, repair using either open or endovascular (EVAR) techniques carries a high mortality that has seen relatively little improvement over the past few decades.

Conversely, the outcomes of elective abdominal aortic aneurysm repair have shown great improvement, with an operative mortality of 4.3% and 1.8% for open repair and EVAR, respectively.[3]

Given that more than 80% of abdominal aortic aneurysm deaths are the result of rupture,[4] new strategies are required to help address the persistently high mortality associated with this condition.

Recent data from the IMPROVE trial suggest that perioperative mortality for ruptured abdominal aortic aneurysms remains high and that a strategy of using EVAR where possible (compared with open surgery) does not appear to improve 30-day mortality—36.4% *versus* 40.6% in patients with confirmed rupture.[5] In addition, even though the instructions for use are sometimes relaxed in the context of ruptured aneurysms, only around 65% of aneurysms are deemed morphologically suitable for EVAR according to liberal instructions for use (proximal neck length ≥10mm, diameter ≤32mm and angle <60 degrees),[6] yet the mortality for EVAR-suitable patients (who are intrinsically lower risk) remains high at 20–25% for either open or endovascular repair.[7,8]

Whilst the IMPROVE trial did not suggest a significant perioperative survival advantage for an EVAR strategy compared to open repair, it did highlight an important observation—that patients undergoing EVAR under local anaesthesia may be three to four times more likely to survive than those patients requiring general anaesthesia, even after adjustment for age, sex, Hardman index and other potential confounders.[9]

In the elective setting, general anaesthesia has been demonstrated to be an independent risk factor for operative complications including death (OR=5.1, 95% CI 1.9–13.3),[10] whilst the EUROSTAR registry (comprising more than 5,500 patients in 164 centres undergoing EVAR) confirmed that patients appear to

benefit from locoregional anaesthesia in elective EVAR to treat infrarenal abdominal aortic aneurysms.[11] EVAR under local anaesthesia may therefore represent a potential opportunity to reduce the perioperative mortality in ruptured abdominal aortic aneurysms.

Local anaesthesia *versus* general anaesthesia in elective and emergency surgery

There is increasing awareness of the limitations and potential negative impact on outcomes for surgical patients undergoing general anaesthesia, particularly those that are high-risk or with serious comorbidities. The use of alternatives to general anaesthesia (including local and regional anaesthesia), have been explored in various surgical contexts, particularly in the emergency situation. Two substudies of the Swedish Hernia Registry have demonstrated improved outcomes for local anaesthesia in elective and emergency hernia surgery. A multicentre randomised trial comparing local *versus* regional anaesthesia *versus* general anaesthesia included 10 non-specialised hospitals (616 patients) and demonstrated that local anaesthesia was associated with reduced postoperative pain and nausea when compared to general anaesthesia (mean visual analogue scale scores—1.8 vs. 3.3 for pain and 1.1 vs. 1.7 for nausea; $p<0.0001$), a reduced frequency of early postoperative complications (15% vs. 44%; $p<0.0001$) and mean hospital stay (3.1 vs. 6.2 days; $p<0.0001$).[12] Further analysis of the Swedish Hernia Registry (comprising 237 patients who died within 30 days of elective or emergency hernia surgery) demonstrated that local anaesthesia was used rarely for elective operations (3%) but more commonly for emergency operations (13%). Although used less commonly than either general anaesthesia or regional anaesthesia, local anaesthesia was used less frequently in those who subsequently died perioperatively (13% vs. 17% in elective surgery, $p<0.001$; 3% vs. 5% in emergency surgery, $p=0.02$).[13] However, no multivariate analysis was performed in this study, therefore confounding factors may be undetected.

The use of local anaesthesia in patients undergoing surgery for peripheral vascular disease has been of increasing interest in recent years. A post-hoc substudy analysis of a study investigating the use of an endovascular intervention for acute stroke, the NASA (North American Solitaire stent retriever acute stroke) registry, found that local anaesthesia was associated with good 90-day neurological outcomes (modified Rankin Scale ≤2, $p=0.01$, OR 1.4 [1.1–1.8]) and that general anaesthesia was associated with mortality in multivariate analysis (OR 3.3 [1.6–7.1], $p=0.001$), in 281 patients who underwent mechanical embolectomy using the Solitaire stent-retrieving device.[14] In contrast, in the GALA (General anaesthesia *versus* local anaesthesia for carotid surgery) trial (a multicentre randomised controlled trial of 3,526 patients with carotid stenosis), no definite benefit of local anaesthesia was demonstrated; however, three events (stroke, myocardial infarction or death within 30 days) per 1,000 patients were prevented under local anaesthesia, although this finding failed to reach statistical significance.[15] Carotid endarterectomy under local anaesthesia is common practice in many UK vascular centres – a large prospective cohort study in the UK (published in 2011) demonstrated that roughly half of all operations were performed under local anaesthesia, with a conversion to general anaesthesia rate of 1.4%.[16] This number is likely to have increased in the intervening years—local anaesthesia for carotid endarterectomy is clearly tolerated

well by vascular patients, surgeons and anaesthetists and is the best method of intraoperative monitoring of brain function. Therefore, the precedent is set for use in other vascular operations.

Regional anaesthesia (*versus* general anaesthesia) for hip fracture surgery in elderly patients has also been associated with reduced early mortality and fewer postoperative complications such as deep vein thrombosis and acute confusion in at least one large systematic review comprising more than 18,000 patients with hip fractures,[17] although definitive evidence for regional anaesthesia as standard preference to general anaesthesia in hip fracture surgery is limited.

Outcomes of elective EVAR under local anaesthesia

The use of local anaesthesia for elective EVAR has been mooted for over a decade,[18,19] and the benefits of this approach were confirmed in the EUROSTAR registry, where patients undergoing EVAR under local anaesthesia had a shorter operation time (115.7±42.2 minutes vs. 133.3±59.1 minutes, p<0.0001), a shorter hospital stay (3.7±3.1 days vs. 6.2±8.5 days, p=0.007), were less likely to require intensive therapy unit (2% vs. 16.2%, p<0.0001) and had fewer systemic complications (6.6% vs. 13.0%, p=0.0015) than those who underwent EVAR under general anaesthesia,[11] when adjusted for possible confounders. A more recent meta-analysis confirmed that local anaesthesia in elective EVAR is faster than general anaesthesia, associated with reduced postoperative complications but failed to demonstrate a reduction in 30-day mortality.[20] A "local anaesthesia first strategy" may be applied to the majority of patients undergoing elective EVAR and is thought to be feasible in up to 75% of patients with infrarenal abdominal aortic aneurysms, as demonstrated in one observational study of more than 200 patients in a high-volume EVAR centre.[21]

Despite evidence of the feasibility and improved outcomes for elective EVAR under local anaesthesia,[11,20,22] there has not been widespread uptake of the technique, possibly due to the traditional surgical preference for operating under general anaesthesia. Therefore, translating this approach in the setting of ruptured abdominal aortic aneurysms may be arguably more challenging; however, patients with ruptured aneurysms represent the highest risk group who are perhaps more likely to develop complications associated with general anaesthesia. Some highly specialised centres already advocate local anaesthesia for ruptured aneurysms where possible,[23] demonstrating that the majority of their patients have been successfully treated using local anaesthesia, with favourable outcomes.[24] However, there remain no randomised trials to assess the feasibility and effectiveness of EVAR under local anaesthesia for ruptured aneurysms in an unselected population.

Benefits of EVAR under local anaesthesia for ruptured abdominal aortic aneurysms

Observational data suggest that 30-day mortality is reduced for patients who undergo EVAR under local anaesthesia for ruptured abdominal aortic aneurysms, compared to EVAR under general anaesthesia for ruptured aneurysms (13–15% and 33%, respectively; OR 0.27, 95% CI 0.10–0.70).[9] Local anaesthesia in the elective setting is associated with a reduction in cardiac events (0.8% *versus* 6.4%,

p=0.02),22 and whilst this has not been formally investigated in the setting of ruptured abdominal aortic aneurysms, the use of local anaesthesia in other vascular emergencies (such as endovascular intervention for stroke) has been associated with improved cardiovascular outcomes and survival (as demonstrated by the Solitaire registry).[14]

Local anaesthesia can be offered to the sickest patients who would otherwise be turned down for general anaesthesia, which avoids the inherent risks associated with general anaesthesia including the loss of sympathetic and abdominal wall tone on induction and the cardiorespiratory effects of artificial ventilation, whilst increasing the proportion of patients suitable for attempted repair. Spontaneous ventilation during local anaesthesia procedures improves venous return, decreasing pulmonary morbidity[25] and local anaesthesia allows improved immediate postoperative analgesia. Importantly, in the context of ruptured aneurysms, the use of local anaesthesia potentially allows more rapid aneurysm exclusion (haemorrhage control) and reduces the operative duration, which in turn reduces risks of prolonged metabolic disturbance, thromboembolism and increased venous blood loss. A reduction in hospital stay and requirement for intensive therapy unit stay has also been demonstrated in the setting of elective EVAR.[11]

It is important to note that the use of regional anaesthesia is generally regarded as unsuitable in ruptured abdominal aortic aneurysms due to the potential for loss of sympathetic tone and further cardiovascular collapse in the already compromised patient.

Feasibility, technical considerations and drawbacks of EVAR under local anaesthesia in ruptured abdominal aortic aneurysm

Not all patients are suitable for EVAR under local anaesthesia. Firstly, the aneurysm must be morphologically and technically suitable for a bifurcated endograft. Those who require an aortouni-iliac graft and femoro-femoral crossover (to revascularise the contralateral leg) are unsuitable for the local anaesthesia approach; however, this is still a common configuration of stents used in ruptured abdominal aortic aneurysms, especially if the operator is less experienced or the patient particularly unstable—of those patients in the IMPROVE trial who complied with the allocated EVAR-first strategy, 23.3% required an aortouni-iliac graft.[5]

The patient must also be suitable for this approach, which necessitates a compliant, conscious and co-operative patient – which may be challenging in ruptured abdominal aortic aneurysms. The patient also needs to be able to lie flat and comply with regular breath-holding instructions; confusion and agitation associated with hypoxia and metabolic disturbance may impede this. The surgeon needs to be comfortable and confident in obtaining vascular access even in the haemodynamically-compromised patient with potentially impalpable femoral pulses. Access vessels must be readily accessed; patient obesity and narrow access vessels can be a barrier to this; however, improved technology (including narrower delivery systems) has gone some way to address these issues.

Preliminary evidence from the National Vascular Registry suggests that 50% of UK vascular centres currently use local anaesthesia for EVAR of ruptured abdominal aortic aneurysms. In order to provide a successful local anaesthesia

service, an experienced team is required, with adequate training to address the various drawbacks of local anaesthesia for EVAR in ruptured aneurysms.

In addition, good anaesthesia input will be required throughout the procedure, in order to minimise the pain associated with performing an endovascular intervention without general anaesthesia. If extensive groin dissection is required, the pain of the procedure may not be tolerable or may necessitate heavy sedation. However, percutaneous access and the use of closure devices can overcome this problem.

Some patients may experience ongoing and unacceptable abdominal pain from the expanding haematoma, which may subsequently lead to respiratory insufficiency due to increased intra-abdominal pressure causing restriction of chest wall movements. Pain at the time of stent deployment, in addition to ischaemic leg and buttock pain from prolonged occlusion of access vessels, may be difficult to control.

Movement artefact from an awake patient may compromise image quality, as will insufficient breath-holding. In the case of a complex EVAR leading to a longer operative duration, local anaesthesia may not be tolerated for a prolonged period and the cardiovascular instability associated with ruptured aneurysms may cause anaesthesia difficulties that are difficult to address in an awake patient. Finally, the conversion to general anaesthesia in a high-risk patient previously deemed unsuitable for general anaesthesia raises difficult questions; certainly the benefit of local anaesthesia is not sustained in those patients who start local anaesthesia but require conversion to general anaesthesia.

Future prospects

The IMPROVE trial suggests that EVAR, where possible, is associated with faster recovery and cost-effectiveness; therefore increasingly more EVARs are likely to be performed for ruptured aneurysms in the future.[26] In addition, recent data demonstrate an increasing prevalence of acute abdominal aortic aneurysm events in the older population (>75 years of age)[27] who may avoid detection during the single screening ultrasound offered at the age of 65 in the UK. We may therefore see an increasing number of elderly patients presenting with ruptured aneurysms, who are likely to have significant medical comorbidities that contribute to greater perioperative risk and are perhaps the most likely to benefit from EVAR and a local anaesthesia approach.

Better strategies to reduce the stubbornly high mortality associated with ruptured aneurysm intervention are required. The benefits of local anaesthesia for elective EVAR have been widely documented, and observational data for emergency EVAR in favour of local anaesthesia are emerging.

Local anaesthesia is often used for the sickest patients, therefore if there is a survival advantage in this selected group (as suggested in recent literature), this may potentially translate to the entire population and could go some way to address the sustained high mortality associated with ruptured aneurysm intervention.

Local anaesthesia may in future be the first choice approach (where possible) for EVAR in ruptured aneurysms; however, further confirmation should be sought from randomised trials, which should be robustly designed, using an intention-to-treat strategy.

Summary

- An EVAR-first strategy for ruptured abdominal aortic aneurysms is commonly performed; however, the mortality rate remains high.
- Local anaesthesia has been associated with improved clinical outcomes (compared to general anaesthesia) for elective EVAR and other elective and emergency operations.
- Recent observational data suggest a significant reduction in 30-day mortality for local anaesthesia in EVAR for ruptured aneurysms, compared to general anaesthesia.
- Other potential benefits of local anaesthesia in EVAR for ruptured aneurysm include shorter operative time, reduced intensive therapy unit and hospital stay, fewer cardiorespiratory complications and improved postoperative analgesia.
- EVAR for ruptured aneurysms is performed under local anaesthesia in approximately half of the UK vascular centres.
- Robust randomised evidence is required to more fully investigate local anaesthesia as a strategy to improve outcomes in ruptured aneurysms.
- The use of local anaesthesia for ruptured aneurysms may increase the proportion of patients offered repair, and may go some way to improve the stubbornly high mortality associated with intervention.

References

1. Ashton HA, Buxton MJ, Day NE, *et al.* Multicentre Aneurysm Screening Study Group. The Multicentre Aneurysm Screening Study (MASS) into the effect of abdominal aortic aneurysm screening on mortality in men: a randomised controlled trial. *Lancet* 2002; **360**: 1531–39.
2. Karthikesalingam A, Holt PJ, Vidal-Diez A, *et al.* Mortality from ruptured abdominal aortic aneurysms: clinical lessons from a comparison of outcomes in England and the USA. *Lancet* 2014; **383** (9921): 963–69.
3. Greenhalgh RM, Brown LC, Powell JT, *et al.* Endovascular *versus* open repair of abdominal aortic aneurysm. *N Engl J Med* 2010; **362** (20): 1863–71.
4. Anjum A, Allmen von R, Greenhalgh R, *et al.* Explaining the decrease in mortality from abdominal aortic aneurysm rupture. *Br J Surg* 2012; **99** (5): 637–45.
5. IMPROVE Trial Investigators, Powell JT, Sweeting MJ, *et al.* Endovascular or open repair strategy for ruptured abdominal aortic aneurysm: 30 day outcomes from IMPROVE randomised trial. *BMJ* 2014; **348** (jan13 2): f7661–f7661.
6. Schanzer A, Greenberg RK, Hevelone N, *et al.* Predictors of abdominal aortic aneurysm sac enlargement after endovascular repair. *Circulation*. 2011; **123** (24): 2848–55.
7. Reimerink JJ, Hoornweg LL, Vahl AC, *et al.* Endovascular repair *versus* open repair of ruptured abdominal aortic aneurysms: a multicenter randomized controlled trial. *Ann Surg* 2013; **258** (2): 248–56.
8. Desgranges P, Kobeiter H, Katsahian S, *et al.* ECAR: Endosvasculaire vs *Chirurgi*e dans les Anévrysmes Rompus: A French Randomized Controlled Trial of endovascular *versus* open surgical repair of ruptured aorto-iliac aneurysms. *Eur J Vasc Endovasc Surg* 2015; **50**: 303–10.
9. IMPROVE Trial Investigators, Powell JT, Hinchliffe RJ, *et al.* Observations from the IMPROVE trial concerning the clinical care of patients with ruptured abdominal aortic aneurysm. *Br J Surg* 2014; **101** (3): 216–24.
10. Walschot LH, Laheij RJ, Verbeek AL. Outcomes after endovascular abdominal aortic aneurysm repair: a meta-analysis. *J Endovasc Ther* 2002; **9** (1): 82–89.

11. Ruppert V, Leurs LJ, Steckmeier B, *et al.* Influence of anesthesia type on outcome after endovascular aortic aneurysm repair: An analysis based on EUROSTAR data. *J Vasc Surg* 2006; **44** (1): 16–21.e2.
12. Nordin P, Zetterström H, Gunnarsson U, *et al.* Local, regional, or general anaesthesia in groin hernia repair: multicentre randomised trial. *Lancet* 2003; **362** (9387): 853–58.
13. Nilsson H, Nilsson E, Angerås U, *et al.* Mortality after groin hernia surgery: delay of treatment and cause of death. **Hernia** 2011; **15** (3): 301–07.
14. Abou-Chebl A, Zaidat OO, Castonguay AC, *et al.* North American SOLITAIRE Stent-Retriever Acute Stroke Registry: choice of anesthesia and outcomes. *Stroke* 2014; **45** (5): 1396–1401.
15. GALA Trial Collaborative Group. General anaesthesia *versus* local anaesthesia for carotid surgery (GALA): a multicentre, randomised controlled trial. *The Lancet*. 2008; **372** (9656): 2132–42.
16. Rudarakanchana N, Halliday AW, Kamugasha D, *et al.* Current practice of carotid endarterectomy in the UK. *Br J Surg* 2012; **99** (2): 209–16.
17. Luger TJ, Kammerlander C, Gosch M, *et al.* Neuroaxial *versus* general anaesthesia in geriatric patients for hip fracture surgery: does it matter? Osteoporos Int. 2010; **21** (Suppl 4): S555–72.
18. Verhoeven ELG, Cinà CS, Tielliu IFJ, *et al.* Local anesthesia for endovascular abdominal aortic aneurysm repair. *J Vasc Surg* 2005; **42** (3): 402–09.
19. Sadat U, Cooper DG, Gillard JH, *et al.* Impact of the Type of Anesthesia on Outcome after Elective Endovascular Aortic Aneurysm Repair: Literature Review. *Vascular* 2008; **16** (6): 340–45.
20. Karthikesalingam A, Thrumurthy SG, Young EL, *et al.* Locoregional anesthesia for endovascular aneurysm repair. *J Vasc Surg* 2012; **56** (2): 510–19.
21. Geisbüsch P, Katzen BT, Machado R, *et al.* Local anaesthesia for endovascular repair of infrarenal aortic aneurysms. *Eur J Vasc Endovasc Surg* 2011; **42** (4): 467–73.
22. Bakker EJ, Van de Luijtgaarden KM, van Lier F, *et al.* General Anaesthesia is Associated with Adverse Cardiac Outcome after Endovascular Aneurysm Repair. *Eur J Vasc Endovasc Surg* 2012; **44** (2): 121–25.
23. Lachat ML, Pfammatter T, Witzke HJ, *et al.* Endovascular repair with bifurcated stent-grafts under local anaesthesia to improve outcome of ruptured aortoiliac aneurysms. *Eur J Vasc Endovasc Surg* 2002; **23** (6): 528–36.
24. Mayer D, Pfammatter T, Rancic Z, *et al.* 10 Years of Emergency Endovascular Aneurysm Repair for Ruptured Abdominal Aortoiliac Aneurysms: Lessons Learned. *Ann Surg* 2009; **249** (3): 510–15.
25. Edwards MS, Andrews JS, Edwards AF, *et al.* Results of endovascular aortic aneurysm repair with general, regional, and local/monitored anesthesia care in the American College of *Surgeon*s National Surgical Quality Improvement Program database. *J Vasc Surg* 2011; **54** (5): 1273–82.
26. IMPROVE Trial Investigators. Endovascular strategy or open repair for ruptured abdominal aortic aneurysm: one-year outcomes from the IMPROVE randomized trial. *Eur Heart J* 2015; **36** (31): 2061–69.
27. Howard DPJ, Banerjee A, Fairhead JF, *et al.* Age-specific incidence, risk factors and outcome of acute abdominal aortic aneurysms in a defined population. *Br J Surg* 2015; **102**: 907–15

Stirrat et al. Journal of Cardiovascular Magnetic Resonance (2016) 18:46
DOI 10.1186/s12968-016-0261-2

Journal of Cardiovascular Magnetic Resonance

RESEARCH Open Access

Ferumoxytol-enhanced magnetic resonance imaging methodology and normal values at 1.5 and 3T

Colin G. Stirrat[1*], Shirjel R. Alam[1], Thomas J. MacGillivray[2,3], Calum D. Gray[2,3], Rachael Forsythe[1], Marc R. Dweck[1], John R. Payne[4], Sanjay K. Prasad[5], Mark C. Petrie[4], Roy S. Gardner[4], Saeed Mirsadraee[2], Peter A. Henriksen[1], David E. Newby[1,2] and Scott I. K. Semple[1,2]

Abstract

Background: Ultrasmall superparamagnetic particles of iron oxide (USPIO)-enhanced magnetic resonance imaging (MRI) can detect tissue-resident macrophage activity and identify cellular inflammation. Clinical studies using this technique are now emerging. We aimed to report a range of normal R2* values at 1.5 and 3 T in the myocardium and other tissues following ferumoxytol administration, outline the methodology used and suggest solutions to commonly encountered analysis problems.

Methods: Twenty volunteers were recruited: 10 imaged each at 1.5 T and 3 T. T2* and late gadolinium enhanced (LGE) MRI was conducted at baseline with further T2* imaging conducted approximately 24 h after USPIO infusion (ferumoxytol, 4 mg/kg). Regions of interest were selected in the myocardium and compared to other tissues.

Results: Following administration, USPIO was detected by changes in R2* from baseline (1/T2*) at 24 h in myocardium, skeletal muscle, kidney, liver, spleen and blood at 1.5 T, and myocardium, kidney, liver, spleen, blood and bone at 3 T ($p < 0.05$ for all). Myocardial changes in R2* due to USPIO were 26.5 ± 7.3 s-1 at 1.5 T, and 37.2 ± 9.6 s-1 at 3 T ($p < 0.0001$ for both). Tissues showing greatest ferumoxytol enhancement were the reticuloendothelial system: the liver, spleen and bone marrow (216.3 ± 32.6 s-1, 336.3 ± 60.3 s-1, 69.9 ± 79.9 s-1; $p < 0.0001$, $p < 0.0001$, p = ns respectively at 1.5 T, and 275.6 ± 69.9 s-1, 463.9 ± 136.7 s-1, 417.9 ± 370.3 s-1; $p < 0.0001$, $p < 0.0001$, $p < 0.01$ respectively at 3 T).

Conclusion: Ferumoxytol-enhanced MRI is feasible at both 1.5 T and 3 T. Careful data selection and dose administration, along with refinements to echo-time acquisition, post-processing and analysis techniques are essential to ensure reliable and robust quantification of tissue enhancement.

Trial registration: ClinicalTrials.gov Identifier - NCT02319278. Registered 03.12.2014.

Keywords: Cardiac, MRI, Inflammation, USPIO

Background

Iron oxide nanoparticles are a class of magnetic resonance imaging (MRI) contrast agents that are generating interest as a method of detecting tissue inflammation. Historically, these nanoparticles were initially used for gastrointestinal, reticuloendothelial system and lymph node imaging [1–3], and subsequently in hepatic and cardiac imaging [4–7]. Recently however, it is in their use as an MRI contrast agent for detecting tissue-resident macrophages that clinical applications are now emerging [8–15].

T2* MRI has been successfully used for over a decade in diagnosing and grading severity of iron accumulation in transfusion-dependent thalassaemia major, and has been instrumental in guiding therapy that improves prognosis, and allows serial disease monitoring [16, 17]. T2* MRI in the assessment of iron accumulation is easily quantifiable, well validated, highly reproducible, clinically robust, and is achievable in a single breath hold [18–22].

* Correspondence: colin.stirrat@ed.ac.uk
[1]British Heart Foundation/University Centre for Cardiovascular Science, University of Edinburgh, Edinburgh, UK
Full list of author information is available at the end of the article

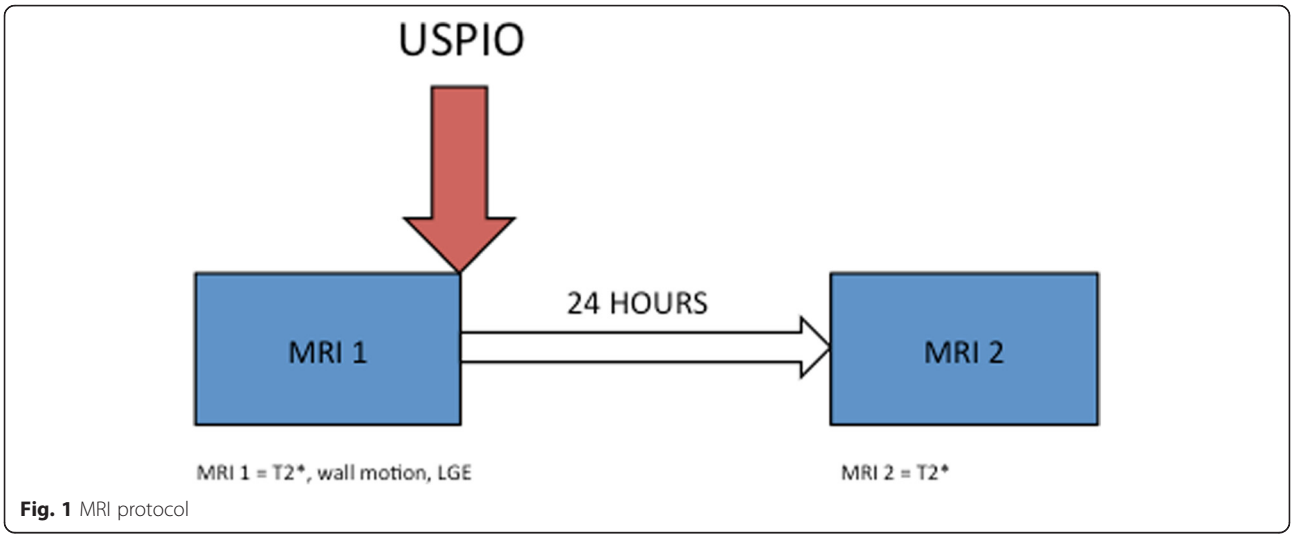

Fig. 1 MRI protocol

Ultrasmall superparamagnetic particles of iron oxide (USPIO) consist of an iron oxide core surrounded by a carbohydrate or polymer coating. These particles can extravasate through damaged capillaries, where they are engulfed and concentrated by tissue-resident macrophages [23]. Gradient echo T2*-weighted (T2*W) sequences are highly sensitive to magnetic field inhomogeneities such as susceptibility artifacts due to the presence of iron, including USPIO. Accumulation of USPIOs in macrophages can be quantified and visualized using T2*W MRI [8, 9] and calculation of, and observing the reduction in, T2* relaxation time due to the presence of iron. Thus USPIO-enhanced MRI can detect tissue-resident macrophage activity and identify localized cellular inflammation within tissues.

In this present study we aimed to observe and quantify the distribution ferumoxytol enhancement following intravenous administration at 1.5 and 3 T MRI and establish a range of normal values for healthy myocardium and other tissue. We also aimed to develop our methodology and describe commonly encountered problems in T2* image analysis of USPIO.

Methods

This was an open-label observational multi-centre cohort study using human volunteers recruited as part of a larger trial, recruiting patients with cardiac inflammation. The study was performed in accordance with the declaration of Helsinki, the approval of the Scotland A research ethics committee, and the written informed consent of all participants.

Subjects

Participants were aged over 18 years of age. Exclusion criteria were contraindication to MRI or ferumoxytol infusion, any systemic inflammatory comorbidity (eg rheumatoid arthritis), renal failure (estimated glomerular filtration rate <30 mL/min), pregnancy, breastfeeding and women of child-bearing age not ensuring reliable contraception.

Magnetic resonance imaging

MRI was performed using 3 T and 1.5 T scanners (Magnetom Verio and Avanto respectively, Siemens Healthcare GmbH, Erlangen, Germany), with dedicated cardiac array coils. All images were acquired using electrocardiogram-gated breath-hold imaging. Routine steady state free precession (TrueFISP) sequences were used to acquire long-axis and short-axis images of the heart. Standard cardiac slice widths (6-mm width with 4-mm gap) and 8 echo times (2.1–17.1 ms range) with matrix size of 256 × 115 were acquired in order to generate T2* maps. The in-plane resolution differed as required for larger or smaller subjects; generally, a field of view of 400 × 300 mm was used with an in-plane resolution of 2.6 × 1.6 mm. T2* relaxation maps were generated before and approximately 24 h after administration of USPIO.

Immediately after the baseline T2* and SSFP cine imaging, breath-held inversion enhancement images were acquired following an intravenous administration of gadolinium contrast medium (0.1 and 0.15 mmol/kg at 3 T and 1.5 T respectively; Gadovist, Bayer Plc, Germany).

Table 1 Participant characteristics

	1.5 T	3 T
Number	9	10
Male;Female	3:6	4:6
Age (years)	52 [45.5–61.5]	50 [45.25–53]
Body-mass Index (kg/m^2)	22.9 [20.1–26.9]	25.9 [22.5–29.4]
Ejection Fraction (%)	63.6 ± 4.9	61.1 ± 4.1

N (%), mean ± SD, or median [interquartile range]

Table 2 Normal values

	1.5 T Pre-USPIO R2*(s^{-1})	1.5 T Post-USPIO R2*(s^{-1})	1.5 T Change R2*(s^{-1})	3 T Pre-USPIO R2*(s^{-1})	3 T Post-USPIO R2*(s^{-1})	1.5 T Change R2*(s^{-1})
Panmyocardial average	33.5 ± 5.4	60.5 ± 7.2	26.5 ± 7.3	46.9 ± 4.1	84.2 ± 12.4	37.2 ± 9.6
Skeletal muscle	34.7 ± 4.2	44.9 ± 4.7	10.2 ± 5.8	55.5 ± 17.1	59.8 ± 6.6	4.3 ± 16.3
Kidney	16.6 ± 2.0	81.2 ± 15.2	64.6 ± 16.1	43.5 ± 39.1	115.2 ± 28.1	71.8 ± 48.8
Liver	36.0 ± 7.2	252.3 ± 34.3	216.3 ± 32.6	65.3 ± 21.2	340.9 ± 57.8	275.6 ± 69.9
Spleen	22.0 ± 7.7	358.3 ± 59.5	336.3 ± 60.3	51.2 ± 21.1	515.1 ± 137.4	463.9 ± 136.7
Blood	11.3 ± 4.1	96.0 ± 26.6	84.7 ± 27.2	18.8 ± 5.3	91.5 ± 20.9	72.6 ± 18.3
Bone	84.4 ± 29.2	154.3 ± 62.0	69.9 ± 79.9	330 ± 168.7	747.9 ± 277.8	417.9 ± 370.3

Mean ± SD

Optimal inversion time (TI) was determined on a slice-by-slice basis using standard late-enhancement TI-scout protocols. The inversion-recovery late-enhancement short-axis slices were acquired using similar slice positions to the myocardial T2* imaging. The T2* acquisitions also included imaging of the liver, spleen and spine to allow quantification of USPIO accumulation within organs of the reticuloendothelial system.

USPIO

Intravenous infusion of USPIO (ferumoxytol, 4 mg/kg; Rienso®, Takeda Italia, Italy) was performed immediately following the baseline magnetic resonance scan over at least 15-min using a concentration of 2–8 mg/mL, diluted in 0.9 % saline or 5 % dextrose. Hemodynamic monitoring was conducted throughout.

Study protocol

Volunteers received 2 MRI scans approximately 24 h apart (Fig. 1).

Image analysis

All T2*-weighted multi-gradient-echo images for each patient were analyzed using Circle CVI software (Circle CVI42, Canada). Regions of interest (ROI) were drawn in the heart using standard cardiac segmentation [24], and panmyocardial values averaged using segments 1–16. Further ROI were drawn in skeletal muscle, kidney, liver, spleen, blood pool (from LV cavity) and bone marrow.

An experimentally determined threshold used in previous work [8] for the coefficient of determination ($r^2 > 0.85$) was used to exclude data that did not have an acceptable exponential decay when signal intensity (SI) was plotted against echo time. The inverse of the mean T2* (R2*) for each ROI was then calculated to assess the uptake of USPIO, where the higher the value, the greater the USPIO accumulation.

Late gadolinium enhancement (LGE), ventricular volume and functional analyses were performed using Circle CVI software (Circle CVI42, Calgary, Canada). T2* data were collected immediately prior to USPIO administration. USPIO-enhanced T2* data were collected 24–25 h following ferumoxytol administration.

Statistical analysis

All statistical analysis was performed with GraphPad Prism, version 6 (GraphPad Software, San Diego, CA). To assess uptake of USPIO in tissues following single administration, R2* increase from pre to 24 h following USPIO were compared using repeated measures one-way ANOVA. Statistical significance was defined as two-sided $p < 0.05$.

Results

Twenty volunteer patients were recruited in total (10 at 1.5 T, 10 at 3 T). Forty MRI scans and 20 infusions of ferumoxytol were completed over the course of the study. Data from one participant at 1.5 T has been removed due to the presence of LGE, (which was included

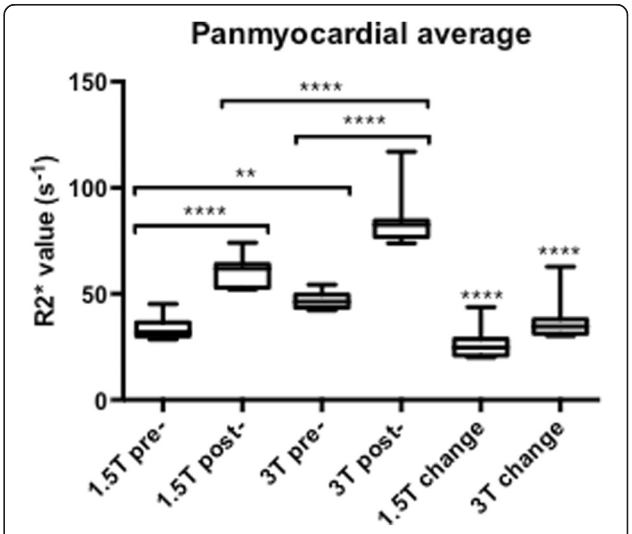

Fig. 2 Myocardial R2* pre- and post-USPIO administration at 1.5 and 3 T. Following administration, USPIO was detected by an increase in R2* at 24 h in the myocardium at both 1.5 and 3 T. (**** = $p < 0.0001$, ** = $p < 0.01$)

in the cardiac MR protocol so that we could exclude volunteers with any detectable cardiac MR abnormalities according to standard cardiac MR protocols). All other volunteers that were included had structurally normal hearts. One participant was prescribed antihypertensive medication but had a normal cardiac MR study and was normotensive so the data was retained for analysis. Administration of ferumoxytol was well tolerated with no adverse reactions reported during or immediately after administration in any of the participants.

Participants were predominantly middle aged, with greater numbers of women in both groups (Table 1). There were no differences between 1.5 T and 3 T groups in BMI or ejection fraction at baseline.

A summary of results is shown in Table 2. At baseline, panmyocardial R2* values were greater at 3 T than 1.5 T (46.9 ± 4.1 versus 33.5 ± 5.4 s^{-1}, Fig. 2, $p < 0.01$) as expected. Baseline R2* values were also greater at 3 T in bone ($P < 0.0001$) but no baseline differences were seen between magnetic field strength in all other tissues (Fig. 3, $p > 0.05$ for all). USPIO increased panmyocardial R2* values at 24 h in both 1.5 T and 3 T scanners ($p < 0.0001$ for both). Post-USPIO panmyocardial R2* values were again greater at 3 T than 1.5 T, as expected (84.2 ± 12.4

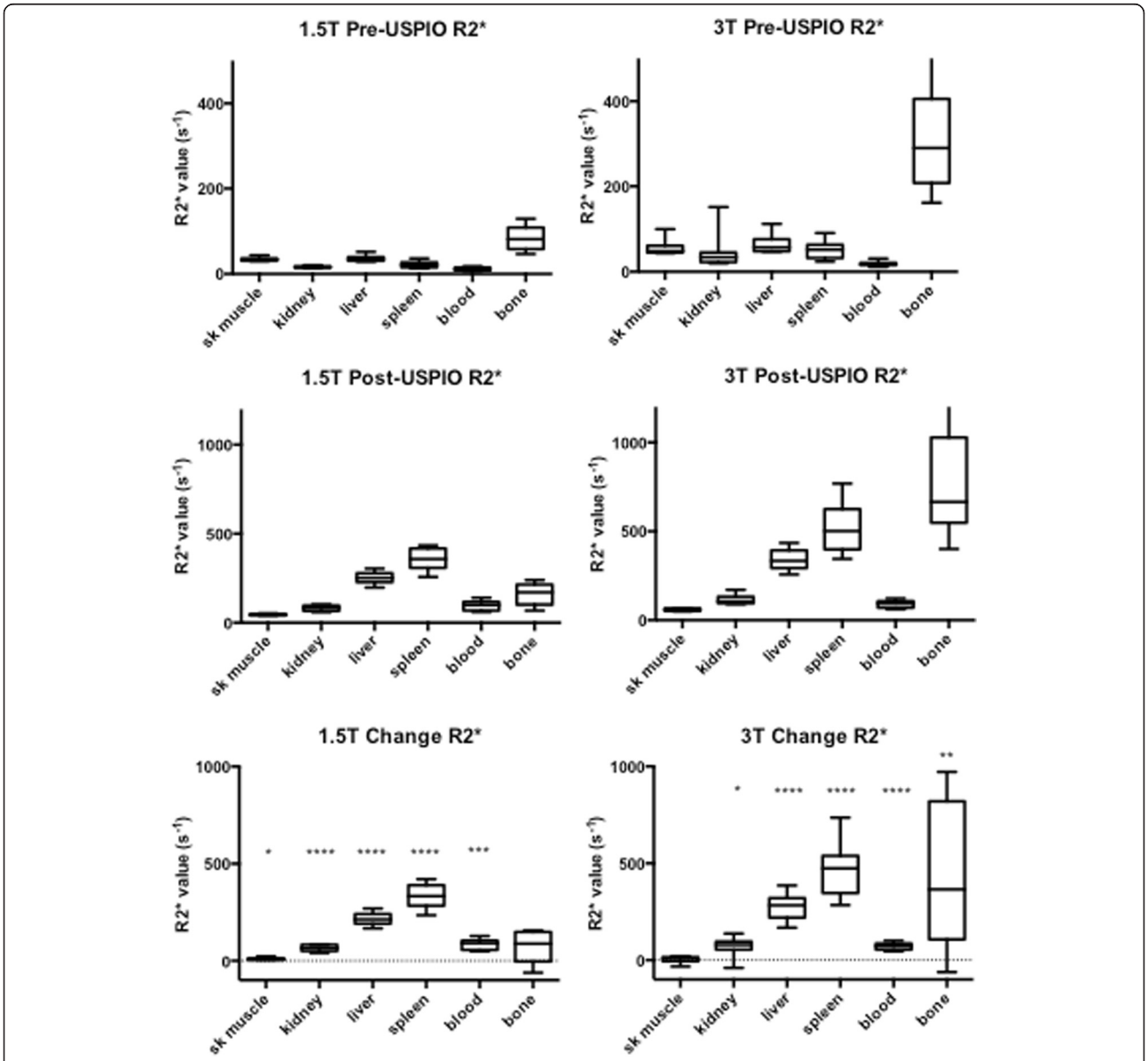

Fig. 3 Tissue R2* pre- and post-USPIO administration at 1.5 and 3 T. Following administration, USPIO was detected by an increase in R2*, 24 h after administration in skeletal muscle, kidney, liver, spleen and blood at 1.5 T, and kidney, liver, spleen, blood and bone at 3 T. (**** = $p < 0.0001$, *** = $p < 0.001$, ** = $p < 0.01$, * = $p < 0.05$)

versus 60.5 ± 7.2 s^{-1}, $p < 0.0001$). Panmyocardial change in R2* between baseline and 24 h post USPIO at 1.5 T was 26.5 ± 7.3 s^{-1} and at 3 T was 37.2 ± 9.6 s^{-1} ($p < 0.0001$ for both). Detectable increases in R2* were also observed at 24 h post-USPIO in skeletal muscle, kidney, liver, spleen and blood at 1.5 T, and kidney, liver, spleen, blood and bone at 3 T. (Fig. 3, $p < 0.05$ for all). BMI correlated with the panmyocardial R2* changes due to USPIO contrast (Fig. 4; $r = 0.72$, $p < 0.001$).

Discussion

For the first time, we report a range of normal T2* values in the healthy human heart and other tissues 24 h after ferumoxytol administration at 1.5 and 3 T. We also report problems, solutions and guidance in ferumoxytol-enhanced T2* image analysis.

Following administration, USPIO is detectable by T2* imaging in the myocardium and other tissues at both 1.5 and 3 T. Tissues with small increases in R2* (less than the blood pool) are likely to represent detection of USPIOs within the intravascular space and include skeletal muscle (at 1.5 T only), myocardium and kidney. In contrast, R2* changes that are greater than the blood pool must be due to accumulation of USPIO, either through iron storage, uptake by macrophages or other phagocytes, or sequestered within tissue interstitium. In the absence of tissue biopsies, we cannot be certain, but as the most pronounced R2* changes were seen in the spleen, liver and bone marrow - organs of the reticulo-endothelial system - it would appear likely that USPIO is incorporated quickly into tissue-resident phagocytes and macrophages.

Detection of USPIO enhancement in skeletal muscle at 1.5 T but not 3 T is due to generally noisier data seen across all tissues at 3 T. Due to wider data confidence intervals, a larger sample size would be required to detected the same mean change in R2*. The variation in data at 3 T is partly artifact in the images, but also because of the lower values at 3 T (USPIO has a faster T2* decay time at 3 T). With the same sampling echo times, there are fewer data points to construct the decay curve at 3 T than 1.5 T so our error in estimation also increases.

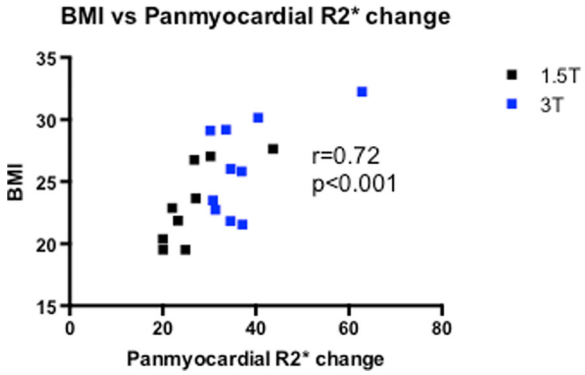

Fig. 4 Body-mass Index vs Panmyocardial R2* change at 1.5 and 3 T. Body-mass index correlates with panmyocardial R2* change pre- and post-USPIO

We chose 24 h post USPIO to re-image participants as myocardial signal attenuation at 24 h has shown to be optimal in the myocardium compared to later time points [8, 9]. In view of this, scanning appointments were generally separated by 25 h, and in practice, this regime worked well for both participants and MRI planning. According to previous work [8], we chose a weight-adjusted USPIO dose of 4 mg Fe/kg body weight. However acknowledging that the distribution of USPIO following administration is predominantly in the organs of the reticuloendothelial system and blood pool, this may not be the optimum administration strategy as blood volume does not increase linearly with weight. We found a correlation between BMI and myocardial R2* change, probably due to increased blood pool USPIO concentration in those with higher BMI. We therefore suggest that a fixed dose approach may also be appropriate depending on the application.

Artifacts were commonly encountered with USPIO-enhanced T2* imaging and made data analysis challenging. Post contrast artifacts at the blood-pool to myocardial interface were commonly seen and needed careful exclusion when selecting myocardial ROI. (Fig. 5A) This limited the assessment of USPIO accumulation at the endocardium. Similarly, blooming artifacts from nearby organs with high iron or blood pool USPIO content, such as lung and liver, commonly created signal deficits within the myocardium. In this situation, examination of T2* decay curves and excluding echo times influenced by artifact aided T2* decay curve fitting (Fig. 5).

The advantage of MRI mapping techniques is that visual assessment and objective quantification can be made using the same image, and these are now entering clinical practice. It seems likely that if UPSIO-enhanced MRI is adopted into clinical practice to detect tissue inflammation, T2* mapping would be used for image interpretation. However based on our experiences, we would recommend caution in interpreting maps alone. Signal attenuation seen on the T2* map may be interpreted as tissue USPIO accumulation, but may be due to blooming artifact from nearby susceptibility effects, and close examination of the T2* decay curve, and individual echoes if possible is suggested in order to distinguish accurately between tissue USPIO accumulation and artifact. In theory, setting an r^2 threshold as we did helps to exclude areas grossly affected by artifact. In practice however, regions with a seemingly acceptable R^2 may still be influenced by artifact (Fig. 5). Manual exclusion of later echoes (influenced by artifact) from the curve may result in an improvement in R^2 (a measure of how well the data

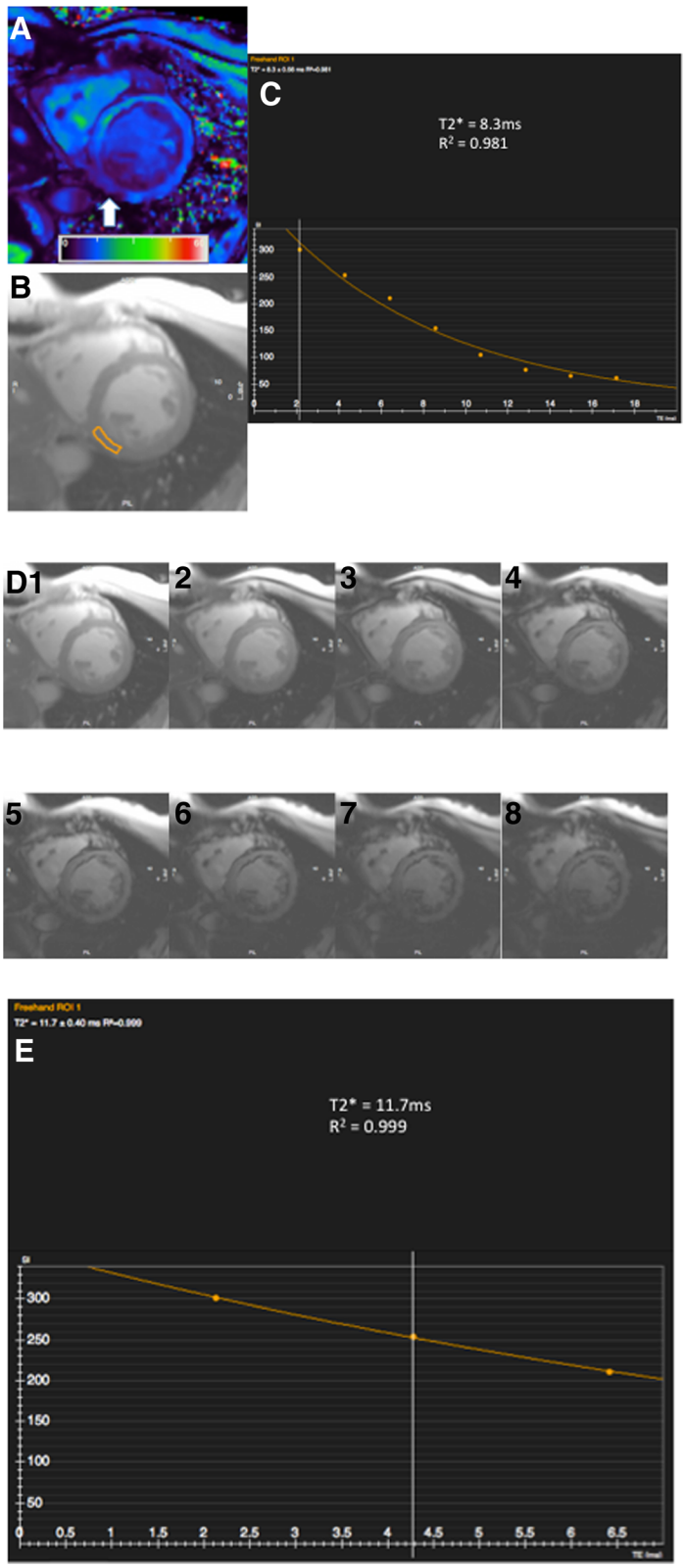

Fig. 5 (See legend on next page.)

(See figure on previous page.)
Fig. 5 Inferior Blooming artifact. Example illustrating the challenge in assessing whether the inferior myocardial signal attenuation seen arrowed on the T2* colourmap (**a**, scale 0-60 ms) is true or caused by artifact. Drawing a region of interest (**b**) and examining the decay curve (**c**) along with visualising individual echos (**d***1-8*) helps determine that this is a 'blooming artifact' from outside the heart is seen to influence echos 4-8. These can be manually removed, forming a new decay curve (**e**) with improvement in curve fitting (R^2 value), although with fewer fitting points

points fit the curve), however there is the danger that reducing the number of fitting points will in fact reduce the overall sampling accuracy. Clearly, automated software capable of detecting and excluding artifact would be advantageous. This could be achieved by excluding, or applying less weight, to later echo times especially data points at a large distance from the initial decay curve trajectory [25, 26]. It should be noted that like all other MRI sequences, poor data quality heavily influenced by breathing or movement artifact is generally non-interpretable and post processing using automated T2* decay curve fitting software is not likely to provide a remedy.

Echo times in this study were specific for cardiac imaging and were selected appropriately. Therefore they were not optimal for imaging tissues with T2* values substantially higher or lower than myocardium. Native blood pool and post USPIO bone marrow (Fig. 6) provide examples of low and high T2* values respectively that we had difficulty accurately fitting a T2* decay curve. With high T2* values, only a short part of the decay curve is plotted over the echo sampling time period, and often the signal has not decayed sufficiently for an accurate decay curve to be plotted. In contrast, regions with particularly short T2* decay times have decayed to a level expected from background noise before sufficient data sampling has been made. Therefore fitting a decay curve from a small number (2–4) of echo times is clearly difficult, and often too much emphasis is

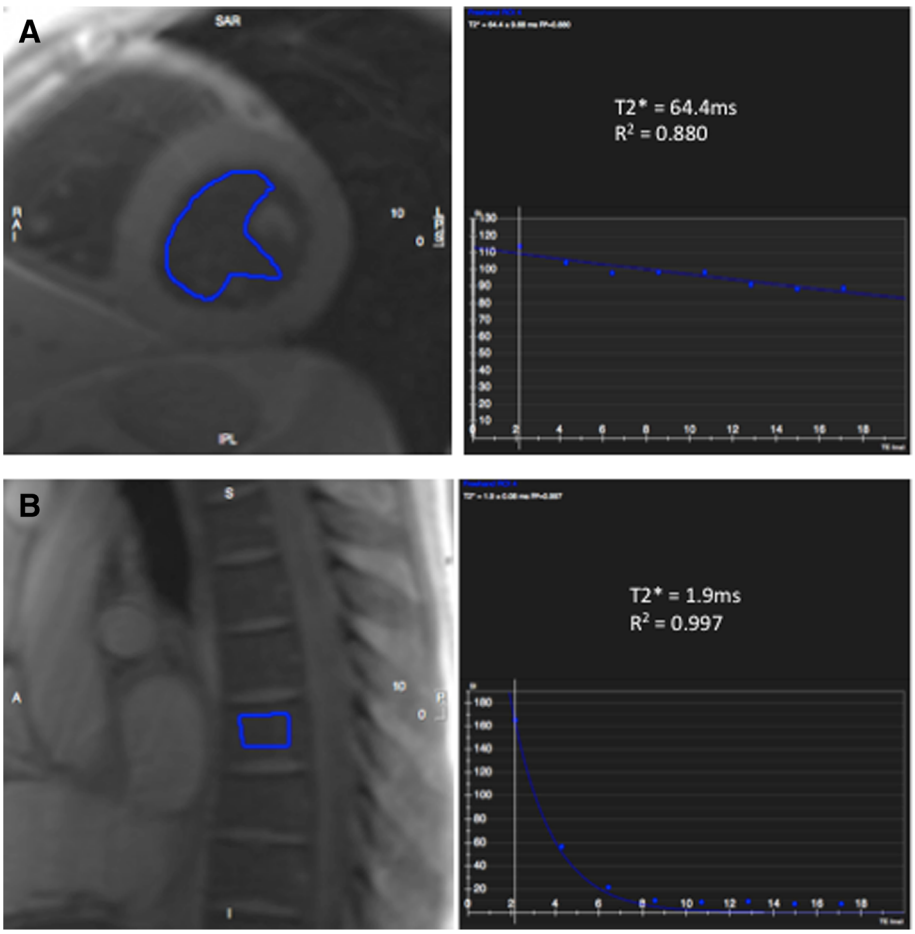

Fig. 6 Example of high and low T2* values. Regions of Interest with excessively low or high T2* value (pre-contrast blood pool, **a**, and post USPIO bone marrow, **b**, respectively) can often be difficult to generate an accurate T2* decay curve. Imaging with tissue-spcific echo times will help generate more accurate T2* decay curves

placed upon data decayed to the baseline level of background noise in order to generate a decay curve. Allowances can be made for background noise but are of limited value in this instance. We strongly advise applying tissue-specific echo times tailored to the expected T2* value in order to achieve the most accurate decay curves possible.

Limitations

There are some limitations that should be taken into account when interpreting these data. First, this study has small numbers and a larger cohort of participants should be studied to further validate these normal values. Furthermore, due to geographical reasons, it was not feasible to scan the same participants at both centres so comparison cohorts at 1.5 T and 3 T were different. Despite this, both were healthy volunteers groups and displayed no differences at baseline so we do not feel this has impacted on the results. Finally, due to problems in interpreting high and low T2* values as mentioned above, we recommend caution in interpreting some high non-cardiac R2* values; especially in the organs of the reticuloendothelial system at 3 T. In these organs, the spread of R2* data above the median value appears wide. This is possibly caused by artifact and most evident at 3 T, and may additionally explain why these regions have disproportionally high R2* values.

Conclusion

We have shown that ferumoxytol-enhanced MRI is feasible at both 1.5 T and 3 T, and suggest a range of expected normal values post-ferumoxytol in a range of tissues. Refinements of dose administration, optimization of acquired echo-times, careful image analysis, and development of post-processing and analysis software capable of excluding common artifacts, are essential to ensure reliable and robust quantification of tissue enhancement.

Abbreviations

LGE: late gadolinium enhancement; MRI: magnetic resonance imaging; ROI: regions of interest; USPIO: ultrasmall superparamagnetic particles of iron oxide.

Funding

This work was supported by the British Heart Foundation (FS/12/83). CS is supported by the Chief Scientist Office (ETM/266). SA and DEN are supported by the British Heart Foundation (FS/12/83; CH/09/002). DEN is the recipient of a Wellcome Trust Senior Investigator Award (WT103782AIA). Edinburgh Clinical Research Facility and the Clinical Research Imaging Centre are supported by NHS Research Scotland (NRS) through NHS Lothian. SS has received funding for this work via the British Heart Foundation Centre of Research Excellence award for the University of Edinburgh.

Authors' contributions

CS, SA, DN and SS designed the study, collected and analysed, data and drafted the manuscript. TM and CG analysed and interpreted data, and drafted the manuscript. MD, JP, SP, MP, RG, SM and PH designed the study and drafted the manuscript. All authors read and approved the manuscript.

Competing interests

The authors declare that they have no competing interests.

Author details

[1]British Heart Foundation/University Centre for Cardiovascular Science, University of Edinburgh, Edinburgh, UK. [2]Clinical Research Imaging Centre, University of Edinburgh, Edinburgh, UK. [3]Edinburgh Clinical Research Facility, University of Edinburgh, Edinburgh, UK. [4]Department of Cardiology, Golden Jubilee National Hospital, Clydebank, UK. [5]Department of Cardiology, Royal Brompton Hospital, London, UK.

Received: 19 January 2016 Accepted: 28 June 2016
Published online: 27 July 2016

References

1. Hahn PF, Stark DD, Lewis JM, Saini S, Elizondo G, Weissleder R, Fretz CJ, Ferrucci JT. First clinical trial of a new superparamagnetic iron oxide for use as an oral gastrointestinal contrast agent in MR imaging. Radiology. 1990; 175:695–700.
2. Saini S, Stark DD, Wittenberg J, Brady TJ, Ferrucci JT. Ferrite particles: a superparamagnetic MR contrast agent for the reticuloendothelial system. Radiology. 1987;162:211–6.
3. Rogers JM, Lewis J, Josephson L. Visualization of superior mesenteric lymph nodes by the combined oral and intravenous administration of the ultrasmall superparamagnetic iron oxide, AMI-227. Magn Reson Imaging. 1994;12:1161–5.
4. Canet E, Revel D, Forrat R, Baldy-Porcher C, de Lorgeril M, Sebbag L, Vallee JP, Didier D, Amiel M. Superparamagnetic iron oxide particles and positive enhancement for myocardial perfusion studies assessed by subsecond T1-weighted MRI. Magn Reson Imaging. 1993;11:1139–45.
5. Ros PR, Freeny PC, Harms SE, Seltzer SE, Davis PL, Chan TW, Stillman AE, Muroff LR, Runge VM, Nissenbaum MA. Hepatic MR imaging with ferumoxides: a multicenter clinical trial of the safety and efficacy in the detection of focal hepatic lesions. Radiology. 1995;196:481–8.
6. Kroft LJM, Doornbos J, van der Geest RJ, van der Laarse A, van der Meulen H, de Roos A. Ultrasmall superparamagnetic particles of iron oxide (USPIO) MR imaging of infarcted myocardium in pigs. Magn Reson Imaging. 1998;16:755–63.
7. Taylor AM, Panting JR, Keegan J, Gatehouse PD, Amin D, Jhooti P, Yang GZ, McGill S, Burman ED, Francis JM, Firmin DN, Pennell DJ. Safety and preliminary findings with the intravascular contrast agent NC100150 injection for MR coronary angiography. J Magn Reson Imaging. 1999;9:220–7.
8. Alam SR, Shah ASV, Richards J, Lang NN, Barnes G, Joshi N, MacGillivray T, McKillop G, Mirsadraee S, Payne J, Fox KAA, Henriksen P, Newby DE, Semple SIK. Ultrasmall Superparamagnetic Particles of Iron Oxide in Patients With Acute Myocardial Infarction: Early Clinical Experience. Circ Cardiovasc Imaging. 2012;5:559–65.
9. Yilmaz A, Dengler MA, van der Kuip H, Yildiz H, Rosch S, Klumpp S, Klingel K, Kandolf R, Helluy X, Hiller KH, Jakob PM, Sechtem U. Imaging of myocardial infarction using ultrasmall superparamagnetic iron oxide nanoparticles: a human study using a multi-parametric cardiovascular magnetic resonance imaging approach. Eur Heart J. 2013;34:462–75.
10. Richards JMJ, Semple SI, MacGillivray TJ, Gray C, Langrish JP, Williams M, Dweck M, Wallace W, McKillop G, Chalmers RTA, Garden OJ, Newby DE. Abdominal Aortic Aneurysm Growth Predicted by Uptake of Ultrasmall Superparamagnetic Particles of Iron Oxide: A Pilot Study. Circ Cardiovasc Imaging. 2011;4:274–81.
11. McBride OMB, Berry C, Burns P, Chalmers RTA, Doyle B, Forsythe R, Garden OJ, Goodman K, Graham C, Hoskins P, Holdsworth R, MacGillivray TJ, McKillop G, Murray G, Oatey K, Robson JMJ, Roditi G, Semple S, Stuart W, van Beek EJR, Vesey A, Newby DE. MRI using ultrasmall superparamagnetic particles of iron oxide in patients under surveillance for abdominal aortic aneurysms to predict rupture or surgical repair: MRI for abdominal aortic aneurysms to predict rupture or surgery-the MA(3)RS study. Open Heart. 2015;2:e000190.
12. Trivedi RA. Identifying Inflamed Carotid Plaques Using In Vivo USPIO-Enhanced MR Imaging to Label Plaque Macrophages. Arterioscler, Thromb, Vasc Biol. 2006;26:1601–6.
13. Trivedi RA, U-King-Im JM, Graves MJ, Cross JJ, Horsley J, Goddard MJ, Skepper JN, Quartey G, Warburton E, Joubert I, Wang L, Kirkpatrick PJ, Brown J, Gillard JH. In vivo detection of macrophages in human carotid atheroma: temporal dependence of ultrasmall superparamagnetic particles of iron oxide-enhanced MRI. Stroke. 2004;35:1631–5.

14. Tang T, Howarth SPS, Miller SR, Trivedi R, Graves MJ, King-Im JU, Li ZY, Brown AP, Kirkpatrick PJ, Gaunt ME, Gillard JH. Assessment of inflammatory burden contralateral to the symptomatic carotid stenosis using high-resolution ultrasmall, superparamagnetic iron oxide-enhanced MRI. Stroke. 2006;37:2266–70.
15. Tang TY, Howarth SPS, Miller SR, Graves MJ, Patterson AJ, U-King-Im J-M, Li ZY, Walsh SR, Brown AP, Kirkpatrick PJ, Warburton EA, Hayes PD, Varty K, Boyle JR, Gaunt ME, Zalewski A, Gillard JH. The ATHEROMA (Atorvastatin Therapy: Effects on Reduction of Macrophage Activity) StudyEvaluation Using Ultrasmall Superparamagnetic Iron Oxide-Enhanced Magnetic Resonance Imaging in Carotid Disease. JAC. 2009;53:2039–50.
16. Anderson LJ, Holden S, Davis B, Prescott E, Charrier CC, Bunce NH, Firmin DN, Wonke B, Porter J, Walker JM, Pennell DJ. Cardiovascular T2-star (T2*) magnetic resonance for the early diagnosis of myocardial iron overload. Eur Heart J. 2001;22:2171–9.
17. Anderson LJ, Westwood MA, Holden S, Davis B, Prescott E, Wonke B, Porter JB, Walker JM, Pennell DJ. Myocardial iron clearance during reversal of siderotic cardiomyopathy with intravenous desferrioxamine: a prospective study using T2* cardiovascular magnetic resonance. Br J Haematol. 2004; 127:348–55.
18. Westwood MA, Anderson LJ, Firmin DN, Gatehouse PD, Lorenz CH, Wonke B, Pennell DJ. Interscanner reproducibility of cardiovascular magnetic resonance T2* measurements of tissue iron in thalassemia. J Magn Reson Imaging. 2003; 18:616–20.
19. Westwood M, Anderson LJ, Firmin DN, Gatehouse PD, Charrier CC, Wonke B, et al. A single breath-hold multiecho T2* cardiovascular magnetic resonance technique for diagnosis of myocardial iron overload. J Magn Reson Imaging. 2003;18:33–9.
20. Carpenter J-P, He T, Kirk P, Anderson LJ, Porter JB, Wood J, Galanello R, Forni G, Catani G, Fucharoen S, Fleming A, House M , Black G, Firmin DN, Pierre TGS, Pennell DJ. Calibration of myocardial iron concentration against T2-star Cardiovascular Magnetic Resonance. J Cardiovasc Magn Reson. 2009; 11:1–2.
21. Kirk P, He T, Anderson LJ, Roughton M, Tanner MA, Lam WWM, Au WY, Chu WCW, Chan G, Galanello R, Matta G, Fogel M, Cohen AR, Tan RS, Chen K, Ng I, Lai A, Fucharoen S, Laothamata J, Chuncharunee S, Jongjirasiri S, Firmin DN, Smith GC, Pennell DJ. International reproducibility of single breathhold T2* MR for cardiac and liver iron assessment among five thalassemia centers. J Magn Reson Imaging. 2010;32:315–9.
22. Carpenter J-P, He T, Kirk P, Roughton M, Anderson LJ, de Noronha SV, Sheppard MN, Porter JB, Walker JM, Wood JC, Galanello R, Forni G, Catani G, Matta G, Fucharoen S, Fleming A, House MJ, Black G, Firmin DN, St Pierre TG, Pennell DJ. On T2* magnetic resonance and cardiac iron. Circulation. 2011;123:1519–28.
23. Ruehm SG, Corot C, Vogt P, Kolb S, Debatin JF. Magnetic Resonance Imaging of Atherosclerotic Plaque With Ultrasmall Superparamagnetic Particles of Iron Oxide in Hyperlipidemic Rabbits. Circulation. 2001;103:415–22.
24. Cerqueira MD, Weissman NJ, Dilsizian V, Jacobs AK, Kaul S, Laskey WK, Pennell DJ, Rumberger JA, Ryan T, Verani MS, Myoca AHAWG . Standardized myocardial segmentation and nomenclature for tomographic imaging of the heart: A statement for healthcare professionals from the Cardiac Imaging Committee of the Council on Clinical Cardiology of the American Heart Association. J Am Soc Echocardiogr. 2002;15:463–7.
25. Shah S, Xue H, Greiser A, Weale P, He T, Firmin DN, Pennell DJ, Zuehlsdorff S, Guehring J. Inline myocardial t2* mapping with iterative robust fitting. J Cardiovasc Magn Reson. 2011;13:P308.
26. He T, Gatehouse PD, Kirk P, Tanner MA, Smith GC, Keegan J, Mohiaddin RH, Pennell DJ, Firmin DN. Black-blood T2* technique for myocardial iron measurement in thalassemia. J Magn Reson Imaging. 2007;25:1205–9.

Heart Online First, published on February 15, 2016 as 10.1136/heartjnl-2015-308779

OPEN ACCESS

Monitoring the biological activity of abdominal aortic aneurysms *Beyond Ultrasound*

Rachael O Forsythe, David E Newby, Jennifer M J Robson

British Heart Foundation Centre for Cardiovascular Science, University of Edinburgh, Edinburgh, UK

Correspondence to
Dr Jennifer M J Robson, British Heart Foundation, Centre for Cardiovascular Science, University of Edinburgh, Little France Crescent, Edinburgh EH164SA, UK; jenny.robson@ed.ac.uk

Received 30 November 2015
Revised 8 January 2016
Accepted 21 January 2016

ABSTRACT

Abdominal aortic aneurysms (AAAs) are an important cause of morbidity and, when ruptured, are associated with >80% mortality. Current management decisions are based on assessment of aneurysm diameter by abdominal ultrasound. However, AAA growth is non-linear and rupture can occur at small diameters or may never occur in those with large AAAs. There is a need to develop better imaging biomarkers that can identify the potential risk of rupture independent of the aneurysm diameter. Key pathobiological processes of AAA progression and rupture include neovascularisation, necrotic inflammation, microcalcification and proteolytic degradation of the extracellular matrix. These processes represent key targets for emerging imaging techniques and may confer an increased risk of expansion or rupture over and above the known patient-related risk factors. Magnetic resonance imaging, using ultrasmall superparamagnetic particles of iron oxide, can identify and track hotspots of macrophage activity. Positron emission tomography, using a variety of targeted tracers, can detect areas of inflammation, angiogenesis, hypoxia and microcalcification. By going beyond the simple monitoring of diameter expansion using ultrasound, these cellular and molecular imaging techniques may have the potential to allow improved prediction of expansion or rupture and to better guide elective surgical intervention.

INTRODUCTION

Abdominal aortic aneurysm (AAA) disease affects up to 5% of men aged between 65 and 74 years in Western Europe and may pass undetected until a patient presents with rupture. The mortality rate of ruptured AAA is over 80%,[1] with a minority of patients surviving long enough to undergo emergency repair. The risks associated with elective AAA repair are also significant, with a 30-day mortality rate of up to 5% for elective endovascular or open repair.[2] Decision-making at an individual patient level is therefore paramount to ensure the best clinical outcome, particularly as AAA shares risk factors for, and typically coexists with, atherosclerotic disease processes that confer substantial perioperative risk.

When planning management of a patient with an AAA, the risks of elective surgery must be weighed against the risk of rupture without intervention. Various risk prediction models have been developed to help evaluate perioperative and postoperative risk. While these scores may help evaluate risk when operative intervention is being considered, the prediction of aneurysm expansion and rupture risk in patients under surveillance remains challenging. Current knowledge of AAA progression is largely based on the tenet that rupture rate rises with increasing aneurysm diameter. However, up to one in five ruptured AAAs occur in small aneurysms (<5.5 cm),[3] while many patients have far larger aneurysms that never rupture and a substantial proportion of patients die of non-AAA-related causes while under surveillance. We would therefore suggest that prediction of disease progression using simple measures and thresholds, such as aneurysm diameter, is too simplistic.

RISK FACTORS FOR DISEASE OCCURRENCE AND PROGRESSION

Various risk factors for the development and progression of AAA disease have been identified, although it remains unclear why some patients develop AAA and others, with identical risk profiles, do not. AAA occurrence is associated with advancing age and male sex. However, female sex is also an independent predictor of accelerated disease progression. Indeed, in comparison to men, women have an increased rate of aneurysm expansion and a threefold higher risk of rupture.[4] Moreover, when rupture takes place in women, it occurs at smaller aneurysm diameters.[5]

Cigarette smoking is the most important modifiable risk factor associated with development, expansion and rupture of AAA: more than 90% of patients with AAA are current or ex-smokers. The relative risk of aneurysm development in current smokers is at least 2,[6] with an increased rate of expansion of the order of 15–20% in patients who continue to smoke.[7]

Although it is often said that AAA shares much of its pathophysiology with atherosclerosis, it has a number of distinct features. While traditional atherosclerotic risk factors (such as hypertension and hypercholesterolaemia) are also associated with AAA formation, diabetes mellitus is protective against its development.[8] The reason for this remains incompletely understood but may relate to diabetes-mediated inhibition of the matrix metalloproteinases (MMPs)[9] that are responsible for proteolytic degradation of the extracellular matrix in AAA disease. The pleiotropic effects of antidiabetic medications, including lipid homeostasis, may also be important.[10]

A strong genetic component to the development of AAA is suggested by the observation that patients with a family history of AAA have the highest risk of AAA development.[11] Connective tissue diseases, such as Marfan's syndrome and Ehlers–Danlos syndrome, are also associated with AAA development.

To cite: Forsythe RO, Newby DE, Robson JMJ. *Heart* Published Online First: [*please include* Day Month Year] doi:10.1136/heartjnl-2015-308779

TOWARDS IMPROVED EVALUATION OF DISEASE PROGRESSION

Current evaluation of AAA disease progression is based on morphological risk factors for expansion—primarily, aneurysm diameter. Serial ultrasound examination is the standard method of monitoring the natural history of AAA disease, using population-derived data to predict the future expansion of an individual patient's aneurysm. The establishment of population-based ultrasound screening in the UK has been associated with a 40–50% decrease in aneurysm-related mortality.[1] Overall, the rate of expansion and risk of rupture generally rises with increasing AAA diameter, and current guidelines recommend that elective repair should be considered when the AAA exceeds 5.5 cm in maximum anteroposterior diameter, or expansion exceeds 1.0 cm/year.

Recent data have demonstrated that many aneurysms exhibit a non-linear, discontinuous staccato growth pattern, with periods of expansion and dormancy.[12] The specific biomechanical and biological factors that lead to this variable and patient-specific AAA expansion patterns cannot be accounted for by current aneurysm diameter measurements and recent growth trends alone. Despite this, maximum anteroposterior diameter, as measured on ultrasound or computed tomography (CT), is still considered the best clinical predictor of AAA expansion and rupture.[7]

Morphological features associated with disease progression include vessel asymmetry[13] and a short, narrow neck configuration.[14] The role of intraluminal thrombus in disease progression remains controversial, although plausibly a large thrombus load may induce local wall hypoxia, triggering further inflammatory activity and inducing changes in local wall strength,[15] potentially leading to rupture. However, beyond maximum diameter none of these is validated as part of standard monitoring of patients with AAA.

As a tool for aneurysm growth surveillance, ultrasound is ideally suited since it is relatively inexpensive, readily available and avoids ionising radiation. CT offers the additional anatomical information required for surgical planning and can diagnose rupture. However, neither modality offers insight into the biological status of the aneurysm that determines disease progression. Future developments in the assessment of AAA disease should go beyond simple morphological parameters with the aim of predicting more accurately the likely evolution of the aneurysm for an individual patient.

PATHOBIOLOGICAL ACTIVITY AS TARGETS FOR DISEASE MONITORING: BIOLOGICAL 'HOTSPOTS'

Aneurysmal degeneration of the aorta involves inflammation, neovascularisation, microcalcification and proteolytic degradation of the extracellular matrix culminating in medial thinning and loss of the structural integrity of the vessel wall. Once again, there are common pathological processes involved in both AAA and atherosclerosis, but also some clear differences (figure 1). Perhaps, the most striking difference is that atherosclerosis affects the arterial intima, causing luminal narrowing, whereas aneurysmal degradation of the vessel wall predominantly affects the media and adventitia, causing vessel dilatation. Furthermore, while aneurysm disease affects only the distal abdominal aorta in 90% of cases, atherosclerosis is typically widespread involving the coronary, cerebral and peripheral circulation systems.

In studies of coronary atherosclerosis, the term 'vulnerable plaque' has been coined to describe plaques at risk of rupture precipitating clinical events. Such plaques are characterised by pathological features that include a thin fibrous cap, large lipid core, increased infiltration of macrophages and a reduction in smooth muscle cells.[16] Analogous to this concept, 'hotspots' have been described in AAA, reflecting the focal and intense biological activity that occurs in specific regions of the aortic wall. Within these hotspots, focal neovascularisation is associated with increased inflammation and proteolysis and is present at the site of rupture.[17] In contrast, the tensile strength of the aortic wall is not uniform and is impaired in areas of increased proteolytic activity,[18] which varies across the aneurysm sac. These biological hotspots appear to represent areas of the aortic wall that are prone to further expansion and rupture.

A number of serum biomarkers of inflammatory and proteolytic activity have been investigated in patients with AAA including MMPs (MMP-2, MMP-8, MMP-9), interleukins (IL-6, IL-10), CRP and other potential mediators (including TNF-α and TIMP-1) that may contribute to connective tissue degradation and depletion of collagen and elastin stores. Increased levels of MMP-8 and MMP-9 have also been identified at the site of AAA rupture.[19] However, measurement of plasma concentrations of these biomarkers has not been demonstrated to be of value in clinical risk prediction of patients and this likely reflects a lack of sensitivity. Ultimately plasma concentrations will represent activity of the entire vasculature rather than potentially small areas of focal vascular injury.

The identification of biological hotspots within the aortic wall using non-invasive imaging may prove to be a more valuable approach that could enable risk prediction and, in addition to the other known risk factors for AAA progression, could form part of a patient-specific risk prediction model. However, this cannot be achieved using conventional cross-sectional imaging techniques and contrast agents. Molecular imaging techniques have the potential to provide such functional biological information and, when used in combination with structural anatomical data, may provide regional and patient-specific information on disease activity. Capitalising on our increased knowledge of the pathogenesis of cardiovascular disease, the field of 'molecular imaging' is one area that has expanded rapidly over the past few decades. Molecular imaging techniques apply both positron-emission tomography (PET) and magnetic resonance imaging (MRI) to identify cell-specific or process-specific probes that assess the biological function of small-scale molecular events, such as gene transcription, or identify surrogate markers for disease activity, such as inflammation and calcification. Knowledge of a relevant biological 'target' is a prerequisite. A suitable tracer needs to be able to bind to the target, be clinically available and offer compatibility with a clinically available imaging modality that provides appropriate spatial and tissue resolution for the disease process. Such techniques have been used in coronary artery disease and valvular heart disease to describe key processes involved in atherosclerosis including inflammation, angiogenesis and apoptosis.[20 21] These techniques can often define and identify evolving disease states at an earlier stage than conventional imaging such as the identification of vulnerable lesions associated with plaque rupture and myocardial infarction. Similarly, the identification, localisation and tracking of disease activity in patients with AAA may provide incremental risk prediction in addition to known risk factors for disease progression (figure 2).

MACROPHAGE ACTIVITY AND MRI

MRI offers high spatial resolution, avoids ionising radiation and results in excellent soft tissue contrast. Molecular MRI

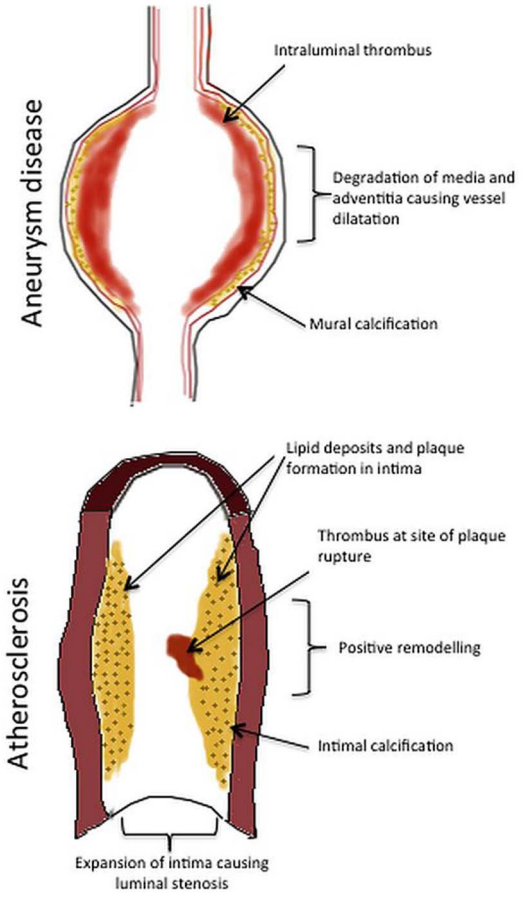

Characteristic	Abdominal Aortic Aneurysm disease	Atherosclerosis
Location	Media and adventitia	Intima
Clinical manifestation of disease	Vessel rupture	Vessel occlusion
Inflammation	Transmural	Intima ± media
Lipid deposition	When associated with atherosclerosis	Marked intimal deposition
Calcification	Transmural	Intimal
Thrombus	Chronic, intraluminal thrombosis.	Acute plaque rupture causing luminal thrombosis and occlusion.
Neovascularisation	Medial and adventitial	Intimal

Figure 1 Comparison of pathobiological characteristics of atherosclerosis and abdominal aortic aneurysm (AAA) disease. While AAA disease shares similar pathobiological processes involved in atherosclerotic disease, there are notable distinctions. In particular, the location of the disease processes is an important difference, with atherosclerosis affecting primarily the vessel intima, whereas AAA disease has a predilection for the media and adventitia. The resulting clinical manifestation is that AAA disease causes vessel dilatation and rupture, whereas atherosclerosis leads to vessel stenosis occlusion. However, the common ground between these two pathological conditions means that molecular imaging techniques thus far used in the study of atherosclerotic vessels (such as the coronary and carotid arteries) may prove useful in the study of AAA disease.

techniques allow coregistration of molecular information with detailed anatomical information and can also be fused with CT data. Paramagnetic MRI agents (such as gadolinium) are used widely in clinical practice. When used as a blood pool agent in AAA, T2-weighted gadolinium-enhanced MRI delineates morphological features such as the blood pool, thrombus and fibrous cap[22] whereas late enhancement reveals areas of fibrosis within vascular tissues. More recently, ultrasmall superparamagnetic particles of iron oxide (USPIOs) have been used as 'smart' contrast agents in cardiovascular molecular MRI studies.[23 24] USPIOs exhibit a dual benefit, in that they can be used both as an initial T1 blood-pool contrast agent as well as visualise tissue inflammation using delayed T2 and T2* imaging. Moreover, USPIOs can be safely used in patients with renal failure, whereas the use of gadolinium is contraindicated in patients with renal failure, due to the risks of nephrogenic systemic fibrosis. With a mean particle diameter of <50 nm, USPIOs are small enough to evade immediate uptake by the reticuloendothelial system and persist in the blood pool with a half-life of 10–15 h. They translocate into tissues and are slowly taken up by tissue-resident macrophages thereby accumulating at sites of inflammation. As such, they have been used to identify and track macrophage activity in situations of cardiovascular disease. In particular, they have been shown to accumulate in vulnerable and ruptured atherosclerotic plaques, but not stable plaques, and atorvastatin therapy reduces USPIO uptake and inflammation in symptomatic carotid plaques.[25] More recently, a small pilot study of 29 patients with asymptomatic AAA (diameter between 4 and 6.6 cm) has demonstrated that focal areas of USPIO uptake in the aortic wall are associated with more rapid AAA expansion.[23] A large, prospective multicentre trial (ISRCTN76413758) of USPIO to predict AAA rupture or surgery in patients with asymptomatic AAA (n=350) is currently in progress.[26] This will establish whether this imaging approach has any potential clinical utility in patient monitoring (figure 3).

Further development of MRI-based techniques may include development of agents that can detect subgroups of macrophages, in addition to other aspects involved in the process of atherosclerosis and AAA disease progression.

MACROPHAGE ACTIVITY AND PET

There is a wide range of PET tracers available that can target different disease processes, many of which could be used in cardiovascular disease. PET has lower spatial resolution (~5 mm) when compared with MRI or CT, and on its own cannot provide optimal anatomical information for detailed evaluation. However, fusion techniques (PET-CT and PET-MRI) allow the integration of molecular information obtained through PET with anatomical detail gained from CT or MRI. Macrophage activity may be tracked using cell-specific PET tracers (table 1).

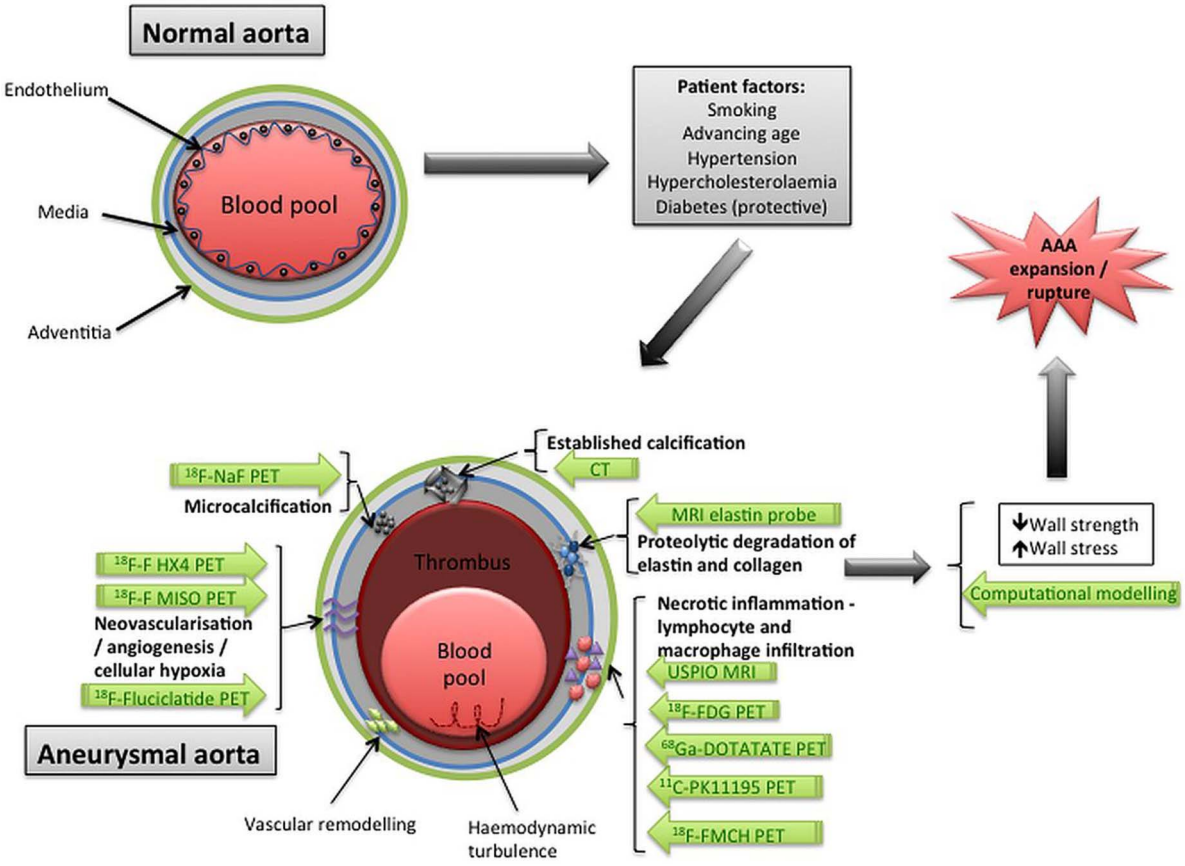

Figure 2 Biological targets and potential molecular imaging techniques in abdominal aortic aneurysm (AAA) disease. As well as patient factors (such as smoking, hypertension and advancing age) that contribute to the risk of AAA formation, biological processes have been identified that are implicit in aneurysm formation. The key processes are illustrated above, along with the corresponding molecular imaging techniques (written in green arrows) that have been used in experimental or clinical studies to date (primarily in the coronary arteries). The combination of patient-related risk factors and biological processes leads to increased wall stress and decreased wall strength (which can be investigated using computational modelling techniques), and all of these factors lead to aneurysm expansion and vulnerability to rupture.

^{18}F-Fluorodeoxyglucose

The most widely used clinical PET tracer is ^{18}F-fluorodeoxyglucose (^{18}F-FDG): a glucose analogue that is taken up by glucose transporters and accumulates in glucose-metabolising cells. It is used as a surrogate marker for metabolic activity and is widely used to identify tumour metastases and monitor response to cancer treatment. In addition, its value in atherosclerosis imaging (by identifying metabolically active macrophages as a marker of inflammation) has been explored largely in the coronary and carotid arteries, as it accumulates within active atherosclerotic plaques.[27]

^{18}F-FDG imaging is the only clinically available tracer that has been explored in AAA disease but its value remains unclear. One small study found that AAA wall biopsies from patients with ^{18}F-FDG uptake showed significantly increased inflammatory infiltrate and a reduction in the number of smooth muscle cells compared with samples from patients with no ^{18}F-FDG uptake.[28] Another small study showed that patients undergoing open repair of symptomatic AAA (n=3) had higher ^{18}F-FDG uptake than asymptomatic patients (n=12), and increased ^{18}F-FDG uptake correlated with histological evidence of increased inflammatory activity.[29] Increased ^{18}F-FDG uptake within the AAA was associated with more aneurysm-related clinical events compared with patients with no ^{18}F-FDG uptake, and interestingly areas of ^{18}F-FDG uptake correlated with increased wall stress on biomechanical modelling.[30] The authors of these papers suggest a potential role of ^{18}F-FDG PET imaging in predicting AAA expansion or rupture.

However, the value of ^{18}F-FDG uptake remains controversial. Data sets are generally small and often derived retrospectively from oncology patient cohorts. Moreover, one larger study has demonstrated no difference in ^{18}F-FDG uptake among patients with AAA when compared with matched controls (n=310).[31] An inverse relationship between ^{18}F-FDG uptake and future AAA expansion has been demonstrated in a small study, suggesting that aneurysms with lower metabolic activity may actually be more prone to expand.[32]

The primary drawback of ^{18}F-FDG PET imaging is that the effect of local cellular hypoxia on glucose uptake may confound the PET signal that is otherwise attributed to macrophage activity,[33] as well as the potential for spillover from adjacent structures that are metabolically active, such as muscle and liver. Thus, ^{18}F-FDG PET imaging of AAA entails many potential confounding factors, lacks specificity and there is currently insufficient evidence to support its routine clinical use in predicting future AAA expansion or rupture risk.

Although other experimental PET tracers have been investigated in studies of inflammation in the context of atherosclerotic plaque, few have been investigated in AAA disease. As aneurysm disease shares some of the common pathways involved in atherosclerosis, some of these tracers may prove useful in the evaluation of AAA disease.

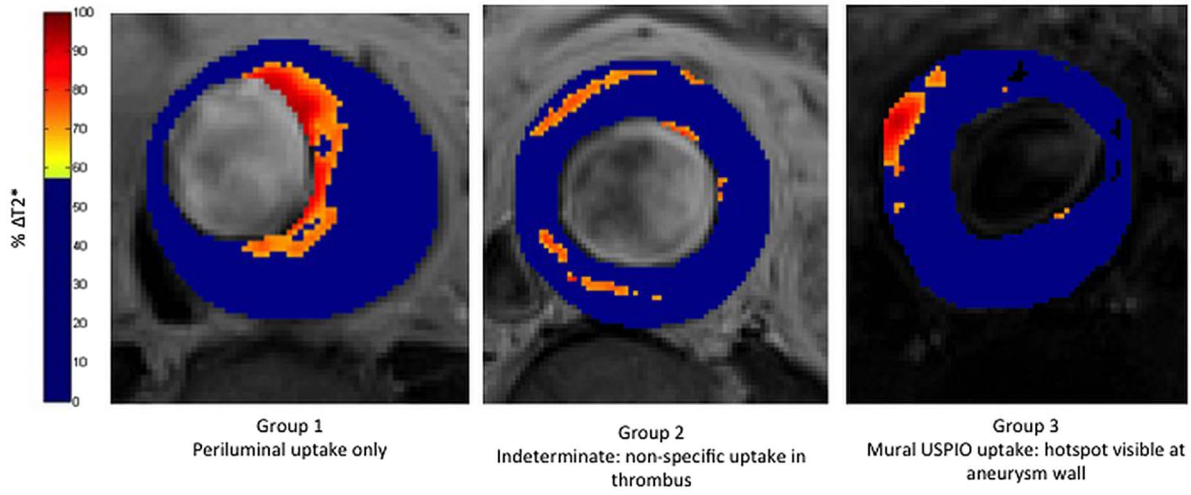

Figure 3 Magnetic resonance imaging (MRI) using ultrasmall superparamagnetic particles of iron oxide (USPIO) in abdominal aortic aneurysm disease. This technique is currently being investigated in the MA^{3}RS study (MRI in Abdominal Aortic Aneurysms to Predict Rupture or Surgery—ISRCTN76413758).

^{68}Ga-DOTATATE

^{68}Ga-DOTATATE (^{68}Ga-[1,4,7,10-tetraazacyclododecane-*N*,*N*′,*N*″,*N*‴-tetraacetic acid]-d-Phe^1,Tyr^3-octreotate) has a specific binding affinity for somatostatin receptors, which play a role in the modulation of inflammation and angiogenesis. Activated macrophages and damaged endothelial cells can cause overexpression of somatostatin receptors (subtype 2), and ^{68}Ga-DOTATATE (which binds to these receptors) exhibits macrophage-specific binding properties that may be more valuable than ^{18}F-FDG. Murine studies have demonstrated ^{68}Ga-DOTATATE uptake in atherosclerotic plaques,[34] while clinical imaging studies have demonstrated an association between ^{68}Ga-DOTATATE uptake in coronary arteries and known cardiovascular risk factors such as the presence of calcified plaques and hypertension.[35] Of note, focal uptake of ^{68}Ga-DOTATATE does not always correlate with ^{18}F-FDG uptake in one comparison study, suggesting that these tracers target slightly different pathobiological pathways. There have been no studies to date investigating the role of ^{68}Ga-DOTATATE in AAA disease progression; however, the abundance of macrophages seen in aneurysmal aortic wall suggests that this may be a suitable tracer for evaluation.

^{11}C-PK11195 and GE180

^{11}C-PK11195 and GE180 selectively bind to the translocator protein (TSPO) and have been used primarily in the assessment of neuronal damage. However, TSPO are also highly expressed by activated macrophages. Studies have demonstrated the

Table 1 PET radiotracers with potential value to track disease processes in AAA

Radiotracer (references)	Pathobiological process	Cellular target	Molecular target	Current clinical use	Applications and limitations
^{18}F-FDG[27–33]	Inflammation	Macrophage	Glucose analogue	Yes—oncology, neurology and cardiology	Uptake influenced by local hypoxia and other resident cell types, therefore may have limited value. Widely used in cardiovascular research; has been studied in AAA disease
^{68}Ga-DOTATATE[34–35]	Inflammation	Macrophage	Somatostatin receptor (subtype 2)	Experimental	No physiological uptake seen in myocardium, therefore clearly detects macrophage accumulation
^{11}C-PK11195[36]	Inflammation	Macrophage	TSPO receptor	Experimental	Non-specific binding and low arterial signal density may preclude its use in clinical setting
GE180[47]	Inflammation	Macrophage	TSPO receptor	Experimental	Binding heterogeneity—10% of the population may lack binding potential due to variant in receptor
^{18}F-FMCH[37–39]	Inflammation	Macrophage	Choline receptor	Yes—oncology	High uptake in liver may obscure analysis in suprarenal aorta. Lower tissue-to-background ratios than FDG, however, may identify areas of evolving inflammation distinct from areas of established calcification
^{18}F-fluciclatide[47]	Angiogenesis	Endothelium, fibroblasts	Integrin $\alpha_v\beta_3$	Experimental	Has been investigated in autoradiography studies of AAA disease
^{18}F-FMISO[48]	Hypoxia	Macrophage	Macromolecules in hypoxic cells	Experimental	Has been used in carotid studies
^{18}F-HX4[48]	Hypoxia	Macrophage	Macromolecules in hypoxic cells	Experimental	Has been used in carotid studies
^{18}F-NaF[46]	Microcalcification	–	Hydroxyapatite	Yes—oncology	Overspill from nearby bone can interfere with uptake interpretation

AAA, abdominal aortic aneurysms; DOTATATE, ^{68}Ga-[1,4,7,10-tetraazacyclododecane-*N*,*N*′,*N*″,*N*‴-tetraacetic acid]-D-Phe^1,Tyr^3-octreotate; FDG, fluorodeoxyglucose; FMCH, fluoromethylcholine; FMISO, fluoromisonidazole; HX4, (3-[18F]fluoro-2-(4-((2-nitro-1H-imidazol-1-yl)methyl)-1H-1,2,3,-triazol-1-yl)-propan-1-ol); NaF, sodium fluoride; PET, positron-emission tomography; TSPO, translocator protein.

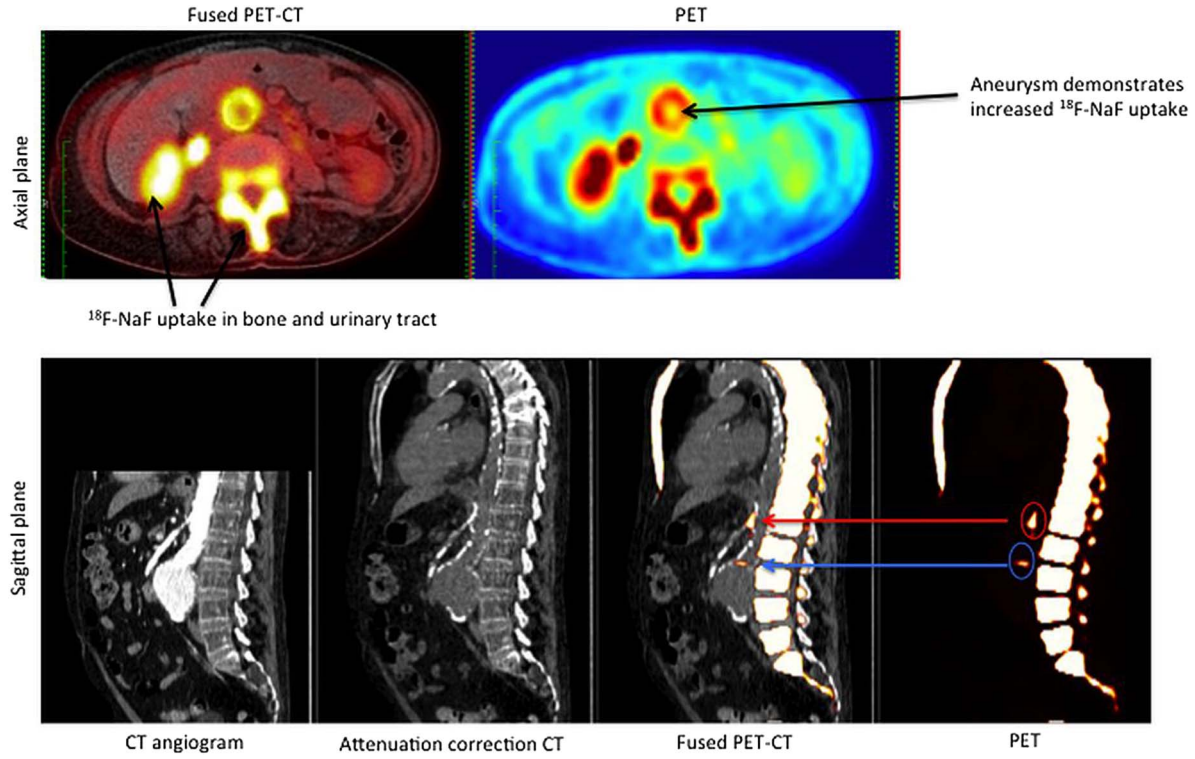

Figure 4 ^{18}F-NaF positron emission tomography–computed tomography (PET-CT) in abdominal aortic aneurysm disease. This technique is currently being investigated in the SoFIA^3 study (Sodium Fluoride Imaging (^{18}F-NaF PET-CT) in Abdominal Aortic Aneurysms—NCT02229006).

potential use of ^{11}C-PK11195 in localising vascular inflammation in atherosclerotic disease states such as symptomatic carotid artery disease and inflamed aortic plaques.[36] GE180 has a superior signal-to-noise ratio compared with ^{11}C-PK11195; however, around 10% of people may have a genetic variant in the GE180 receptor, which leads to poor binding of the ligand. Binding heterogeneity would be a barrier to widespread use of GE180, as it would require pre-emptive genotyping. Neither tracer has been investigated in AAA disease to date.

^{18}F-Fluoromethylcholine

^{18}F-Fluoromethylcholine (^{18}F-FMCH) binds to choline receptors and was introduced as a radiotracer for neuroimaging and prostate cancer. However, increased choline uptake is also seen in activated macrophages. ^{18}F-FMCH uptake has been seen in murine atherosclerotic plaques, with a higher sensitivity than ^{18}F-FDG,[37] while one retrospective clinical study in oncology patients demonstrated ^{18}F-FMCH uptake in structurally abnormal aortic wall,[38] but not in areas that only exhibited established calcification. This suggests that ^{18}F-FMCH may identify areas of current biological activity, distinct from areas of macroscopic calcification that are biologically inert. However, a comparison study of rat AAA has demonstrated that ^{18}F-FMCH achieved lower tissue-to-background ratios than ^{18}F-FDG, which was more sensitive when detecting activated macrophages.[39]

CALCIFICATION IN AAAS

Vascular calcification is associated with increased cardiovascular risk. Molecular imaging studies have suggested that inflammation and calcification occur at different stages of the atherosclerotic disease process.[40] 18F-FDG does not always colocalise with areas of calcification seen on CT,[41] and it is postulated that vascular calcification occurs as part of the healing response to necrotic inflammation, and is regulated in a similar manner to bone formation.[42] Established deposits of vascular calcification are considered part of a chain of pathological processes relating to atherosclerosis.[41] Therefore, macroscopically visible vascular calcification (macrocalcification) may correlate with overall disease burden and can be visualised on CT.

Mural calcification is common in AAA disease, is a predictor of future cardiovascular events and may also be linked with an increased risk of rupture.[43] Calcification, resulting from necrotic inflammation, may therefore cause aneurysm wall weakness.[44] Although widespread macrocalcification is very common in AAA disease, macrocalcification on CT does not identify those at high risk of AAA events. However, early evolving areas of calcification (microcalcification) could be a more significant and useful measurement of biological activity in the aneurysm wall, as microcalcification precedes the laying down of macrocalcification. Recent evidence suggests that plaque vulnerability is inversely associated with calcification density—established dense calcification may stabilise a plaque whereas less dense, spotty areas of microcalcification can trigger plaque rupture by causing a disproportionate increase in local stresses in the thin collagenous plaque, leading to a mismatch in compliance and vulnerability to rupture.[45] Identifying and localising microcalcification are beyond the resolution of CT scanning and require a molecular imaging approach to detect its presence.

MICROCALCIFICATION AND ^{18}F-NAF PET IMAGING

The PET radiotracer ^{18}F-sodium fluoride (^{18}F-NaF) has been used as a bone tracer for decades in the clinical arena. ^{18}F-NaF acts as a novel marker of vascular calcification activity, by binding to hydroxyapatite, which is a key component of bone and vascular calcification. ^{18}F-NaF preferentially binds to areas of developing calcification (microcalcification) and has been used to identify high-risk coronary plaques and culprit lesions in acute myocardial infarction.[46] 18F-NaF may also be useful in

patients with AAA to identify those with increased biological activity. Microcalcification represents necrotic inflammation which, in turn, weakens the vessel wall and may predispose to aneurysm expansion or rupture. By combining ^{18}F-NaF PET with CT and CT angiography, identification of hotspots of increased microcalcification in the aneurysm wall could allow identification of high-risk AAAs. These data, when combined with known clinical risk factors for disease progression, may allow patient-specific evaluation of AAA expansion or rupture risk. This is currently being investigated as part of the prospective sodium fluoride imaging (^{18}F-NaF PET-CT) in AAAs (SoFIA^3) study (NCT02229006) (figure 4).

OTHER TARGETS FOR MONITORING BIOLOGICAL ACTIVITY

Other potential PET tracers that may be useful in evaluating AAA disease do exist,[47] although research has so far been confined largely to preclinical autoradiography studies. ^{18}F-fluciclatide binds to integrins and has a high affinity for $\alpha_v\beta_3$, which is expressed on endothelial cells, fibroblasts and inflammatory cells, and is known to be upregulated in angiogenesis. One autoradiography study demonstrated that ^{18}F-fluciclatide detects areas of angiogenesis in AAA in vitro.[47] 18F-FMISO (fluoromisonidazole) and ^{18}F-HX4 are radiotracers that selectively identify areas of hypoxia and have been used to localise high-risk carotid artery plaque reflecting increased macrophage activity.[48] Proteolytic degradation of collagen and elastin in the extracellular matrix is another key component in AAA formation. Gadolinium-based contrast agents, using MRI tropoelastin-binding probes, have recently shown promise in imaging impaired elastinogenesis in atherosclerotic mice[49] and in humans following myocardial infarction.[50]

CONCLUSIONS AND FUTURE CHALLENGES

Current evaluation of AAA disease (using the basic morphological parameter of maximum aneurysm diameter) facilitates only a generic, population-based estimate of future aneurysm progression. However, more sophisticated methods of risk prediction are now required to plan timely surgical intervention, to allow appropriate screening intervals during AAA surveillance and to rationalise health resources.

While aneurysm disease shares some of the common pathways of atherosclerosis, its unique and, as yet, incompletely understood pathobiology means that further AAA-specific research is required to assess the value of promising imaging techniques that have been explored in the carotid and coronary arteries. There is a pressing need to understand the evolving biology of AAAs and its contribution to future AAA-related events. Emerging molecular imaging techniques offer the potential to add this additional biological information to the established risk factors for disease progression and may facilitate individual patient risk assessment.

Acknowledgements ROF is a principal investigator for the MRI in Abdominal Aortic Aneurysms to Predict Rupture or Surgery (MA^{3}RS) study (ISRCTN76413758) and the Sodium Fluoride Imaging (^{18}F-NaF PET-CT) in Abdominal Aortic Aneurysms (SoFIA^3) study (NCT02229006). DEN is the chief investigator for the MA^{3}RS study. JMJR is the chief investigator for the SoFIA^3 study.

Contributors ROF wrote and revised the manuscript. DEN and JMJR made substantial revisions. All authors approved the final draft.

Funding ROF is supported by a grant from the Medical Research Council National Institute for Health Research Efficacy and Mechanism Evaluation (NIHR EME) programme, which funds the MA^{3}RS study (funding reference 11/20/03). The SoFIA^3 study is funded by a grant from the Chief Scientist Office (funding reference ETM/365). DEN is supported by the British Heart Foundation (CH/09/002) and is the recipient of a Wellcome Trust Senior Investigator Award (WT103782AIA).

Competing interests None declared.

Provenance and peer review Commissioned; externally peer reviewed.

REFERENCES

1 Ashton HA, Buxton MJ, Day NE, *et al*, Multicentre Aneurysm Screening Study Group. The Multicentre Aneurysm Screening Study (MASS) into the effect of abdominal aortic aneurysm screening on mortality in men: a randomised controlled trial". *Lancet* 2002;360:1531–9.
2 The United Kingdom EVAR Trial Investigators. Endovascular versus open repair of abdominal aortic aneurysm. *N Eng J Med* 2010;362:1863–71.
3 Nicholls SC, Gardner JB, Meissner MH, *et al*. Rupture in small abdominal aortic aneurysms. *J Vasc Surg* 1998;28:884–8.
4 Mofidi R, Goldie VJ, Kelman J, *et al*. Influence of sex on expansion rate of abdominal aortic aneurysms. *Br J Surg* 2007;94:310–14.
5 Katz DJ, Stanley JC, Zelenock GB. Gender differences in abdominal aortic aneurysm prevalence, treatment, and outcome. *J Vasc Surg* 1997;25:561–8.
6 Golledge J, Muller J, Daugherty A, *et al*. Abdominal aortic aneurysm: pathogenesis and implications for management. *Arterioscler Thromb Vasc Biol* 2006;26:2605–13.
7 Brady AR, Thompson SG, Fowkes FGR, *et al*. Abdominal aortic aneurysm expansion: risk factors and time intervals for surveillance. *Circulation* 2004;110:16–21.
8 De Rango P, Farchioni L, Fiorucci B, *et al*. Diabetes and Abdominal Aortic Aneurysms. *Eur J Vasc Endovasc Surg* 2014;47:243–61.
9 Golledge J, Karan M, Moran CS, *et al*. Reduced expansion rate of abdominal aortic aneurysms in patients with diabetes May be related to aberrant monocyte-matrix interactions. *Eur Heart J* 2008;29:665–72.
10 Torsney E, Pirianov G, Cockerill GW. Diabetes as a negative risk factor for abdominal aortic aneurysm—does the disease aetiology or the treatment provide the mechanism of protection? *Curr Vasc Pharmacol* 2013;11:293–8.
11 Larsson E, Granath F, Swedenborg J, *et al*. A population-based case-control study of the familial risk of abdominal aortic aneurysm. *J Vasc Surg* 2009;49:47–50; discussion 51.
12 Kurvers H, Veith FJ, Lipsitz EC, *et al*. Discontinuous, staccato growth of abdominal aortic aneurysms. *J Am Coll Surg* 2004;199:709–15.
13 Fillinger MF, Racusin J, Baker RK, *et al*. Anatomic characteristics of ruptured abdominal aortic aneurysm on conventional CT scans: implications for rupture risk. *J Vasc Surg* 2004;39:1243–52.
14 Hinchliffe RJ, Alric P, Rose D, *et al*. Comparison of morphologic features of intact and ruptured aneurysms of infrarenal abdominal aorta. *J Vasc Surg* 2003;38:88–92.
15 Vorp DA, Lee PC, Wang D, *et al*. Association of intraluminal thrombus in abdominal aortic aneurysm with local hypoxia and wall weakening. *J Vasc Surg* 2001;34:291–9.
16 Naghavi M, Libby P, Falk E, *et al*. From vulnerable plaque to vulnerable patient: a call for new definitions and risk assessment strategies: Part II. *Circulation* 2003;108:1772–8.
17 Thompson MM, Jones L, Nasim A, *et al*. Angiogenesis in abdominal aortic aneurysms. *Eur J Vasc Endovasc Surg* 1996;11:464–9.
18 Vallabhaneni SR, Gilling-Smith GL, How TV, *et al*. Heterogeneity of tensile strength and matrix metalloproteinase activity in the wall of abdominal aortic aneurysms. *J Endovasc Ther* 2004;11:494–502.
19 Wilson WRW, Anderton M, Schwalbe EC, *et al*. Matrix metalloproteinase-8 and -9 are increased at the site of abdominal aortic aneurysm rupture. *Circulation* 2006;113:438–45.
20 Jaffer FA, Weissleder R. Molecular Imaging in the Clinical Arena. *JAMA* 2005;293:855–62.
21 Adamson PD, Dweck MR, Newby DE. The vulnerable atherosclerotic plaque: in vivo identification and potential therapeutic avenues. *Heart* 2015;101:1755–66.
22 Kramer CM, Cerilli LA, Hagspiel K, *et al*. Magnetic resonance imaging identifies the fibrous cap in atherosclerotic abdominal aortic aneurysm. *Circulation* 2004;109:1016–21.
23 Richards JMJ, Semple SI, MacGillivray TJ, *et al*. Abdominal aortic aneurysm growth predicted by uptake of ultrasmall superparamagnetic particles of iron oxide: a pilot study. *Circ Cardiovasc Imaging* 2011;4:274–81.
24 Alam S, Spath N, Richards J, *et al*. Nanoparticle enhanced MRI: a novel method of investigating myocardial infarction. *JACC* 2013;61(10_S):E1072.
25 Tang TY, Howarth SPS, Miller SR, *et al*. The ATHEROMA (Atorvastatin Therapy: Effects on Reduction of Macrophage Activity) Study. Evaluation using ultrasmall superparamagnetic iron oxide-enhanced magnetic resonance imaging in carotid disease. *J Am Coll Cardiol* 2009;53:2039–50.
26 McBride OMB, Berry C, Burns P, *et al*. MRI using ultrasmall superparamagnetic particles of iron oxide in patients under surveillance for abdominal aortic aneurysms

to predict rupture or surgical repair: MRI for abdominal aortic aneurysms to predict rupture or surgery—the MA3RS study. *Open Heart* 2015;2:e000190.
27 Tarkin JM, Joshi FR, Rudd JHF. PET imaging of inflammation in atherosclerosis. *Nat Rev Cardiol* 2014;11:443–57.
28 Courtois A, Nusgens BV, Hustinx R, *et al*. 18F-FDG Uptake Assessed by PET/CT in abdominal aortic aneurysms is associated with cellular and molecular alterations prefacing wall deterioration and rupture. *J Nuc Med* 2013;54:1740–7.
29 Reeps C, Essler M, Pelisek J, *et al*. Increased 18F-fluorodeoxyglucose uptake in abdominal aortic aneurysms in positron emission/computed tomography is associated with inflammation, aortic wall instability, and acute symptoms. *J Vasc Surg* 2008;48:417–23; discussion 424.
30 Nchimi A, Cheramy-Bien JP, Gasser TC, *et al*. Multifactorial relationship between 18F-fluoro-deoxy-glucose positron emission tomography signaling and biomechanical properties in unruptured aortic aneurysms. *Circ Cardiovasc Imaging* 2014;7:82–91.
31 Barwick TD, Lyons OTA, Mikhaeel NG, *et al*. 18F-FDG PET-CT uptake is a feature of both normal diameter and aneurysmal aortic wall and is not related to aneurysm size. *Eur J Nuc Med Mol Imaging* 2014;41:2310–18.
32 Kotze CW, Groves AM, Menezes LJ, *et al*. What is the relationship between 18F-FDG aortic aneurysm uptake on PET/CT and future growth rate? *Eur J Nuc Med Mol Imaging* 2011;38:1493–9.
33 Folco EJ, Sheikine Y, Rocha VZ, *et al*. Hypoxia but not inflammation augments glucose uptake in human macrophages: implications for imaging atherosclerosis with fluorine-labeled 2-Deoxy-D-glucose positron emission tomography. *J Am Coll Cardiol* 2011;58:603–14.
34 Rinne P, Hellberg S, Kiugel M, *et al*. Comparison of Somatostatin Receptor 2-Targeting PET Tracers in the Detection of Mouse Atherosclerotic Plaques. *Mol Imaging Biol* 2016;18:99–108.
35 Li X, Samnick S, Lapa C, *et al*. 68Ga-DOTATATE PET/CT for the detection of inflammation of large arteries: correlation with18F-FDG, calcium burden and risk factors. *EJNMMI Res* 2012;2:52.
36 Gaemperli O, Shalhoub J, Owen DRJ, *et al*. Imaging intraplaque inflammation in carotid atherosclerosis with 11C-PK11195 positron emission tomography/computed tomography. *Eur Heart J* 2012;33:1902–10.
37 Matter CM, Wyss MT, Meier P, *et al*. F-Choline Images Murine Atherosclerotic Plaques Ex Vivo. *Arterioscler Thromb Vasc Biol* 2006;26:584–9.
38 Bucerius J, Schmaljohann J, Bohm I, *et al*. Feasibility of 18-F-fluoromethylcholine PET/CT for imaging of vessel wall alterations in humans—first results. *Eur J Nuc Med Mol Imaging* 2008;35:815–20.
39 Sarda-Mantel L, Alsac JM, Boisgard R, *et al*. Comparison of 18F-fluoro-deoxy-glucose, 18F-fluoro-methyl-choline, and 18F-DPA714 for positron-emission tomography imaging of leukocyte accumulation in the aortic wall of experimental abdominal aneurysms. *J Vasc Surg* 2012;56:765–73.
40 Aikawa E, Nahrendorf M, Figueiredo JL, *et al*. Osteogenesis associates with inflammation in early-stage atherosclerosis evaluated by molecular imaging in vivo. *Circulation* 2007;116:2841–50.
41 Rudd JHF, Myers KS, Bansilal S, *et al*. Relationships among regional arterial inflammation, calcification, risk factors, and biomarkers a prospective fluorodeoxyglucose positron-emission tomography/computed tomography imaging study. *Circ Cardiovasc Imaging* 2009;2:107–15.
42 Duer MJ, Friscić T, Proudfoot D, *et al*. Mineral surface in calcified plaque is like that of bone: further evidence for regulated mineralization. *Arterioscler Thromb Vasc Biol* 2008;28:2030–4.
43 Buijs RVC, Willems TP, Tio RA, *et al*. Calcification as a Risk Factor for Rupture of Abdominal Aortic Aneurysm. *EurJ Vasc Endovasc Surg* 2013;46:542–8.
44 Reeps C, Maier A, Pelisek J, *et al*. Measuring and modeling patient-specific distributions of material properties in abdominal aortic aneurysm wall. *Biomech Model Mechanobiol* 2013;12:717–33.
45 Kelly-Arnold A, Maldonado N, Laudier D, *et al*. Revised microcalcification hypothesis for fibrous cap rupture in human coronary arteries. *Proc Natl Acad Sci USA* 2013;110:10741–6.
46 Joshi NV, Vesey AT, Williams MC, *et al*. 18F-fluoride positron emission tomography for identification of ruptured and high-risk coronary atherosclerotic plaques: a prospective clinical trial. *Lancet* 2014;383:705–13.
47 Tegler G, Estrada S, Hall H, *et al*. Autoradiography screening of potential positron emission tomography tracers for asymptomatic abdominal aortic aneurysms. *Ups J Med Sci* 2014;119:229–35.
48 van der Valk FM, Sluimer JC, Vöö SA, *et al*. In Vivo Imaging of Hypoxia in Atherosclerotic Plaques in Humans. *JACC Cardiovasc Imaging* 2015;8:1340–1.
49 Lacerda S, Andia ME, Botnar R. Development of a tropoelastin-binding MR contrast agent for in vivo imaging of impaired elastogenesis in atherosclerosis. *J Cardiovasc Magn Reson* 2015;17(Suppl 1):O102.
50 Protti A, Lavin B, Dong X, *et al*. Assessment of Myocardial Remodeling Using an Elastin/Tropoelastin Specific Agent with High Field Magnetic Resonance Imaging (MRI). *J Am Heart Assoc* 2015;4:e001851.

Heart

Monitoring the biological activity of abdominal aortic aneurysms *Beyond Ultrasound*

Rachael O Forsythe, David E Newby and Jennifer M J Robson

Heart published online February 15, 2016

openheart

MRI using ultrasmall superparamagnetic particles of iron oxide in patients under surveillance for abdominal aortic aneurysms to predict rupture or surgical repair: MRI for abdominal aortic aneurysms to predict rupture or surgery—the MA^{3}RS study

Olivia M B McBride,[1] Colin Berry,[2] Paul Burns,[1] Roderick T A Chalmers,[1] Barry Doyle,[1] Rachael Forsythe,[1] O James Garden,[1] Kirsteen Goodman,[1] Catriona Graham,[1] Peter Hoskins,[1] Richard Holdsworth,[3] Thomas J MacGillivray,[1] Graham McKillop,[1] Gordon Murray,[1] Katherine Oatey,[1] Jennifer M J Robson,[2] Giles Roditi,[2] Scott Semple,[1] Wesley Stuart,[2] Edwin J R van Beek,[1] Alex Vesey,[1] David E Newby[1]

To cite: McBride OMB, Berry C, Burns P, *et al*. MRI using ultrasmall superparamagnetic particles of iron oxide in patients under surveillance for abdominal aortic aneurysms to predict rupture or surgical repair: MRI for abdominal aortic aneurysms to predict rupture or surgery—the MA^{3}RS study. *Open Heart* 2015;**2**:e000190. doi:10.1136/openhrt-2014-000190

► Additional material is available. To view please visit the journal (http://dx.doi.org/10.1136/openhrt-2014-000190).

Received 7 October 2014
Accepted 18 January 2015

For numbered affiliations see end of article.

Correspondence to
Dr Olivia M B McBride;
olivia.mcbride@ed.ac.uk

ABSTRACT

Introduction: Population screening for abdominal aortic aneurysms (AAA) halves the associated mortality and has led to the establishment of national screening programmes. Prediction of aneurysm growth and rupture is challenging and currently relies on serial diameter measurements with ultrasound. Recently, a novel MRI-based technique using ultrasmall superparamagnetic particles of iron oxide (USPIO) has demonstrated considerable promise as a method of identifying aneurysm inflammation and expansion.

Methods and analysis: The MA^{3}RS study is a prospective observational multicentre cohort study of 350 patients with AAA in three centres across Scotland. All participants will undergo MRI with USPIO and aneurysm expansion will be measured over 2 years with CT in addition to standard clinical ultrasound surveillance. The relationship between mural USPIO uptake and subsequent clinical outcomes, including expansion, rupture and repair, will be evaluated and used to determine whether the technique augments standard risk prediction markers. To ensure adequate sensitivity to answer the primary question, we need to observe 130 events (composite of rupture or repair) with an estimated event rate of 41% over 2 years of follow-up. The MA^{3}RS study is currently recruiting and expects to report in 2017.

Discussion: This is the first study to evaluate the use of USPIO-enhanced MRI to provide additional information to aid risk prediction models in patients with AAA. If successful, this study will lay the foundation for a large randomised controlled trial targeted at applying this technique to determine clinical management.

KEY MESSAGES

What is already known about this subject?

- Current techniques for estimation of rupture risk in abdominal aortic aneurysm disease rely solely on diameter measurements from ultrasound. However, the absolute diameter of the aneurysm is not the sole determinant of the risk of rupture.
- USPIO-enhanced MRI can be used to detect focal hotspots of inflammation in asymptomatic aneurysms, and mural USPIO uptake is associated with more rapid expansion of aneurysms.

What does this study add?

- The aim of the MA^{3}RS study is to examine the relationship between mural USPIO uptake and subsequent clinical outcomes.

How might this impact on clinical practice?

- This technique may provide an improved method of risk stratification of patients with abdominal aortic aneurysms that extends beyond simple anatomical measurements of aneurysm diameter.

Trial registration number: Current Controlled Trials: ISRCTN76413758.

INTRODUCTION

Abdominal aortic aneurysm (AAA) disease is particularly prevalent in elderly men,

affecting 5% of men over the age of 65 years[1] and causing 2–3% of deaths within this group.[2] Aneurysm rupture is associated with a mortality rate in excess of 80%.[3 4] Population screening halves the mortality associated with AAA and has led to the establishment of national screening and surveillance programmes.[1] However, once an aneurysm has been diagnosed, there is currently no accurate method of predicting which patients are at risk of rupture and would benefit from elective surgical or endovascular intervention.

The aetiology of AAA is multifactorial, with environmental and genetic factors playing a part. Aneurysms typically occur in patients with atherosclerosis and there are a number of common risk factors, however, there are also distinct differences between the two disease processes. Atherosclerotic lesions are predominantly located within the tunica intima, whereas aneurysm disease affects the media and also the adventitia. Aneurysm disease is most commonly confined to the infrarenal aorta, whereas atherosclerosis is generally more widespread throughout the arterial tree. In aneurysm disease, cigarette smoking and hypertension are more strongly correlated with incidence and risk of rupture.[5]

The combined effects of biomechanical factors and biological processes weaken the aortic wall, and lead to aneurysm formation, expansion and rupture. Histopathologically, the aneurysmal aortic wall is characterised by focal medial neovascularisation, infiltration of inflammatory cells (principally macrophages) and fragmentation of elastin and collagen fibres within the extracellular matrix. Regions of intense biological activity represent sites of potential rupture, and can be considered as putative targets for novel imaging techniques to predict aneurysm expansion and assess the risk of rupture. In addition, tissue and wall stresses vary spatially within the aneurysm, and tensile strength varies in different parts of the aneurysm sac.[6 7] It is likely that expansion and rupture occur where regions of high biomechanical stress coincide with these biological 'hotspots' in the aneurysm wall that have become weakened. Indeed, there is strong evidence that aneurysm rupture is seen in those patients with more rapid aneurysm expansion rates.[8 9]

MRI

MRI is increasingly being used as an investigative tool for cardiovascular disease, enabling distinction between the different atherosclerotic plaque components, such as the lipid-rich necrotic core, fibrous cap and areas of calcification.[10] Standard gadolinium-based MRI is able to identify areas of thrombus formation and fibrosis in AAA.[11] However, recent innovations in cellular and molecular imaging methods have enabled the detection of key biological processes and vessel characteristics that may correlate with aneurysm disease progression.[12–14]

Superparamagnetic particles of iron oxide (SPIO) are part of a novel class of MRI contrast agents that provide additional biological and functional information through the detection of cellular inflammation within tissues. Current preparations of ultrasmall SPIO (USPIO) are biodegradable and safe for clinical administration.[15–17] USPIO are phagocytosed by macrophages within vascular and lymphatic tissues,[18–21] and can be used to detect tissue inflammation. USPIO accumulate in ruptured and vulnerable carotid plaques, and USPIO-enhanced MRI can detect a reduction in plaque inflammation following treatment with high-dose atorvastatin.[22] USPIO uptake has also been demonstrated in other regions of the vasculature, including the aorta, in preclinical models and also in small clinical studies.[23 24]

We have recently conducted a series of MRI studies in patients with AAA and shown that uptake of USPIO in the aortic wall correlates with macrophage activity, and identifies cellular inflammation.[25] Using a 3 T MR scanner, patients with asymptomatic AAA (n=29; aneurysm diameter 4.0–6.6 cm) attending our surveillance programme were imaged before and 24–36 h after intravenous administration of USPIO. Histological examination of aneurysm tissue confirmed co-localisation and uptake of USPIO in areas of macrophage infiltration.

Patients exhibiting USPIO uptake and inflammation within the wall of their aneurysm had a threefold higher aneurysm expansion rate (n=11, 0.66 cm/year; p=0.020) than patients with no (n=6, 0.22 cm/y) or non-specific (n=8, 0.24 cm/y) USPIO uptake, despite similar baseline anteroposterior diameters.[25] Indeed, one patient with a hotspot of USPIO uptake and biological activity within the wall of an aneurysm, died suddenly 2 months after scanning, from presumed aneurysm rupture.

We have shown that USPIO-enhanced MRI holds major promise as a new method of risk-stratification of patients with AAA and extends beyond simple anatomical measurements of aneurysm diameter. The aim of this present study is to validate this technique within a larger multicentre cohort study and to examine the relationship between baseline USPIO uptake and subsequent aneurysm expansion, requirement for elective repair and incidence of rupture.

METHODS AND ANALYSIS

Study design

The study is a prospective observational multicentre cohort study of patients with AAA disease under routine clinical surveillance, and will assess the role of MRI with USPIO to predict clinical disease progression.

Study objectives

Our previous proof-of-concept study[25] demonstrated that MRI with USPIO had the potential to predict clinical disease progression in patients with asymptomatic AAA. The aim of this study is to validate these findings, focusing on the relationship between baseline USPIO uptake and the subsequent clinical outcome and aneurysm expansion rates.

The primary objective of the study is to determine whether mural uptake of USPIO in AAA provides

incremental risk prediction in addition to standard risk markers such as aneurysm diameter, smoking and blood pressure.

Secondary objectives of the study are to ascertain whether mural uptake of USPIO in AAA: (1) correlates with the rate of aneurysm expansion; (2) occurs more commonly in patients who progress to surgery or whose aneurysm subsequently ruptures; (3) co-localises with, or relates to, areas of biomechanical stress and (4) occurs in a reproducible manner.

We will also investigate other inter-related mechanisms associated with aneurysm growth. We will specifically explore the added value of biomechanical stress modelling as we suspect co-localisation of USPIO uptake and areas of high mechanical stress could act synergistically, and cause more marked aneurysm growth. We will also examine correlates with other blood biomarkers including regulators of extracellular matrix turnover (such as matrix metalloproteinases and tissue inhibitors of metalloproteinases) and vascular inflammation (such as C reactive protein and interleukin 6).

Reproducibility of the technique will be assessed in a subgroup (n=20) of study participants (from the Edinburgh study centre) who will undergo repeat MRI and USPIO administration at <1 month and 1 year. Short-term (<1 month) reproducibility is likely to reflect the variability in USPIO uptake whereas long-term (1 year) reproducibility is likely to represent the variation in biology of the aortic aneurysm with time.

This will lay the foundation for a large multicentre randomised controlled trial targeted at applying this technique to determine clinical management and surgical intervention. This will be particularly important given the fact that screening programmes for the detection of AAA are being rolled out in many countries and this is likely to increase substantially the number of patients being entered into surveillance programmes.

Study end points

The primary endpoint of the study will be the composite rate of aneurysm rupture or repair. The following secondary endpoints will be evaluated: (1) the rate of aneurysm rupture; (2) the rate of surgical or endovascular repair of the aneurysm; (3) the aneurysm growth rate and (4) all-cause and aneurysm-related mortality.

We will conduct exploratory analyses examining the interactions between mural USPIO uptake, biomechanical stress, clinical risk factors, and serum biomarkers of extracellular matrix turnover and inflammation.

Study population

Participants will be identified from clinical surveillance programmes and databases at three centres: Royal Infirmary of Edinburgh, Western Infirmary in Glasgow and Forth Valley Royal Hospital (FVRH). We will recruit 350 participants over a 24-month period with recruitment having begun on 6 November 2012. Recruitment rate and summary statistics can be viewed at online supplementary appendix 2.

Inclusion criteria will be: (1) AAA measuring ≥4.0 cm in anteroposterior diameter on ultrasound scanning and (2) age ≥40 years. Patients under the age of 40 years will be excluded since they may have a connective tissue disorder accounting for their disease.

Exclusion criteria will be: (1) patients expected to undergo imminent elective or emergency surgical or endovascular repair; (2) contraindication to MRI scanning identified from MRI safety questionnaire; (3) patients refusing or unable to give informed consent; (4) women with childbearing potential or who are breast feeding will not be enrolled into the study (women who are currently pregnant or have experienced menarche but are premenopausal and have not been sterilised will be excluded); (5) intercurrent illness including patients with a systemic inflammatory disorder or underlying malignancy (life expectancy <2 years); (6) renal dysfunction (estimated glomerular filtration rate ≤30 mL/min/1.73 m^2); (7) polycythaemia; (8) contraindication to ferumoxytol (evidence of known iron overload, haemochromatosis, known hypersensitivity to ferumoxytol or its components or anaemia not caused by iron deficiency) and (9) contraindication to iodine-based contrast.

Participant selection and enrolment

Eligible participants will be identified from the clinical aneurysm surveillance database and will be approached by a member of the study team at their ultrasound appointment. Participants will be supplied with the study information sheet either in person or by post. Written informed consent will be obtained from patients willing to participate in the study. Participants are free to withdraw from the study at any point or the investigator can choose to withdraw a participant. If a participant has consented for the study and then wishes to withdraw, providing they have not been administered ferumoxytol, another participant will be recruited in their place.

Study drug

Ferumoxytol

Ferumoxytol (Rienso) is composed of USPIO coated with polyglucose sorbitol carboxymethylether. It is supplied as an aqueous colloidal product that is formulated with mannitol and presented in single use vials ready for intravenous infusion. Each vial contains 510 mg of elemental iron in a volume of 17 mL of mannitol.

The ferumoxytol dose (4 mg/kg) is removed from the vial and administered intravenously at a rate of up to 1 mL/s. The single dose is given immediately following the baseline MRI and 24–36 h before the postcontrast scan. Blood pressure is recorded before and 30 min after administration to monitor for hypotension. In a subset of patients (n=20), MRI scanning and USPIO administration will be repeated at <1 month and 1 year (up to a total of 3 doses of ferumoxytol in 1 year). Each

dose of ferumoxytol equates to approximately 7% of total body iron.

The study drug is manufactured by AMAG Pharmaceuticals Inc (Lexington, Massachusetts, USA), and distributed and released by Takeda Italia Farmaceutica SPA in Europe.

Buscopan

Intravenous Buscopan (hyoscine butylbromide) 20 mg will be administered before each MRI to reduce artefact from bowel peristalsis in patients who do not have a contraindication (allergic reaction, narrow angle glaucoma, paralytic ileus, myasthaenia gravis, obstructive prostatic hypertrophy).

Study assessments and data collection

Online supplementary appendix 1 outlines the assessments performed at each study visit. Figure 1 shows the study flow chart. Patients recruited in Edinburgh and Glasgow will undergo all study investigations in their respective centre. For patients recruited from FVRH, they will have the choice of attending the study in either Edinburgh or Glasgow. They will continue to have their surveillance ultrasound scan at FVRH.

Clinical assessment

Patients will have a full formal and standardised clinical assessment at baseline that will include history, examination and documentation of cardiovascular risk factor profile (smoking status, family history, hypertension, hyperlipidaemia, diabetes mellitus). Concomitant medications (antihypertensive medication, etc) will be recorded at baseline and at the end of the study.

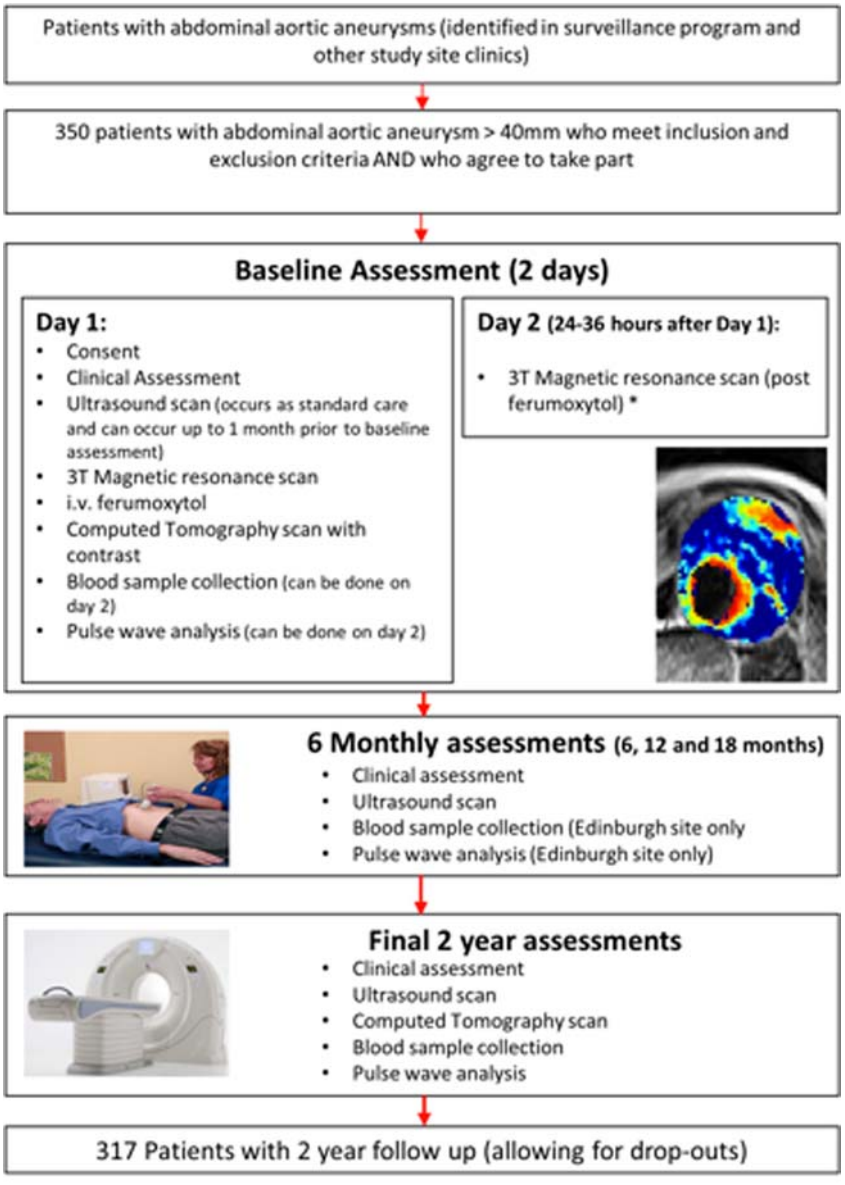

Figure 1 Study flow chart (i.v., intravenous).

Blood sampling

Blood samples (20 mL on each visit) will be collected at baseline and at 24 months, for routine haematology and biochemistry including full blood count, urea, creatinine and electrolytes, liver function tests, total cholesterol and glucose.

For patients recruited and imaged in the Edinburgh centre, a further blood sample (9 mL) will be collected at baseline and at 6, 12, 18 and 24 months. Samples will be processed (plasma and serum) and stored at −80°C for later analysis of potential extracellular matrix and inflammatory biomarkers.

Pulse wave analysis and velocity

Pulse wave analysis and velocity will be measured in triplicate in fasted patients using applanation tonometry (SphygmoCor, AtCor Medical, Sydney Australia). This will facilitate the measurement of central aortic pressure to assist in the modelling of biomechanical stress within the aneurysm. This will be measured at baseline and at 6, 12, 18 and 24 months.

Ultrasound of the abdominal aorta

Patients will undergo ultrasound imaging as part of the standard clinical surveillance programme with measurement of the maximum anteroposterior diameter of the aneurysm. Ultrasound scans will be performed every 6 ±2 months. A 3.5 MHz linear array transducer will be used to provide standard real time longitudinal B-scan images of the AAA at the point of maximum diameter. Maximum anteroposterior AAA diameter and distensibility (pressure strain elastic modulus and stiffness) will be assessed. Scans will be undertaken by accredited clinical vascular scientists with interobserver coefficient of variation of aortic diameter measurements of 3.5% in our laboratory.[26]

CT of the abdominal aorta

Contrast-enhanced images of the abdominal aorta will be obtained using a 320-multidetector (Edinburgh; Aquilion ONE; Toshiba) or 64-multidetector CT scanner (Glasgow; Brilliance 64; Philips), at baseline and 2 years. These data will be reconstructed into three dimensions (3D) using volumetric matrices to enable a more comprehensive assessment of the aneurysm geometry and growth than that provided by the ultrasound assessment of the unidimensional aortic anteroposterior diameter. In cases where study participants undergo emergency repair of a ruptured AAA, a CT scan may not be performed. In the event of patients not receiving the CT scan at baseline it will be performed within 1 month of the baseline visit.

MRI of the abdominal aorta

MRI will be conducted using a 3 T Siemens Magnetom Verio scanner (Siemens, Erlangen, Germany) before and 24–36 h after administration of the USPIO in Edinburgh or Glasgow. Scanning protocols from the two centres were validated prior to study initiation. The MRI safety questionnaire will be applied to identify patients with a contraindication to scanning. Patients will be given intravenous Buscopan (hyoscine butylbromide) prior to imaging to minimise bowel motion artefacts. Routine clinical coronal and sagittal breath-held T2-weighted (T2W) multislice HASTE sequences will be used to identify the position and extent of the aneurysm, following which a respiratory-gated, T2W turbo spin echo sequence will be used to acquire detailed anatomical data (TR/TE 2500/252 ms; matrix 365×384; field of view 300×400 mm; slice width 5 mm). These data are acquired with and without Spectral Attenuated Inversion Recovery fat suppression in order to allow segmentation of aortic wall. A multiecho, gradient echo T2*W sequence (TE 4.9, 7.7, 10.5, 13.3 ms; TR 133 ms; flip angle 15°; matrix 192×256; field of view 400×400 mm; slice width 5 mm) will be used to acquire contiguous axial images of the entire aneurysm (from the neck of the aneurysm down to the iliac bifurcation) with slice positions corresponding to those of the T2W images. Saturation bands are placed over the anterior abdomen for the T2*W acquisition in order to minimise breathing-related artefact.

Clinical management of AAA

The management of AAA in NHS Scotland follows international[27] and national guidelines.[28] Elective AAA repair is considered when the anteroposterior diameter, as measured by ultrasound scanning, reaches 5.5 cm, the AAA grows >1 cm in 1 year or the AAA is symptomatic. Furthermore, the decision for elective AAA repair will be made by independent clinicians who will be unaware of the USPIO-enhanced MRI. These clinicians do not have routine access to the CT scans. However, clinically important incidental findings will be communicated to the clinicians. Study investigators will not be directly involved in the patient's care or treatment decisions. In the case of patients undergoing surgery where repair of the AAA is not the primary intention (eg, in the case of repair of a common iliac aneurysm with concomitant AAA), they will be included in the primary analysis on an intention-to-treat analysis.

Follow-up for patients in certain circumstances

If a patient undergoes an open or endovascular repair of their aneurysm, we will record the results of any scans that are carried out for clinical reasons (such as extra CT or ultrasound scans). Those undergoing open repair will have aneurysm wall tissue collected and stored for the assessment of tissue resident macrophages and matrix metalloproteinases. These patients will be invited to return every 6 months for blood tests but not ultrasound or pulse wave analysis or velocity.

Proposed analysis

Image analysis of ultrasound

Cursors will be locked onto echoes representing the anterior and posterior aortic walls and the movement of both tracked with each cardiac cycle. The longitudinal image will be used for analysis as experience with the technique and data from formal reproducibility studies indicate that the quality of the data obtained from a longitudinal section is superior to that obtained from a transverse view. Images will be captured digitally for later offline core laboratory review.

Image analysis of CT

CT of the abdominal aorta will be performed at baseline and 2 years to assess regional and volumetric growth rates. These two CT scans will be spatially co-registered so that areas of expansion and growth can be more accurately defined, and can permit correlation with areas of USPIO uptake and finite element analysis modelling.

Three-dimensional computer models will be generated from segmented, contrast-enhanced images, allowing geometric indices to be quantified. Semiautomatic segmentation is achievable due to the intensity differences between the aneurysm, and surrounding tissues and structures. Intensity thresholding will be used to identify the lumen. To detect the thrombus and complete the segmentation, we will use a 3D deformable model approach that utilises the level set algorithm as well as modelling the thrombus contour as a radial function starting from the aortic centre line as calculated from the lumen segmentation.

Image analysis of MRI

A region of interest encompassing the aortic wall and thrombus but excluding the lumen will be drawn on each slice of the precontrast T2W image. The precontrast T2W scan will be used as the base image to which subsequent scans will be co-registered using a semiautomatic rigid 3D voxel registration protocol utilising a normalised mutual information algorithm. To minimise the contribution of bowel and abdominal wall motion in the MRI datasets, a region for registration will include the aorta, vertebrae and spinal musculature that remain relatively static during the respiratory cycle, but exclude the more mobile abdominal wall and bowel.

The four echoes in the multiecho T2*W sequence will be combined to generate T2* and R2* maps. The T2* value is the decay constant for the exponential decay of signal intensity with time and its inverse is the R2* value. A 3×3 voxel Gaussian filter will be applied to the individual echoes to reduce noise, and the coefficient of determination will be used to exclude data that do not have an acceptable straight line fit when the log of signal intensity is plotted against echo time. Images will be co-registered to allow direct comparison of the precontrast and postcontrast T2*W MRI. USPIO uptake will be presented visually as a colour map of change in T2* or R2* values between pre-USPIO and post-USPIO scans, with our previously validated threshold of significance applied (figure 2).[25] The change in T2* or R2* colour maps from the MRI will be spatially co-registered to the CT datasets.

Finite element analysis

Using Abaqus/Complete Abaqus Environment, the vessel wall will be modelled as a constant thickness layer of 1.5 mm, with a hyperelastic constitutive model. Thrombus will be modelled as homogeneous and isotropic with Young's modulus 0.1 MPa. The model will be inflated from diastolic to systolic pressure using a homogeneous pressure-modelling regime. Peak wall stress and other rupture indices will be calculated and compared against areas of USPIO uptake.

Statistics and data analysis

Sample size calculation

The sample size is determined by the numbers required to build robust prognostic models for rupture or surgical

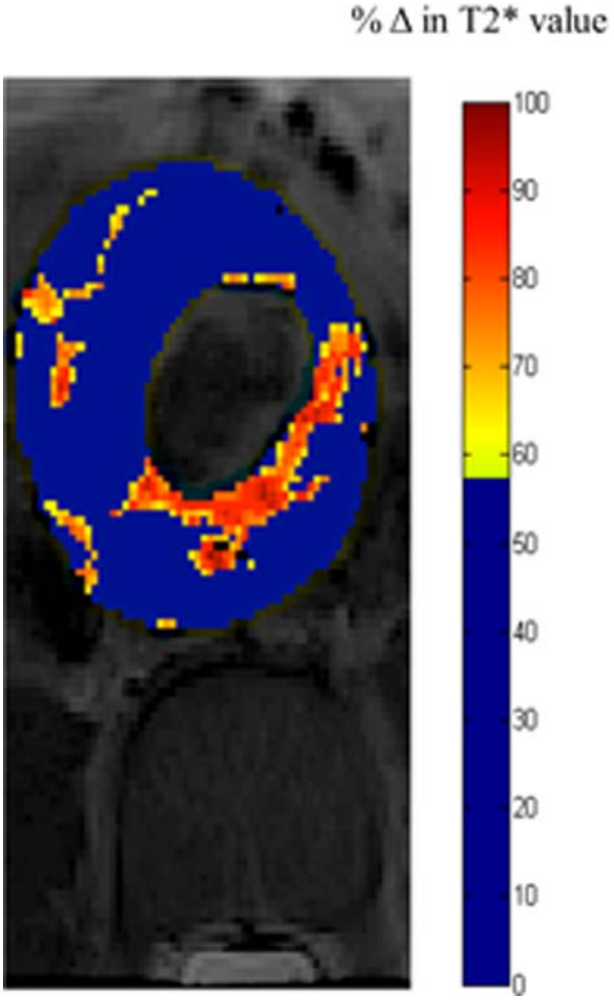

Figure 2 Colour map of MRI of an abdominal aortic aneurysm. Red and yellow pixels indicate areas of increased T2* value, indicative of ultrasmall superparamagnetic particles of iron oxide uptake.

repair, and in particular to measure the additional prognostic value of mural USPIO uptake when added to such a prognostic model based only on conventional clinical risk factors. There is a widely accepted 'rule of thumb' that one needs at least 10 and ideally 20 outcome events per covariate to be included in a prognostic model.[29] As described in more detail below, we plan to use the net reclassification index (NRI) as the primary measure of the clinical relevance of the added prognostic value of mural USPIO uptake.[30 31] Based on two recent papers using the NRI,[32 33] and also taking account of the Harrell 'rule of thumb', we estimate that we need to observe 130 events (ie, the composite of rupture or surgical repair) to have adequate sensitivity to answer the primary question. With our estimated event rate of 41% over the mean duration of follow-up of 2 years,[34] this equates to 317 patients. The estimated event rate is based on a composite endpoint of rupture and repair. This is taken from a previous study at our centre,[34] where rupture rates were 13% and elective intervention rates were in the region of 30% over a 2-year period.

The sample size has been derived so that the study will allow us to assess the 'added value' of USPIO uptake over and above conventional clinical risk factors in predicting rupture and/or the need for surgical intervention. As such, conventional type I and II errors are not relevant. However, the approach we have adopted is extremely conservative in terms of a conventional power calculation. For example, if we assume that 40% of the patients are 'positive' for USPIO uptake, and that their event rate is 55%, compared with an event rate of 30% in the uptake 'negative' patients, then the statistical power to detect such an effect would be over 99% at the 5% significance level (2-sided). In other words, the study has extremely high power to detect an effect of the order that would be required if USPIO uptake is to add usefully to conventional prognostic factors.

There should be very modest losses to follow-up for the primary analysis, since all study recruits are already enrolled in a surveillance programme. Moreover, we shall seek consent at the time of recruitment to flag the patients so that if any patients are lost to follow-up they can be traced to identify any hospital admissions or to identify if they have died. In addition, some patients will drop out due to technical failure of the scan, such as claustrophobia or a severe reduction in image quality preventing analysis. Image quality will be assessed on a four-point Likert scale (1=excellent; 2=mild reduction in image quality; 3=moderate reduction in image quality; and 4=severe reduction in image quality). We have, therefore, conservatively accounted for a 10% drop out rate and we will recruit 350 patients to the study.

Statistical analysis

The baseline assessment will include the baseline aneurysm diameter, sex, smoking habit and blood pressure. Using these covariates, a prognostic model predicting the time to the composite outcome event of rupture or surgical repair will be developed using Cox proportional hazards regression. The added prognostic value of adding mural USPIO uptake to this model will be assessed using the increase in the area under the receiver operator characteristic curve, the Nagelkerke partial R^2 and, primarily, the NRI.[32 33] The NRI is a direct measure of the clinical relevance of adding a covariate to a prognostic model. It is an overall measure of how many patients move from a low predicted risk to a high predicted risk when the covariate is added (and whether these individuals are indeed high risk), and how many move from a high predicted risk to a low predicted risk (and whether these individuals are indeed low risk). For the primary analysis, the USPIO will be taken as a binary covariate (as in Richards *et al*[25]), but a sensitivity analysis will explore the potential for including a quantification of the USPIO uptake. Some but not all of the patients will also have a measure of current aneurysm growth rate at baseline, and a further sensitivity analysis will explore using growth rate as a further prognostic factor, using imputation when the estimated growth rate is not available.

A secondary analysis will follow a similar analytical strategy to that set out above, but using prognostic models to predict aneurysm growth rate. This analysis will be far more complex with the inclusion of serial measures of aneurysm diameter and with these measurements being censored on rupture or on surgical repair. Further exploratory analysis will look at the predictive ability of measures of wall stress and how these interact with regional USPIO uptake.

The reproducibility of the technique will be assessed with participants categorised with respect to the presence or absence of USPIO uptake at 1 month and 1 year, to define the proportionate agreement, with 95% CIs.

ETHICS AND DISSEMINATION

Research sponsorship is provided by the Academic and Clinical Central Office for Research and Development (ACCORD), a partnership between the University of Edinburgh and NHS Lothian Health Board.

The results of the study will be submitted for publication in peer-reviewed journals.

Results will also be disseminated through presentations at national and international conferences.

DISCUSSION

The multicentre MA^{3}RS study will assess the ability of USPIO-enhanced MRI to augment standard risk markers for AAA expansion or rupture in 350 patients attending aneurysm surveillance clinics. This is the first study to assess novel MRI-based imaging approaches to improve risk prediction in this common and potentially fatal condition.

Mortality from ruptured AAA is very high, at approximately 90%. In contrast, the risk of death from open

surgical or endovascular repair is low, at 1–5%.[35] The aim is therefore to identify AAA prior to rupture and consider surgery when the risk of rupture exceeds that of elective repair. Aneurysm screening reduces the risk of aneurysm-related death by 53–73%, and has been introduced throughout the UK and in many countries across the world.[1 36 37] Evaluation of rupture risk is currently based on the maximum anteroposterior diameter of the aneurysm. Elective aneurysm repair is offered to patients with an aneurysm diameter of >5.5 cm or if aneurysm expansion is >1.0 cm/year. However, while the risk of rupture increases with diameter,[8 38 39] the absolute diameter of the aneurysm is not the sole determinant of the risk of rupture,[40] and elective repair when the diameter is <5.5 cm offers no survival benefit over continued surveillance.[41] Furthermore, 1 in 14 screen-detected aneurysms <5.5 cm in diameter will rupture within 3 years of detection, and up to one-fifth of ruptured AAA are <5.5 cm in diameter, while many patients present with diameters considerably >5.5 cm without prior symptoms or rupture.[8 41 42] The increase in patients under long-term surveillance with the introduction of nationwide screening, coupled with the unpredictability and non-linearity of aneurysm growth, highlight the need for an improved method of risk prediction in aneurysm disease. This will then enable preventative surgical or endovascular repair to be targeted to the high-risk patients.

We have previously demonstrated that the assessment of USPIO uptake with MRI can be used to detect focal hotspots of inflammation in asymptomatic aneurysms, and that mural USPIO uptake is associated with more rapid expansion of aneurysms.[25] By assessing these biological processes and evaluating them with this novel technique, the MA^{3}RS study aims to develop an improved method of assessing rupture risk in AAA in a large prospective clinical study with a long duration of follow-up.

We will model differing thresholds of risk predictors that have the potential to inform future interventional trials. For example, this study could define USPIO-enhanced MRI features that predict aneurysm rupture. This could lead to the design of a major interventional trial whereby surgical intervention could be targeted at those aneurysms that are vulnerable or prone to rupture. This could include surgery in patients with aneurysms <5.5 cm or mandate conservative management in those with aneurysms >5.5 cm. A more sophisticated stratified approach has the potential to save lives as well as avoid unnecessary high-risk surgery in those who are unlikely to come to harm.

Trial status

The study has been approved by the East of Scotland Research Ethics Committee. Recruitment is underway at all sites and two-thirds of the study population have already been recruited. Completion of study enrolment is anticipated in autumn 2014.

Author affiliations
[1]British Heart Foundation/University of Edinburgh Centre for Cardiovascular Science, Edinburgh, UK
[2]BHF Glasgow Cardiovascular Research Centre, University of Glasgow, Glasgow, UK
[3]Forth Valley Royal Hospital, Larbert, UK

Collaborators *MA^{3}RS Trialists*: Chief Investigator: DEN. Principal Investigators Edinburgh: OMBM, RF and AV. Principal Investigator Glasgow: WS. Principal Investigator Forth Valley Royal Hospital: RH. Grant applicants: DEN, GMc, RTAC, PB, JMJR, SS, TJM, CG, OJG, PH, BD, EJRvB, GMu, CB and WS. *Trial Steering Committee*: Professor Julie Brittenden (Chair), Professor Graeme Houston, Robert Lambie, Professor John Norrie, DEN, GMc, SS, PB, GMu, KG, KO and OMBM. *Edinburgh Clinical Trials Unit*: GMu, KG, KO, Lynsey Milne, Garry Milne and CG.

Contributors DEN and JMJR conceived the study, participated in its design and coordination, and helped draft the manuscript. OMBM helped to draft the manuscript. All authors read and approved the final manuscript.

Funding The study was funded by a grant from the Medical Research Council National Institute for Health Research Efficacy and Mechanism Evaluation (NIHR EME) programme. Additional contributions came from the Chief Scientists Office (CSO; ETM/365). DEN is supported by the British Heart Foundation (CH/09/002) and the Wellcome Trust (WT103782AIA). OMBM is supported by the Academic Department of Military Surgery and Trauma. The Clinical Research Imaging Centre and Wellcome Trust Clinical Research Facility (Edinburgh), and the Clinical Research Facility Glasgow, are supported by National Health Service Research Scotland (NRS). The Glasgow Cardiovascular Research Centre is supported by the British Heart Foundation.

Competing interests None.

Ethics approval East of Scotland Research Ethics Committee (A).

Provenance and peer review Not commissioned; externally peer reviewed.

Data sharing statement No additional data are available.

REFERENCES

1. Ashton HA, Buxton MJ, Day NE, *et al*., Multicentre Aneurysm Screening Study Group. The Multicentre Aneurysm Screening Study (MASS) into the effect of abdominal aortic aneurysm screening on mortality in men: a randomised controlled trial. *Lancet* 2002;360:1531–9.
2. Gillum RF. Epidemiology of aortic aneurysm in the United States. *J Clin Epidemiol* 1995;48:1289–98.
3. Logan AJ, Bourantas NI, Moseley LG, *et al*. Mortality from ruptured abdominal aortic aneurysm in Wales. *Br J Surg* 2000;87:966–7.
4. Johnston KW. Ruptured abdominal aortic aneurysm: six-year follow-up results of a multicenter prospective study. Canadian Society for Vascular Surgery Aneurysm Study Group. *J Vasc Surg* 1994;19:888–900.
5. Brady AR, Thompson SG, Fowkes FG, *et al*. Abdominal aortic aneurysm expansion: risk factors and time intervals for surveillance. *Circulation* 2004;110:16–21.
6. Raghavan ML, Vorp DA. Toward a biomechanical tool to evaluate rupture potential of abdominal aortic aneurysm: identification of a finite strain constitutive model and evaluation of its applicability. *J Biomech* 2000;33:475–82.
7. Vallabhaneni SR, Gilling-Smith GL, How TV, *et al*. Heterogeneity of tensile strength and matrix metalloproteinase activity in the wall of abdominal aortic aneurysms. *J Endovasc Ther* 2004;11:494–502.
8. Thompson AR, Cooper JA, Ashton HA, *et al*. Growth rates of small abdominal aortic aneurysms correlate with clinical events. *Br J Surg* 2009;97:37–44.
9. Brown PM, Zelt DT, Sobolev B. The risk of rupture in untreated aneurysms: the impact of size, gender, and expansion rate. *J Vasc Surg* 2003;37:280–4.

10. Cai J, Hatsukami TS, Ferguson MS, *et al*. In vivo quantitative measurement of intact fibrous cap and lipid-rich necrotic core size in atherosclerotic carotid plaque: comparison of high-resolution, contrast-enhanced magnetic resonance imaging and histology. *Circulation* 2005;112:3437–44.
11. Kramer CM, Cerilli LA, Hagspiel K, *et al*. Magnetic resonance imaging identifies the fibrous cap in atherosclerotic abdominal aortic aneurysm. *Circulation* 2004;109:1016–21.
12. Jaffer FA, Libby P, Weissleder R. Molecular imaging of cardiovascular disease. *Circulation* 2007;116:1052–61.
13. Rajani N, Joshi FR, Tarkin JM, *et al*. Advances in imaging vascular inflammation. *Clin Transl Imaging* 2013;1:305–14.
14. Choudhury RP, Fisher EA. Molecular imaging in atherosclerosis, thrombosis, and vascular inflammation. *Arterioscler Thromb Vasc Biol* 2009;29:983–91.
15. Bernd H, De Kerviler E, Gaillard S, *et al*. Safety and tolerability of ultrasmall superparamagnetic iron oxide contrast agent: comprehensive analysis of a clinical development program. *Invest Radiol* 2009;44:336–42.
16. Bourrinet P, Bengele HH, Bonnemain B, *et al*. Preclinical safety and pharmacokinetic profile of ferumoxtran-10, an ultrasmall superparamagnetic iron oxide magnetic resonance contrast agent. *Invest Radiol* 2006;41:313–24.
17. Müller K, Skepper JN, Posfai M, *et al*. Effect of ultrasmall superparamagnetic iron oxide nanoparticles (Ferumoxtran-10) on human monocyte-macrophages in vitro. *Biomaterials* 2007;28:1629–42.
18. Harisinghani MG, Barentsz J, Hahn PF, *et al*. Noninvasive detection of clinically occult lymph-node metastases in prostate cancer. *N Engl J Med* 2003;348:2491–9.
19. Heesakkers R, Hövels AM, Jager GJ, *et al*. MRI with a lymph-node-specific contrast agent as an alternative to CT scan and lymph-node dissection in patients with prostate cancer: a prospective multicohort study. *Lancet Oncol* 2008;9:850–6.
20. Kooi ME, Cappendijk VC, Cleutjens KBJM, *et al*. Accumulation of ultrasmall superparamagnetic particles of iron oxide in human atherosclerotic plaques can be detected by in vivo magnetic resonance imaging. *Circulation* 2003;107:2453–8.
21. Trivedi RA, Mallawarachi C, U-King-Im J-M, *et al*. Identifying inflamed carotid plaques using in vivo USPIO-enhanced MR imaging to label plaque macrophages. *Arterioscler Thromb Vasc Biol* 2006;26:1601–6.
22. Tang TY, Howarth SPS, Miller SR, *et al*. The ATHEROMA (Atorvastatin Therapy: Effects on Reduction of Macrophage Activity) Study. Evaluation using ultrasmall superparamagnetic iron oxide-enhanced magnetic resonance imaging in carotid disease. *Journal Am Coll Cardio* 2009;53:2039–50.
23. Sadat U, Taviani V, Patterson AJ, *et al*. Ultrasmall superparamagnetic iron oxide-enhanced magnetic resonance imaging of abdominal aortic aneurysms—a feasibility study. *Eur J Vasc Endovasc Surg* 2011;41:167–74.
24. Turner GH, Olzinski AR, Bernard RE, *et al*. Assessment of macrophage infiltration in a Murine model of abdominal aortic aneurysm. *J Magn Reson Imaging* 2009;30:455–60.
25. Richards JMJ, Semple SI, MacGillivray TJ, *et al*. Abdominal aortic aneurysm growth predicted by uptake of ultrasmall superparamagnetic particles of iron oxide: a pilot Study. *Circ Cardiovasc Imaging* 2011;4:274–81.
26. Wilson KA, Hoskins PR, Lee AJ, *et al*. Ultrasonic measurement of abdominal aortic aneurysm wall compliance: a reproducibility study. *J Vasc Surg* 2000;31:507–13.
27. Hirsch AT, Haskal ZJ, Hertzer NR, *et al*. ACC/AHA 2005 practice guidelines for the management of patients with peripheral arterial disease (lower extremity, renal, mesenteric, and abdominal aortic). *Circulation* 2006;113:e463–5.
28. *Nice.org.Uk* (http://www.nice.org.uk)
29. Harrell FE, Lee KL, Califf RM, *et al*. Regression modelling strategies for improved prognostic prediction. *Stat Med* 1984;3:143–52.
30. Pencina MJ, D'Agostino RB, D'Agostino RB, *et al*. Evaluating the added predictive ability of a new marker: from area under the ROC curve to reclassification and beyond. *Stat Med* 2008;27:157–72; discussion 207–12.
31. Pencina MJ, D'Agostino RB, Steyerberg EW. Extensions of net reclassification improvement calculations to measure usefulness of new biomarkers. *Stat Med* 2011;30:11–21.
32. Fellahi J-L, Le Manach Y, Daccache G, *et al*. Combination of EuroSCORE and cardiac troponin I improves the prediction of adverse outcome after cardiac surgery. *Anesthesiology* 2011;114:330–9.
33. Polak JF, Pencina MJ, Pencina KM, *et al*. Carotid-wall intima-media thickness and cardiovascular events. *N Engl J Med* 2011;365:213–21.
34. Wilson KA, Lee AJ, Lee AJ, *et al*. The relationship between aortic wall distensibility and rupture of infrarenal abdominal aortic aneurysm. *J Vasc Surg* 2003;37:112–17.
35. National Vascular Registry. 2013 Report on Surgical Outcomes Consultant-level statistics. 2013:1–62.
36. Fleming C, Whitlock EP, Beil TL, *et al*. Screening for abdominal aortic aneurysm: a best-evidence systematic review for the U.S. Preventive Services Task Force. *Ann Intern Med* 2005;142:203–11.
37. Lindholt JS, Juul S, Fasting H, *et al*. Screening for abdominal aortic aneurysms: single centre randomised controlled trial. *BMJ* 2005;330:750.
38. Mofidi R, Goldie VJ, Kelman J, *et al*. Influence of sex on expansion rate of abdominal aortic aneurysms. *Br J Surg* 2007;94:310–14.
39. Vorp DA, Vande Geest JP. Biomechanical determinants of abdominal aortic aneurysm rupture. *Arterioscler Thromb Vasc Biol* 2005;25:1558–66.
40. Darling RC, Messina CR, Brewster DC, *et al*. Autopsy study of unoperated abdominal aortic aneurysms. The case for early resection. *Circulation* 1977;56:II161–4.
41. Greenhalgh RM, Brady AR, Brown LC, *et al*. Mortality results for randomised controlled trial of early elective surgery or ultrasonographic surveillance for small abdominal aortic aneurysms. The UK Small Aneurysm Trial Participants. *Lancet* 2005;352:1649–55.
42. Nicholls SC, Gardner JB, Meissner MH, *et al*. Rupture in small abdominal aortic aneurysms. *J Vasc Surg* 1998;28:884–8.

MRI using ultrasmall superparamagnetic particles of iron oxide in patients under surveillance for abdominal aortic aneurysms to predict rupture or surgical repair: MRI for abdominal aortic aneurysms to predict rupture or surgery––the MA^{3}RS study

Olivia M B McBride, Colin Berry, Paul Burns, Roderick T A Chalmers, Barry Doyle, Rachael Forsythe, O James Garden, Kirsteen Goodman, Catriona Graham, Peter Hoskins, Richard Holdsworth, Thomas J MacGillivray, Graham McKillop, Gordon Murray, Katherine Oatey, Jennifer M J Robson, Giles Roditi, Scott Semple, Wesley Stuart, Edwin J R van Beek, Alex Vesey and David E Newby

Open Heart 2015 2:
doi: 10.1136/openhrt-2014-000190

APPENDIX ii

Manuscripts Under Submission

ORIGINAL ARTICLE

^{18}F-Sodium Fluoride Uptake in Abdominal Aortic Aneurysms

The SoFIA^3 Study

Rachael O Forsythe MD,[1-3] Marc R Dweck MD,[1-3] Olivia MB McBride MD,[1-3] Alex T Vesey MD,[1,2] Scott I Semple PhD,[1-3] Anoop SV Shah MD,[1] Philip D Adamson MD,[1] William Wallace MD,[3] Jakub Kaczynski MD,[1-3] Weiyang Ho MD,[1] Edwin JR van Beek MD,[2,3] Calum D Gray PhD,[2] Alison Fletcher PhD,[2] Christophe Lucatelli PhD,[2] Aleksander Marin MD,[1,2] Paul Burns MD,[3] Andrew Tambaraja MD,[3] Roderick TA Chalmers MD,[3] Graeme Weir MD,[2,3] Neil Mitchard BSc,[2] Adriana Tavares PhD,[1,2] Jennifer MJ Robson MD,[1-3] David E Newby MD[1-3]

Affiliations:

[1]British Heart Foundation Centre for Cardiovascular Science, University of Edinburgh, 49 Little France Crescent, Edinburgh, UK, EH16 4SB
[2]Edinburgh Imaging Facility, Queen's Medical Research Institute, University of Edinburgh, 47 Little France Crescent, Edinburgh, UK, EH16 4SA
[3]NHS Lothian, Royal Infirmary of Edinburgh, Little France Crescent, Edinburgh, EH16 4SB

Corresponding author:

Professor David Newby, British Heart Foundation Centre for Cardiovascular Science, University of Edinburgh, 49 Little France Crescent, Edinburgh, UK, EH16 4SB
Fax: +44 131 242 6379
Phone: +44 131 242 6515
Email: d.e.newby@ed.ac.uk

Sponsor
The University of Edinburgh and NHS Lothian Health Board were co-sponsors.

Trial Registration
NCT02229006 and ISRCTN76413758

Keywords
Abdominal aortic aneurysm, positron emission tomography, rupture, repair.

Word count: 4,543

Abstract

Background: ^{18}F-Sodium fluoride (^{18}F-NaF) uptake is a marker of active vascular calcification associated with high-risk atherosclerotic plaque.

Objectives: In patients with abdominal aortic aneurysm (AAA), we assessed whether ^{18}F-NaF positron emission tomography and computed tomography (PET-CT) predicts AAA growth and clinical outcomes.

Methods: In prospective case-control (n=20 /group) and longitudinal cohort (n=72) studies, patients with AAA (aortic diameter >40 mm) and control subjects (diameter <30 mm) underwent abdominal ultrasound, ^{18}F-NaF PET-CT, CT angiography and calcium scoring. Clinical endpoints were aneurysm expansion and the composite of AAA repair or rupture.

Results: ^{18}F-NaF uptake was increased in AAA compared to non-aneurysmal regions within the same aorta (p=0·004), or aortae of control subjects (p=0·023). Histological and micro-PET-CT analysis demonstrated that ^{18}F-NaF uptake localised to areas of aneurysm disease and active calcification. In 72 patients within the longitudinal cohort study (age 73±7 years, men 85%, baseline aneurysm diameter 48·8±7·7 mm), there were 19 aneurysm repairs (26·4%) and 3 ruptures (4·2%) after 510±196 days. Aneurysms in the highest tertile of ^{18}F-NaF uptake expanded 2·5 times more rapidly than those in the lowest tertile (3·10 [2·34-5·92] versus 1·24 [0·52-2·92] mm/year, p=0·008) and were nearly three times as likely to experience AAA repair or rupture (15·3% versus 5·6%, log-rank p=0·043).

Conclusions: ^{18}F-NaF PET-CT is a novel and promising approach to the identification of disease activity in patients with AAA, and is an additive predictor of aneurysm growth and future clinical events.

Condensed Abstract

^{18}F-sodium fluoride uptake specifically localizes to areas of abdominal aortic aneurysm disease, and is a major predictor of aneurysm expansion and clinical outcome, independent of established clinical risk factors including aneurysm diameter. ^{18}F-Sodium fluoride positron emission tomography may be a useful adjunctive test in patients with high-risk or borderline aneurysms, or those with larger aneurysms where the balance of risk and benefit is uncertain. Future clinical trials will be needed to validate this approach and to establish whether clinical and surgical decisions based on ^{18}F-sodium fluoride positron emission tomography findings can improve the outcome of patients with abdominal aortic aneurysms.

Abbreviations

AAA	Abdominal aortic aneurysm
CT	Computed tomography
ECG	Electrocardiogram
^{18}F-NaF	^{18}F-Sodium fluoride
MA^{3}RS	Magnetic resonance imaging in Abdominal Aortic Aneurysms to predict Rupture or Surgery
MDS	Most diseased segment
PET	Positron emission tomography
ROI	Regions of interest
SUV	Standardized uptake value
TBR	Tissue to background ratio

Introduction

Abdominal aortic aneurysm (AAA) disease affects up to 5% of males aged 64 to 75 years and its prevalence is increasing in more elderly populations (1). With progressive AAA expansion over time, there is an increasing risk of often fatal rupture, representing the twelfth commonest cause of death amongst older men (2). Consequently, patients with AAA enter an ultrasound-based surveillance programme, with the aim of facilitating pre-emptive elective aneurysm repair in order to avoid fatal rupture. AAA surveillance relies on serial measurements of aneurysm diameter, which is currently the best clinical predictor of further expansion and rupture (3,4). However, AAA growth is non-linear, unpredictable and influenced by biomechanical processes that cannot be predicted by conventional anatomical imaging alone (5). Indeed, aneurysms not infrequently rupture below the current threshold (55 mm diameter) for elective repair, and many patients with aneurysms larger than 70 mm never experience rupture (6). There is therefore a need to develop more reliable methods of identifying those patients at particular risk of abdominal aortic aneurysm expansion and rupture (7).

In AAA disease, degradation of the extracellular matrix occurs in response to the accumulation of inflammatory cells, such as macrophages and lymphocytes, and the activation of matrix metalloproteinases. The resulting milieu of cellular inflammation, tissue destruction and necrosis can lead to cycles of further inflammation (8). Focal 'hotspots' of such intense biological activity have been identified in active aneurysm disease and can occur at the site of rupture (9). We have recently demonstrated that the positron emitting radiotracer, ^{18}F-sodium fluoride (^{18}F-NaF), can identify areas of

early microcalcification (10) that occur in response to necrotic inflammation in ruptured or high-risk human carotid (11) and coronary (12) atherosclerotic plaques. This tracer has not been assessed in patients with AAA although loss of tissue integrity and necrotic inflammation may be central to its pathophysiology, underlie aneurysm expansion and ultimately predict disease progression and outcome (7). We hypothesized that ^{18}F-NaF uptake on positron emission tomography (PET) would highlight areas of microcalcification and AAA disease activity, representing regions prone to expansion and rupture. The main aims of this study were to determine whether ^{18}F-NaF uptake on combined PET and computed tomography (CT) is increased in AAA, and whether this is associated with aneurysm growth (primary endpoint), and the subsequent rates of AAA repair or rupture.

Methods

Study Population

Consecutive patients over 50 years of age under routine clinical surveillance with asymptomatic AAA (≥40 mm anteroposterior diameter) were recruited from the Magnetic resonance imaging in Abdominal Aortic Aneurysms to predict Rupture or Surgery (MA^3RS) study (ISRCTN76413758) database (13). Control subjects were recruited through the NHS Lothian National Abdominal Aortic Aneurysm Screening Programme or the Vascular Laboratory at the Royal Infirmary of Edinburgh, and had a documented normal calibre aorta (<30 mm anteroposterior diameter).

Study Design

This was a prospective single-centre case-control and observational cohort study of patients with asymptomatic AAA, who were under ultrasound-based surveillance as part of routine clinical follow-up, and control subjects with a normal calibre abdominal aorta demonstrated on targeted screening ultrasound. The study (www.clinicaltrials.gov, NCT02229006) was conducted with the written informed consent of all subjects, approval by the Research Ethics Committee, and in accordance with the Declaration of Helsinki.

Study Assessments

Participants underwent a clinical evaluation including documentation of medical history, concomitant medications and family history as well as an ultrasound evaluation of the maximum anteroposterior abdominal aortic diameter. Ultrasound scans were carried out in an accredited clinical vascular science laboratory using a

standardized protocol with a known inter-observer variability of 3·4% (14). The AAA growth rate was determined using the AAA maximum anteroposterior diameter obtained at baseline and the last ultrasound performed during study follow-up. Abdominal aortic tissue was obtained at post-mortem or from patients undergoing elective AAA repair, and analysed by micro-PET-CT and histology (Supplementary Material).

^{18}F-Sodium Fluoride PET-CT

Patients were administered a target dose of 125 MBq of ^{18}F-NaF intravenously, and after 60 min, were imaged on a hybrid 128-detector array PET-CT scanner (Biograph mCT, Siemens) (10). A low-dose attenuation correction CT scan was performed (120 kV, 50 mAs; 5/3 mm), followed by acquisition of PET data, using three 10-min bed positions to ensure coverage from the thoracic aorta to the aortic bifurcation. An ECG-gated calcium scoring CT scan (120 kV, 120 mAs, 3/3 mm; prospective ECG-gating at 50% of the R-R interval) and a contrast-enhanced CT angiogram (120 kV, 145 mAs; 3/3 mm, 400 field of view; and 1/1 mm, 300 field of view; triggered at 181 HU) were performed, centred on the AAA (or abdominal aorta in control patients) and extending to the aortic bifurcation (Figure 1).

To estimate ^{18}F-NaF uptake, the maximum standardized uptake values (SUV_{max}, a validated measure of tissue radiotracer uptake) were quantified from regions of interest (ROI; Supplementary Material) (15). Maximum tissue-to-background ratios (TBR_{max}) were then calculated, after correction for blood pool activity using the averaged SUV_{mean} values of 3 consecutive ROIs from the right atrium, according to our previously described technique (16). Although TBR_{max} was used for our primary

analysis (12), we also investigated other methods for quantification including SUV_{max} and the corrected SUV_{max} ($cSUV_{max}$; calculated by subtracting the blood pool activity from the SUV_{max}) (15). Finally, we adopted the 'most-diseased segment' (MDS) approach as suggested by others (11,16,18-20). The MDS TBR_{max} was calculated as the average TBR_{max} across three axial slices centred on the region of the aneurysm with the highest tracer activity (11).

Clinical Endpoints and Adjudication

Clinical data from clinic visits, research database, electronic health records, primary care contacts and General Register Office were reviewed and clinical endpoints adjudicated by an independent Clinical Endpoint Committee (Supplementary Material). The committee members were blinded to the PET-CT findings. Follow-up was censored at 10th January 2017 or at the time of event.

Statistics and Data Analysis

Baseline characteristics are reported as number (percentages) for categorical variables and mean ± standard deviation or median [interquartile range] for continuous variables, as appropriate. We stratified our patient cohort by AAA MDS TBR_{max} tertiles to assess associations with aneurysm expansion (primary endpoint) and the clinical outcomes of aneurysm repair or rupture (secondary endpoint). For the aneurysm growth and outcomes analysis, AAA expansion rate and MDS TBR_{max} were log-transformed [log_2] to normalize the data. One-way analysis of variance was used to compare continuous data across multiple factors, with post-hoc analysis using the Bonferroni test where appropriate. The Kruskall-Wallis test was used for non-parametric continuous data and the log-rank test for comparisons of AAA event rate

and mortality between tertiles. Categorical data were compared using chi-squared or Fisher's exact tests, and unpaired Student's *t*-test was used to compare continuous outcomes between two independent groups. Two-tailed Pearson's correlation and linear regression analysis were performed to investigate the relationship between ^{18}F-NaF uptake and aneurysm expansion. Finally, we performed Kaplan-Meier and Cox's regression analysis to investigate time to AAA event by tertile, censored at the date of death. Statistical analysis was undertaken using IBM SPSS Statistics 23 and significance was taken at the two-sided 5% level ($p<0{\cdot}05$).

Results

A total of 145 patients with AAA were screened for inclusion: 136 were approached and 76 patients ultimately attended for the scanning visit. Four patients underwent protocol development scans, had incomplete data and were excluded from the final analysis, leaving a total of 72 patients with AAA and 20 control subjects (Figure 2). Patients were predominantly elderly (72·5±6·9 years) men (84·7%) with multiple cardiovascular risk factors including hypertension (65·3%) and hypercholesterolemia (81·9%; Table 1). Over 90% were current or ex-smokers (27·8% and 65·3% respectively) with a mean baseline AAA diameter of 48·8±7·7 mm. Control subjects were younger (65·2±2·8 years), but also predominantly (95·0%) men and 40% were current (25·0%) or prior (15·0%) smokers.

Case-control Study

Twenty AAA patients were matched for age, sex and smoking status with the 20 control subjects (Table 1). Background blood pool activity in the right atrium was similar between groups (log_2SUV_{mean} -0·570±0·517 versus -0·588±0·531; difference 0·018 (95% confidence interval (CI) -0·340 to 0·376), p=0·919). ^{18}F-NaF uptake was higher in the AAA when compared to the abdominal aorta of control subjects irrespective of the method of quantification (e.g. log_2MDS TBR_{max} 1·712±0·560 versus 1·314±0·489; difference 0·398 (95% CI 0·057 to 0·739), p=0·023; Supplementary Table 1). In contrast to control aortic tissue, AAA tissue demonstrated *ex vivo* ^{18}F-NaF uptake that correlated with areas of tissue disruption with necrotic debris and active calcification (r=0·808, P=0·015; Figure 3). Areas of ^{18}F-NaF uptake on PET were distinct from areas of macrocalcification on CT (Supplementary Movie).

Patients with AAA had more cardiovascular risk factors and higher abdominal aortic CT calcium scores (log_2Agatston score, 11·444±1·760 versus 7·338±3·811; difference 4·105 (95% CI 2·013 to 6·198), p=0·001; Supplementary Table 1) than control subjects. However, no differences in ^{18}F-NaF uptake were observed between these groups in either the descending thoracic aorta, or the non-aneurysmal abdominal aorta.

Observational Cohort Study

^{18}F-NaF uptake was again higher in the aneurysm than in the non-aneurysmal portion of the abdominal aorta (log_2TBR_{max} 1·647±0·537 versus 1·332±0·497; difference 0·314 (95% CI 0·0685 to 0·560), p=0·004) and almost double the uptake observed in the descending thoracic aorta (log_2TBR_{max} 1·647±0.537 versus 0·881±0.414; difference 0·766 (95% CI 0·517 to 1·011), p<0·0001). These differences were consistently observed regardless of the method of PET quantification.

Across the tertiles of AAA MDS TBR_{max}, there were no differences in most risk factors for AAA disease including age, sex, smoking habit, aneurysm diameter, hypertension and hypercholesterolemia. Whilst there appeared to be some differences with respect to diastolic blood pressure, body-mass index and peripheral arterial disease, the trend was inconsistent across the tertiles (Table 1).

^{18}F-NaF Uptake and Aneurysm Growth

During 510±196 days of follow-up, the median AAA expansion rate was 2·20 [0.96-3.72] mm/year (Table 2). Baseline ^{18}F-NaF activity in the aneurysm was associated with future expansion regardless of the method of quantification (e.g. $\log_2$MDS TBR_{max} r=0·365, p=0·006). When stratified by tertiles, aneurysms in the highest tertile expanded 2.5 times more rapidly than those in the lowest tertile (3·10 [2.34-5.92] mm/year versus 1·24 [0.52-2.92] mm/year, p=0·008; Figure 4). Moreover, in multivariable analysis, ^{18}F-NaF activity in the AAA (MDS TBR_{max}) emerged as a predictor of growth independent of age, sex, baseline diameter, body-mass index, blood pressure, smoking, renal function or peripheral arterial disease (p=0·042; Supplementary Table 2). In contrast, the aneurysm Agatston score was not associated with future expansion (r=0·199, p=0·141).

^{18}F-NaF Uptake and Clinical Events

In total, 22 (30·6%) patients met the composite endpoint of AAA repair or rupture. Of these 19 (26·4%) underwent elective AAA repair and 3 (4·2%) experienced AAA rupture, all of whom died without repair. Five other patients died during study follow-up, all from non-AAA causes.

Patients with aneurysms in the highest tertile of ^{18}F-NaF uptake were more likely to experience AAA repair or rupture during follow up (15·3% versus 5·6%, log-rank p=0·043; Table 2). They also had a reduced time to AAA event: 572 versus 735 days for AAA repair (log-rank p=0·014), and 572 versus 709 days for the composite of AAA repair or rupture (log-rank p=0·043; Figure 4). In those patients who experienced an AAA event, ^{18}F-NaF activity was higher than those who continued

under surveillance without an event (log_2MDS TBR_{max} 2·20±0·58 versus 1·87±0·54, difference 0·330 (95% CI 0·047 to 0·613), p=0·023). In unadjusted analysis, a doubling of ^{18}F-NaF activity in the MDS was associated with a more than 2-fold risk of experiencing AAA rupture or repair (HR 2·16, 95% CI 1·03 to 4·50; p=0·041; Table 2). When adjusted for age, sex, baseline diameter, systolic blood pressure, body-mass index and smoking, this risk remained (HR 2·49, 95% CI 1·07 to 5·78; p=0·034; Supplementary Table 2).

Discussion

In this prospective series of clinical studies, we have demonstrated for the first time that ^{18}F-NaF uptake is specifically increased in AAA, and relates to areas of advanced aneurysmal disease. Moreover, ^{18}F-NaF uptake is a major predictor of aneurysm expansion and clinical outcome that is additive to standard clinical risk factors including aneurysm diameter. This is the first study to demonstrate that an imaging biomarker of disease activity can add to the risk prediction of AAA and to suggest that this approach might refine clinical decisions regarding the need for surgery and improve patient outcomes (Central Illustration).

Our studies have several major strengths and prominent observations. First, we have shown AAA tissue demonstrates markedly increased levels of ^{18}F-NaF uptake that far exceeds those seen in control volunteers. Perhaps more importantly, uptake of the AAA also exceeds that observed in the non-aneurysmal aorta within the same patient. Second, we demonstrate that ^{18}F-NaF uptake localized to areas of AAA disease, highlighting diseased areas of poor tissue integrity that may be susceptible to aneurysm expansion and clinical events. Third, we assessed the potential clinical value of this technique in a cohort of patients with extended follow-up where the clinicians responsible for the patient's care were unaware of the PET-CT findings. It is therefore salient to note that ^{18}F-NaF uptake predicted expansion and clinical outcomes in addition to clinical risk factors including AAA diameter, especially as the latter drives the decision for elective AAA repair. Four, this is the largest dedicated PET-CT study in AAA disease to date and the first clinical study to investigate ^{18}F-NaF PET-CT in AAA disease progression (21). Finally, this was a prospective

clinical cohort study which contrasts with many previous studies of PET-CT in patients with AAA that are based on retrospective data, often obtained from cohorts derived from oncological imaging practice.

We have previously demonstrated that ^{18}F-NaF selectively binds to microcalcification in coronary[11] and carotid atherosclerotic plaques (10,11), and that this is associated with plaque vulnerability and rupture. We (11,12) and others (22) have also shown that ^{18}F-NaF binds to areas of tissue necrosis associated myocardial and cerebral infarction. In our present study, histological and micro-PET-CT data indicate that this tracer is behaving in a similar fashion in AAA. Increased ^{18}F-NaF uptake was most marked in AAA tissue with advanced disease and active calcification. We suggest that ^{18}F-NaF uptake again relates to microcalcification and is particular to the most diseased areas associated with tissue disruption and loss of integrity. Interestingly, we also showed that 18F-NaF was distinct from AAA macrocalcification detected by computed tomography, and that the latter is not associated with expansion or AAA events, suggesting that once established, dense calcified deposits represent a more stabilized biological state.

Most previous clinical PET-CT studies of AAA disease have focussed on the use of ^{18}F-fluorodeoxyglucose (^{18}F-FDG) to identify inflammation, with variable results and no clear clinical application. Whilst some groups have suggested a potential role for ^{18}F-FDG PET-CT in predicting AAA expansion or rupture (23-25), others have disputed this and reported contradictory findings (26,27). This in part relates to the small study sample sizes and whether patients had symptomatic or inflammatory AAAs but to date there is no clear relationship between ^{18}F-FDG and aneurysm

expansion or clinical outcome (22). Our current study was nested within another larger clinical cohort study, the MA^{3}RS trial. This was a multicentre study of 342 patients with AAA who underwent ultrasmall superparamagnetic particles of iron oxide (USPIO)-enhanced magnetic resonance imaging (MRI) to identify cellular inflammation within the aortic wall (13). This study recently reported and demonstrated that while USPIO-enhanced MRI did predict AAA expansion and clinical outcome, the association was modest and was not independent of established clinical factors including ultrasound AAA diameter (28). This suggests that imaging of cellular inflammation alone, either by ^{18}F-FDG or USPIO-enhanced MRI, is insufficient to provide additive clinical information beyond established clinical risk factors and AAA diameter. In contrast, ^{18}F-NaF PET-CT identifies focal areas of microcalcification indicative of more advanced aneurysm disease, and independently predicts both disease progression and clinical events.

We have demonstrated an important clinical application of ^{18}F-NaF PET-CT in AAA disease. Until now, future prediction of aneurysm expansion has relied on the simple morphological parameter of aneurysm diameter. However it is clear that AAA growth is non-linear and cannot be predicted accurately from a simple anatomical measure, such as AAA diameter. While we know that larger aneurysms tend to expand more rapidly and are more prone to rupture, disease evolution is not straightforward. Better AAA disease prediction using ^{18}F-NaF uptake could be particularly useful for patients in whom the decision to intervene is challenging. For example, those with high-risk aneurysms below 55 mm, those with borderline aneurysm sizes, or those with larger aneurysms where the balance of risk and benefit is uncertain.

Our study has a number of limitations. This is a single-centre proof-of-concept study with a low number of rupture events that makes adjustment for potential confounders and covariates challenging. Although we observed no marked differences in gender across the tertiles of ^{18}F-NaF uptake, our study population had a strong male bias (typical of this disease population) and we cannot be certain that our findings are truly representative for both men and women. The clinical impact of this technique has not been assessed, and would require a larger trial where clinical and surgical decisions would be influenced or dictated by the ^{18}F-NaF PET-CT findings. The widespread implementation of this technique may be challenging, especially given the relative expense and complexity of PET-CT compared to ultrasound. However, we have demonstrated the feasibility of this technique that uses a well-established, widely available and relatively cheap radiotracer. Moreover, with the more widespread use and availability of PET-CT scanners, barriers to implementation are declining. There are also some inherent limitations of ^{18}F-NaF image analysis that merit comment. Being a bone tracer, ^{18}F-NaF is readily taken up by the vertebrae, which lie in close proximity to the abdominal aorta. In our study, it was necessary to exclude some areas of the posterior aorta due to overspill of signal. However, this is not unique to ^{18}F-NaF with similar issues seen with ^{18}F-FDG uptake in regions of interest adjacent to bowel, muscle or other metabolically active tissues. Finally, further validation of the tissue binding characteristics and time course of change in ^{18}F-NaF uptake in aneurysmal and non-aneurysmal aortae are needed and this would be interesting to explore in future studies.

In conclusion, this novel proof-of-concept PET-CT study of patients with asymptomatic AAA demonstrates that ^{18}F-NaF uptake identifies advanced

aneurysmal disease, and is associated with aneurysm growth and clinical AAA events independent of established clinical risk factors including aneurysm diameter. This technique holds major promise for the future management of patients with AAA disease.

Acknowledgements

This study was funded by the Chief Scientist Office (CSO; ETM/365). The MA^{3}RS study was funded by the Medical Research Council (MRC) and managed by National Institute of Healthcare Research (NIHR) on behalf of the MRC-NIHR partnership (NIHR Efficacy and Mechanism Evaluation Programme: funding reference 11/20/03). The views expressed in this publication are those of the authors and not necessarily those of the CSO, MRC, National Health Service (NHS), NIHR or the Department of Health. DEN is supported by the British Heart Foundation (CH/09/002, RE/13/3/30183, RM/13/2/30158) and is the recipient of a Wellcome Trust Senior Investigator Award (WT103782AIA). MRD is supported by the British Heart Foundation FS/14/78/31020 and is the recipient of the Sir Jules Thorn Award for Biomedical Research 2015. OMBM is supported by the Academic Department of Military Surgery and Trauma. The Edinburgh Clinical Research Facility and Edinburgh Imaging Facility are supported by NHS Research Scotland. We would like to acknowledge the support of Karen Gallagher, Janet Jeffrey, Janice Taylor, Jo Singleton, Melanie McMillan, David Brian and Colin Young during the conduct of this study.

Declaration of Interests

None

Perspectives

Clinical Competency: ^{18}F-Sodium fluoride uptake is specific to abdominal aortic aneurysm tissue, is proportional to the rate of aneurysm expansion, and predicts the risk of repair or rupture independent of aneurysm diameter.

Translational Outlook: This is the first study to demonstrate that an imaging biomarker of disease activity can add to the risk prediction of abdominal aortic aneurysms, and to suggest that this approach might refine clinical decisions regarding the need for surgery and improve patient outcomes. This needs to be established in future randomized controlled clinical trials.

References

1. Howard DPJ, Banerjee A, Fairhead JF, et al. Age-specific incidence, risk factors and outcome of acute abdominal aortic aneurysms in a defined population. Br J Surg. 2015;102:907-915.

2. Office for National Statistics. Leading causes of death 2013. Office for National Statistics. http://visual.ons.gov.uk/wp-content/uploads/2015/02/Leading-Causes-of-Deaths-20131.csv. Published 2013. Accessed February 16, 2017.

3. Brady AR, Thompson SG, Fowkes FGR, Greenhalgh RM, Powell JT, UK Small Aneurysm Trial Participants. Abdominal aortic aneurysm expansion: risk factors and time intervals for surveillance. Circulation. 2004;110:16-21.

4. RESCAN Collaborators, Bown MJ, Sweeting MJ, Brown LC, Powell JT, Thompson SG. Surveillance intervals for small abdominal aortic aneurysms: a meta-analysis. JAMA. 2013;309:806-13.

5. Kurvers H, Veith F, Lipsitz E, et al. Discontinuous, staccato growth of abdominal aortic aneurysms. J Am Coll Surg. 2004;199:709-715.

6. Darling RC, Messina CR, Brewster DC, Ottinger LW. Autopsy study of unoperated abdominal aortic-aneurysms - case for early resection. Circulation. 1977;56:161-164.

7. Forsythe RO, Newby DE, Robson JMJ. Monitoring the biological activity of abdominal aortic aneurysms: beyond ultrasound. Heart. 2016;102:817-824.

8. Golledge ALV, Walker P, Norman PE, Golledge J. A systematic review of studies examining inflammation associated cytokines in human abdominal aortic aneurysm samples. Dis Markers. 2009;26:181-188.

9. Thompson MM, Jones L, Nasim A, Sayers RD, Bell P. Angiogenesis in abdominal aortic aneurysms. Eur J Vasc Endovasc Surg. 1996;11:464-469.

10. Irkle A, Vesey AT, Lewis DY, et al. Identifying active vascular micro-calcification by 18F-sodium fluoride positron emission tomography. Nat Commun. 2015;6:1-11.

11. Vesey AT, Jenkins W, Irkle A, et al. 18F-Fluoride and 18F-Fluorodeoxyglucose positron emission tomography after transient ischemic attack or minor ischemic stroke. case-control study. Circ Cardiovasc Imaging. 2017;10:e004976.

12. Joshi NV, Vesey AT, Williams MC, et al. 18F-fluoride positron emission tomography for identification of ruptured and high-risk coronary atherosclerotic plaques: a prospective clinical trial. Lancet. 2014;383:705-713.

13. McBride OMB, Berry C, Burns P, et al. MRI using ultrasmall superparamagnetic particles of iron oxide in patients under surveillance for

abdominal aortic aneurysms to predict rupture or surgical repair: MRI for abdominal aortic aneurysms to predict rupture or surgery - the MA3RS Study. Open Heart 2015:2:e000190.

14. Wilson KA, Hoskins PR, Lee AJ, Fowkes FG, Ruckley CV, Bradbury AW. Ultrasonic measurement of abdominal aortic aneurysm wall compliance: a reproducibility study. J Vasc Surg. 2000;31:507-513.

15. Vallabhaneni SR, Gilling-Smith GL, How TV, Carter SD, Brennan JA, Harris PL. Heterogeneity of tensile strength and matrix metalloproteinase activity in the wall of abdominal aortic aneurysms. J Endovasc Ther. 2004;11:494-502.

16. Pawade TA, Cartlidge TRG, Jenkins WSA, et al. Optimization and Reproducibility of aortic valve 18F-fluoride positron emission tomography in patients with aortic stenosis. Circ Cardiovasc Imaging. 2016;9:e005131.

17. Chen W, Dilsizian V. PET assessment of vascular inflammation and atherosclerotic plaques: SUV or TBR? J Nucl Med. 2015;56:503-504.

18. Fayad ZA, Mani V, Woodward M, et al. Safety and efficacy of dalcetrapib on atherosclerotic disease using novel non-invasive multimodality imaging (dal-PLAQUE): a randomised clinical trial. Lancet. 2011;378:1547-1559.

19. Fayad ZA, Mani V, Woodward M, et al. Rationale and design of dal-PLAQUE: A study assessing efficacy and safety of dalcetrapib on progression or regression of atherosclerosis using magnetic resonance imaging and 18F-fluorodeoxyglucose positron emission tomography/computed tomography. Am Heart J. 2011;162:214–221.

20. Tawakol A, Fayad ZA, Mogg R, et al. Intensification of statin therapy results in a rapid reduction in atherosclerotic inflammation results of a multicenter fluorodeoxyglucose-positron emission tomography/computed tomography feasibility study. J Am Coll Cardiol. 2013;62:909-917.

21. Jalalzadeh H, Indrakusuma R, Planken RN, Legemate DA, Koelemay MJW, Balm R. Inflammation as a predictor of abdominal aortic aneurysm growth and rupture: a systematic review of imaging biomarkers. Eur J Vasc Endovasc Surg. 2016;52:333-342.

22. Marchesseau S, Seneviratna A, Sjöholm AT, Qin DL, Ho JXM, Hausenloy DJ, Townsend DW, Richards AM, Totman JJ, Chan MYY. Hybrid PET/CT and PET/MRI imaging of vulnerable coronary plaque and myocardial scar tissue in acute myocardial infarction. J Nucl Cardiol. 2017; in press. doi: 10.1007/s12350-017-0918-8. [Epub ahead of print]

23. Courtois A, Nusgens BV, Hustinx R, et al. 18F-FDG uptake assessed by pet/ct in abdominal aortic aneurysms is associated with cellular and molecular alterations prefacing wall deterioration and rupture. J Nucl Med. 2013;54:1740-1747.

24. Reeps C, Essler M, Pelisek J, Seidl S, Eckstein H-H, Krause B-J. Increased 18F-fluorodeoxyglucose uptake in abdominal aortic aneurysms in positron

emission/computed tomography is associated with inflammation, aortic wall instability, and acute symptoms. J Vasc Surg. 2008;48:417-423. doi:10.1016/j.jvs.2008.03.059.

25. Nchimi A, Cheramy-Bien J-P, Gasser TC, et al. Multifactorial relationship between 18F-fluoro-deoxy-glucose positron emission tomography signaling and biomechanical properties in unruptured aortic aneurysms. Circ Cardiovasc Imaging. 2014;7:82-91.

26. Barwick TD, Lyons OTA, Mikhael NG, Waltham M, O'Doherty MJ. 18F-FDG PET-CT uptake is a feature of both normal diameter and aneurysmal aortic wall and is not related to aneurysm size. Eur J Nucl Med Mol Imaging. 2014;41:2310-2318.

27. Kotze CW, Groves AM, Menezes LJ, et al. What is the relationship between 18F-FDG aortic aneurysm uptake on PET/CT and future growth rate? Eur J Nucl Med Mol Imaging. 2011;38:1493-1499.

28. The MA^{3}RS Study Investigators. Aortic wall inflammation predicts abdominal aortic aneurysm expansion, rupture and need for surgical repair. Circulation. 2017;136:787-797.

Figure Legends

Central Illustration

^{18}F-Sodium Fluoride Uptake in Abdominal Aortic Aneurysms

^{18}F-Sodium fluoride uptake is specific to abdominal aortic aneurysm tissue, is proportional to the rate of aneurysm expansion, and predicts the risk of repair or rupture independent of aneurysm diameter.

Figure 1

Positron emission tomography and computed tomography images of abdominal aortic aneurysms.

(A) Structural image of computed tomography (CT) angiogram, (B) ^{18}F-sodium fluoride uptake on positron emission tomography (PET), and (C) fused PET-CT co-localizing ^{18}F-sodium fluoride uptake with the skeleton and abdominal aortic aneurysm.

Figure 2

Study populations.

The 20 patients for the case-control study were selected from within the cohort study population. AAA, abdominal aortic aneurysm.

Figure 3

Correlation of histology with micro-positron emission tomography and computed tomography of abdominal aortic tissue.

Ex vivo micro-positron emission tomography and computed tomography (left panels), and histology (right panels) of aortic wall excised (A) at post-mortem in a patient without an aneurysm, and (B) during open abdominal aortic aneurysm repair. Regions of interest (dashed circle) of ^{18}F-sodium fluoride (^{18}F-NaF) uptake demonstrate atheromatous disease with necrosis (hematoxyin and eosin stain; magnification x100; B1) and calcification (black, Von Kossa stain; magnification x200; B2) in the aortic aneurysm tissue that is not apparent in control aorta (A1 and A2).

Figure 4

Prediction of disease progression and clinical outcome by ^{18}F-sodium fluoride positron emission tomography

Association of ^{18}F-sodium fluoride (^{18}F-NaF) uptake with disease progression and clinical outcome. (A) Rate of aneurysm expansion (mm/year: logarithm base 2 transformed) across the tertiles of ^{18}F-sodium fluoride uptake. The highest tertile expanded more rapidly than those in the lowest tertile (3·10 versus 1·24 mm/year respectively, p=0·008). Cumulative event rate (censored at date of death) across the tertiles of ^{18}F-sodium fluoride uptake for (B) abdominal aortic aneurysm repair or rupture (log-rank p=0·043), and (C) abdominal aortic aneurysm repair (log-rank p=0·014).

SUPPLEMENTARY MATERIAL

^{18}F-Sodium Fluoride Uptake in Abdominal Aortic Aneurysms

The SoFIA^3 Study

Rachael O Forsythe MD,[1-3] Marc R Dweck MD,[1-3] Olivia MB McBride MD,[1-3] Alex T Vesey MD,[1,2] Scott I Semple PhD,[1-3] Anoop SV Shah MD,[1] Philip D Adamson MD,[1] William Wallace MD,[3] Jakub Kaczynski MD,[1-3] Weiyang Ho PhD,[1] Edwin JR van Beek MD,[2,3] Calum D Gray PhD,[2] Alison Fletcher PhD,[2] Christophe Lucatelli PhD,[2] Aleksander Marin MD,[1,2] Paul Burns MD,[3] Andrew Tambaraja MD,[3] Roderick TA Chalmers MD,[3] Graeme Weir MD,[2,3] Neil Mitchard,[2] Adriana Tavares PhD,[1,2] Jennifer MJ Robson MD,[1-3] David E Newby MD[1-3]

Affiliations:
[1]British Heart Foundation Centre for Cardiovascular Science, University of Edinburgh, 49 Little France Crescent, Edinburgh, UK, EH16 4SB
[2]Edinburgh Imaging Facility, Queen's Medical Research Institute, University of Edinburgh, 47 Little France Crescent, Edinburgh, UK, EH16 4SA
[3]NHS Lothian, Royal Infirmary of Edinburgh, Little France Crescent, Edinburgh, EH16 4SB

Supplementary Methods

Patient Population: Exclusion Criteria

Participants were excluded if they were unable to give informed written consent, or had contraindications to iodine-based contrast media, estimated glomerular filtration rate <30 mL/min/1·73 m^2, a collagen vascular disorder, an intercurrent illness, a life expectancy <1 year, or were women of child-bearing potential without contraception.

Tissue Collection and Micro-Positron Emission Tomography

In two patients, aneurysmal aortic tissue was obtained during open abdominal aortic aneurysm (AAA) repair and was excised from the anterior wall of the native aorta prior to plication around the tube graft. Non-aneurysmal (control) aortic tissue was obtained during post-mortem examination of a sudden cardiac death victim, following written consent from relatives and the approval of the Research Ethics Committee.

Aneurysmal and non-aneurysmal aortic tissues were incubated using optimized protocol conditions, specifically: 20-min incubation with ^{18}F-sodium fluoride (100 kBq/mL, in 0.1 M phosphate buffer saline) at room temperature. Following incubation, samples were washed twice in assay buffer (1 min per wash) and mounted on a petri dish for micro-positron emission tomography (PET) and computed tomography (CT) imaging. This incubation protocol was designed to capture pseudo-secular equilibrium of ^{18}F-sodium fluoride binding to calcium particles and aggregates in tissue, mimicking *in vivo* conditions, while minimizing tissue degradation during incubation process with the aim to retain tissue properties for subsequent histology. Incubation conditions were optimized using calcium phosphate particles (CPPs, 200-300 nm) and varying concentrations of ^{18}F-sodium fluoride, as well as, incubation time with and without competing non-homologous inhibitor (alendronate 25 μM).

In brief, results from those optimization experiments demonstrated that ^{18}F-sodium fluoride total and specific binding to CPPs was rapid and reached pseudo-secular equilibrium at 20 min following incubation. The affinity, K_D, of ^{18}F-sodium fluoride to CPPs was 1 nM. For molar activity of ^{18}F-sodium fluoride of 100 GBq/μmol, incubations total volume of 200 mL and activity of 20 MBq equals 100 kBq/mL of ^{18}F-sodium fluoride (i.e. 1 nM).

Following incubation of the aortic specimen with ^{18}F-sodium fluoride, a 30-min emission scan was obtained using a micro-PET-CT scanner (nanoPET/CT; Mediso, Hungary) in a 1:5 co-incidence mode. A CT scan was acquired (semi-circular full trajectory, maximum field of view, 720 projections, 55 kVp, 300 ms and 1:4 binning) for attenuation correction. PET data were reconstructed using Mediso's iterative Tera-Tomo 3D reconstruction algorithm using 4 iterations, 6 subsets, full detector model, normal regularisation, spike filter on, voxel size 0.4 mm and 400-600 keV energy window.

Histopathological analysis

Regions of interest (ROI) were identified on the reconstructed micro-PET-CT images of the AAA and control aortic specimens. Specimens of tissue corresponding to the site of each ROI were stained with hemotoxylin and eosin to determine cellular structure, and Von Kossa to identify focal calcification.

^{18}F-NaF PET-CT Image Analysis

Static PET-CT images were reconstructed with correction applied for attenuation, dead time, scatter and random coincidences, using an optimized iterative reconstruction algorithm (ultra-HD; TrueX + TOF, matrix 200, zoom 1; Gaussian filter). Scans were visually assessed for registration, patient movement, scan quality and tracer uptake, with minor adjustments in co-

registration made manually as required, using fixed boney landmarks. PET analysis was performed using an OsiriX workstation (OsiriX, version 8·0·1 64 bit; OsiriX Imaging Software, Geneva, Switzerland). Care was taken to exclude tracer uptake that originated from nearby bone structures or from the urinary tract.

CT Calcium Scoring

CT Calcium scoring was performed by an experienced observer on a dedicated workstation (Vitrea Advanced, Vital Imaging, Toshiba Systems, Minnesota, USA). Taking care to exclude calcium originating from the vertebrae, the aortic calcium burden was extracted using axial slices of the ECG-gated calcium scoring CT and recorded as the Agatston score. The cumulative Agatston score was used to determine the macroscopic calcium burden for each region of the aorta: descending thoracic aorta, non-aneurysmal abdominal aorta and the aneurysm (or infra-renal abdominal aorta in control subjects) using a threshold of 130 Hounsfield Units.

Clinical Endpoint Adjudication

There are no consensus guidelines to direct investigators when adjudicating endpoints relating to death in patients with known abdominal aortic aneurysms who have no definitive proof of causality (such as post-mortem examination). Most of the recently proposed classification systems relating to abdominal aortic aneurysms events require radiological or operative evidence to classify abdominal aortic aneurysms events. In the event that no such confirmation was available, the end points were assessed and determined by each member of the end-point committee and any disagreement settled by consensus, with oversight from the Chairperson. ‘Cold pursuit’ of relevant data included obtaining information from primary care or hospital records as to likely cause of death, cause of death listed on death certificate

obtained from public registry, and data from the Information and Statistics Division of NHS Scotland. The following guidelines and classification system were used as part of the assessment for adjudication of cause of death:

Abdominal Aortic Aneurysms-related Events

1) Abdominal aortic aneurysm-related death, confirmed

- Death occurs in hospital following confirmed abdominal aortic aneurysm rupture on computed tomography, or intra-operative findings
- Death occurs following treatment for abdominal aortic aneurysm during same admission (elective or emergency)
- Death arising from complications relating to abdominal aortic aneurysm treatment
- Death occurs out of hospital, confirmed abdominal aortic aneurysm rupture on post-mortem
- Death occurs out of hospital, confirmed abdominal aortic aneurysm treatment related complication on post-mortem

2) Abdominal aortic aneurysm-related death, probable

- Death occurs in circumstances with high probability of abdominal aortic aneurysm rupture (e.g. patient admitted to hospital following collapse, known abdominal aortic aneurysm, hypotension, no other obvious cause of symptoms, death shortly after presentation)
- Death occurs in circumstances with high probability of complications relating to abdominal aortic aneurysm treatment (e.g. known endoleak, suspected rupture post-endovascular aortic repair)

- Death occurs out of hospital, no post-mortem performed but highly likely as no other obvious cause of death (e.g. witnessed collapse at home, known abdominal aortic aneurysm, sudden death, no other obvious cause)
- Sudden unexplained death in a patient with known abdominal aortic aneurysm ≥7 cm, with no other cause of death identified

3) Abdominal aortic aneurysm-related death, possible

- Death occurs in hospital, no post-mortem performed and cannot be judged as highly likely to be abdominal aortic aneurysm-related, but no other circumstances to suggest other definitive cause
- Death occurs out of hospital, no post-mortem performed and cannot be judged as highly likely to be abdominal aortic aneurysm-related, but no other circumstances to suggest other definitive cause

Non-abdominal Aortic Aneurysm related events

Cardiovascular death (non-abdominal aortic aneurysm):

Death resulting from an acute myocardial infarction, sudden cardiac death, death due to heart failure, death due to stroke, death due to cardiovascular procedures, death due to other cardiovascular causes (excluding abdominal aortic aneurysm-related deaths).

Non-cardiovascular death:

Death resulting from all other causes, excluding cardiovascular or abdominal aortic aneurysm-related deaths.

Supplementary Results

Table 2
Expansion Rate and Clinical Outcomes According to Tertiles of ^{18}F-Sodium Fluo

Outcome	All patients with AAA (n=72)	Tertile 1 (n=24)	Tertile 2 (n=24)	
AAA expansion rate (mm/year)	2·20 [0·96-3·73]	1·24 [0·52-2·92]]	1·55 [0·81-3·12]	3·
AAA events				
Composite events	22 (30·6)	4 (16·7)	7 (29·2)	
Repair	19 (26·4)	3 (12·5)	5 (20·8)	
Rupture	3 (4·2)	1 (4·2)	2 (8·3)	
Deaths				
All-cause	8 (11·1)	4 (16.7)	4 (16.7)	
AAA-related	3 (4·2)	1 (4·2)	2 (8·3)	

Values are presented as n (%), median [interquartile range]
AAA: abdominal aortic aneurysm
*P-value for trend across the tertiles

Table 1
Characteristics of Study Participants

	Cohort study					Case control study	
	All Patients with AAA (n=72)	**Tertile 1** (n=24)	**Tertile 2** (n=24)	**Tertile 3** (n=24)	**P-value***	**Patients with AAA** (n=20)	**Control Subjects** (n=20)
Characteristics							
Age (years)	72·5±6·9	73·3±7·2	72·8±7·5	71·4±6·1	0·640	66·2±2·6	65·2±2·8
Male	61 (84·7)	20 (83·3)	21 (85·7)	20 (83· 3)	1·000	19 (95·0)	19 (95·0)
Systolic blood pressure (mmHg)	136·7±18·3	142·1±18·2	132·5±16·2	135·6±19·9	0·178	138·1±22·5	141·6±14·2
Diastolic blood pressure (mmHg)	81·6±11·6	84·8±12·0	76·4±9·4	83·5±11·9	0·024	84·2±16·6	80·5±8·2
Heart rate (/min)	71±9	72±10	70±8	70±8	0·694	70·2±9·7	66·7±13·5
Body-mass index (kg/m^2)	27·6±3·5	27·6±3·4	26·2±3·3	29·0±3·3	0·019	28·4±3·1	29·3±6·4
Current smoker	20 (27·8)	6 (25·0)	9 (37·5)	5 (20·8)	0·407	5 (25·0)	5 (25·0)
Medical history							
Hypertension	47 (65·3)	14 (58·3)	16 (66·7)	17 (70·8)	0·651	12 (60·0)	6 (30·0)
Hypercholesterolemia	59 (81·9)	21 (87·5)	21 (87·5)	17 (70·8)	0·264	15 (75·0)	7 (35·0)
Diabetes	10 (13·9)	3 (12·5)	4 (16·7)	3 (12·5)	1·000	1 (5·0)	2 (10·0)
Ischemic heart disease	22 (30·6)	7 (29·2)	7 (29·2)	8 (33·3)	0·937	5 (25·0)	1 (5·0)
Peripheral arterial disease	11 (15·3)	2 (8·3)	8 (33·3)	1 (4·2)	0·021	2 (10·0)	1 (5·0)
Cerebrovascular disease	10 (13·9)	1 (4·2)	4 (16·7)	5 (20·8)	0·316	1 (5·0)	0 (0·0)
Positive family history of AAA	9 (12·5)	2 (8·3)	4 (16·7)	3 (12·5)	0·903	3 (15·0)	2 (10·0)
Medications							
Anti-platelet	51 (70·8)	19 (79·2)	18 (75·0)	14 (58·3)	0·350	11 (55·0)	3 (15·0)
Statin	58 (80·6)	21 (87·5)	21 (87·5)	16 (66·7)	0·141	13 (65·0)	8 (40·0)
Anti-coagulant	2 (2·8)	1 (4·2)	0 (0·0)	1 (4·2)	1·000	0 (0·0)	1 (5·0)
Beta-blocker	19 (26·4)	8 (33·3)	5 (20·8)	6 (25·0)	0·711	6 (30·0)	2 (10·0)
ACE inhibitor	25 (34·7)	8 (33·3)	8 (33·3)	9 (37·5)	1·000	5 (25·0)	2 (10·0)
Aorta							
Aortic diameter (mm)	48·8±7·7	47·5±9·2	48·7±7·8	50·1±5·8	0·510	45·7±4·0	17·6±2·3
Concurrent iliac aneurysm	13 (18·1)	4 (16·7)	5 (20·8)	4 (16·7)	1·000	3 (15·0)	0·0 (0·0)

Values are presented as n (%) or mean ± standard deviation.

Supplementary Table 1
^{18}F-Sodium Fluoride Uptake and Agatston Score in Patients with Abdominal Aortic Aneurysm and Control Subjects

Region	Uptake Measure [log_2]	Population			
		Patients with AAA (n=20)	**Control Subjects** (n=20)	**Mean difference (95% CI for difference)**	**P-value**
Right atrium					
	SUV_{mean}	-0·570±0·571	-0·588±0·531	0·018 (-0·340 to 0·376)	0·919
Descending thoracic aorta					
	SUV_{max}	0·281±0·316	0·268±0·473	0·013 (-0·250 to 0·275)	0·920
	TBR_{max}	0·851±0·415	0·856±0·418	-0·005 (-0·275 to 0·265)	0·970
	$cSUV_{max}$	-1·089±0·684	-1·115±1·025	0·027 (-0·542 to 0·595)	0·925
	MDS SUV_{max}	0·618±0·334	0·717±0·438	-0·099 (-0·348 to 0·150)	0·426
	MDS TBR_{max}	1·156±0·450	1·306±0·443	-0·148 (-0·450 to 0·154)	0·328
Abdominal aorta (non-aneurysmal)					
	SUV_{max}	0·762±0·316	0·726±0·366	0·037 (-0·186 to 0·259)	0·741
	TBR_{max}	1·333±0·532	1·314±0·489	0·018 (-0·313 to 0·350)	0·911
	$cSUV_{max}$	-0·104±0·652	-0·1058±0·556	0·002 (-0·392 to 0·397)	0·991
	MDS SUV_{max}	1·158±0·363	0·995±0·369	0·163 (-0·724, to 0·399)	0·170
	MDS TBR_{max}	1·697±0·537	1·583±0·510	0·114 (-0·221 to 0·449)	0·494
Abdominal aorta (AAA)					
	SUV_{max}	1·142±0·283	0·726±0·366	0·416 (0·203 to 0·629)	<0·0001
	TBR_{max}	1·712±0·560	1·314±0·489	0·398 (0·057 to 0·739)	0·023
	$cSUV_{max}$	0·543±0·432	-0·1058±0·556	0·649 (0·324 to 0·973)	<0·0001
	MDS SUV_{max}	1·427±0·356	0·995±0·369	0·432 (0·197 to 0·668)	0·001
	MDS TBR_{max}	1·997±0·568	1·583±0·510	0·414 (0·064 to 0·764)	0·022
	Agatston score	11·444±1·760	7·338±3·811	4·105 (2·013 to 6·198)	0·001

Values are logarithm base 2 transformed and presented as mean±standard deviation
AAA, abdominal aortic aneurysm; ^{18}F-NaF, ^{18}F-sodium fluoride; MDS, most-diseased segment; CI, confidence interval

Supplementary Table 2
Multivariable Analysis of ^{18}F-Sodium Fluoride Uptake and Clinical Outcomes

	Increase in Expansion (mm/year; 95% CI)	**P-value**	**Hazard Ratio (95% CI) for Composite AAA Events**	**P-value**
Model 1	0·365 (0·34 to 1·90)	0·006	2·16 (1·03 to 4·51)	0·041
Model 2	0·375 (0·39 to 1·91)	0·004	2·26 (1·97 to 4·76)	0·033
Model 3	0·259 (0·029 to 1·56)	0·042	2·49 (1·07 to 5·78)	0·034
Model 4	0.357 (0.315-1.880)	0.007	2.096 (1.004-4.375)	0.049
Model 5	0.346 (0.295-1.834)	0.008	2.103 (1.002-4.412)	0.049
Model 6	0.267 (0.052-1.589)	0.037	2.162 (0.970-4.819)	0.059
Model 7	0.266 (0.026-1.597)	0.041	2.194 (0.955-5.028)	0.064

Expansion rate was logarithm base 2 transformed

Model 1: unadjusted
Model 2: adjusted for age, sex
Model 3: adjusted for age, sex, baseline diameter, body-mass index, systolic blood pressure, smoking
Model 4: adjusted for diastolic blood pressure
Model 5: adjusted for diastolic blood pressure, eGFR
Model 6: adjusted for age, sex, body-mass index, diastolic blood pressure, smoking, diameter, eGFR
Model 7: adjusted for age, sex, body-mass index, diastolic blood pressure, smoking, diameter, eGFR, peripheral arterial disease

AAA, abdominal aortic aneurysm; CI, confidence intervals; eGFR, estimated glomerular filtration rate

Figure 1

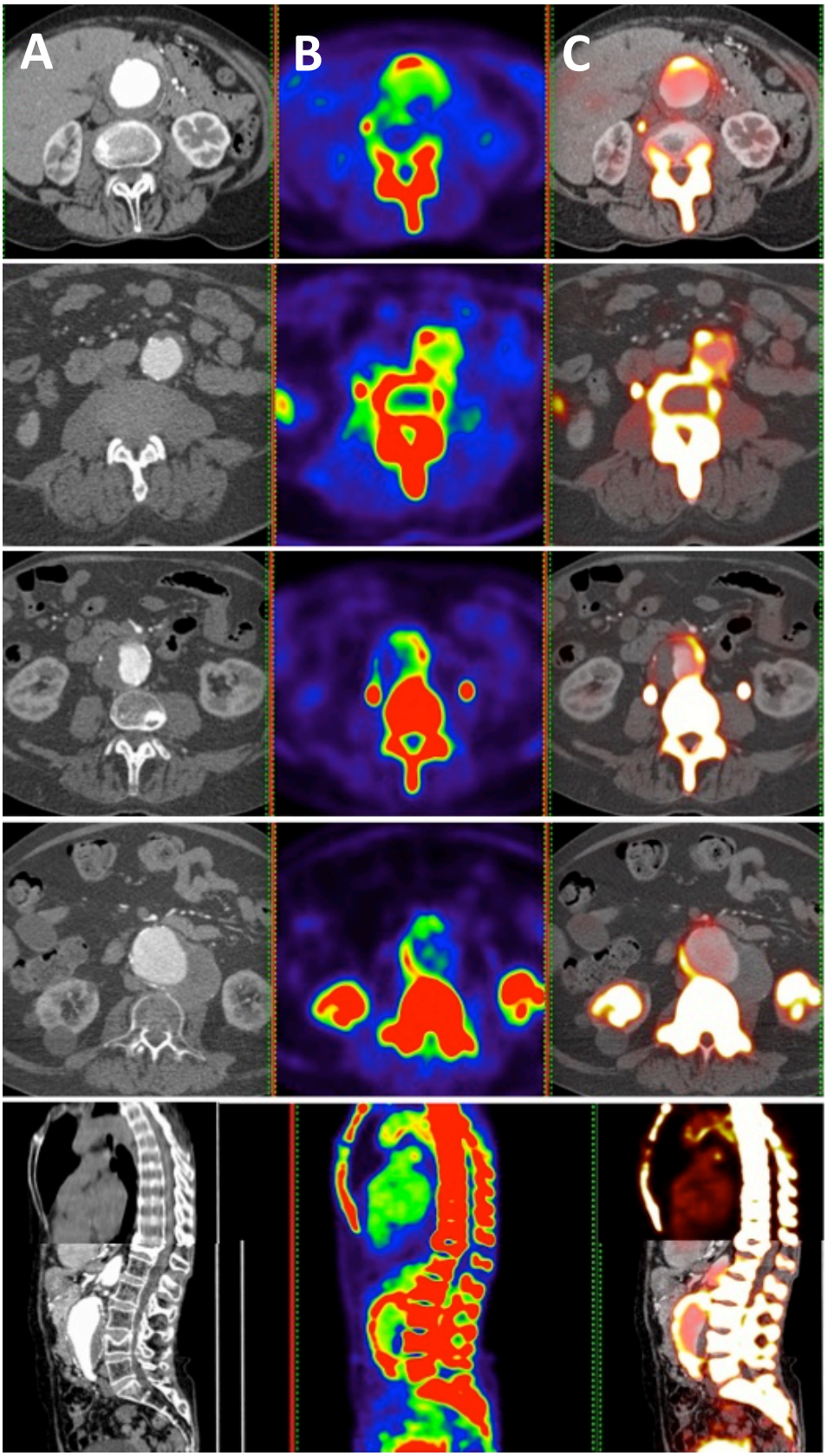

Figure 3

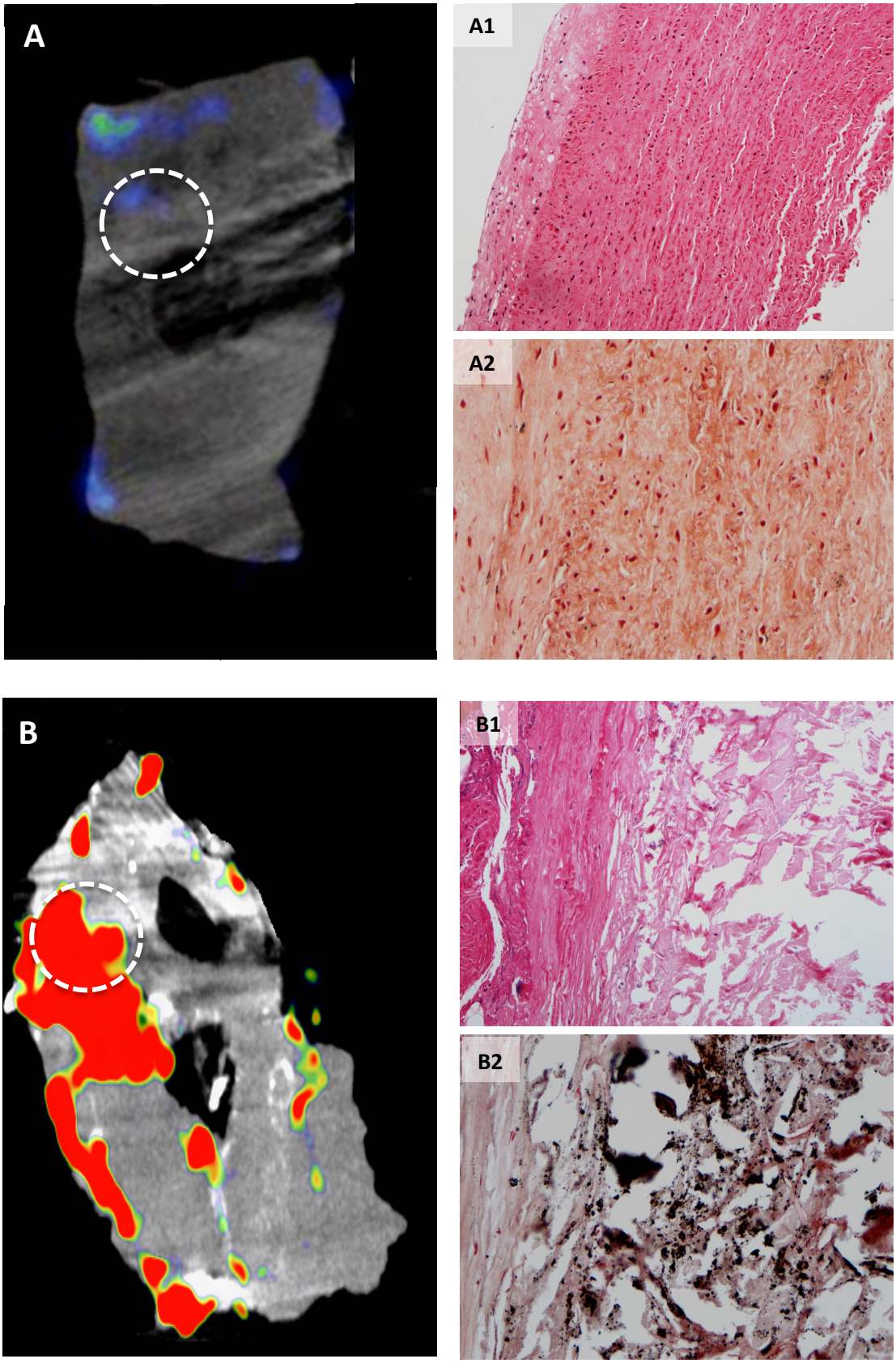

Figure 4

A

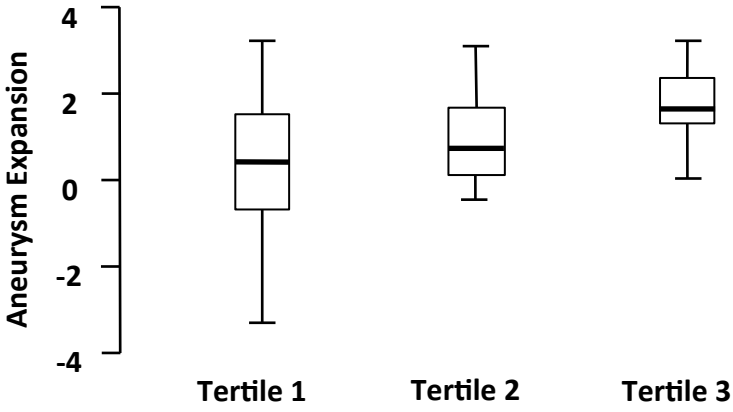

B

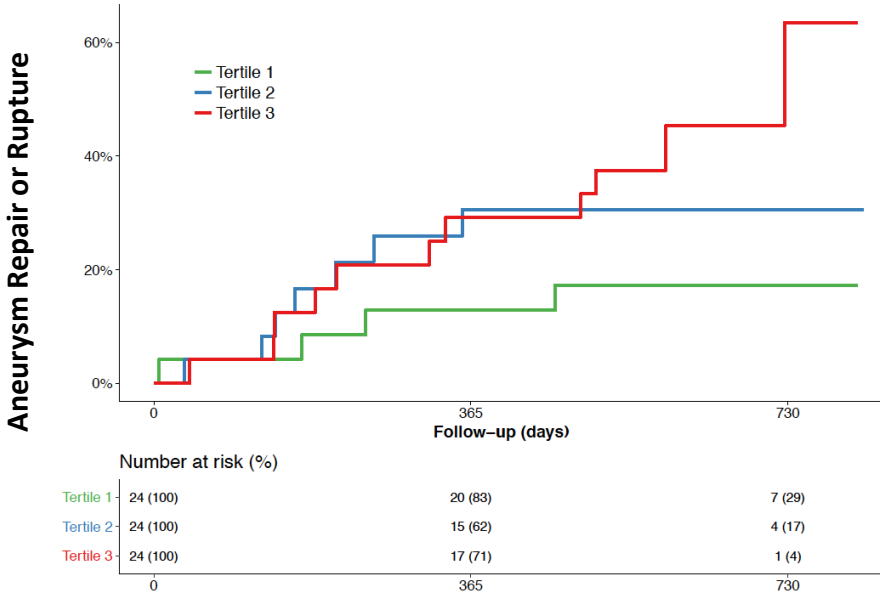

Number at risk (%)

Tertile 1	24 (100)	20 (83)	7 (29)
Tertile 2	24 (100)	15 (62)	4 (17)
Tertile 3	24 (100)	17 (71)	1 (4)
	0	365	730

C

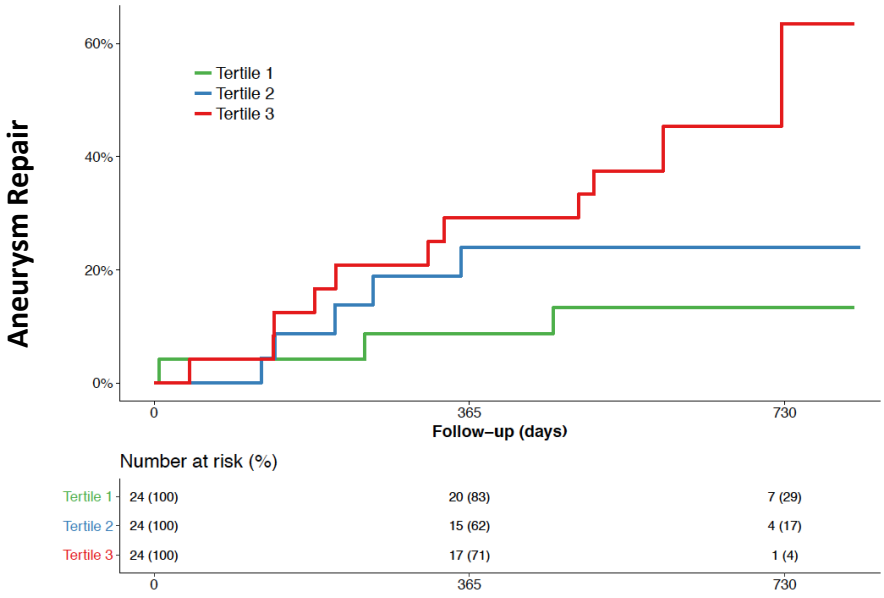

Number at risk (%)

Tertile 1	24 (100)	20 (83)	7 (29)
Tertile 2	24 (100)	15 (62)	4 (17)
Tertile 3	24 (100)	17 (71)	1 (4)
	0	365	730

APPENDIX iii

Study Protocols

Study Protocol

Magnetic Resonance Imaging Using Ultrasmall Superparamagnetic Particles of Iron Oxide in Patients Under Surveillance for Abdominal Aortic Aneurysms to Predict Rupture or Surgical Repair

__M__RI for __A__bdominal __A__ortic __A__neurysms to predict __R__upture or __S__urgery: The MA^{3}RS trial

Co-sponsors	University of Edinburgh & NHS Lothian ACCORD The Queen's Medical Research Institute 47 Little France Crescent Edinburgh EH16 4TJ
Funder	Medical Research Council
Funding Reference Number	11/20/03
Chief Investigator	Professor David Newby
EudraCT Number	2012-002488-25
REC Number	12/ES/0068
Version Number and Date	Version 8.0, 18th March 2015

COORDINATING CENTRE

Chief Investigator	**Co-sponsor Representative**
Professor David E Newby Centre of Cardiovascular Science Chancellor's Building 51 Little France Crescent Edinburgh EH16 4SB Tel: 0131 242 6515 Fax: 0131 242 6379 Email: d.e.newby@ed.ac.uk	Marise Bucukoglu University of Edinburgh Queen's Medical Research Institute 47 Little France Crescent Edinburgh EH16 4SB Tel: 0131 242 9262 Fax: 0131 242 9447 Email: marise.bucukoglu@ed.ac.uk
Trial Manager	**Trial Statisticians**
Fiona Wee Clinical Trials Manager Edinburgh Clinical Trials Unit University of Edinburgh Western General Hospital EH4 2XU Tel: 0131 537 2562/3841 Fax: 0131 537 3851 Email: fiona.wee@ed.ac.uk	Gordon Murray Edinburgh MRC Hub for Trials and Research University of Edinburgh Teviot Place Edinburgh EH8 9AG Tel: 0131 650 3233 Fax: 0131 650 3224 Email: Gordon.murray@ed.ac.uk
Principal Investigator Rachael Forsythe Research Fellow Centre of Cardiovascular Science Chancellor's Building 51 Little France Crescent Edinburgh, EH16 4SB Tel: 0131 242 6364 Email: rachael.forsythe@ed.ac.uk	

PARTICIPATING SITES

Glasgow	**Fife and Forth Valley**
Principal Investigator Mr Wesley Stuart Consultant Vascular Surgeon Western Infirmary Glasgow G11 6NT Email: Wesley.stuart@ggc.scot.nhs.uk	**Principal Investigator** Mr Richard Holdsworth Consultant Vascular Surgeon Forth Valley Royal Hospital Stirling Road, Larbert FK5 4WR Tel: 01324 566830 Email: Richard.holdsworth@nhs.net

CONTENTS

contents **3**

protocol approval **5**

list of abbreviations **6**

summary **7**

1 INTRODUCTION **8**

1.1 BACKGROUND 8

1.2 RATIONALE FOR STUDY 10

2 STUDY OBJECTIVES **11**

2.1 OBJECTIVES 11

2.1.1 Primary Objective 11

2.1.2 Secondary Objectives 11

2.2 ENDPOINTS 11

2.2.1 Primary Endpoint 11

3 STUDY DESIGN **12**

4 STUDY POPULATION **14**

4.1 NUMBER OF PARTICIPANTS 14

4.2 INCLUSION CRITERIA 14

4.3 EXCLUSION CRITERIA 14

5 PARTICIPANT SELECTION AND ENROLMENT **15**

5.1 IDENTIFYING PARTICIPANTS 15

5.2 CONSENTING PARTICIPANTS 15

5.3 SCREENING FOR ELIGIBILITY 15

5.4 INELIGIBLE AND NON-RECRUITED PARTICIPANTS 15

5.5 PREMATURE WITHDRAWAL

5.6 RANDOMISATION 15

5.7 SOFIA3 SUB-STUDY

6 INVESTIGATIONAL MEDICINAL PRODUCT AND PLACEBO **15**

6.1 STUDY DRUG 16

6.1.1 Study Drug Identification 16

6.1.2 Study Drug Manufacturer 16

6.1.3 Marketing Authorisation Holder 16

6.1.4 Labelling and Packaging 16

6.1.5 Storage 16

6.1.6 Summary of Product Characteristics or Investigators Brochure 16

6.2 PLACEBO 16

6.3 DOSING REGIME 16

6.4 DOSE CHANGES 17

6.5 PARTICIPANT COMPLIANCE 17

6.6 OVERDOSE 17

6.7 OTHER MEDICATIONS 18

6.7.1 Buscopan 18

6.7.2 Permitted Medications 18

6.7.3 Prohibited Medications 18

7 STUDY ASSESSMENTS **18**

7.2 STUDY ASSESSMENTS 19

8 DATA COLLECTION **21**

9 STATISTICS AND DATA ANALYSIS **22**

9.1 SAMPLE SIZE CALCULATION 22

9.2 PROPOSED ANALYSES 23
10 ADVERSE EVENTS 25
10.1 DEFINITIONS 25
10.2 DETECTING AEs AND SAEs 26
10.3 RECORDING AEs AND SAEs 26
10.4 ASSESSMENT OF AEs AND SAEs 26
10.4.1 Assessment of Seriousness 26
10.4.2 Assessment of Causality 26
10.4.3 Assessment of Severity 27
10.4.4 Assessment of Expectedness 27
10.5 REPORTING OF SAEs/SARs/SUSARs 27
10.6 REGULATORY REPORTING REQUIREMENTS 28
10.7 FOLLOW UP PROCEDURES 28
11. PREGNANCY 28
12 TRIAL MANAGEMENT AND OVERSIGHT ARRANGEMENTS 28
12.1 TRIAL MANAGEMENT GROUP 28
12.2 TRIAL STEERING COMMITTEE 28
12.3 DATA MONITORING COMMITTEE 29
12.4 INSPECTION OF RECORDS 29
12.5 RISK ASSESSMENT 29
12.6 STUDY MONITORING AND AUDIT 31
13 GOOD CLINICAL PRACTICE 31
13.1 ETHICAL CONDUCT 31
13.2 REGULATORY COMPLIANCE 31
13.3 INVESTIGATOR RESPONSIBILITIES 31
13.3.1 Informed Consent 31
13.3.2 Study Site Staff 32
13.3.3 Data Recording 32
13.3.4 Investigator Documentation 32
13.3.5 GCP Training 32
13.3.6 Confidentiality 32
13.3.7 Data Protection 33
14 STUDY CONDUCT RESPONSIBILITIES 33
14.1 PROTOCOL AMENDMENTS 33
14.2 PROTOCOL VIOLATIONS AND DEVIATIONS 33
14.3 SERIOUS BREACH REQUIREMENTS 34
14.4 STUDY RECORD RETENTION 34
14.5 END OF STUDY 34
14.6 CONTINUATION OF DRUG FOLLOWING THE END OF STUDY 34
14.7 INSURANCE AND INDEMNITY 34
15 REPORTING, PUBLICATIONS AND NOTIFICATION OF RESULTS 35
15.1 AUTHORSHIP POLICY 35
15.2 PUBLICATION 35
15.3 PEER REVIEW 35
16 REFERENCES 35

PROTOCOL APPROVAL

Magnetic Resonance Imaging Using Ultrasmall Superparamagnetic Particles of Iron Oxide to Predict Clinical Outcome in Patients Under Surveillance for Abdominal Aortic Aneurysms

EudraCT number 2012-002448-25

Signatures

Chief Investigator	_____ Signature	_____ Date
Trial Statistician	_____ Signature	_____ Date
Sponsor(s) Representative	_____ Signature	_____ Date
Principal Investigator	_____ Signature	_____ Date

LIST OF ABBREVIATIONS

GCP	Good Clinical Practice
ICH	International Conference on Harmonisation
IMP	Investigational Medicinal Product
ISF	Investigator Site File
TMF	Trial Master File
SOP	Standard Operating Procedure
CRF	Case Report Form
AE	Adverse Event
SAE	Serious Adverse Event
AR	Adverse Reaction
SAR	Serious Adverse Reaction
UAR	Unexpected Adverse Reaction
SUSAR	Suspected Unexpected Serious Adverse Reaction
ACCORD	Academic and Clinical Central Office for Research & Development - Joint office for University of Edinburgh and NHS Lothian
WTCRF	Wellcome Trust Clinical Research Facility
MRI	Magnetic Resonance Imaging
CT	Computed Tomography
US	Ultrasound
AAA	Abdominal Aortic Aneurysm
Fe	Iron

SUMMARY

Abdominal aortic aneurysms have a prevalence of 5% in 65-74 year-old men and when ruptured, are associated with a mortality of up to 90%. Ruptured aortic aneurysms are a common cause of death in the United Kingdom, being the thirteenth commonest cause of death and accounting for 6,800 deaths each year in England and Wales.[1] Open surgical or endovascular intervention to prevent rupture is considered when the aortic aneurysm diameter exceeds 55 mm or expansion rates are greater than 10 mm/year.

Population screening halves the mortality associated with abdominal aortic aneurysms[1] and has led to the establishment of a national screening and surveillance programme. Currently, abdominal aortic aneurysm surveillance is complex because of the non-linearity and unpredictability of expansion rates, although the best predictor of aneurysm expansion is the baseline aneurysm diameter. However, up to one fifth of ruptured abdominal aortic aneurysm are less than 55 mm in diameter[2] and many patients present with diameters considerably greater than 55 mm without prior symptoms or rupture. Taken together, these data highlight the need for a more accurate method of rupture prediction that would better inform decisions to undertake preventative and potentially life-saving surgery.

We have developed a novel magnetic resonance imaging method that is based upon the known biological processes underlying aneurysm expansion and rupture. For the first time, the MA^{3}RS study proposes to assess this novel approach to identify aneurysms that are likely to expand more rapidly and potentially rupture. This technique would provide potentially important additional information to the current simplistic gold-standard of ultrasound measurement of aneurysm diameter.

1 INTRODUCTION

1.1 BACKGROUND

Aortic aneurysms frequently occur in patients with atherosclerosis and the two disease processes share several common risk factors. However, there are distinct differences. Atherosclerotic lesions are pre-dominantly located in the intima, whereas the media and adventitia are primarily involved in aneurysms. Aneurysm disease is also much more closely associated with smoking and hypertension, and has a particular predilection for the abdominal aorta.

The formation, growth and rupture of aneurysms are now recognised to be the result of a complex interplay between biological and mechanical factors. Aneurysm tissue is characterised by excessive medial neovascularisation, infiltration of inflammatory cells (principally macrophages) and irreversible remodeling of the extracellular matrix. These pathological processes do not affect the aorta uniformly but are focal in nature. Shear wall stress varies spatially within the aneurysm[3] and tensile strength varies in different parts of the aneurysm sac.[4] Focal neovascularisation occurs at the site of rupture and its presence corresponds to the degree of inflammation. These biological 'hotspots' represent sites of potential rupture and are putative targets for novel imaging strategies aiming to predict aneurysm expansion and assess the risk of rupture. In addition, tissue and wall stresses vary spatially within the aneurysm and tensile strength varies in different parts of the aneurysm sac. Synergy between these biological 'hotspots' and areas of intense biomechanical stress may be the focal point precipitating aneurysm rupture. Indeed, there is strong evidence that aneurysm rupture is seen in those patients with more rapid aneurysm expansion rates.[5, 6]

1.1.1 Magnetic Resonance Imaging

Magnetic resonance imaging is emerging as a useful investigative tool for cardiovascular disease that can distinguish the different atherosclerotic plaque components, such as the lipid-rich core and areas of calcification.[7] Standard gadolinium-based magnetic resonance imaging identifies areas of thrombus formation and fibrosis in abdominal aortic aneurysms.[8] Newer contrast agents containing superparamagnetic particles of iron oxide (SPIO) have been developed that provide additional biological and functional information through the detection of cellular inflammation within tissues. Ultrasmall SPIO (USPIO), with particle sizes in the range 10-30 nm, escape immediate recognition by the reticulo-endothelial system and persist for longer in the bloodstream allowing them to be used to assess the accumulation of macrophages within vascular and lymphatic tissues.[9, 10, 11, 12, 13] Current preparations are biodegradable and safe for clinical administration.[14, 15, 16]

USPIO accumulate in the aortae of hypercholesterolaemic rabbits[17] and in murine models of abdominal aortic aneurysms.[18] In humans, USPIO accumulate in ruptured or rupture-prone carotid plaques rather than stable plaques,[11, 12] and treatment with atorvastatin reduces both inflammation and USPIO uptake in carotid plaques.[13]

We have recently conducted a series of magnetic resonance imaging studies in patients with abdominal aortic aneurysms and shown that uptake of USPIO in the aortic wall correlates with macrophage activity and identifies cellular inflammation.[19, 20] Using a 3T magnetic resonance scanner, patients with asymptomatic abdominal aortic aneurysms (n=29; aneurysm diameter 4.0- 6.6 cm) attending our surveillance programme were imaged before and 24-36 hours after intravenous administration of USPIO. Histological examination of aneurysm tissue confirmed co-localization and uptake of USPIO in areas of macrophage infiltration (Figure 1).[19]

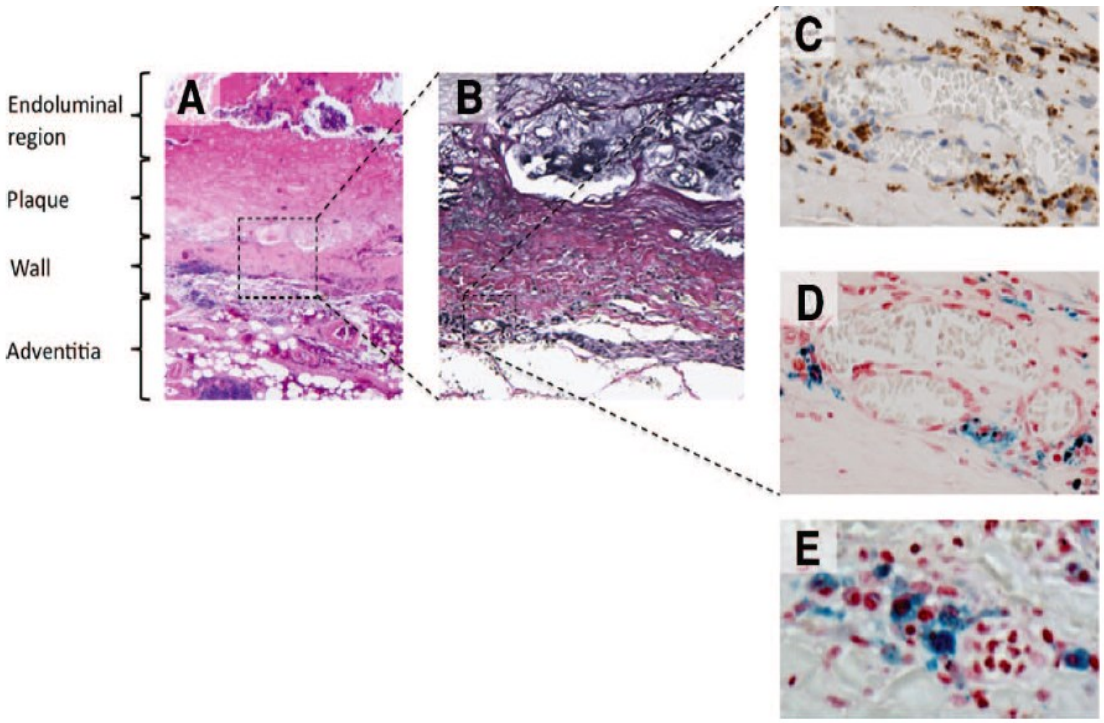

Figure 1. Representative histological sections of the aortic wall. **A**, Haematoxoylin and eosin (x20) of the full thickness of the aortic wall including atherosclerotic plaque, adherent thrombus and periadventitial fatty tissue. **B,** Elastin-van Gieson stain (x100) of the aortic wall showing complete destruction of the normal wall structure, including fibrosis (collagen, pink) of the media and adventitia and virtual absence of intact medial elastic fibers (black). **C,** Prussian blue staining for iron demonstrating co-localisation of CD68-positive macrophages (x400; brown) with **D,** Ultrasmall super-paramagnetic particles of iron oxide particles (x400; blue), **E,** High power (x1000) Prussian blue staining shows intracytoplasmic accumulation of USPIO within macrophages.

Furthermore, aortic aneurysms with mural USPIO uptake had a three-fold higher expansion rate when compared to abdominal aortic aneurysms with no or non-specific USPIO uptake despite similar baseline anteroposterior diameters (Figure 2).[19] Indeed, one patient with substantial mural USPIO uptake died suddenly 2 months after scanning from presumed aneurysm rupture. We have therefore shown that this technique holds major promise as a new method of risk-stratification of patients with abdominal aortic aneurysm that extends beyond simple anatomical measurements of aneurysm diameter.

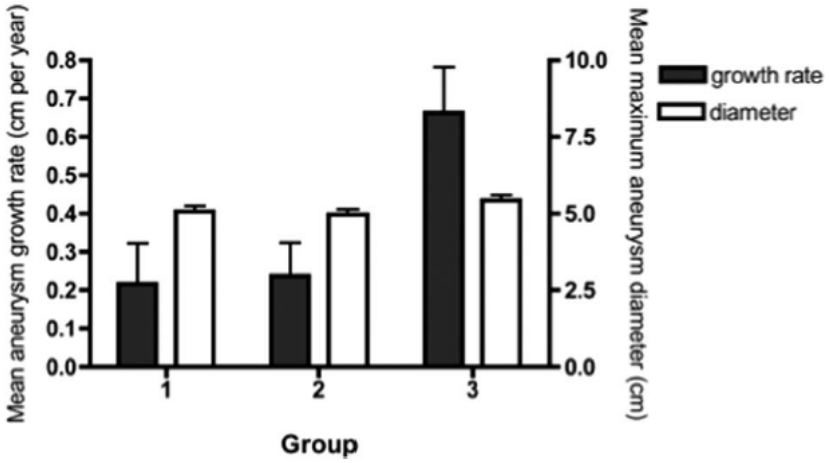

Figure 2. USPIO uptake in the aortic wall (group 3; 45% of total population) predicted a 3-fold increase in aneurysm expansion rate despite similar aortic diameters.

To date, the assessment of USPIO uptake has been qualitative or based on relative changes in signal intensity within regions of interest defined by vessel quadrants.[12, 13] However, this change in signal intensity can be caused by other factors including imaging artifacts. During the process of our studies, we have developed a more robust semi-quantitative image acquisition methodology for the detection of iron nanoparticle accumulation in humans using 3T magnetic resonance imaging.[19, 20] Here we apply a multi-echo gradient sequence to define the T2* value of the tissue. Images before and after USPIO administration are then co-registered and the difference in T2* value quantified. Following repeatability measurements in patients with abdominal aortic aneurysms, we have identified a threshold of change in signal intensity (59%) that defines USPIO accumulation in tissues (Figure 3).[20]

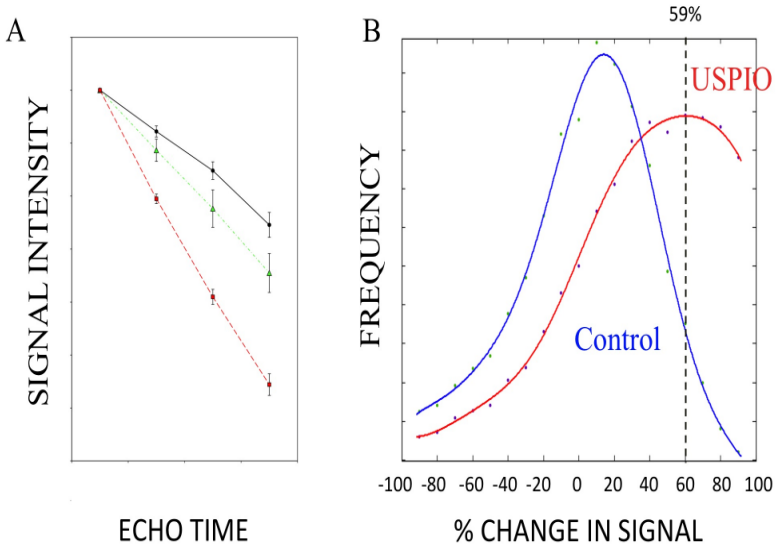

Figure 3. A. Signal intensity as percentage of first echo time (4.9 ms) within the multi-echo sequence of pre-contrast and post- contrast images in areas of no (black circles), low (green triangles) and high (red squares) USPIO uptake. **B.** Frequency of voxels with per cent change in T2* for patients who did (red) or did not (blue) receive USPIO. The upper 95% threshold of per cent change in T2* in the absence of USPIO was 59%.

1.1.2 Biomechanical Stress

Another potential predictive marker of aneurysm rupture is wall tissue stress. Information on aneurysm geometry is provided by computed tomography and magnetic resonance imaging, and this can be combined with finite element analysis to enable prediction of tissue stresses within the aneurysm wall.[3, 21] Peak wall tissue stress is higher in patients with symptomatic aneurysms[22] and co-localises with regions of inflammation identified by 18F-fluorodeoxyglucose positron emission tomography.[23] This suggests combining stress analysis with imaging of inflammation may provide added predictive value in the assessment of aneurysm expansion and potential rupture.

1.2 RATIONALE FOR STUDY

Ruptured AAA is the thirteenth commonest cause of death in the United Kingdom and accounts for 6,800 deaths each year in England and Wales. Population screening halves the mortality associated with AAA, and has led to the establishment of national screening and surveillance programmes. However, AAA surveillance is complex because of the non-linearity and unpredictability of expansion rates. Although the best predictor of aneurysm expansion is the aneurysm diameter, up to one fifth of ruptured AAA are less than 55 mm in diameter, and many patients present with diameters considerably greater than 55 mm without prior symptoms or rupture. There is therefore a major unmet clinical need to

predict aneurysm growth and rupture more accurately so that surgeons can better target preventative potentially life-saving surgery. We have developed a novel magnetic resonance imaging method that is based upon the known biological processes underlying aneurysm expansion and rupture. For the first time, this study proposes to assess this novel approach to identify aneurysms that are likely to expand more rapidly and potentially rupture. This technique would provide potentially important additional information to the current simplistic gold-standard of ultrasound measurement of aneurysm diameter.

2 STUDY OBJECTIVES

2.1 OBJECTIVES

2.1.1 Primary Objective

To determine whether mural uptake of USPIO provides incremental risk prediction in addition to standard risk markers such as aneurysm diameter, smoking and blood pressure.

2.1.2 Secondary Objectives

In patients under surveillance for abdominal aortic aneurysms, to determine whether mural uptake of USPIO:

i. Correlates with the rate of aneurysm expansion

ii. Occurs more commonly in patients who progress to surgery or whose aneurysm subsequently ruptures

iii. Co-localises with, or relates to, areas of biomechanical stress

iv. Occurs in a reproducible manner

We will investigate other inter-related mechanisms associated with aneurysm growth. We will specifically explore the added value of biomechanical stress modeling as we suspect co-localisation of both USPIO uptake and areas of high mechanical stress could act synergistically and cause more marked aneurysm growth. We will also examine correlates with other blood biomarkers including regulators of extracellular matrix turnover (such as matrix metalloproteinases and tissue inhibitors of metalloproteinases) and vascular inflammation (such as C-reactive protein and interleukin-6).

2.2 ENDPOINTS

2.2.1 Primary Endpoint

The primary end-point of the study will be the composite of aneurysm rupture or aortic aneurysm repair.

2.2.2 Secondary Endpoints

Secondary end-points will include:

i. the rate of aneurysm rupture
ii. the rate of surgical repair of the aneurysm
iii. the aneurysm growth rate
iv. all-cause and aneurysm-related mortality

We will conduct exploratory analyses examining the interactions between mural USPIO uptake, biomechanical stress, clinical risk factors and serum biomarkers of extracellular

matrix turnover and inflammation.

Clinicians involved directly with patient surveillance and care will be blinded to the magnetic resonance imaging findings of mural USPIO uptake.

3 STUDY DESIGN

The study will be a prospective observational cohort study of patients participating in abdominal aortic aneurysm surveillance programmes with blinded assessments of USPIO uptake. The study aims to recruit 350 participants in three study centres, with participants being followed up at six monthly intervals for 2 years.

We aim to validate the findings of our previous proof-of-concept study,[19] focusing on the relationship between baseline USPIO uptake and the subsequent clinical outcome and aneurysmal expansion rates. We will also look at the interplay between various risk factors affecting the growth rates and aneurysm-related adverse clinical events such as rupture, surgical repair, and death. This will lay the foundation for a large multicentre randomised controlled trial targeted at applying this technique to determine clinical management and surgical intervention. This will be particularly important given that screening programmes for the detection of abdominal aortic aneurysms are being rolled out across the United Kingdom and this is likely to increase substantially the number of patients being entered into surveillance programmes.

Reproducibility of the technique will be assessed in a subgroup of study participants (from the Edinburgh study centre) who will undergo repeat magnetic resonance scanning and USPIO administration at 1 month and 1 year (n=20), 1 year(n=60) and 2 year (n=40). Short-term (1 month) reproducibility is likely to reflect the variability in USPIO uptake whereas long-term (1 and 2 year) reproducibility is likely to represent the variation in biology of the aortic aneurysm with time. Patients recruited in Edinburgh who undergo elective surgery will also have AAA wall tissue collected and stored for the assessment of tissue resident macrophages and matrix metalloproteinases. Figure 4 shows the study flow chart.

Patients with abdominal aortic aneurysms (identified in surveillance program and other study site clinics)

350 patients with abdominal aortic aneurysm > 40mm who meet inclusion and exclusion criteria AND who agree to take part

Baseline Assessment (2 days)

Day 1:

- Consent
- Clinical Assessment
- Ultrasound scan (occurs as standard care and can occur up to 1 month prior to baseline assessment)
- 3T Magnetic resonance scan
- i.v. ferumoxytol
- Computed Tomography scan with contrast (can be done on day 2)
- Blood sample collection (can be done on day 2)
- Pulse wave analysis (can be done on day 2)

Day 2
(24-36 hours after Day 1):

- 3T Magnetic resonance scan (post ferumoxytol) *

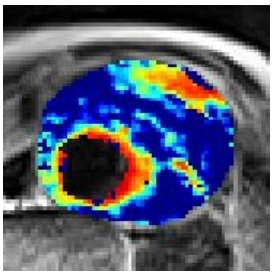

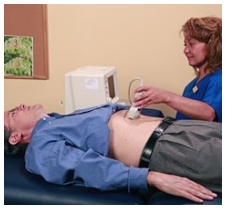

6 Monthly assessments (6, 12 and 18 months)
+/- 8 weeks, assessments can be performed on separate days
Clinical assessment
Ultrasound scan
Blood sample collection (**Edinburgh site only)**
Pulse wave analysis (**Edinburgh site only)**

Final 2 year assessments
+/- 8 weeks, assessments can be performed on separate days

- Clinical assessment
- Ultrasound scan
- Computed Tomography scan
- Blood sample collection
- Pulse wave analysis

317 Patients with 2 year follow up (allowing for drop-outs)

* 20 patients will undergo MRI reproducibility assessments at 1 month and 1 year,60 will have the assessment at 1 year only and 40 will have the assessment at 2 years only.

Figure 4: Study Flow Chart

4 STUDY POPULATION

Participants will be identified from the clinical surveillance program and given a patient information leaflet about the study. Eligible participants who are interested in the study will attend a baseline visit where they will provide written informed consent. All other study assessments for this baseline visit and the visits though-out the study are detailed in section 7.2

4.1 NUMBER OF PARTICIPANTS

We will recruit 350 patients with abdominal aortic aneurysms from the clinical surveillance program. Patients will be recruited from three centres; Royal Infirmary of Edinburgh, Western Infirmary in Glasgow and Forth Valley Royal Hospital. Patients recruited from Edinburgh will undergo limited additional procedures. Full details are in section 7.2.

4.2 INCLUSION CRITERIA

1. Abdominal aortic aneurysms measuring ≥40 mm in anteroposterior diameter on ultrasound scanning.
2. Age ≥40 years. Patients with abdominal aortic aneurysms less than 40 years may have a connective tissue disorder and a different aetiology to their disease.

4.3 EXCLUSION CRITERIA

1. Patients expected to, or already received, imminent elective or emergency surgical or endovascular repair.
2. Contraindication to magnetic resonance imaging scanning identified from magnetic resonance imaging safety questionnaire
3. Patients refusing or unable to give informed consent
4. Woman with child-bearing potential and who are breastfeeding will not be enrolled into the trial (woman who have experienced menarche, are pre-menopausal, have not been sterilised or who are currently pregnant).
5. Intercurrent illness including patients with a systemic inflammatory disorder or underlying malignancy (life expectancy < 2 years)
6. Renal dysfunction (eGFR ≤30 mL/min/1.73m^2)
7. Polycythemia
8. Contraindication to ferumoxytol (evidence of known iron overload, hemochromatosis, known hypersensitivity to ferumoxytol or its components or anaemia not caused by iron deficiency)9. Contraindication to Iodine.
10. Patients with any known history of drug allergy (including hypersensitivity) to other parenteral iron products.

5 PARTICIPANT SELECTION AND ENROLMENT

5.1 IDENTIFYING PARTICIPANTS

Patients will be identified from the clinical surveillance programmes and databases in Edinburgh, Glasgow and Forth Valley.

5.2 CONSENTING PARTICIPANTS

Written informed consent will be obtained by a suitably qualified member of the research team at study entry.

5.3 SCREENING FOR ELIGIBILITY

Once patients have been identified from the surveillance service database, they will be seen at their surveillance ultrasound appointment (standard clinical care) and eligibility will be assessed. Eligibility will be confirmed prior to consent. If patients are not seen in the ultrasound appointment, the study will be discussed with the patient over the phone and study information sent to them in the post. An appointment will be made for a baseline visit (where consent takes place) for all patients who are eligible and are interested in taking part.

5.4 INELIGIBLE AND NON-RECRUITED PARTICIPANTS

Ineligible and non-recruited patients will receive standard medical care. An anonymised log will be kept for patients who were screened for the study and subsequently found to be ineligible or not recruited.

5.5 CO-ENROLMENT

Co-enrolment is permitted into the 18F-Sodium Fluoride Imaging of Abdominal Aortic Aneurysms (SoFIA3) substudy. Study participants at the Edinburgh site may be invited to take part in this sub-study, which is detailed in a separate protocol.

Co-enrolment should not be considered with other interventional studies without prior discussion and agreement from the Sponsors and the Chief Investigators of both studies.

5.6 PREMATURE WITHDRAWAL

Participants are free to withdraw from the study at any point or a participant can be withdrawn by the investigator. If withdrawal occurs, the primary reason for withdrawal will be documented in the participant's Case Report Form (CRF).

If a patient who has consented for the study states that they wish to be withdrawn from the study before they have been administered ferumoxytol, they will be withdrawn from the study and another participant will be recruited in their place.

Clinicians should not withdraw participants who have received ferumoxytol but have not undergone the baseline MRI scanning protocol. These participants should continue to be followed up.

5.7 RANDOMISATION

There is no randomisation in this study.

6 INVESTIGATIONAL MEDICINAL PRODUCT AND PLACEBO

6.1 STUDY DRUG

6.1.1 Study Drug Identification

Rienso® (ferumoxytol) is composed of ultrasmall superparamagnetic particles of iron oxide (USPIOs) coated with polyglucose sorbitol carboxymethylether. It is supplied as an aqueous colloidal product that is formulated with mannitol and presented in single use vials

6.1.2 Study Drug Manufacturer

AMAG Pharmaceuticals Inc.Lexington, MA 02421, USA

Takeda Italia Farmaceutici S.p.A. Via Crosa, 86, 28065 Cerano (NO), Italy are responsible for batch release.

6.1.3 Marketing Authorisation Holder

Takeda Pharma A/S, Langebjerg 1, DK-4000 Roskilde, Denmark

6.1.4 Labelling and Packaging

Rienso® is supplied in a labelled vial containing 510 mg of elemental iron in a volume of 17mL of mannitol. Each mL of the sterile colloidal solution contains 30 mg of elemental iron and 44 mg of mannitol.

6.1.5 Storage

Consistent with the Summary of Product Characteristics (November 2012), Rienso® will be stored in the original package in order to protect from light and will not be frozen.

6.1.6 Summary of Product Characteristics or Investigators Brochure

A copy of the latest version of the Summary of Product Characteristics (SmPC) is available in the Investigator Site File.

6.2 PLACEBO

No placebo will be used in this study.

6.3 DOSING REGIME

The single use vials are diluted and administered as an intravenous infusion over 15-30 minutes. The ferumoxytol dose (4.0 mg/kg) is diluted in sterile 0.9% sodium chloride up to a final concentration of 2-8 mg iron per mL.

Patients should be reclined or in a semi-reclining position during infusion and for 30 minutes thereafter. Blood pressure (systolic and diastolic) will be recorded before ferumoxytol infusion and 30 minutes after the infusion to monitor for hypotension as detailed in the Summary of Product Characteristics.

The single dose is given 24-36 hours before magnetic resonance imaging.

In a subset of patients (n=20), repeated magnetic resonance imaging scans will be performed at 1 month and 1 year. These patients will receive a further dose (4.0 mg/kg) of ferumoxytol 24 (± 6) - 36 hours before each magnetic resonance imaging (total of 3 doses of ferumoxytol in one year).

A second subset of patients (n=60), repeated magnetic resonance imaging scans will be performed at 1 year only. These patients will receive a further dose (4.0 mg/kg) of ferumoxytol 24 (± 6) - 36 hours before each magnetic resonance imaging (total of 2 doses of ferumoxytol in one year).

In a further subset of patients (n=40), repeated magnetic resonance imaging scans will be performed at 2 years (±1 month). These patients will receive a further dose (4.0mg/kg) ferumoxytol 24 (± 6) - 36 hours before each magnetic resonance imaging (total of 1 doses of ferumoxytol in 1 year).

6.4 DOSE CHANGES

All patients will receive the same dose (4.0 mg/kg) 24-36 hours before magnetic resonance imaging.

In a subset of patients (n=20), magnetic resonance imaging will be repeated at 1 month (± 1 week) and 1 year (± 1 month) to determine short and long-term reproducibility respectively. These patients will receive a further dose (4.0 mg/kg) of ferumoxytol 24 (±6h) -36 hours before each magnetic resonance imaging (total of 3 doses of ferumoxytol in one year).

Another subset of patients (n=60), repeated magnetic resonance imaging scans will be performed at 1 year (± 1 month) only. These patients will receive a further dose (4.0 mg/kg) of ferumoxytol 24 (± 6) - 36 hours before each magnetic resonance imaging (total of 2 doses of ferumoxytol in one year).

In a further subset of patients (n=40), repeated magnetic resonance imaging scans will be performed at 2 years (±1 month). These patients will receive a further dose (4.0mg/kg) ferumoxytol 24 (± 6) - 36 hours before each magnetic resonance imaging (total of 1 doses of ferumoxytol in one year).

All study participants who agree to be part of the reproducibility sub-study will consent for the extra scans. Consecutive patients imaged in the Edinburgh centre will be approached until 20 patients have undergone repeated scanning at 1 month and 1 year, 60 patients have undergone repeated scanning at 1 year and 40 patients have undergone repeated scanning at 2 years.

6.5 PARTICIPANT COMPLIANCE

Responsibility for the infusion of ferumoxytol will be with the research team. Timing and volume of administration will be noted in the CRF. Any reason for non-administration of the ferumoxytol will be noted.

If intolerable side effects are experienced during the infusion of Ferumoxytol, the infusion will be abandoned and appropriate medical care will be delivered to the participant.

6.6 OVERDOSE

Overdose is unlikely as ferumoxytol will be prescribed and administered in the hospital. If accidental overdose is suspected, the patient will be followed up for signs of iron excess and will be referred for specialist assessment if appropriate.

For 270 patients, a single dose of ferumoxytol will be administered. In a random subset of patients (n=20) magnetic resonance imaging will be repeated at 1 month (± 1 week) and 1 year (± 1 month) to determine short and long-term reproducibility respectively. These patients will receive a further dose (4.0 mg/kg) of ferumoxytol 24 (±6h) -36 hours before each magnetic resonance imaging (a total of 3 doses of ferumoxytol in one year

and a total of 6 MRI scans). In a second subset of patients (n=60), magnetic resonance imaging will be repeated at 1 year (± 1 month) only. These patients will receive a further dose (4.0 mg/kg) of ferumoxytol 24 (±6h) -36 hours before each magnetic resonance imaging (a total of 2 doses of ferumoxytol in one year and a total of 4 MRI scans). In a further subset of patients (n=40), repeated magnetic resonance imaging scans will be performed at 2 years (±1 month). These patients will receive a further dose (4.0mg/kg) ferumoxytol 24 (± 6) - 36 hours before each magnetic resonance imaging (total of 1 doses of ferumoxytol in one year).

The manufacturers have good evidence of repeated dosing of Ferumoxytol in more than 200 patients, where repeat dosing occurred as short as 22 days, without adverse effect on the patient. In addition, serial data from patients undergoing multiple MRIs over a 2-week period, following a single dose of ferumoxytol show no residual ferumoxytol in the brain by 5-7 days.

Each dose of ferumoxytol equates to approximately 7% of total body iron.

6.7 OTHER MEDICATIONS

6.7.1 Buscopan

20mg of intravenous Buscopan (hyoscine butylbromide) will be given before each MRI scan. If patients have a contraindication (allergic reaction, narrow angle glaucoma, paralytic ileus, myasthenia gravis, obstructive prostatic hypertrophy) to this drug they will not receive it but will proceed with MRI scanning.

6.7.2 Permitted Medications

Any other medication necessary for clinical care can be taken.

For patients taking Metformin refer to section 7.1.

6.7.3 Prohibited Medications

Any other medication necessary for clinical care can be taken.

For patients taking Metformin refer to section 7.1.

7 STUDY ASSESSMENTS

7.1 SAFETY ASSESSMENTS

In patients with no history of renal disease, hypertension or diabetes, a normal eGFR within the last six months will be considered to be acceptable. For patients with risk factors for renal dysfunction or no blood tests within the last 6 months, clinical biochemical analysis of a blood sample will be performed prior to receiving contrast agent.

All patients are advised to drink water prior to their scan for adequate hydration.

For patients with a normal eGFR (60 mL/min/1.73m^2) and taking Metformin they should continue taking the medication up until the scan. After the scan they should withhold Metformin for 48 hours and then have a blood test to check renal function. They will be informed when they are to restart the Metformin following the result of this.

For patients with an eGFR 30 – 60 mL/min/1.73m^2 and taking Metformin they will be advised to stop the medication for 48 hours before and 48 hours after the scan. They

will then have a blood test to check renal function and informed when they are to restart the Metformin following the result of this.

These safety assessments are part of standard clinical care with regards to CT scanning with an intravenous contrast agent.

The magnetic resonance imaging safety questionnaire will be applied to identify patients with a contraindication to scanning.

Blood pressure (systolic and diastolic) will be recorded before ferumoxytol infusion and 30 minutes after the infusion to monitor for hypotension as detailed in the Summary of Product Characteristics. Patients should be reclined or in a semi-reclining position during infusion and for 30 minutes thereafter.

7.2 STUDY ASSESSMENTS

A preliminary assessment of eligibility will be conducted by a suitably qualified member of the research team. See tables 1.0 and 2.0 for the assessments performed at each study visit.

Additional assessments:

In patients that are to undergo elective repair of their aneurysms during the course of their follow-up, a repeat computed tomography scan may be performed immediately prior to surgery.

Patients recruited in Edinburgh who undergo elective surgery will also have AAA wall tissue collected and stored for the assessment of tissue resident macrophages and matrix metalloproteinases. Samples will **not** be collected for patients undergoing EVAR or from elective surgeries where unexpected complications arise.

Table 1.0 Table of study assessments for patients (not taking part in reproducibility study).

Assessments	Visits						
	SV	BV (a)	BV (b)	6 Mo	12 Mo	18 Mo	24 Mo
Screening/Eligibility	√						
Medical History/Demographics and concomitant medications		√					
Consent		√					
Ultrasound of AAA (**Standard clinical care)**	√			√	√	√	√
Clinical Assessment		√		√	√	√	√
Pulse Wave analysis and velocity		√		√ **	√ **	√ **	√
Blood sampling		√		√ **	√ **	√ **	√
CT scan of AAA *		√					√
MRI scan of AAA (pre-ferumoxytol)		√					
i.v. administration of ferumoxytol		√					
Post ferumoxytol MRI scan of AAA			√				
AE/SAE Reporting		←	—	—	—	—	→

SV = surveillance clinic; BV(a) = Baseline visit (occurs within 1 month of SV); BV (b) Baseline visit part B; 24-36 hours after part (a);

- * Where patients are to undergo elective repair of their aneurysms during follow up, a repeat CT scan may be performed prior to surgery.
- ** Bloods and pulse wave analysis will only occur every 6 months in Edinburgh only

6 month follow-up visits, 24 month visits and reproducibility scans can be performed within +/- 8 weeks of the due date.

Table 2.0 Table of study assessments for patients taking part in reproducibility part study

Assessments	Visits									
	SV	BV (a)	BV (b)	RP (a) (1 Mo)	RP (b) (1 Mo)	6 mo	RP (a) 1 yr	RP (b) 1 yr	18 Mo	24 Mo
Screening/Eligibility	√									
Medical History/Demographics and concomitant medications		√								
Consent		√								
Ultrasound of AAA **(Standard clinical care)**	√					√				
Clinical Assessment		√		√	√	√	√	√	√	√
Pulse Wave analysis and velocity		√				√			√	√
Blood sampling		√		√	√	√	√	√	√	√
CT scan of AAA		√								√
MRI scan of AAA (pre-ferumoxytol)		√		√			√		√	√
i.v. administration of ferumoxytol		√		√			√			
Post ferumoxytol MRI scan of AAA			√		√			√		
AE/SAE Reporting		←	—	—	—	—	—	—	—	→

SV = surveillance clinic; BV (a)= Baseline visit; BV (b) Baseline visit part B; 24-36 hours after part (a); RP = Reproducibility visit where (b) is 24-36 hours after RP (a)

8 DATA COLLECTION

8.1 CLINICAL ASSESSMENT

Patients will have a full formal and standardized clinical assessment at baseline that will include history, examination, documentation of cardiovascular risk factor profile (smoking status, family history, hypertension, hyperlipidaemia, diabetes mellitus) and concomitant medications (anti-hypertensive medication, etc). Concomitant medication will be recorded at baseline and at end of trial.

Brachial artery systolic and diastolic blood pressure, pulse pressure, and mean arterial pressure will be measured after a 30-min supine rest period using an automated oscillometric sphygmomanometer (model 711, Omron Healthcare GmbH, Hamburg, Germany). The mean of three recordings will be taken.

8.2 BLOOD SAMPLING

Blood samples (20 mL on each visit) will be collected at baseline and at 24 months for patients for routine biochemistry and haematology (including full blood count, U&Es, Liver Function Tests, total cholesterol and glucose)

For patients recruited and imaged in the Edinburgh centre a blood sample will be processed (plasma and serum) and stored at -80°C for later analysis of potential extracellular matrix and inflammatory biomarkers. This will happen at baseline, 6, 12,18 and 24 months. Full details for processing and shipment of serum biomarker samples will be provided in the ISF.

8.3 PULSE WAVE ANALYSIS AND VELOCITY

Pulse wave analysis and velocity will be measured in triplicate using the SphygmoCor™ apparatus (AtCor Medical, Sydney Australia) as previously described [McLeod *et al*, 2004]. This will facilitate the measurement of central aortic pressure to assist in the modelling of biomechanical stress within the aneurysm. This will be measured at baseline and every 6 months (6,12,18 and 24 months) for the patients recruited at the Edinburgh centre. This procedure will be carried out at baseline and at 24 months for patients in other recruiting centres. Pulse wave analysis and velocity measurements should always be done before the MRI scan and CT scans (this can be on day 1 or day 2 of the baseline visit). Patients will be fasted for this procedure.

In some instances, it may not be possible to perform pulse wave analysis and pulse wave velocity on some of the study patients. For example, if they are in atrial fibrillation or a weak pulse. In these instances, we will record that it was not possible to obtain these measurements and no further measurements will be obtained at the relevant follow up timelines.

8.4 ULTRASOUND OF THE ABDOMINAL AORTA

Patients will undergo 6-month ultrasound imaging as part of standard care for the surveillance programme to measure the maximal anteroposterior diameter of the aneurysm (Ultrasound scans should be every 6 months ± 2 months from the last ultrasound scan) A 3.5-MHz linear array transducer will be used to provide standard real time longitudinal B-scan images of the abdominal aortic aneurysm at the point of maximum diameter. Maximum anteroposterior abdominal aortic aneurysm diameter and distensibility (pressure strain elastic modulus and stiffness) will be assessed. Scans will be undertaken by accredited clinical vascular scientists with interobserver coefficient of variation of aortic diameter measurements of 3.5% in our laboratory.[24]

8.5 COMPUTED TOMOGRAPHY OF THE ABDOMINAL AORTA

Contrast enhanced images of the abdominal aorta will be obtained using a 320-multidetector computed tomography scanner (Aquilion ONE; Toshiba) or a 64 slice multi-detector computed tomography detector (Brilliance 64; Philips_at baseline and 2 years at either the Clinical Research Imaging Centre or the Western Infirmary of Glasgow. These data will be reconstructed into three dimensions using volumetric matrices to enable a more comprehensive assessment of the aneurysm geometry and growth than that provided by the ultrasound assessment of the unidimensional aortic anteroposterior diameter. In cases where study participants undergo emergency repair of a ruptured abdominal aortic aneurysm then a CT scan may not be performed. In the event of patients not receiving the CT scan at baseline (due to a CT scanner issue, or other clinical issue), the CT scan will be performed within 1 month of the baseline visit.

8.6 MAGNETIC RESONANCE IMAGING OF THE ABDOMINAL AORTA

Magnetic resonance imaging will be conducted using a 3T Siemens Magnetom Verio scanner (Siemens, Erlangen, Germany) before and 24-36 hours after administration of the USPIO in Edinburgh or Glasgow. Patients will be given intravenous buscopan (hyoscine butylbromide), prior to imaging to minimise bowel motion artifacts. Routine clinical coronal and sagittal breath-held T2-weighted multi-slice HASTE sequences will be used to identify the position and extent of the aneurysm following which a respiratory-gated, electrocardiographically-triggered T2 weighted (T2W) turbo- spin echo sequence will be used to acquire detailed anatomical data (TR/TE 2R-R intervals/72 ms; flip angle 180°; matrix 192 x 256; field of view 400 x 400 mm; slice width 5 mm). A multi-echo, gradient-echo T2*W sequence (TE 4.9, 7.7, 10.5, 13.3 ms; TR 133 ms; flip angle 15°; matrix 192 x 256; field of view 400 x 400 mm; slice width 5 mm) will be used to acquire contiguous axial images of the entire aneurysm (from the neck of the aneurysm down to the iliac bifurcation) with slice positions corresponding to those of the T2W images.

8.7 FOLLOW UP FOR PATIENTS IN CERTAIN CIRCUMSTANCES

If a patient undergoes an open or endovascular repair of their AAA they will not return routinely for US or pulse wave analysis or velocity every 6 months but will be invited to return every 6 months for blood tests and at 2 years for a CT scan.

If a patient is considered not fit for elective surgery then they would normally be discharged from the care of the Vascular Surgeons. However, we will invite these patients to attend for the standard study assessments.

9 STATISTICS AND DATA ANALYSIS

9.1 SAMPLE SIZE CALCULATION

The sample size is determined by the numbers required to build robust prognostic models for rupture and/or surgical repair, and in particular to measure the additional prognostic value of mural USPIO uptake when added to such a prognostic model based only on conventional clinical risk factors. There is a widely accepted ‘rule of thumb’ that one needs at least 10 and ideally 20 outcome events per covariate to be included in a prognostic model.[25] As described in more detail below, we plan to use the net reclassification index (NRI) as the primary measure of the clinical relevance of the added prognostic value of mural USPIO uptake.[26, 27] Based on two recent papers using the NRI,[28, 29] and also taking account of the Harrell ‘rule of thumb, we estimate that we need to observe 130 events (i.e. the composite of rupture or surgical repair) to have adequate sensitivity to answer the primary question. With our estimated event rate of 41% over the mean duration of follow-up of two years,[30] this equates to 317 patients.

There should be very modest losses to follow up for the primary analysis, since all study recruits are already enrolled on a surveillance programme. Moreover we shall seek consent at the time of recruitment to flag the patients so that if any patients are lost to follow up they can be traced to identify any hospital admissions or to identify if they have died. In addition, some patients will drop out due to technical failure of the scan, such as claustrophobia or poor image quality. We have therefore conservatively accounted for a 10% drop-out rate and we will recruit 350 patients to the study.

9.2 PROPOSED ANALYSES

9.2.1 Image analysis of ultrasound

Cursors will be locked onto echoes representing the anterior and posterior aortic walls and the movement of both tracked with each cardiac cycle. The longitudinal image will be used for analysis as experience with the technique and data from formal reproducibility studies indicates that the quality of the data obtained from a longitudinal section is superior to that obtained from a transverse view. Images will be captured digitally for later off-line core laboratory review.

9.2.2 Image analysis of computed tomography

Computed tomography of the abdominal aorta will be performed at baseline and 2 years to assess regional and volumetric growth rates. These two computed tomography scans will be spatially co-registered so that areas of expansion and growth can be more accurately defined and permit correlation with areas of USPIO uptake and fine element analysis modeling.

Three-dimensional computer models will be generated from segmented, contrast-enhanced images allowing geometric indices to be quantified. Semi-automatic segmentation is achievable due to the intensity differences between the aneurysm and surrounding tissues and structures. Intensity thresholding will be used to identify the lumen. To detect the thrombus and complete the segmentation, we will use a 3-D deformable model approach that utilises the level set algorithm as well as modeling the thrombus contour as a radial function starting from the aortic centre line as calculated from the lumen segmentation.

9.2.3 Image analysis of magnetic resonance imaging

A region of interest (ROI) encompassing the aortic wall and thrombus but excluding the lumen will be drawn on each slice of the pre-contrast T2W image. The pre-contrast T2W scan will be used as the base image to which subsequent scans will be co-registered using a semi-automatic rigid three-dimensional voxel registration protocol utilising a normalised mutual information algorithm. To minimise the contribution of bowel and abdominal wall motion in the magnetic resonance imaging datasets, a region for registration will include the aorta, vertebrae and spinal musculature that remain relatively static during the respiratory cycle but exclude the more mobile abdominal wall and bowel.

The four echoes in the multi-echo T2*W sequence will be combined to generate T2* and R2* maps. The T2* value is the decay constant for the exponential decay of signal intensity with time (Figure 3) and its inverse is the R2* value. A 3 x 3 voxel Gaussian filter will be applied to the individual echoes to reduce noise, and the co-efficient of determination will be used to exclude data that do not have an acceptable straight line fit when ln(signal intensity) is plotted against echo time. Images will be co-registered to allow direct comparison of the pre-and post-contrast T2*W magnetic resonance images. USPIO uptake will be presented visually as a colour map of per cent change in T2* or R2* values between pre- and post-USPIO scans, with our previously validated threshold

of significance applied[19, 20] (Figures 3 and 4).

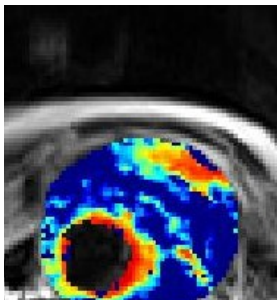

Figure 4. Colour map of magnetic resonance imaging of an abdominal aortic aneurysm. Red and yellow pixels indicate areas of increase T2* value, indicative of USPIO uptake.

The change in T2* or R2* colour maps from the magnetic resonance images will be spatially co-registered to the computed tomography datasets.

9.2.4 Finite element and stress analysis

Using Abaqus, the vessel wall will be modeled as a constant thickness layer of 1.5 mm, with a hyperelastic constitutive model. Thrombus will be modeled as homogenous and isotropic with Young's modulus 0.1 MPa. The model will be inflated from diastolic to systolic pressure using a homogeneous pressure-modeling regime. Peak wall stress and other rupture indices will be calculated and compared against areas of USPIO uptake.

9.2.5 Statistical analysis

The baseline assessment will include the baseline aneurysm diameter, sex, smoking habit and blood pressure. Using these covariates, a prognostic model predicting the time to the composite outcome event of rupture or surgical repair will be developed using Cox proportional hazards regression. The added prognostic value of adding mural USPIO uptake to this model will be assessed using the increase in the area under the receiver operator characteristic (ROC) curve, the Nagelkerke partial R^2, and primarily, the net reclassification index.[26, 27] The NCI is a direct measure of the clinical relevance of adding a covariate to a prognostic model. It is an overall measure of how many patients move from a low predicted risk to a high predicted risk when the covariate is added (and whether these individuals are indeed high risk), and how many move from a high predicted risk to a low predicted risk (and whether these individuals are indeed low risk). For the primary analysis, the USPIO will be taken as a binary covariate (as in Richards *et al*, 2011a), but a sensitivity analysis will explore the potential for including a quantification of the USPIO uptake. Some but not all of the patients will also have a measure of current aneurysm growth rate at baseline, and a further sensitivity analysis will explore using grown rate as a further prognostic factor, using imputation when the estimated growth rate is not available.

A secondary analysis will follow a similar analytical strategy to that set out above, but using prognostic models to predict aneurysm growth rate. This analysis will be far more complex with there being serial measures of aneurysm diameter, and with these measurements being censored on rupture or on surgical repair. Further exploratory analysis will look at the predictive ability of measures of wall stress and how these interact with regional USPIO uptake.

The analysis will be conducted by the study statistician, Catriona Graham (Senior Statistician Wellcome Trust Clinical Research Facility), under the supervision of Gordon Murray (Professor of Medical Statistics).

Reproducibility of the technique will be assessed in a subgroup of study participants who will undergo repeat magnetic resonance scanning and USPIO administration at 1 month and 1 year (n=20), 1 year only (n=60) and at 2 years (n=40). Short-term (1 month)

repeatability is likely to reflect the variability in USPIO uptake whereas long-term (1 and 2 years) reproducibility is likely to represent the variation in biology of the aortic aneurysm with time. Subjects will be categorised with respect to the presence or absence of USPIO uptake to define the proportionate agreement, with 95% confidence intervals.

For the 2 year repro sub-study, missing data is expected to be minimal as participants will be recruited for this component of the study as they are attending their regular 2 year study visit. A sample size has been determined as follows:

The following table shows width of a two-sided 95% confidence interval around expected proportions from 0.5 [column 1] up to 0.9 [column 5] based on a sample size of 40.

Confidence interval for proportion using normal approximation (n large)					
	1	**2**	**3**	**4**	**5**
Confidence level, 1-α	0.950	0.950	0.950	0.950	0.950
1 or 2 sided interval?	2	2	2	2	2
Expected proportion, π	0.500	0.600	0.700	0.800	0.900
Distance from proportion to limit, ω	0.155	0.152	0.142	0.124	0.093
n	40	40	40	40	40

As the expected proportion increases the width of the confidence interval decreases however with a sample size of 40 we would be able to express the proportional agreement to within ±0.155. This is based on a proportional agreement of 0.5 as this represents the 'worst-case scenario' i.e. the point at which the width of the CI is as its widest.

10 ADVERSE EVENTS

The Investigator is responsible for the detection and documentation of events meeting the criteria and definitions detailed below.

Full details of contraindications and side effects that have been reported following administration of the IMP can be found in the relevant Summary of Product Characteristics (SmPC).

Participants will be instructed to contact their Investigator at any time after consenting to join the study if any symptoms develop. All adverse events (AE) that require medical attention (for example, visit to a GP, hospital etc) which occur after having received ferumoxytol must be reported in detail in the Case Report Form (CRF) or AE form. In the case of an AE, the Investigator should initiate the appropriate treatment according to their medical judgment. Participants with AEs present at the last visit must be followed up until resolution of the event. For patients that have an aneurysm rupture or repair (elective or emergency), this will be recorded in the AAA case report form and entered into the database (this is one of secondary outcomes). This event will not be recorded as an AE.

10.1 DEFINITIONS

An **adverse event** (AE) is any untoward medical occurrence in a clinical trial participant which does not necessarily have a causal relationship with an investigational medicinal product (IMP).

An **adverse reaction** (AR) is any untoward or unintended response to an IMP which is related to any dose administered to that participant.

An **unexpected adverse reaction** (UAR) is an adverse reaction that is not consistent with the applicable product information for the IMP, e.g. the Investigator Brochure (IB) for a non licensed IMP or the SmPC for a licensed product.

A **serious adverse event** (SAE), **serious adverse reaction** (SAR) or **suspected unexpected serious adverse reaction** (SUSAR) is any AE, AR or UAR that at any dose:

- results in death;
- is life threatening* (i.e. the participant was at risk of death at the time of the event; it does not refer to an event which hypothetically might have caused death if it were more severe);
- requires in-patient hospitalisation or prolongation of existing hospitalisation;
- results in persistent or significant disability or incapacity;
- is a congenital anomaly or birth defect.

10.2 DETECTING AEs AND SAEs

All AEs and SAEs will be recorded from the time a participant signs the consent form to take part in the study until the last study visit.

Participants will be asked about the occurrence of AEs/SAEs at every visit during the study. Open-ended and non-leading verbal questioning of the participant will be used to enquire about AE/SAE occurrence. Participants will also be asked if they have been admitted to hospital or had any accidents. If there is any doubt as to whether a clinical observation is an AE, the event will be recorded.

AEs and SAEs may also be identified by support departments e.g. laboratories.

10.3 RECORDING AEs AND SAEs

When an AE/SAE occurs, it is the responsibility of the Investigator to review all documentation (e.g. hospital notes, laboratory and diagnostic reports) related to the event. The Investigator will then record all relevant information in the CRF and on the SAE form (if the AE meets the criteria of serious).

Information to be collected includes dose, type of event, onset date, Investigator assessment of severity and causality, date of resolution as well as treatment required, investigations needed and outcome.

10.4 ASSESSMENT OF AEs AND SAEs

Seriousness, causality, severity and expectedness will be assessed as though the participant is taking active IMP. The Investigator is responsible for assessing each AE.

The Chief Investigator (CI) may not downgrade an event that has been assessed by an Investigator as an SAE or SUSAR, but can upgrade an AE to an SAE, SAR or SUSAR if appropriate.

10.4.1 Assessment of Seriousness

The Investigator will make an assessment of seriousness as defined in Section 10.1.

10.4.2 Assessment of Causality

The Investigator will make an assessment of whether the AE/SAE is likely to be related to the IMP according to the definitions below.

All AEs/SAEs judged as having a reasonable suspected causal relationship (e.g. possibly related or unrelated) to the IMP will be considered as related to the IMP (ARs/SARs).

Where non Investigational Medicinal Products (NIMPs) e.g. rescue/escape drugs are given: if the AE is considered to be related to an interaction between the IMP and the NIMP, or where the AE might be linked to either the IMP or the NIMP but cannot be clearly attributed to either one of these, the event will be considered as an AR/SAR.

Unrelated: where an event is not considered to be related to the IMP.

Possibly related: The nature of the event, the underlying medical condition, concomitant medication or temporal relationship make it possible that the AE has a causal relationship to the study drug.

Probably related: The temporal relationship and absence of a more likely explanation suggest the event could be related to the study drug.

Definitely related: The known effects of the study drug or its therapeutic class, or based on challenge testing, suggest that study drug is the most likely cause.

Alternative causes such as natural history of the underlying disease, other risk factors and the temporal relationship of the event to the treatment should be considered and investigated.

10.4.3 Assessment of Severity

The Investigator will make an assessment of severity for each AE/SAE and record this on the CRF or AE form according to one of the following categories:

Mild: an event that is easily tolerated by the participant, causing minimal discomfort and not interfering with every day activities.

Moderate: an event that is sufficiently discomforting to interfere with normal everyday activities.

Severe: an event that prevents normal everyday activities.

Note: the term ‘severe’, used to describe the intensity, should not be confused with ‘serious’ which is a regulatory definition based on participant/event outcome or action criteria. For example, a headache may be severe but not serious, while a minor stroke is serious but may not be severe.

10.4.4 Assessment of Expectedness

If an event is judged to be an AR/SAR, the evaluation of expectedness will be made based on knowledge of the reaction and the relevant product information documented in the SmPC/IB.

The event may be classed as either:

Expected: the AR is consistent with the toxicity of the IMP listed in the SmPC/IB.

Unexpected: the AR is not consistent with the toxicity in the SmPC/IB.

10.5 REPORTING OF SAEs/SARs/SUSARs

Once the Investigator becomes aware that an SAE has occurred in a study participant, the information will be reported to the ACCORD Research Governance & QA Office **immediately or within 24 hours**. If the Investigator does not have all information regarding an SAE, they should not wait for this additional information before notifying ACCORD. The SAE report form can be updated when the additional information is received.

The SAE report will provide an assessment of causality and expectedness at the time of the initial report to ACCORD according to Sections 10.4.2, Assessment of Causality and 10.4.4, Assessment of Expectedness.

The SAE form will be transmitted by fax to ACCORD on **+44 (0)131 242 9447** or may be transmitted by hand to the office.

All reports faxed to ACCORD and any follow up information will be retained by the Investigator in the Investigator Site File (ISF).

10.6 REGULATORY REPORTING REQUIREMENTS

The ACCORD Research Governance & QA Office is responsible for pharmacovigilance reporting on behalf of the co-sponsors (Edinburgh University and NHS Lothian).

The ACCORD Research Governance & QA Office has a legal responsibility to notify the regulatory competent authority and relevant ethics committee (Research Ethics Committee (REC) that approved the trial). Fatal or life threatening SUSARs will be reported no later than 7 calendar days and all other SUSARs will be reported no later than 15 calendar days after ACCORD is first aware of the reaction.

ACCORD will inform Investigators at participating sites of all SUSARs and any other arising safety information.

An Annual Safety Report will be submitted to the regulatory competent authority and main REC listing all SARs and SUSARs.

10.7 FOLLOW UP PROCEDURES

After initially recording an AE or recording and reporting an SAE, the Investigator will follow each participant until resolution or death of the participant. Follow up information on an SAE will be reported to the ACCORD office.

AEs still present in participants at the last study visit will be monitored until resolution of the event or until no longer medically indicated.

11. PREGNANCY

Woman with child-bearing potential will not be enrolled into the trial (woman who have experienced menarche, are pre-menopausal, have not been sterilised or who are currently pregnant).

12 TRIAL MANAGEMENT AND OVERSIGHT ARRANGEMENTS

12.1 TRIAL MANAGEMENT GROUP

The study will be coordinated by a Project Management Group, consisting of the grant holders (Chief Investigator and Principal Investigator in Edinburgh), Trial Manager and coordinating nurse.

The Trial Manager will oversee the study and will be accountable to the Chief Investigator. The Trial Manager will be responsible for checking the CRFs for completeness, plausibility and consistency. Any queries will be resolved by the Investigator or delegated member of the study team.

A Delegation Log will be prepared for each site, detailing the responsibilities of each member of staff working on the study.

12.2 TRIAL STEERING COMMITTEE

A Trial Steering Committee (TSC) will be established to oversee the conduct and progress of the study, in particular the TSC will monitor the trial event rate. The terms of reference of the Trial Steering Committee, the draft template for reporting and the names and contact details are detailed in the TSC charter.

12.3 DATA MONITORING COMMITTEE

An independent Data Monitoring Committee (DMC) will not be convened for this study. The investigators will report all adverse events to the Sponsor and the Trial Steering Committee. As there is no blinded intervention and the investigational medicinal product will be given to all subjects, there is no risk to the scientific integrity of the study or requirement for a DMC.

12.4 INSPECTION OF RECORDS

Investigators and institutions involved in the study will permit trial related monitoring and audits on behalf of the sponsor, REC review, and regulatory inspection(s). In the event of an audit or monitoring, the Investigator agrees to allow the representatives of the sponsor direct access to all study records and source documentation. In the event of regulatory inspection, the Investigator agrees to allow inspectors direct access to all study records and source documentation.

12.5 RISK ASSESSMENT

An independent risk assessment will be performed by an ACCORD Clinical Trials Monitor to determine if monitoring is required and if so, at what level. An independent risk assessment will also be carried out by the ACCORD Quality Assurance Group to determine if an audit should be performed before/during/after the study and if so, at what locations and at what frequency.

12.5.1 RISKS

The risks to the participants of the study are very modest and are mainly attributable to the magnetic resonance and computed tomography scans and their respective contrast agents.

12.5.1.1 Magnetic resonance imaging

Magnetic resonance imaging is a standard clinical imaging technique that is applied across the world. Contraindications for magnetic resonance imaging are the presence of certain metallic objects, electrical devices and claustrophobia. Patients with implanted electrical devices, such as pacemakers or defibrillators, will be excluded. We have the provision of a wide-bore scanner (diameter, 70 cm) that will minimise the risk of experiencing claustrophobia.

12.5.1.2 Ferumoxytol

Ferumoxytol (Rienso®) was originally developed for the treatment of iron-deficiency anaemia in patients with chronic kidney disease. It consists of a suspension of USPIO with an ultrasmall core (diameter ~7 nm) and a semi-synthetic carbohydrate coating giving an overall particle size of 30 nm. The size of the particle prevents any early redistribution outside the vascular space and therefore can act as a blood-pool imaging agent with a plasma elimination half-life of approximately 10 - 14 hours in humans.

Herborn and colleagues examined the utility of ferumoxytol for imaging atheroma in the aortae of hyperlipidaemic rabbits using a 1.5T magnetic resonance scanner.[31] Susceptibility artifacts were detectable in the aortic wall at day 2 to 3 post administration of contrast. Signal voids were observed as a result of T2/T2* effects and were more homogenous than those seen in similar animals administered ferumoxtran-10. Histology revealed the accumulation of iron particles under the endothelium and into the medial layer of diseased vessels.[31]

Ferumoxytol has been administered safely as a bolus dose of 4 mg/kg for use as a magnetic resonance imaging contrast agent in humans.[32, 33, 34, 35, 36] Most of these studies have examined and confirmed its utility as a blood-pool contrast agent. However, it has also been assessed for its use in lymph node imaging for cancer staging. In a study of patients with prostate cancer, ferumoxytol was administered at 4 mg/kg and imaging performed at baseline, 5, 8 and 24 hours post dose using a 1.5 T scanner. Maximum signal-to-noise ratio was observed in lymph nodes at 24 hours on T2*-weighted MR imaging.[37]

Ferumoxytol is generally very well tolerated. We have administered ferumoxytol to 16 patients with abdominal aortic aneurysms, 28 patients who have undergone coronary artery bypass surgery and 12 patients with a recent acute myocardial infarction. None have experienced any significant major side-effects or serious adverse events. One subject did experience brief muscle cramps; a previously reported mild side effect. Common reported side-effects of ferumoxytol include constipation, diarrhoea, dizziness and nausea. Reported severe reactions include serious hypersensitivity reactions and hypotension, but are rare.

Buscopan is an anticholinergic drug and is generally used to provide relief from spasm of the genito-urinary tract or gastro-intestinal tract. In this study it is used to minimise bowel motion during the imaging protocol of this study to decrease artefacts seen due to digestive movements. Any side effects reported are uncommon or rare and consist of dry mouth and constipation.

12.5.1.3 Computed tomography

As part of the protocol, subjects will receive two extra computed tomography scans with intravenous contrast. This will expose the patient to ionising radiation (~6 mSv per scan for the Glasgow centre and 3mSv in Edinburgh centre) and the potential hazard of allergic reactions and transient renal dysfunction in response to the contrast agent. Thus the maximum total research protocol dose is 12 mSv.

The level of dose is comparable to the average cumulated dose from 5 years of natural background radiation to the UK population. It is equal to 60% of the whole body dose limit for radiation workers.

The associated excess risk of death from radiation induced cancer is approximately 1 in 3000 compared with the cancer mortality rate in the UK of just over 1 in 4.

The risks of exposure to the contrast medium include allergic reactions and impairment of kidney function. Amongst patients with moderate-to-severe chronic kidney disease, there is a 2-4% risk of kidney impairment after computed tomography angiography.[38] The risk of contrast exposure in this study will be minimised by exclusion of high risk patients who have significant kidney disease (estimated glomerular filtration rate ≤30 mL/min/1.73m^2).

12.5.2 Benefits

Patients will benefit from inclusion in a clinical study that includes close clinical supervision. Based on our previous studies and the demographics of the study population, the study may identify other important clinical conditions that require intervention or treatment because of incidental findings on the magnetic resonance or computed tomography scans. This could be viewed as a potential risk but most patients are grateful if covert conditions are detected early and treated more promptly. In addition, patients will benefit from the additional and closer supervision and care that clinical studies deliver.

Society and some of the participants will benefit if the findings of our study demonstrate that USPIO can successfully identify which patients are at risk of more rapid aneurysm expansion and clinical events. This is the main purpose of the study and we hope this will represent an important new method that may become standard of care.

12.5.3 Risk-to-Benefit

The risks associated with the additional scans and the administration of contrast agents are very low and consistent with many routine clinical imaging procedures. Conversely, if this technique is proven to be successful, the major gains in risk stratification and better selection of patients with abdominal aortic aneurysms who should receive surgical intervention, could have major morbidity and mortality benefits. Deferring unnecessary major surgery or bringing forward potentially life-saving surgery will ensure appropriate use of limited health care resources for maximum patient benefit.

12.6 STUDY MONITORING AND AUDIT

An ACCORD Clinical Trials Monitor or an appointed monitor will visit the Investigator site prior to the start of the study and during the course of the study if required, in accordance with the monitoring plan if required. Investigator sites will be risk assessed by the ACCORD QA Manager, or designee, in order to determine if audit by the ACCORD QA group is required.

13 GOOD CLINICAL PRACTICE

13.1 ETHICAL CONDUCT

The study will be conducted in accordance with the principles of the International Conference on Harmonisation Tripartite Guideline for Good Clinical Practice (ICH GCP).

A favorable ethical opinion will be obtained from the appropriate REC and local R&D approval will be obtained prior to commencement of the study.

13.2 REGULATORY COMPLIANCE

The study will not commence until a Clinical Trial Authorisation (CTA) is obtained from the appropriate Regulatory Authority. The protocol and study conduct will comply with the Medicines for Human Use (Clinical Trials) Regulations 2004, and any relevant amendments.

13.3 INVESTIGATOR RESPONSIBILITIES

The Investigator is responsible for the overall conduct of the study at the site and compliance with the protocol and any protocol amendments. In accordance with the principles of ICH GCP, the following areas listed in this section are also the responsibility of the Investigator. Responsibilities may be delegated to an appropriate member of study site staff.

13.3.1 Informed Consent

The Investigator is responsible for ensuring informed consent is obtained before any protocol specific procedures are carried out. The decision of a participant to participate in clinical research is voluntary and should be based on a clear understanding of what is involved.

Participants must receive adequate oral and written information – appropriate Participant Information and Informed Consent Forms will be provided. The oral explanation to the participant will be performed by the Investigator or qualified delegated person, and must cover all the elements specified in the Participant Information Sheet and Consent Form.

The participant must be given every opportunity to clarify any points they do not understand and, if necessary, ask for more information. The participant must be given sufficient time to consider the information provided. It should be emphasised that the participant may withdraw their consent to participate at any time without loss of benefits to which they otherwise would be entitled.

The participant will be informed and agree to their medical records being inspected by regulatory authorities and representatives of the sponsor(s) but understand that their name will not be disclosed outside the research team.

The Investigator or delegated member of the study team and the participant will sign and date the Informed Consent Form(s) to confirm that consent has been obtained. The participant will receive a copy of this document and a copy filed in the Investigator Site File (ISF) and participant's medical notes.

13.3.2 Study Site Staff

The Investigator must be familiar with the IMP, protocol and the study requirements. It is the Investigator's responsibility to ensure that all staff assisting with the study are adequately informed about the IMP, protocol and their study related duties.

13.3.3 Data Recording

The Principal Investigator is responsible for the quality of the data recorded in the CRF at each Investigator Site.

13.3.4 Investigator Documentation

Prior to beginning the study, each Investigator will be asked to provide particular essential documents to the ACCORD Research Governance & QA Office, including but not limited to:

- An original signed Investigator's Declaration (as part of the Clinical Trial Agreement documents);
- Curriculum vitae (CV) signed and dated by the Investigator indicating that it is accurate and current.

The ACCORD Research Governance & QA Office will ensure all other documents required by ICH GCP are retained in a Trial Master File (TMF), where required, and that appropriate documentation is available in local ISFs.

13.3.5 GCP Training

All study staff must hold evidence of appropriate GCP training.

13.3.6 Confidentiality

All laboratory specimens, evaluation forms, reports, and other records must be identified in a manner designed to maintain participant confidentiality. All records must be kept in a secure storage area with limited access. Clinical information will not be released without the written permission of the participant. The Investigator and study site staff

involved with this study may not disclose or use for any purpose other than performance of the study, any data, record, or other unpublished, confidential information disclosed to those individuals for the purpose of the study. Prior written agreement from the sponsor or its designee must be obtained for the disclosure of any said confidential information to other parties.

13.3.7 Data Protection

All Investigators and study site staff involved with this study must comply with the requirements of the Data Protection Act 1998 with regard to the collection, storage, processing and disclosure of personal information and will uphold the Act's core principles. Access to collated participant data will be restricted to those clinicians treating the participants.

Computers used to collate the data will have limited access measures via user names and passwords.

Published results will not contain any personal data that could allow identification of individual participants.

13.3.8 Sharing of anonymised data

Toshiba Medical Visualisation Systems (TMVS) have requested permission to use some of the anatomical MA3RS MRI and CT imaging data for the purposes of developing and evaluating registration algorithms. This will enable development of a framework allowing quantitative comparison of various registration algorithms and will only look at the anatomical/structural data that is acquired during the MA3RS imaging protocol. No MA3RS primary outcome data will be included.

The data provided will be fully anonymised (identifiable by MA3RS study ID only). An agreement will be put in place so that only TMVS members that are named on the agreement will be allowed to access the data provided and TMVS will not publish without explicitly requesting consent. Any further use of the data by TMVS for any purpose will require approval by the University of Edinburgh and the Trial Steering Committee.

14 STUDY CONDUCT RESPONSIBILITIES

14.1 PROTOCOL AMENDMENTS

Any changes in research activity, except those necessary to remove an apparent, immediate hazard to the participant in the case of an urgent safety measure, must be reviewed and approved by the Chief Investigator.

Amendments to the protocol must be submitted in writing to the appropriate REC, Regulatory Authority and local R&D for approval prior to participants being enrolled into an amended protocol.

14.2 PROTOCOL VIOLATIONS AND DEVIATIONS

Investigators will not implement any deviation from the protocol without agreement from the Chief Investigator and appropriate REC, Regulatory Authority and R&D approval except where necessary to eliminate an immediate hazard to study participants.

In the event that an Investigator needs to deviate from the protocol, the nature of and reasons for the deviation will be recorded in the CRF. If this necessitates a subsequent

protocol amendment, this should be submitted to the REC, Regulatory Authority and local R&D for review and approval if appropriate.

14.3 SERIOUS BREACH REQUIREMENTS

A serious breach is a breach which is likely to effect to a significant degree:

(a) the safety or physical or mental integrity of the participants of the study; or

b) the scientific value of the study.

If a potential serious breach is identified by the Chief investigator, Principal Investigator or delegates, the co-sponsors (accord.seriousbreach@ed.ac.uk) must be notified within 24 hours. It is the responsibility of the co-sponsors to assess the impact of the breach on the scientific value of the study, to determine whether the incident constitutes a serious breach and take the appropriate action.

Not every violation from the protocol needs to be reported to the regulatory authority as a serious breach. If the sponsor(s) deem the incident to be a violation that does not constitute a serious breach from the protocol when identified, corrective and preventative actions will be taken where appropriate and they will be recorded in file notes, held within the TMF and ISF.

14.4 STUDY RECORD RETENTION

All study documentation will be kept for a minimum of 5 years from the protocol defined end of study point. When the minimum retention period has elapsed, study documentation will not be destroyed without permission from the sponsor.

14.5 END OF STUDY

The end of study is defined as the last participant's last visit.

The Investigators and/or the trial steering committee and/or the co-sponsor(s) have the right at any time to terminate the study for clinical or administrative reasons.

The end of the study will be reported to the REC and Regulatory Authority within 90 days, or 15 days if the study is terminated prematurely. The Investigators will inform participants of the premature study closure and ensure that the appropriate follow up is arranged for all participants involved.

A summary report of the study will be provided to the REC and Regulatory Authority within 1 year of the end of the study.

14.6 CONTINUATION OF DRUG FOLLOWING THE END OF STUDY

Study participants will not receive ferumoxytol once they have completed the study.

14.7 INSURANCE AND INDEMNITY

The co-sponsors are responsible for ensuring proper provision has been made for insurance or indemnity to cover their liability and the liability of the Chief Investigator and staff.

The following arrangements are in place to fulfil the co-sponsors' responsibilities:

- The Protocol has been designed by the Chief Investigator and researchers employed by the University and collaborators. The University has insurance in place (which includes no-fault compensation) for negligent harm caused by poor protocol design by the Chief Investigator and researchers employed by the University.
- Sites participating in the study will be liable for clinical negligence and other negligent harm to individuals taking part in the study and covered by the duty of care owed to them by the sites concerned. The co-sponsors require individual sites participating in the study to arrange for their own insurance or indemnity in respect of these liabilities.
- Sites which are part of the United Kingdom's Nation Health Service will have the benefit of NHS Indemnity.

  Sites out with the United Kingdom will be responsible for arranging their own indemnity or insurance for their participation in the study, as well as for compliance with local law applicable to their participation in the study.

15 REPORTING, PUBLICATIONS AND NOTIFICATION OF RESULTS

15.1 AUTHORSHIP POLICY

Ownership of the data arising from this study resides with the study team. On completion of the study, the study data will be analysed and tabulated, and a clinical study report will be prepared in accordance with ICH guidelines.

15.2 PUBLICATION

The clinical study report will be used for publication and presentation at scientific meetings. Investigators have the right to publish orally or in writing the results of the study.

Summaries of results will also be made available to Investigators for dissemination within their clinics (where appropriate and according to their discretion).

15.3 PEER REVIEW

The protocol has undergone extensive peer review by the funders (Medical Research Council, Efficacy and Mechanism Evaluation programme) and by the Trial Steering Committee of the study.

16 REFERENCES

1. Multicentre Aneurysm Screening Study Group. Multicentre Aneurysm Screening Study (MASS) into the effect of abdominal aortic aneurysm screening on mortality in men: a randomised controlled trial. *Lancet* 2002;360:1531-1539.
2. Darling RC, Messina CR, Brewster DC, Ottinger LW. Autopsy study of unoperated abdominal aortic aneurysms: the case for early resection. *Circulation.* 1977;56:II161–II164.
3. Raghavan ML, Vorp DA. Toward a biomechanical tool to evaluate rupture potential of abdominal aortic aneurysm: identification of a finite strain constitutive model and evaluation of its applicability. *J Biomech* 2000;33:475–482.
4. Vallabhaneni, S.R. et al. Heterogeneity of tensile strength and matrix metalloproteinase activity in the wall of abdominal aortic aneurysms. *J Endovasc Ther* **11**, 494-502 (2004).
5. Brown PM, Zelt DT, Sobolev B. The risk of rupture in untreated aneurysms: the impact of size, gender, and expansion rate. *J Vasc Surg* 2003;37:280-284.
6. Thompson AR, Cooper JA, Ashton HA, Hafez H. Growth rates of small abdominal aortic aneurysms correlate with clinical events. *Br J Surg*. 2010;97:37-44.
7. Cai J, Hatsukami TS, Ferguson MS, Kerwin WS, Saam T, Chu B, Takaya N, Polissar NL, Yuan C. In vivo quantitative measurement of intact fibrous cap and lipid-rich necrotic core

size in atherosclerotic carotid plaque: comparison of high-resolution, contrast-enhanced magnetic resonance imaging and histology. *Circulation.* 2005;112:3437-3444.

8. Kramer CM, Cerilli LA, Hagspiel K, DiMaria JM, Epstein FH, Kern JA. Magnetic resonance imaging identifies the fibrous cap in atherosclerotic abdominal aortic aneurysm. *Circulation.* 2004;109:1016-1021.
9. Harisinghani MG, Barentsz J, Hahn PF, Deserno WM, Tabatabaei S, van de Kaa CH, de la Rosette J, Weissleder R. Noninvasive detection of clinically occult lymph-node metastases in prostate cancer. *N Engl J Med.* 2003;348:2491-2499.
10. Heesakkers RA, Hovels AM, Jager GJ, van den Bosch HC, Witjes JA, Raat HP, Severens JL, Adang EM, van der Kaa CH, Futterer JJ, Barentsz J. MRI with a lymph-node-specific contrast agent as an alternative to CT scan and lymph-node dissection in patients with prostate cancer: a prospective multicohort study. *Lancet Oncol.* 2008;9:850-856.
11. Kooi ME, Cappendijk VC, Cleutjens KB, Kessels AG, Kitslaar PJ, Borgers M, Frederik PM, Daemen MJ, van Engelshoven JM. Accumulation of ultrasmall superparamagnetic particles of iron oxide in human atherosclerotic plaques can be detected by in vivo magnetic resonance imaging. *Circulation.* 2003;107:2453-2458.
12. Trivedi RA, Mallawarachi C, JM UK-I, Graves MJ, Horsley J, Goddard MJ, Brown A, Wang L, Kirkpatrick PJ, Brown J, Gillard JH. Identifying inflamed carotid plaques using in vivo USPIO-enhanced MR imaging to label plaque macrophages. *Arterioscler Thromb Vasc Biol.* 2006;26:1601-1606.
13. Tang TY, Howarth SP, Miller SR, Graves MJ, Patterson AJ, JM UK-I, Li ZY, Walsh SR, Brown AP, Kirkpatrick PJ, Warburton EA, Hayes PD, Varty K, Boyle JR, Gaunt ME, Zalewski A, Gillard JH. The ATHEROMA (Atorvastatin Therapy: Effects on Reduction of Macrophage Activity) Study. Evaluation using ultrasmall superparamagnetic iron oxide-enhanced magnetic resonance imaging in carotid disease. *J Am Coll Cardiol.* 2009;53:2039-2050.
14. Bernd H, De Kerviler E, Gaillard S, Bonnemain B. Safety and tolerability of ultrasmall superparamagnetic iron oxide contrast agent: comprehensive analysis of a clinical development program. *Invest Radiol.* 2009;44:336-342.
15. Bourrinet P, Bengele HH, Bonnemain B, Dencausse A, Idee JM, Jacobs PM, Lewis JM. Preclinical safety and pharmacokinetic profile of ferumoxtran-10, an ultrasmall superparamagnetic iron oxide magnetic resonance contrast agent. *Invest Radiol.* 2006;41:313-324.
16. Muller K, Skepper JN, Posfai M, Trivedi R, Howarth S, Corot C, Lancelot E, Thompson PW, Brown AP, Gillard JH. Effect of ultrasmall superparamagnetic iron oxide nanoparticles (Ferumoxtran-10) on human monocyte-macrophages in vitro. *Biomaterials.* 2007;28:1629-1642.
17. Ruehm SG, Corot C, Vogt P, Kolb S, Debatin JF. Magnetic resonance imaging of atherosclerotic plaque with ultrasmall superparamagnetic particles of iron oxide in hyperlipidemic rabbits. *Circulation.* 2001;103:415-422.
18. Turner GH, Olzinski AR, Bernard RE, Aravindhan K, Boyle RJ, Newman MJ, Gardner SD, Willette RN, Gough PJ, Jucker BM. Assessment of macrophage infiltration in a murine model of abdominal aortic aneurysm. *J Magn Reson Imaging.* 2009;30:455-460.
19. Richards JMJ, Semple SI, MacGillivray TJ, Gray C, Langrish JP, Williams M, Dweck M, Wallace MD, McKillop G, Chalmers RTA, Garden OJ, Newby DE. Abdominal aortic aneurysm growth predicted by uptake of ultrasmall superparamagnetic particles of iron oxide. *Circ Cardiovasc Imaging* 2011a;4:274-81.
20. Richards JMJ, Semple SI, MacGillivray TJ, Gray C, Langrish JP, Williams M, Dweck M, Wallace MD, McKillop G, Chalmers RTA, Garden OJ, Newby DE. Uptake of ultrasmall superparamagnetic particles of iron oxide predicts growth in abdominal aortic aneurysms. *Heart* 2011b;97 Supplement 1: Abstract Young Research Worker's Prize.
21. Doyle BJ, Corbett TC, Callanan A, Walsh MT, Vorp DA, McGloughlin TM. An experimental and numerical comparison of the rupture locations of an abdominal aortic aneurysm. *J Endovasc Ther* 2009;16:322–335
22. Fillinger MF, Raghavan ML, Marra SP, Cronenwett JL, Kennedy FE. In vivo analysis of mechanical wall stress and abdominal aortic aneurysm rupture risk. *J Vasc Surg* 2002;36:589–597.
23. Xu XY, Borghi A, Nchimi A, Leung J, Gomez P, Cheng Z, Defraigne JO, Sakalihasan N. High levels of 18f-fdg uptake in aortic aneurysm wall are associated with high wall stress. Eur J Vasc Endovasc Surg. 2010; 39:295-301.
24. Wilson KA, Hoskins PR, Lee AJ, Fowkes FG, Ruckley CV, Bradbury AW. Ultrasonic measurement of abdominal aortic aneurysm wall compliance: a reproducibility study. *J Vasc Surg.* 2000;31:507-513.

25. Harrell FE, Lee KL, Califf RM, Pryor DB, Rosati RA. Regression modelling strategies for improved prognostic prediction. *Stat. Med*. 1984;3:143-152.

26. Pencina MJ, D'Agostino RB Sr, D'Agostino RB Jr, Vasan RS. Evaluating the added predictive ability of a new marker: from area under the ROC curve to reclassification and beyond. Stat. Med. 2008:27;157-172.

27. Pencina MJ, D'Agostino RB, Steyerberg EW. Extensions of net reclassification improvement calculations to measure usefulness of new biomarkers. *Stat. Med*. 2011:30;11-21

28. Fellahi JL, Le Manach Y, Daccache G, Riou B, Gerard JL, Hanouz JL. Combination of EuroSCORE and cardiac troponin 1 improves the prediction of adverse outcome after cardiac surgery. *Anesthesiology* 2011;114:330-339.

29. Polak JF, Pencina MJ, Pencina KM, o'Donnell CJ, Wolf PA, D'Agostino RB. Carotid-wall intima-media thickness and cardiovascular events. *N. Engl. J. Med*. 2011;365:213-221

30. Wilson KA, Lee AJ, Hoskins PR, Fowkes FG, Ruckley CV, Bradbury AW. The relationship between aortic wall distensibility and rupture of infrarenal abdominal aortic aneurysm. *J Vasc Surg*. 2003;37:112-117.

31. Herborn CU, Vogt FM, Lauenstein TC, Dirsch O, Corot C, Robert P, Ruehm SG. Magnetic resonance imaging of experimental atherosclerotic plaque: comparison of two ultrasmall superparamagnetic particles of iron oxide. *J Magn Reson Imaging.* 2006;24:388-393.

32. Prince MR, Zhang HL, Chabra SG, Jacobs P, Wang Y. A pilot investigation of new superparamagnetic iron oxide as a contrast agent for cardiovascular MRI. *Journal of X-Ray Science and Technology.* 2003;11:231-240.

33. Ersoy H, Jacobs P, Kent CK, Prince MR. Blood pool MR angiography of aortic stent-graft endoleak. *AJR Am J Roentgenol.* 2004;182:1181-1186.

34. Li W, Tutton S, Vu AT, Pierchala L, Li BSY, Lewis JM, Prasad PV, Edelman RR. First-pass contrast-enhanced magnetic resonance angiography in humans using ferumoxytol, a novel ultrasmall superparamagnetic iron oxide (USPIO)-based blood pool agent. *J Magn Reson Imaging.* 2005;21:46-52.

35. Li W, Salanitri J, Tutton S, Dunkle EE, Schneider JR, Caprini JA, Pierchala LN, Jacobs PM, Edelman RR. Lower extremity deep venous thrombosis: evaluation with ferumoxytol-enhanced MR imaging and dual-contrast mechanism--preliminary experience. *Radiology.* 2007;242:873-881.

36. Neuwelt EA, Várallyay CG, Manninger S, Solymosi D, Haluska M, Hunt MA, Nesbit G, Stevens A, Jerosch-Herold M, Jacobs PM, Hoffman JM. The potential of ferumoxytol nanoparticle magnetic resonance imaging, perfusion, and angiography in central nervous system malignancy: a pilot study. *Neurosurgery.* 2007;60:601-611.

37. Harisinghani M, Ross RW, Guimaraes AR, Weissleder R. Utility of a new bolus-injectable nanoparticle for clinical cancer staging. *Neoplasia.* 2007;9:1160-1165.

38. Barrett BJ, Katzberg RW, Thomsen HS, Chen N, Sahani D, Soulez G, Heiken JP, Lepanto L, Ni ZH, Ni ZH, Nelson R. Contrast-induced nephropathy in patients with chronic kidney disease undergoing computed tomography: a double-blind comparison of iodixanol and iopamidol. *Invest Radiol*. 2006;41:815-821.

SoFIA^3

Sodium Fluoride Imaging of Abdominal Aortic Aneurysms: The SoFIA^3 Study

STUDY PROTOCOL

Version 4.2

18^F-Sodium Fluoride PET-CT in Abdominal Aortic Aneurysms

Co-sponsors	University of Edinburgh & NHS Lothian ACCORD The Queen's Medical Research Institute 47 Little France Crescent Edinburgh EH16 4TJ
Funder/	Chief Scientist Office
Funding Reference Number	ETM/365
Chief Investigator	Dr Jenny Robson
Principal Investigator	Dr Rachael Forsythe
IRAS Project ID	152670
REC number	14\SS\0080
NCT number	
Version Number / Date	Version 4.2; 10/11/15

CO-ORDINATING CENTRE

Chief Investigator:	**Co-sponsor Representative 1:**
Jennifer Robson* Lecturer in Vascular Surgery Room F3304, Department of Surgery Royal Infirmary of Edinburgh Little France Crescent Edinburgh EH16 4SA Tel: 07967827942 Email: Jenny.Robson@ed.ac.uk!	Raymond French Research Governance Manager ACCORD Research & Development Suite The Queens Medical Research Institute 47 Little France Crescent Edinburgh EH16 4TJ Tel: 0131 242 6226 Email: Raymond.French@ed.ac.uk!
Principal Investigator:! Rachael Forsythe*! Clinical Research Fellow Centre of Cardiovascular Science Chancellor's Building 51 Little France Crescent Edinburgh EH16 4SB Tel: 07739967481! Email: rachaelforsythe@doctors.org.uk! !	**Co-sponsor Representative 2:**! Susan Shepherd Research & Development Department Room 4F/2/070 Western General Hospital Crewe Road South EH4 2XU Tel: 0131 537 2912 Email: susan.shepherd@nhslothian.scot.nhs.uk !
Trial Manager:! Rachael Forsythe! Clinical Research Fellow Centre of Cardiovascular Science Chancellor's Building 51 Little France Crescent Edinburgh EH16 4SB Tel: 07739967481! Email: rachaelforsythe@doctors.org.uk!	**Trial Statistician:**! Gordon D Murray Professor of Medical Statistics Centre for Population Health Sciences University of Edinburgh Medical School Teviot Place, Edinburgh EH8 9AG Tel: +44 (0) 131 650 3233 Email: Gordon.Murray@ed.ac.uk!

* Protocol authors

Sodium Fluoride Imaging of Abdominal Aortic Aneurysms:
The SoFIA[3] Study

Chief Investigator	Signature	Date
Trial Statistician	Signature	Date
Sponsor(s) Representative	Signature	Date
Principal Investigator	Signature	Date

LIST OF ABBREVIATIONS

AAA	Abdominal Aortic Aneurysm
ACCORD	Academic and Clinical Central Office for Research and Development
AE	Adverse Event
CI	Chief Investigator
CRIC	Clinical Research Imaging Centre, Edinburgh
CRIF	Clinical Research Imaging Facility, Dundee
CT	Computed Tomography
eGFR	estimated Glomerular Filtration Rate
MA^{3}RS	MRI in Abdominal Aortic Aneurysms to predict Rupture or Surgery
MRI	Magnetic Resonance Imaging
NHS	National Health Service
NAAASP	National Abdominal Aortic Aneurysm Screening Programme
PET-CT	Positron Emission Tomography-Computed Tomography
PI	Principal Investigator
REC	Research Ethics Committee
R&D	Research and Development
USPIO	Ultrasmall supramagnetic Particles of Iron Oxide
USS	Ultrasound scan
SAE	Serious Adverse Event
^{18}F-NaF	^{18}F-Sodium Fluoride

SUMMARY

Ruptured abdominal aortic aneurysms (AAAs) have a 90% mortality rate but there are currently no accurate methods of establishing the risk of rupture for an individual patient with an asymptomatic AAA. In vascular disease, microcalcification occurs in response to necrotic inflammation. Using computed tomography and positron emission tomography, we can identify early microcalcification using uptake of the radiotracer ^{18}F-sodium fluoride. This can identify high risk-lesions in the aorta, coronary and carotid arteries, and appears to be indicative of necrotic and heavily inflamed tissue. We therefore propose to evaluate the ability of ^{18}F-sodium fluoride to identify regions of necrotic inflammation in AAA and predict AAA expansion. We will also explore its value as part of an ongoing clinical trial assessing the identification of macrophage activity using magnetic resonance imaging (the MA^{3}RS study).

1 INTRODUCTION

1.1 BACKGROUND

Abdominal aortic aneurysms (AAA) are the 13th leading cause of death in the United Kingdom and other western countries, with around 6,800 deaths each year in the United Kingdom and 15,000 deaths annually in the United States[1]. The condition is most prevalent amongst men, with 5-8% of men over the age of 65 years affected. The mortality of ruptured AAA is extremely high at ~90%. In contrast, the risk of death from elective open surgical or endovascular repair is low at 1-5%[2].

The focus is therefore to identify AAA before rupture and offer surgery when the risk of rupture exceeds that of elective repair. Indeed, the early identification of AAA through screening programmes can reduce aneurysm-related mortality by up to 50% and nationwide screening has recently been established in the United Kingdom. Currently, patients diagnosed with an aneurysm are entered into an ultrasound-based surveillance programme with a view to offering those at high risk of rupture preventative surgical or endovascular repair. Evaluation of rupture risk is currently based on the maximum anteroposterior diameter of the aneurysm. Aneurysms <55 mm in diameter have an annual risk of rupture of <1%, and early repair affords no survival benefit over continued surveillance in this group[3].

Elective aneurysm repair is offered to patients with an aneurysm diameter >55 mm or where the aneurysm expansion rate is >10 mm/year. However, up to one in five ruptured AAA has a diameter of <55 mm and many patients have aneurysms considerably larger than 55 mm without symptoms or rupture[4]. Furthermore, although aneurysm size is currently the best predictor of clinical risk, the unpredictability and non-linearity of aneurysm growth makes risk prediction complex.

There is an urgent unmet clinical need for an improved method of predicting disease progression and rupture in patients with AAA so that preventative surgical or endovascular repair can be targeted at high-risk patients. In this proposed study, we intend to conduct an exploratory analysis of the uptake of ^{18}F-NaF in aneurysmal aortae and investigate whether there is a relationship with ^{18}F-NaF uptake and AAA expansion.

1.1.1 ANEURYSM BIOLOGY

Aneurysm disease typically coexists with atherosclerosis and the two processes share a number of risk factors. However, there are distinct and important differences[5]. Atherosclerotic lesions originate in the tunica intima whilst aneurysmal degeneration affects the tunica media and adventitia[6]. Aneurysm disease has a particular predilection for the infrarenal abdominal aorta, whilst atherosclerotic disease is more widespread. Furthermore, aneurysm disease is more strongly associated with hypertension and smoking, and correlates negatively with the presence of diabetes mellitus[7].

Aneurysm disease results from a complex interaction between biomechanical factors and biological processes that include neovascularisation, inflammation and proteolytic degradation of the extracellular matrix[8]. These processes do not affect the aorta uniformly but are focal in nature. Indeed biological and biomechanical “hotspots” are thought to represent regions of the aortic wall at risk of further expansion and rupture. Focal neovascularisation occurs at the site of rupture and corresponds to the degree of inflammation. Increased proteolytic activity occurs in regions of the wall with low tensile

strength and also at the site of rupture. Wall stresses vary in different parts of the aneurysm and it seems likely that rupture occurs where intense radial wall stress is applied to a biologically active and inflamed region of the aortic wall with reduced tensile strength[9].

1.1.2 VASCULAR SMOOTH MUSCLE CELL APOPTOSIS

Vascular smooth muscle cells are the major source of extracellular matrix proteins including collagen and elastin. In atherosclerosis, vascular smooth muscle cells migrate into the intima, and can stabilise the plaque by maintaining the fibrous cap. Conversely, chronic vascular smooth muscle cell apoptosis is associated with plaque vulnerability and calcification as well as medial atrophy and aneurysm formation[10 11]. In aneurysm disease, wasting of the extracellular matrix occurs through both vascular smooth muscle cell apoptosis (reduced extracellular matrix production) and matrix metalloproteinase activity (degradation of existing collagen and elastin). Fragmentation and loss of first elastin and then collagen weakens the aortic wall leaving it vulnerable to expansion and rupture. In otherwise healthy arteries, vascular smooth muscle cell apoptosis is inconspicuous since phagocytic cells rapidly clear the cellular debris. In diseased arteries, however, apoptotic bodies appear to persist leading to a secondary pro-inflammatory necrotic response[12]. We hypothesise that it is the balance between tissue degradation by macrophages, and extracellular matrix deposition by vascular smooth muscle cells that determines the initiation, progression and complications of AAA disease.

1.1.3 CALCIFICATION

In atherosclerotic disease, microcalcification is a key indicator of plaque vulnerability and its presence is associated with chronic vascular smooth muscle cell apoptosis and necrotic inflammation. Indeed coronary microcalcification is a strong predictor of plaque rupture and future cardiovascular events[13]. The relative risk of clinical events associated with coronary calcification is greater than that associated with established risk factors such as smoking, hypertension and diabetes mellitus, and is independently associated with a 3-4 fold increased risk of death[14].

Calcification is widely observed in aortic aneurysm disease and, like coronary atheroma, co-localises to areas of apoptosis and necrotic inflammation. In established aneurysm disease, regions of medial calcification contribute to increased Young's elastic modulus, greater aortic stiffness and loss of mechanical anisotropy[15]. Load–bearing becomes concentrated in regions of calcification causing heterogeneity in the distribution of wall stress across the aneurysm wall with an increase in the peak stresses. Irregular calcification therefore has the potential to induce aortic wall instability and increase vulnerability to rupture. We hypothesise that micro-calcification and later macro-calcification will occur at sites of vascular smooth muscle cell apoptosis and extracellular matrix depletion, and thereby localise to weakened areas of the aneurysmal aortic wall that are prone to expansion and rupture.

1.1.4 IMAGING IN ANEURYSM DISEASE

Current imaging techniques in aneurysm disease are limited to the assessment of aneurysm dimensions and morphology, and offer no prognostic information beyond size-based risk stratification. Molecular imaging techniques targeted against these biological 'hotspots' in the aneurysm wall could allow the identification of patients with aneurysms at high risk of expansion and rupture. Positron emission and computed tomography

(PET-CT) combine functional molecular imaging with high-resolution anatomical imaging. We have recently explored the PET radiotracer ^{18}F -sodium fluoride (^{18}F-NaF) as a marker of calcification activity in valvular heart disease and coronary atherosclerosis[16 17]. ^{18}F-NaF has in fact been used as a bone tracer for >40 years, binding to hydroxyapatite, a key crystalline component of both bone and vascular calcification. The surface area of hydroxyapatite is much higher in regions of powdery, novel calcification compared to macroscopic field calcification (where much of the hydroxyapatite is internalized and not available for binding) so that ^{18}F-NaF preferentially binds to regions of developing calcification. It therefore acts as a marker of vascular calcification activity, providing complementary information to the presence of established calcium on CT and demonstrating a close correlation with immunohistochemical markers of calcification activity in excised aortic valve tissue (alkaline phosphatase: r=0.65, p=0.04)[18].

In previous studies we have established the methodology to measure ^{18}F-NaF uptake in the cardiovascular system. In patients with aortic stenosis, ^{18}F-NaF was detected within the aortic valve, often in areas of no macroscopic calcification or in areas adjacent to established macroscopic calcification. Moreover, baseline ^{18}F-NaF uptake correlated not only with disease severity and histological measures of calcification activity, but also progression of valvular calcification over 1 year of follow-up [19 20].

In the vasculature, ^{18}F-NaF acts as a marker of novel calcification activity [21 22 23]. Similar to other conditions, calcification in coronary atheroma occurs as a healing response to intense necrotic inflammation, making ^{18}F-NaF a useful marker of high-risk atherosclerotic plaque. We have previously demonstrated increased uptake of this tracer in the coronary vasculature localising to individual coronary lesions and identifying patients with increased cardiovascular risk factor profiles[24].

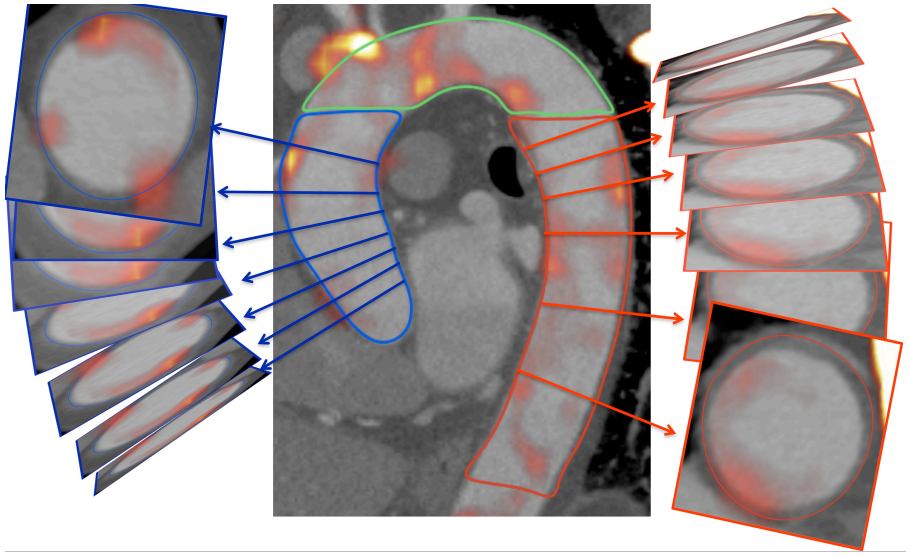

Figure 1: Fused PET-CT of atherosclerotic thoracic aorta. *Uptake of ^{18}F -sodium fluoride in the wall of the ascending aorta, arch and descending aorta in patients with coronary artery disease.*

More recently we have conducted a prospective study of 40 patients with myocardial infarction in whom ^{18}F-NaF localised to the culprit plaque in over 90% of patients[25]. This finding was confirmed in 12 patients with a recent stroke undergoing carotid endarterectomy where ^{18}F-NaF uptake was observed at the site of plaque rupture in 100% of patients and this uptake correlated with increased calcification activity and areas of

necrosis on histology. Finally we studied 40 patients with stable coronary artery disease. Increased uptake was observed in 45% of these patients and this again localised to individual coronary plaques. Interestingly these lesions were associated with multiple high-risk markers on radiofrequency and gray-scale intravascular ultrasound: necrotic core, positive remodelling and micro-calcification.

During our cardiac studies, ^{18}F-NaF uptake was observed incidentally in atherosclerotic regions of the thoracic and abdominal aorta as well as in aneurysmal aortae (Figure 1). This activity is distinct from uptake of other radiotracers, such as ^{18}F-fluorodeoxyglucose, with which it correlated poorly[26]. We have also demonstrated ^{18}F-NaF uptake in *ex vivo* autoradiography studies of human aortic wall tissue acquired from patients undergoing open AAA surgery and this maps to areas of tissue necrosis and degradation (Figure 2). Thus, as with atherosclerosis, ^{18}F -NaF uptake identifies areas of tissue necrosis and apoptosis that is actively calcifying in order to limit and contain destructive tissue inflammation and degradation. Moreover, novel planes of calcification can serve to magnify and focus incident tissue stresses such that this may encourage rather than prevent AAA rupture.

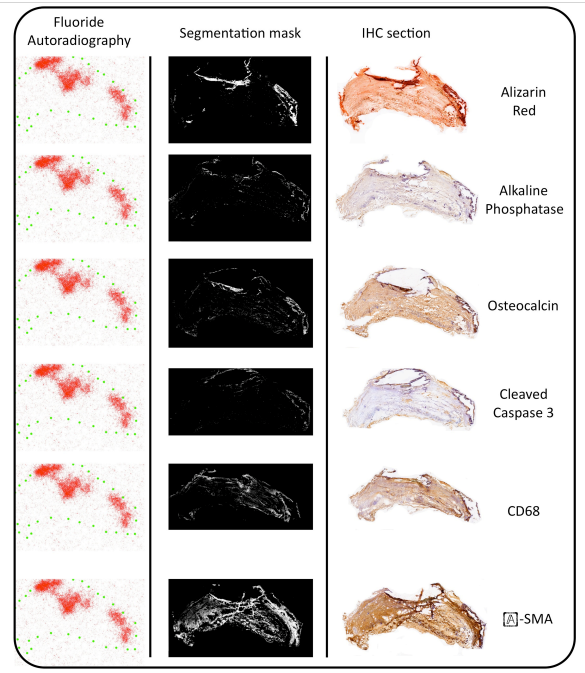

Figure 2: ^{18}F -NaF is seen to localise to areas of mineralisation activity and apoptosis in aneurysmal aortic wall. *Histological and immunohistochemical staining of aortic wall for calcium (alizarin red), mineralisation metabolic activity (Alkaline phosphatase), osteocalcin (structural protein strongly associated with hydroxyapatite), apoptotic cells (cleaved caspase 3), macrophages (CD68) and smooth muscle cells (α-SMA). The computer generated segmentation masks clearly demonstrate positive staining. The ^{18}F-sodium fluoride autoradiography shows areas of high uptake (the green section outline is added to aid interpretation of co-localization). ^{18}F-NaF can be seen to localise to areas of mineralisation activity and apoptosis.*

In our pilot study of 29 patients, we used magnetic resonance imaging (MRI) with ultrasmall superparamagnetic particles of iron oxide (USPIO) to identify cellular inflammation in the wall of AAA[27]. This approach exploits the fact that active tissue-resident macrophages phagocytose and concentrate the USPIOs that can then be detected using T2*-weighted MRI. This addresses the first mechanism of our hypothesis that

AAA disease initiation and progression is the result of tissue degradation by resident macrophages. Indeed, in this study, we were able to show that patients with focal USPIO uptake and inflammation in the wall of the AAA had an aneurysm expansion rate that was three-fold higher than those who did not[28]. We are currently confirming these findings and investigating whether USPIO-MRI can predict rupture and the need for elective surgery in patients with AAA under surveillance (MA^{3}RS study: MRI in AAA to predict rupture and the need for surgery; MRC EME £2.2 million). As part of the MA^{3}RS trial, we are currently recruiting 350 patients with AAA >40 mm in diameter who will undergo MRI scanning with USPIO and be followed up for 2 years to determine aneurysm expansion, rupture and rate of repair.

1.2 RATIONALE FOR STUDY

The national screening programme for AAA (NAAASP) currently uses serial US assessments to identify patients with AAA and to monitor AAA expansion. Elective surgical or endovascular AAA repair is offered to patients at high risk of rupture and this screening programme has reduced aneurysm-related mortality by 50% in the UK. Evaluation of rupture risk is currently based on aneurysm size; patients are offered elective repair if AAA maximum AP diameter is greater than 55 mm, or if AAA diameter expansion is found to exceed 10 mm per year. However, the screening programme and risk evaluation are complex processes, as the growth rate of AAA is neither linear nor predictable. ^{18}F-NaF PET-CT has been used in the coronary circulation to accurately identify atherosclerotic plaque at high risk of rupture. We therefore propose to investigate the use of this imaging modality in AAA, to identify regions of necrotic inflammation and predict AAA expansion. This study will run in parallel to the MA^{3}RS Study, and will take advantage of some of the follow-up data that will already be collected for the
MA^{3}RS Study.

2 STUDY OBJECTIVES

2.1 OBJECTIVES

2.1.1 Primary objective

To explore whether ^{18}F-NaF uptake in the aortic wall correlates with aneurysm expansion.

2.1.2 Secondary objectives

1) In patients under surveillance for AAA, to determine whether uptake of ^{18}F-NaF:

   - occurs in regions of the aneurysm wall that show evidence of active calcification, necrotic inflammation and proteolytic degradation
   - is associated with focal areas of USPIO uptake on MRI
   - corresponds with regions of high biomechanical stress

2) In volunteers who do not have an AAA, to determine whether there is any uptake of ^{18}F-NaF and to compare these results with those patients who do have an AAA.

We aim to investigate whether there are regions of ^{18}F-NaF uptake and active calcification in the wall of abdominal aortic aneurysms and whether ^{18}F-NaF uptake occurs in areas of mural inflammation (USPIO uptake on MRI, data to be obtained from The MA^{3}RS Study), necrotic inflammation and extracellular matrix destruction. We propose to exploit the resources and platform of the MA^{3}RS study to undertake ^{18}F-NaF PET-CT imaging in a subset of the study cohort. This will allow us to detect any potential interaction between macrophage activity and necrotic inflammation, as well as assessing whether inflammation, vascular smooth muscle cell apoptosis and tissue necrosis contribute to the initiation, progression and complications of AAA disease. Through finite element analysis computational modelling, we will also be able to explore the relationship between ^{18}F-NaF uptake and wall stresses.

We will use data obtained from The MA^{3}RS Study to assess peripheral blood biomarkers of inflammation (C-reactive protein and inflammatory cytokines) and protease activity (serum matrix metalloproteinases), as well as pulse wave analysis and an assessment of the biomechanical environment within the aneurysm. These data will already be collected from the MA^{3}RS Study, however we will also collect blood for biomarkers at the time of the SoFIA^3 Study, in order to gain real-time information about biomarkers present at the time of PET-CT scanning. All other information will be shared from the MA^{3}RS Study results and outcome data.

In addition, we will carry out a PET-CT, CT angiogram, a calcium scoring scan and Pulse Wave Analysis on 20 volunteers who have undergone an ultrasound as part of NAAASP who do not have an AAA. This will allow comparison of age-matched controls with those patients who are known to have an AAA.

The AAA patients will not be required to undergo any further pulse wave analysis as part of the study, as they will have already undergone this assessment during the MA^{3}RS study visits. The pulse wave data from AAA patients (obtained as part of MA^{3}RS) will be compared to the pulse wave data from volunteers (obtained as part of SoFIA^3).

2.2 ENDPOINTS

2.2.1 Primary endpoint

- Aneurysm expansion rate.

2.2.2 Secondary endpoints

- Co-localisation of ^{18}F-NaF with USPIO uptake on MRI scanning
- Co-localisation of ^{18}F-NaF with histological evidence of active calcification, necrotic inflammation and proteolytic degradation of the aneurysm wall
- Relationship with areas of high wall stress (finite element analysis)
- Comparison of ^{18}F-NaF uptake in people with AAA versus volunteers with no AAA
- Comparison of Pulse Wave Analysis data in people with AAA versus volunteers with no AAA (using Pulse Wave Analysis data from AAA patients obtained as part of MA^{3}RS)

3 STUDY DESIGN

This will be a prospective observational cohort study. In patients with a known AAA, using ^{18}F-NaF PET-CT, we will identify regions of active calcification and necrotic inflammation within the aortic aneurysm sac. These data will be combined with data obtained from the MA^{3}RS study, including histological analysis of tissue samples taken from participants who undergo open surgical aneurysm repair. AAA patients will continue to be followed up as part of the MA^{3}RS study and will require only one additional visit to participate in this current study. These results will be compared with the results from age-matched controls (ie volunteers who do not have an AAA). See Figure 3 and Figure 4 for diagrams of patient and volunteer participation in this study.

Number of study visits: 1

Procedures involved:

- Clinical: PET-CT scan including administration of IV contrast and administration of radiopharmaceutical ^{18}F-NaF – this will take place either in the Clinical Research Imaging Centre (CRIC), Edinburgh or the Clinical Research Imaging Facility, Dundee (CRIF)
- Clinical: CT angiogram and calcium scoring CT – this will take place in the CRIC / CRIF
- Clinical: Measurement of blood pressure and pulse – this will take place before the PET-CT scan at the CRIC / CRIF
- Clinical: Withdrawal of 9ml of blood from cannula required for contrast injection. Blood sampling will not require any additional needles.
- Clinical (Volunteers only): Pulse Wave Analysis – this will take place at the CRF
- Non-clinical: Informed consent – written information will be given to the participant at the ultrasound surveillance clinic or via post. Written informed consent will be taken at the baseline study visit prior to the scan at the CRIC / CRIF. This will be carried out by the PI (Dr Forsythe)

Total time for study visit: 60-90 minutes for AAA patients, 2-2.5 hours for volunteers

We will conduct exploratory analyses examining the interactions between ^{18}F-NaF uptake, biomechanical stress, clinical risk factors and serum biomarkers of extracellular matrix turnover and inflammation.

Clinicians involved directly with patient surveillance and care will be blinded to the PET-CT findings of ^{18}F-NaF uptake.

Figure 3: PATIENTS WITH KNOWN AAA

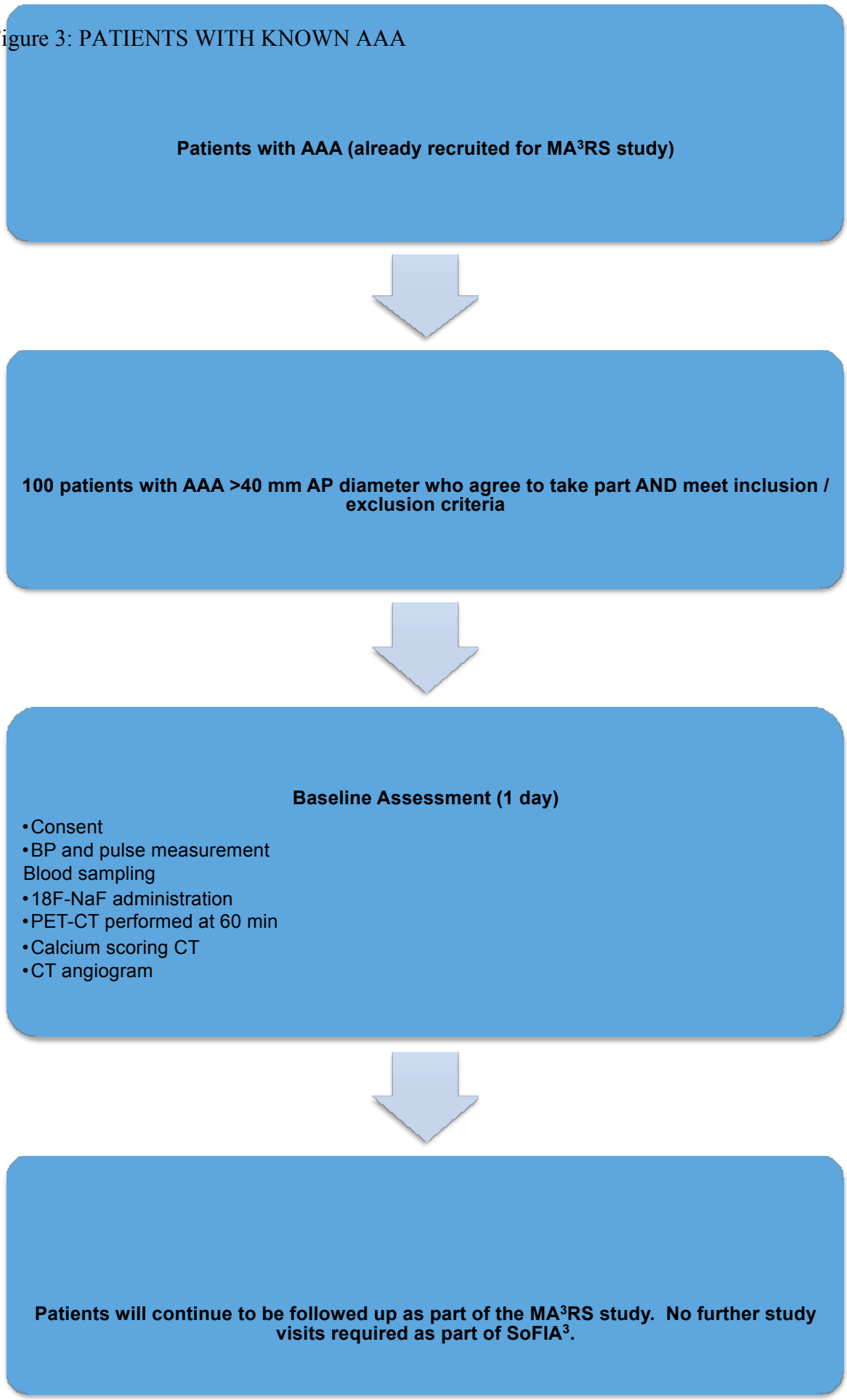

Figure 4: VOLUNTEERS (no AAA)

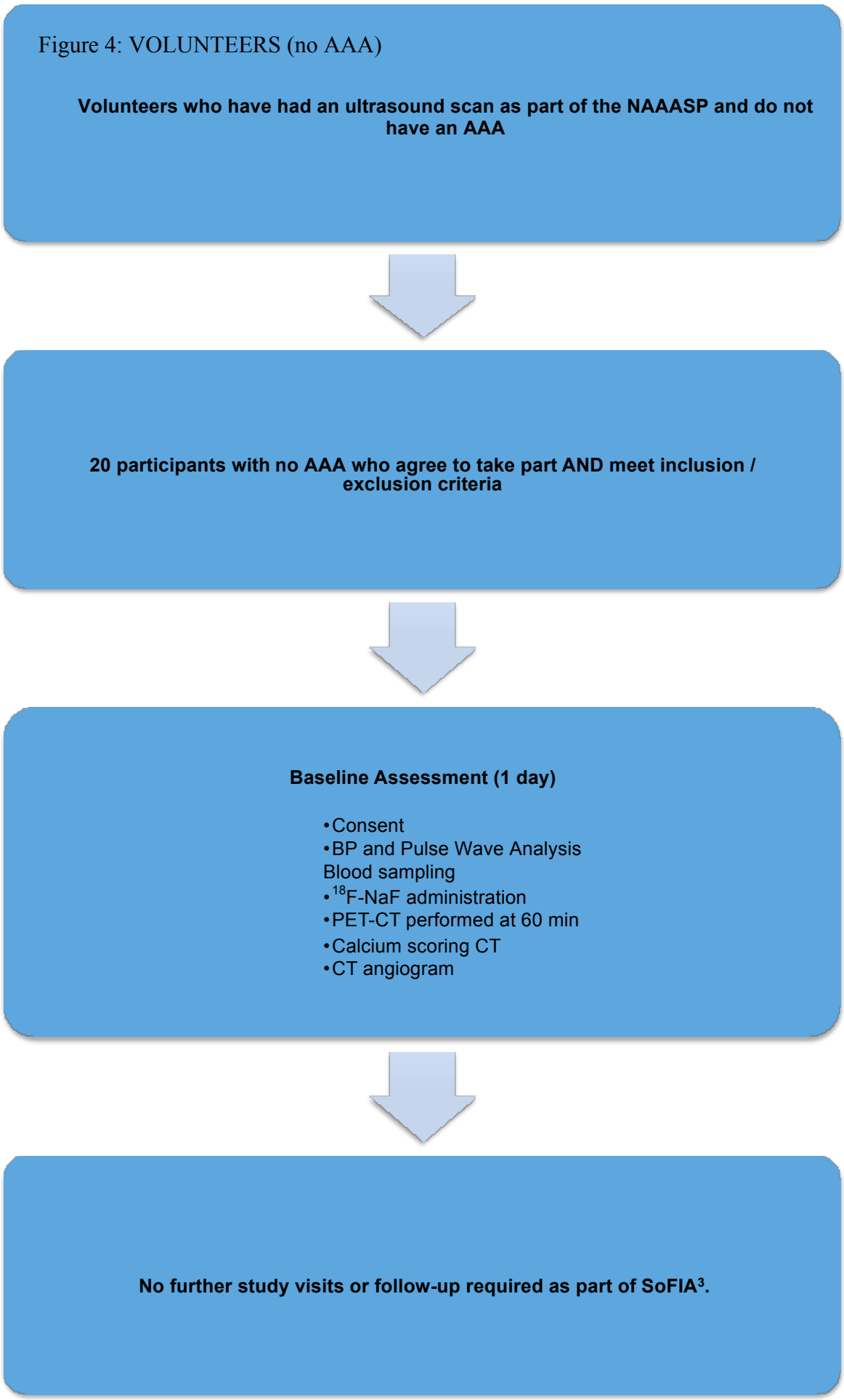

4 STUDY POPULATION

Participants with AAA will be identified from the MA^{3}RS study database. Participants will already be enrolled and under follow up in the MA^{3}RS study (ISRCTN76413758). Volunteers will be identified through the NAAASP ultrasound clinic – they will have attended for an ultrasound scan, which has demonstrated that they do not have an AAA.

4.1. Number of participants

Patients with AAA:

We aim to recruit 100 patients with AAA. AAA patients will already be enrolled and under follow up in the MA^{3}RS study. Enrolment for the MA^{3}RS study commenced in November 2012 and was completed in December 2014. As part of the MA^{3}RS study, a subset (n=80) of patients will undergo reproducibility MRI scans at 12 months. We will also aim to carry out repeat MRI scans at 2 years in a further 40 patients. The patients involved in repeat MRI scanning will also be approached for co-enrolment in SoFIA^3.

Volunteers with no AAA:

We aim to recruit 20 volunteers with no AAA, as demonstrated on an ultrasound scan performed as part of the NAAASP.

4.2 Inclusion criteria

AAA patients:

- Patients already enrolled in the MA^{3}RS study
- Patients with abdominal aortic aneurysm with AP diameter >40 mm on ultrasound
- >50 years of age. Patients <50 years of age may have a connective tissue disorder and a different disease aetiology

Volunteers:

- Participants who have attended for an ultrasound scan as part of the NAAASP who do not have an AAA
- >50 years of age

4.3 Exclusion criteria

AAA patients:

- Patients expected to undergo imminent AAA repair
- Patients who refuse or are unable to give informed consent
- Women of child-bearing potential without contraception
- Patients who are unable to undergo PET-CT scan
- Patients with collagen vascular disease
- Intercurrent illness, malignancy or comorbidity with life expectancy <1 year
- Renal dysfunction (eGFR <30ml/min/1.73m2)

- Contraindication to PET-CT or CTA
- Iodine allergy

Volunteers:

- Volunteers who refuse or are unable to give informed consent
- Women of child-bearing potential without contraception
- Patients who are unable to undergo PET-CT scan
- Participants with collagen vascular disease
- Intercurrent illness, malignancy or comorbidity with life expectancy <1 year
- Renal dysfunction (eGFR <30ml/min/1.73m2)
- Contraindication to PET-CT or CTA
- Iodine allergy

5 PARTICIPANT SELECTION AND ENROLMENT

5.1 IDENTIFYING PARTICIPANTS

AAA participants will be identified from the participant list of the MA^{3}RS study, which is based on ultrasound surveillance programme databases at the Royal Infirmary of Edinburgh. Volunteers will be identified from the NAAASP database at the Royal Infirmary of Edinburgh.

5.2 CONSENTING PARTICIPANTS

Participants will be given written information (in the form of a Patient Information Leaflet) at the time of screening at the ultrasound surveillance clinic or via post, following initial contact with the PI. Written informed consent will be taken by the PI (Dr Rachael Forsythe) prior to the PET-CT scan at the baseline scan visit. This will take place at the CRIC, Edinburgh or the CRIF, Dundee.

5.3 SCREENING FOR ELIGIBILITY

AAA patients: Once AAA patients have been identified from the MA^{3}RS database, they will be seen at their 12 month surveillance US appointment (standard clinical care) and eligibility will be assessed. Eligibility will be confirmed prior to consent. If patients are not seen in the US appointment, the study will be discussed with the patient over the phone and study information sent to them in the post.

Volunteers: Once volunteers have been identified from the NAAASP database, they will be assessed for eligibility after their NAAASP scan visit (standard clinical care). If volunteers are not seen at the NAAASP visit, the study will be discussed over the phone and information sent to them in the post.

All participants: An appointment will be made for a baseline visit (where consent takes place) for all patients and volunteers who are eligible and are interested in taking part.

5.4 INELIGIBLE AND NON-RECRUITED PARTICIPANTS

Ineligible and non-recruited participants will receive standard medical care. An anonymised log will be kept for participants who were screened for the study and subsequently found to be ineligible or not recruited.

5.5 PREMATURE WITHDRAWAL

Participants are free to withdraw from the study at any point and a participant can also be withdrawn from the study by an investigator. If withdrawal occurs, the primary reason for withdrawal will be documented in the participant's Case Report Form (CRF).

If a participant who has consented for the study states that they wish to be withdrawn from the study before they have been administered ^{18}F-NaF, they will be withdrawn from the study and another participant will be recruited in their place.

5.6 RANDOMISATION

There is no randomisation in this study

6 INVESTIGATIONAL MEDICAL PRODUCT AND PLACEBO

This study does not involve investigational medical products

7 STUDY ASSESSMENTS

A preliminary assessment of eligibility will be conducted by a suitably qualified member of the research team. See Table 1 for the assessments performed at each study visit. This table does not illustrate the assessments which will already be planned for the patient as part of the MA^{3}RS study.

Assessments	**Visits***!*	
	SV	BV
Screening/Eligibility*!*	√*!*	
Consent		√
Blood sampling, PET-CT scan, calcium scoring scan and CT		√
Pulse Wave Analysis (volunteers only)		√
AE/SAE Reporting*!*	*!*	

Table 1
SV = surveillance clinic visit; BV(a) = Baseline visit (occurs within 1 month of SV)
* Where patients are to undergo elective repair of their aneurysms during follow up, a repeat CT scan will be performed prior to surgery.

7.1 Additional assessments:

All AAA patients will already be enrolled in the MA^{3}RS study, which involves additional assessments not detailed in this protocol. These include MRI scan, CT angiogram, clinical assessment, pulse wave analysis, blood tests, tissue sampling. Data from the MA^{3}RS study will be shared with this current study, in order to reduce the number of additional assessments required. Volunteers will not require any additional assessments.

7.2 Safety assessments

In participants with no history of renal disease, hypertension or diabetes, a normal eGFR within the last six months will be considered to be acceptable. For patients with risk factors for renal dysfunction or no blood tests within the last 6 months, clinical biochemical analysis of a blood sample will be performed prior to receiving contrast agent.

All participants are advised to drink water prior to their scan for adequate hydration. For participants with a normal eGFR ($\geq$60 mL/min/1.73 m^2) and taking metformin they should continue taking the medication up until the scan. After the scan they should withhold metformin for 48 h and then have a blood test to check renal function. They will be informed when they are to restart the Metformin following the result of this.

For participants with an eGFR 30–60 mL/min/1.73 m^2 and taking metformin they will be advised to stop the medication for 48 h before and 48 h after the scan. They will then have a blood test to check renal function and informed when they are to restart the metformin following the result of this.

These safety assessments are part of standard clinical care with regards to PET-CT scanning with an intravenous contrast agent.

Participants will be advised to avoid close contact with children for 12 h following the PET- CT scan. This is precautionary and is part of standard clinical care with regards to the use of PET-CT scans.

8 DATA COLLECTION

8.1 Clinical Assessment

All AAA patients will undergo clinical evaluation as part of the MA^{3}RS study. Apart from blood pressure and pulse measurement before and after administration of ^{18}F-NaF, no additional clinical assessment will be performed as part of the current study, however

clinical assessment information will be shared between the two studies. This is in order to minimise duplication of assessments and to reduce the extra time required for participation in the SoFIA^3 study.

8.2 Blood and Tissue Assays

Information from the MA^{3}RS study will be shared with the current study. A further sample of blood will be obtained from the cannula required for the SoFIA^3 study, in order that we have real-time information about serum biomarkers present at the time of PET-CT scanning.

8.3 Positron emission and computed tomography (PET-CT)

Participants will undergo combined positron emission tomography computed tomography (PET-CT) scanning 60 min after the administration of ^{18}F-NaF. Previous studies have shown that this time point provides excellent contrast between the artery wall and blood pool. A scout CT scan will be followed by a low-dose computed tomography scan, to allow attenuation correction, and a calcium scoring CT scan Positron emission tomographic data will then be acquired over two bed positions centred over the aneurysm for 10 min each. Finally a CT angiogram will be acquired of the aneurysm following contrast administration to provide detailed anatomical information on which to co-register the PET data.

8.4 Follow-up

AAA patients will continue to be followed up as part of the MA^{3}RS study. They will also continue with standard care using ultrasound scanning (baseline, 6 months and 12 months) to determine the aneurysm expansion rate. Volunteers will not require any further follow up after the SoFIA^3 scan visit.

9 STATISTICS AND DATA ANALYSIS

9.1 SAMPLE SIZE CALCULATION

The sample size for the study is based on data from our previous pilot studies where the overall aneurysm growth rates were 4.2±4.0 mm/year.[29] We have previously observed a difference in growth rate of 6.6 *versus* 2.2 mm/year in AAA with and without USPIO uptake respectively.[29] To observe a more conservative effect size of 50% of this difference (2.2 mm/yr) at 80% power and assuming that half of all aneurysms will demonstrate ^{18}F-NaF uptake (c.f. coronary atheroma [Joshi et al, 2014]), we will need a total study sample size of 100 patients (50 patients per group). We aim to recruit 100 patients.

9.2 PROPOSED ANALYSES

9.2.1 Image analysis of 18F-NaF PET-CT

^{18}F-NaF uptake: Static positron emission and computed tomographic images will be reconstructed with corrections applied for attenuation, dead time, scatter and random coincidences, using an optimised iterative reconstruction algorithm. To estimate ^{18}F-NaF concentrations, 3D volumes of interest (VOI) will be drawn around the aorta on the

computed tomography images. From these VOI, we will derive the mean and maximum standardised uptake values (SUV): a widely used, validated measure of tissue ^{18}F-NaF uptake. Tissue-to-background ratios (TBR) will be calculated after correction for blood pool activity in the superior vena cava. Increased ^{18}F -NaF uptake will be defined as TBR ≥1.25 as previously defined in a study using healthy controls to set the threshold.[30 31] We will explore the patterns of uptake throughout the AAA wall, to identify areas of active (TBR ≥1.25) and inactive (TBR <1.25) calcification. We will explore whether there are focal areas of increased ^{18}F–NaF uptake (TBR ≥1.25) that correspond to focal areas of USPIO uptake (as identified in the MA^{3}RS study) and/or focal or overall aneurysm expansion. We also explore modelling of different thresholds to assess the optimum sensitivity for detecting higher aneurysm growth rates and we will identify the threshold which gives a 50:50 split of patients into those with and without uptake, to maximise the sensitivity of the primary comparison described in Section 9.1.

Calcium Scoring: The aortic calcium score will be calculated on axial scans using calcium score analysis software (VScore, Vital Images, Minnetonka, Minnesota).

Computed tomography growth assessment*:* Three-dimensional computer models will be generated from segmented, contrast-enhanced images allowing geometric indices to be quantified. Semi-automatic segmentation is achievable due to the intensity differences between the aneurysm and surrounding tissues and structures. Intensity thresholding will be used to identify the lumen. To detect the thrombus and complete the segmentation, we will use a 3-D deformable model approach that utilises the level set algorithm as well as modelling the thrombus contour as a radial function starting from the aortic centre line as calculated from the lumen segmentation.

Assessment of growth changes: Changes in AAA growth will be determined using the measurement of AAA maximum AP diameter on the screening ultrasound scan performed 6 months prior to the SoFIA^3 scanning visit (ie as part of normal clinical care) and the ultrasound scan performed 6 months after the SoFIA^3 scanning visit (ie as part of normal clinical care). We will also explore the effect of ^{18}F–NaF uptake on focal aneurysm expansion using baseline and final CT aortograms.

9.2.2 Biomechanical analysis

Using Abaqus, the vessel wall will be modelled as a constant thickness layer of 1.5 mm, with a hyperelastic constitutive model. Thrombus will be modelled as homogenous and isotropic with Young's modulus 0.1 MPa. The model will be inflated from diastolic to systolic pressure using a homogeneous pressure-modelling regime. Peak wall stress and other rupture indices will be calculated and compared against areas of USPIO uptake.

9.2.3 Statistical analysis

Data sharing: A summary of demographics will be shared with the SoFIA^3 study from the MA^{3}RS study. The SoFIA^3 researchers will have access to the images obtained during the SoFIA^3 scanning visit and the MRI images obtained during the MA^{3}RS scanning visits. The SoFIA^3 study will require access to a cleaned, quality-checked extract of data from the MA^{3}RS study, however this will not include clinical data pertaining to MA^{3}RS primary outcomes.

The primary end-point of AAA growth rate will be compared between those with and those without ^{18}F-NaF uptake using an unpaired Student's *t*-test. Statistical significance

will be taken at the two-sided 5% level. We will assess the level of agreement between ^{18}F-NaF uptake and histological evidence of necrotic inflammation and MRI USPIO uptake using regression analysis and the kappa statistic. Statistical analysis will be carried out by the PI under the supervision of the CI and study statistician.

We may also explore whether ^{18}F-NaF uptake adds value to the MA^{3}RS analysis in this small subset of patients, using clinical data obtained from the MA^{3}RS study. This would be on a strictly exploratory basis, as the SoFIA^3 study is not sufficiently powered to predict clinical outcomes.

10 ADVERSE EVENTS

The Investigator is responsible for the detection and documentation of events meeting the criteria and definitions detailed below.

Participants will be instructed to contact their Investigator at any time after consenting to join the study if any symptoms develop. All adverse events (AE) that require medical attention (for example, visit to a GP, hospital etc) must be reported in detail in the Case Report Form (CRF) or AE form. In the case of an AE, the Investigator should initiate the appropriate treatment according to their medical judgment. Participants with AEs present at the last visit must be followed up until resolution of the event.

10.1 DEFINITIONS

An **adverse event** (AE) is any untoward medical occurrence in a clinical trial participant which does not necessarily have a causal relationship with an investigational medicinal product (IMP).

A **serious adverse event** (SAE), is any AE:

- results in death;
- is life threatening* (i.e. the participant was at risk of death at the time of the event; it does not refer to an event which hypothetically might have caused death if it were more severe);
- requires in-patient hospitalisation or prolongation of existing hospitalisation;
- results in persistent or significant disability or incapacity;
- is a congenital anomaly or birth defect.

10.2 DETECTING AEs AND SAEs

All AEs and SAEs will be recorded from the time a participant signs the consent form to take part in the study until the last study visit.

Participants will be asked about the occurrence of AEs/SAEs at every visit during the study. Open-ended and non-leading verbal questioning of the participant will be used to enquire about AE/SAE occurrence. Participants will also be asked if they have been admitted to hospital or had any accidents. If there is any doubt as to whether a clinical observation is an AE, the event will be recorded.

AEs and SAEs may also be identified by support departments e.g. laboratories.

10.3 RECORDING AEs AND SAEs

When an AE/SAE occurs, it is the responsibility of the Investigator to review all documentation (e.g. hospital notes, laboratory and diagnostic reports) related to the event. The Investigator will then record all relevant information in the CRF and on the SAE form (if the AE meets the criteria of serious).

Information to be collected includes dose, type of event, onset date, Investigator assessment of severity and causality, date of resolution as well as treatment required, investigations needed and outcome.

10.4 ASSESSMENT OF AEs AND SAEs

The Investigator is responsible for assessing each AE.

10.4.1 Assessment of Seriousness

The Investigator will make an assessment of seriousness as defined in Section 10.1.

10.4.2 Assessment of Severity

The Investigator will make an assessment of severity for each AE/SAE and record this on the CRF or AE form according to one of the following categories:

Mild: an event that is easily tolerated by the participant, causing minimal discomfort and not interfering with every day activities.

Moderate: an event that is sufficiently discomforting to interfere with normal everyday activities.

Severe: an event that prevents normal everyday activities.

Note: the term 'severe', used to describe the intensity, should not be confused with 'serious' which is a regulatory definition based on participant/event outcome or action criteria. For example, a headache may be severe but not serious, while a minor stroke is serious but may not be severe.

10.5 REPORTING OF SAEs

Once the Investigator becomes aware that an SAE has occurred in a study participant, the information will be reported to the ACCORD Research Governance & QA Office **immediately or within 24 hours**. If the Investigator does not have all information regarding an SAE, they should not wait for this additional information before notifying ACCORD. The SAE report form can be updated when the additional information is received.

The SAE form will be transmitted by fax to ACCORD on **+44 (0)131 242 9447** or may be transmitted by hand to the office.

All reports faxed to ACCORD and any follow up information will be retained by the Investigator in the Investigator Site File (ISF).

10.6 FOLLOW UP PROCEDURES

After initially recording an AE or recording and reporting an SAE, the Investigator will follow each participant until resolution or death of the participant. Follow up information on an SAE will be reported to the ACCORD office.

AEs still present in participants at the last study visit will be monitored until resolution of the event or until no longer medically indicated.

11. PREGNANCY

Woman with child-bearing potential will not be enrolled into the trial (woman who have experienced menarche, are pre-menopausal, have not been sterilised or who are currently pregnant).

12. STUDY MANAGEMENT AND OVERSIGHT ARRANGEMENTS

Study management will be overseen by the Principal Investigator, who will be accountable to the Chief Investigator. Any requirement for monitoring or audit by the appropriate REC or NHS body will be facilitated by the investigators.

12.1.1 RISK ASSESSMENT

12.1 PET-CT, calcium scoring CT and CT angiogram

As part of the protocol, subjects will receive ^{18}F-NaF PET-CT scans. This will expose the patient to ionising radiation and a mildly radioactive tracer (^{18}F-NaF), as well as the potential hazard of allergic reactions and transient renal dysfunction in response to the contrast agent. See Table 2 and Table 3.

The risks of exposure to the contrast medium include allergic reactions and impairment of kidney function. Amongst participants with moderate-to-severe chronic kidney disease, there is a 2-4% risk of kidney impairment after computed tomography angiography.[38]
The risk of contrast exposure in this study will be minimised by exclusion of high risk participants who have significant kidney disease (estimated glomerular filtration rate $\leq$30 mL/min/1.73 m^2).

Participants undergoing PET-CT are routinely advised to avoid close contact with children for 12 hours following the scan. This is to avoid any unnecessary exposure to radioactive material, however the risks of this are small and this is largely precautionary.

Procedure	PET-CT attenuation	CT angiogram[b]	Calcium scoring CT[c]
Number of procedures	1	1	1
Estimated procedure dose[d]	3	5	5

Table 2: Radionuclide

[a] ARSAC Notes for Guidance on the Clinical Administration of Radiopharmaceuticals and Use of Sealed Radioactive Sources -March 2006 (updated 2014) Appendix VII

Table 3: Other ionizing radiation

[b] Typical patient dose , based on average patient doses for study centre

[c] Taken from Chuang et al. Academic Radiology. 20 (11) (pp 1422-1428) 2013, with uplift to account for variation between scanner models

[d] Utilising scanner –specific dose-length product to effective dose conversion factor based on ICRP 103 tissue weighting factors

13. GOOD CLINICAL PRACTICE

13.1 Ethical conduct

A favourable ethical opinion will be obtained from the appropriate REC and local R&D approval will be obtained prior to commencement of this study.

13.2 Investigator responsibilities

The Chief Investigator will be responsible for the overall conduct of the study, however tasks may be delegated to other members of the team.

13.3 Informed consent

The Investigators are responsible for ensuring informed written consent is obtained prior to involvement in the study. The decision to participate in the study is voluntary and should be based on a clear understanding of what is involved.

Formal written and verbal information will be given to prospective participants, including Patient Information Sheets and Consent Forms, which will also be signed and dated by the person taking consent.

Participants must be given every opportunity to ask questions before and during the study and to withdraw consent at any time.

Participants will be aware that their medical records may be accessed for additional information and confidential data shared only with members of the study team. Any patient identifiable data will be anonymised prior to use.

13.4 Confidentiality

All records must be identified in a manner designed to maintain confidentiality, in a secure area with limited access. The study team members shall not disclose any confidential information for any other reason outside of this study.

13.5 Data Protection

All study team members must comply with the requirement of the Data Protection Act 1998 with regards to the collection, storage, processing and disclosure of personal information and will uphold the Act's core principles. Access to participant data will be restricted to those clinicians directly involved in the study or patient care.

Computers used to access participant details will have password protection and limited access.

Published results will not include any patient identifiable data.

14. STUDY CONDUCT RESPONSIBILITIES

14.1 Protocol amendments

Any changes or amendments must be approved by the Supervising Investigator. Any major amendments must be submitted for re-review.

14.2 End of Study

The end of the study will be defined by the participation of the total number of participants required as per the power calculation.

14.3 Insurance and indemnity

Sites participating in the study will be liable for clinical negligence and covered by the duty of care owed to them by the sites concerned.
There will be the benefit of NHS indemnity in sites which are part of the UK NHS.
The details of indemnity and insurance will be clarified in the REC application.

15. REPORTING, PUBLICATION AND NOTIFICATION OF RESULTS

15.1 Authorship policy

Ownership of this study results resides with the study team.

15.2 Publications

Results of this study may be used for publication and presentation at scientific meetings. The Principal Investigator has the right to publish the results of the study orally or in writing. Summaries of the results may also be made available for dissemination in clinics, if appropriate.

15.3 Peer review

Prior to commencement of this study, it shall undergo peer review by the local REC.

REFERENCES

[1] Office for National Statistics in England and Wales, Mortality Statistics 2008
[2] National Vascular Registry 2013 Report on Surgical Outcomes – Consultant-level statistics 2013
[3] Mortality results for randomised controlled trial of early elective surgery or ultrasonographic surveillance for small abdominal aortic aneurysms. The UK Small Aneurysm Trial Participants. Lancet 1998;352(9141):1649-1655
[4] Darling RC, Messina CR, Brewster DC, Ottinger LW. Autopsy study of unoperated abdominal aortic aneurysms. The case for early resection. Circulation 1977;56(3 Suppl):II161-164
[5] Reed D, Reed C, Stemmermann G, Hayashi T. Are aortic aneurysms caused by atherosclerosis? Circulation 1992;85(1):205-211.
[6] Choke E, Cockerill G, Wilson WR, et al. A review of biological factors implicated in abdominal aortic aneurysm rupture. Eur J Vasc Endovasc Surg 2005;30(3):227-244
[7] Brady AR, Thompson SG, Fowkes FG, Greenhalgh RM, Powell JT. Abdominal aortic aneurysm expansion: risk factors and time intervals for surveillance. Circulation 2004;110(1):16-21
[8] Choke E, Cockerill G, Wilson WR, et al. A review of biological factors implicated in abdominal aortic aneurysm rupture. Eur J Vasc Endovasc Surg 2005;30(3):227-244
[9] Raghavan ML, Vorp DA, Federle MP, Makaroun MS, Webster MW. Wall stress distribution on three-dimensionally reconstructed models of human abdominal aortic aneurysm. J Vasc Surg 2000;31(4):760-769
[10] Clarke MC, Littlewood TD, Figg N, et al. Chronic apoptosis of vascular smooth muscle cells accelerates atherosclerosis and promotes calcification and medial degeneration. Circ Res 2008;102(12):1529-1538
[11] Clarke MC, Figg N, Maguire JJ, et al. Apoptosis of vascular smooth muscle cells induces features of plaque vulnerability in atherosclerosis. Nat Med 2006;12(9):1075-1080
[12] Clarke MC, Figg N, Maguire JJ, et al. Apoptosis of vascular smooth muscle cells induces features of plaque vulnerability in atherosclerosis. Nat Med 2006;12(9):1075-1080
[13] Motoyama S, Kondo T, Sarai M, et al. Multislice computed tomographic characteristics of coronary lesions in acute coronary syndromes. J Am Coll Cardiol 2007;50(4):319-326
[14] Detrano R, Guerci AD, Carr JJ, et al. Coronary calcium as a predictor of coronary events in four racial or ethnic groups. N Engl J Med 2008;358(13):1336-1345
[15] Li ZY, J UK-I, Tang TY, Soh E, See TC, Gillard JH. Impact of calcification and intraluminal thrombus on the computed wall stresses of abdominal aortic aneurysm. J Vasc Surg 2008;47(5):928-935
[16] Dweck MR, Joshi NV, Rudd JH, Newby DE. Imaging of inflammation and calcification in aortic stenosis. Curr Cardiol Rep;15(1):320
[17] Dweck MR, Khaw HJ, Sng GK, et al. Aortic stenosis, atherosclerosis, and skeletal bone: is there a common link with calcification and inflammation? Eur Heart J 2013;34(21):1567-1574
[18] Dweck M, Jenkins WA, Vesey AT, Pringle MAH, MAlley TS, Cowie WJA, Tasmpasia V, Richardson H, Fletcher A, Wallace WA, Pessotto R, Boon NA, Rudd JHF, Newby DE. 18F-NAF uptake is a marker of active calcification and disease progression in patients with aortic stenosis. Under review 2013
[19] Dweck MR, Jones C, Joshi NV, et al. Assessment of valvular calcification and inflammation by positron emission tomography in patients with aortic stenosis. Circulation 2012;125(1):76-86
[20] Dweck MR, Chow MW, Joshi NV, et al. Coronary arterial 18F-sodium fluoride uptake: a novel marker of plaque biology. J Am Coll Cardiol 2012;59(17):1539-1548
[21] Dweck MR, Khaw HJ, Sng GK, et al. Aortic stenosis, atherosclerosis, and skeletal bone: is there a common link with calcification and inflammation? Eur Heart J 2013;34(21):1567-1574
[22] Dweck MR, Jones C, Joshi NV, et al. Assessment of valvular calcification and inflammation by positron emission tomography in patients with aortic stenosis. Circulation 2012;125(1):76-86
[23] Dweck MR, Chow MW, Joshi NV, et al. Coronary arterial 18F-sodium fluoride uptake: a novel marker of plaque biology. J Am Coll Cardiol 2012;59(17):1539-1548
[24] Dweck MR, Chow MW, Joshi NV, et al. Coronary arterial 18F-sodium fluoride uptake: a novel marker of plaque biology. J Am Coll Cardiol 2012;59(17):1539-1548
[25] Joshi NV, Vesey AT, Williams MC, et al. F-fluoride positron emission tomography for identification of ruptured and high-risk coronary atherosclerotic plaques: a prospective clinical trial. Lancet 2013
[26] Dweck MR, Khaw HJ, Sng GK, et al. Aortic stenosis, atherosclerosis, and skeletal bone: is there a common link with calcification and inflammation? Eur Heart J 2013;34(21):1567-1574
[27] Richards JM, Semple SI, Macgillivray TJ, et al. Abdominal aortic aneurysm growth predicted by uptake of ultrasmall superparamagnetic particles of iron oxide: a pilot study. Circ Cardiovasc Imaging 2011;4(3):274-281
[28] Richards JM, Semple SI, Macgillivray TJ, et al. Abdominal aortic aneurysm growth predicted by uptake of ultrasmall superparamagnetic particles of iron oxide: a pilot study. Circ Cardiovasc Imaging 2011;4(3):274-281
[29] Richards JM, Semple SI, Macgillivray TJ, et al. Abdominal aortic aneurysm growth predicted by uptake of ultrasmall superparamagnetic particles of iron oxide: a pilot study. Circ Cardiovasc Imaging 2011;4(3):274-281
[30] Dweck MR, Chow MW, Joshi NV, et al. Coronary arterial 18F-sodium fluoride uptake: a novel marker of plaque biology. J Am Coll Cardiol 2012;59(17):1539-1548

[31] Joshi NV, Vesey AT, Williams MC, et al. F-fluoride positron emission tomography for identification of ruptured and high-risk coronary atherosclerotic plaques: a prospective clinical trial. Lancet 2013

Study Protocol

Hybrid ^{18}F-Fluoride Positron Emission Tomography-Magnetic Resonance Imaging in Patients with Symptomatic Carotid Artery Stenosis.

Co-sponsors	University of Edinburgh & NHS Lothian ACCORD The Queen's Medical Research Institute 47 Little France Crescent Edinburgh EH16 4TJ
Funder	Princess Margaret Research Development Fellowship and British Heart Foundation Clinical Training Fellowship
Chief Investigator	Professor David Newby
REC Number	
Version number and Date	v 1.0, 5th June 2017

List of abbreviations

ACCORD	**Academic and Clinical Central Office for Research & Development**
AE	**Adverse Event**
AR	**Adverse Reactions**
BHF	**British Heart Foundation**
CEA	**Carotid Endarterectomy**
CI	**Chief Investigator**
CT	**Computed Tomography**
CTA	**Computed Tomography Angiography**
CRF	**Case Report Form**
eGFR	**Estimated Glomerular Filtration Rate**
^{18}F PET-CT	**^{18}F-Fluoride Positron Emission Tomography - Computed Tomography**
^{18}F PET-MRI	**^{18}F-Fluoride Positron Emission Tomography - Magnetic Resonance Imaging**
FOV	**Field of View**
MBq	**Megabecquerel**
MES	**Microembolic Signals**
mL	**Millilitres**
MRA	**Magnetic Resonance Angiography**
MRI	**Magnetic Resonance Imaging**
MRS	**Magnetic Resonance Spectroscopy**
NASCET	**North American Symptomatic Carotid Endarterectomy Trial**
OMT	**Optimal Medical Therapy**
PET	**Positron Emission Tomography**
PI	**Principal Investigator**
QMRI	**Queen's Medical Research Institute**
SAE	**Serious Adverse Event**
SAR	**Serious Adverse Reaction**
SCAS	**Symptomatic Carotid Artery Stenosis**
SUSAR	**Suspected Unexpected Serious Adverse Reaction**
SUV	**Standardized Uptake Value**
TCD	**Transcranial Doppler**
TIA	**Transient Ischaemic Attack**
TBR	**Tissue to Background Ratio**
UAR	**Unexpected Adverse Reaction**
VOI	**Volume of Interest**
WTCRF	**Welcome Trust Clinical Research Facility**

1. BACKGROUND

1.1. Carotid Artery Stenosis

Ischaemic stroke remains a major global cause of disability and death that is associated with an enormous social and economic burden.[1] Up to 20% of ischaemic strokes are caused by atherosclerosis of the internal carotid artery.[2] Atherosclerosis is a complex disease of the large arteries characterised by persistent inflammation, lipid accumulation, angiogenesis, and necrosis.[3] In the carotid circulation, it usually remains asymptomatic until a critical burden of luminal atheroma is reached that may ultimately rupture, thrombose and embolise.[3] When this occurs in carotid arteries or in the aortic arch, the resulting thromboembolism can lead to a stroke, transient ischaemic attack (TIA) or retinal ischaemia (amaurosis fugax).[4]

Carotid endarterectomy (CEA) is an established surgical intervention that is associated with a reduction in the future risk of stroke in *symptomatic* patients.[4] However, the procedure is associated with a perioperative risk of stroke and death between 1-6%.[5-9] Current guidelines suggest that CEA is indicated when luminal stenosis of carotid artery exceeds 50% in men and 70% in women, as at this threshold the recurrent risk of stroke equals or exceeds the risk of surgery.[10] [11] Unfortunately, this anatomical quantification of luminal stenosis has limitations. First, it does not take account of positive remodelling, which plays an important role in lumen preservation that is responsible for a delayed clinical manifestation of atherosclerosis.[3] [12] [13] Thus, it may underestimate the degree of cross-sectional area stenosis including associated risks. Second, luminal stenosis provides no information on the biological activity of the plaque. Histological data show that inflammation, cell death, microcalcification and intraplaque haemorrhage are key features in driving both carotid plaque formation and instability.[14-17] These high-risk plaques add to the independent risk of ipsilateral TIA or ischaemic stroke provided by the severity of carotid artery stenosis alone.[15] [18] [19] Third, only 50-60% of recently symptomatic carotid plaques removed during CEA demonstrate rupture.[6]

Strong evidence from histological and imaging derived markers of risk have so far made no impact on the North American Symptomatic Carotid Endarterectomy Trial (NASCET) recommendations.[18-22] These observations indicate that assessment of carotid artery stenosis remains complex and that ipsilateral plaque morphology requires re-evaluation. Selection of patients based solely on the severity of a stenosis is no longer adequate and should be supported by relevant information on plaque composition. Therefore, robust identification of culprit plaque features is a promising strategy to identify patients who are at highest risk of further cerebral events to better target intervention strategies.

1.2 Standard imaging techniques

The ability to identify the culprit carotid plaque represents a key goal in carotid artery imaging. However, this remains challenging for number of reasons including the suboptimal evaluation of carotid plaque morphology, disease activity and future stroke risk stratification.

Current non-invasive imaging technologies have been validated without any standardised methodology of grading the severity of carotid artery stenosis with the outdated intra-arterial angiography often used as a reference point.[23-26] This has resulted in a biased consensus in the literature that tends to overestimate true sensitivity and specificity of non-invasive imaging techniques.[26 27] Meta-analyses demonstrate that contrast-enhanced magnetic resonance was the most sensitive and specific technique for detection of symptomatic 70-99% carotid artery stenosis when compared with Duplex Ultrasound, Computed Tomography Angiography and Magnetic Resonance Angiography.[23 26] However, each of the aforementioned imaging modalities demonstrated low sensitivity in the detection of moderate (50-70%) carotid artery stenosis.[26] This was particularly evident when images were obtained by Duplex Ultrasound and Magnetic Resonance Angiography.[26] This is an important issue because imprecise stenosis calculation can lead either to unnecessary surgical intervention or at the other end of the spectrum patients, not undergoing surgery that would otherwise be indicated.[23 27]

Almost 20 years have passed since the large randomised trials demonstrating the efficacy of carotid endarterectomy, and despite significant improvements in optimal medical therapy, the risk of stroke remains unchanged.[28] Recent data have shown that patients with symptomatic mild (20-49%) carotid artery stenosis treated with optimal medical therapy (OMT) had a higher risk of recurrent ipsilateral stroke of 7.4% when compared with both an asymptomatic group with similar degree of stenosis and a symptomatic cohort with moderate or severe stenoses.[29] This implies that we need to look beyond the traditional paradigm where the basis for CEA were formulated by an invasive imaging modality that provided no information on the arterial wall composition.[30]

Finally, overwhelming histological data suggests that specific plaque components identify patients at high-risk for future ipsilateral stroke and cardiovascular events.[31 32] Although an array of non-invasive imaging techniques can detect a wide spectrum of complementary high-risk characteristics, no single modality can reliably identify vulnerable plaques associated with future stroke development.[15 31] Alternative imaging strategies are therefore required targeting not only *in vivo* carotid morphology but also plaque biology and disease activity.

Colour Duplex Ultrasound is the first-line imaging modality in the pre operative assessment of carotid artery stenosis. It is a repeatable and a low-cost tool that is well tolerated by patients. Colour Duplex Ultrasound offers reliable quantification of a severe luminal carotid

artery stenosis with less accurate assessment of moderate stenoses.[26] Therefore, in those with 50%-70% stenosis, diagnosis should be confirmed by another imaging modality to avoid unnecessary CEA and vice versa.[24 27]

Colour duplex ultrasound can differentiate lipid-rich plaques (low echogenicity) from fibro-calcific tissue (high echogenicity).[33-35] Additionally, it measures fibrous cap thickness, can identify plaque rupture and intra-plaque haemorrhage.[36-40] Although, differentiation between intra-plaque haemorrhage and large necrotic core is poor because both appear as echolucent areas.[31 36] Unfortunately, as with most real-time imaging techniques, colour duplex ultrasound is limited by high operator dependency due to subjective plaque morphology grading and moderate specificity.[31 36 40 41] Extensive carotid artery calcification may obscure plaque features and may occasionally impede stenosis measurements.[37 38] Furthermore, colour duplex ultrasound provides no information about other potential sources of an embolism at other sites in the aortic arch, including the origins of its major branches, that can be identified by other imaging modalities.

Computed Tomography Angiography (CTA) is another confirmatory investigation performed prior to any vascular intervention. CTA can delineate a heterogeneous, calcified[30] and ulcerated atheroma,[30 41] and can identify intra-plaque haemorrhage and intra-luminal thrombus.[31 42] When colour duplex ultrasound may be overestimating the degree of carotid artery stenosis or lacks the ability to image high carotid bifurcations, CTA is desirable.[24 31] Although CTA is the best imaging modality in the analysis of plaque calcification, ultimately it is the calcium artefact that limits image interpretation.[30 31] Furthermore, the utility of CTA is diminished by limited soft tissue contrast, radiation exposure, and contrast load.[35 42]

Magnetic Resonance Angiography (MRA) is a reproducible modality that allows for detailed carotid plaque morphology evaluation with moderate to good agreement.[31 43] MRA detects lipid-rich necrotic core, intra-plaque haemorrhage, cap thickness, ulceration and plaque rupture.[15 31 43 44] However, MRA use is limited by the exclusion of patients with certain metallic implants and claustrophobia, it is also more expensive, takes longer to perform, and requires a greater degree of co-operation than either colour duplex ultrasound or CTA.[31] Although existing literature on the imaging of *in vivo* carotid plaque features with histological data is vast and promising, all studies lack standardised histological analysis as well as imaging protocols.[32] This precludes meta-analysis. Nevertheless, MRA is at present the most multifaceted technique to assess the breadth of culprit plaque characteristics.[32]

Overall, currently available imaging technologies have strengths but are unable to characterise carotid plaque biology and activity fully, and lack the capacity to identify culprit carotid plaque reliably. This is fundamental to optimal risk-stratification and appropriate selection of patients for high-risk vascular intervention. One new approach is to use non-invasive molecular imaging targeted at plaque biology using hybrid systems such as positron emission tomography-magnetic resonance imaging.

1.3 ^{18}F-Fluoride Positron Emission Tomography - Computed Tomography

Positron emission tomography demonstrates high sensitivity for the non-invasive, *in vivo* detection of radiolabelled biomolecules in a variety of pathophysiological processes. Atherosclerotic calcification in carotid arteries occurs in response to unresolved chronic inflammation within the plaque and represents an attempt to contain and isolate the necrotic area, thus preventing plaque rupture with its thrombotic consequences. However, detection of early vascular calcification is difficult because we can only monitor the late stages of the disease when calcium deposition has become confluent and large enough (macrocalcification, diameter >50 µm) to be detected by computed tomography. Our research group has pioneered research into the early microcalcification (<50 µm) in human diseased cardiovascular tissue using ^{18}F-Fluoride by validating the mechanism of action of ^{18}F-Fluoride in highlighting high-risk atherosclerotic plaque. We have shown that the phenomenon is likely to be mediated by the ability of the radiotracer to identify early and pathologically high-risk micro-calcification well beyond the resolution of clinical computed tomography.[13] We have demonstrated that ^{18}F-Fluoride Positron Emission Tomography-Computed Tomography (^{18}F PET-CT) identifies both culprit plaque in patients following myocardial infarction and plaques with high-risk features in patients with stable angina.[12] We have also confirmed ^{18}F-Fluoride uptake in the aortic valve correlates with stenosis severity and identifies areas of newly developing calcification that are beyond standard computed tomography resolution.

We have recently reported *ex vivo* and *in vivo* carotid plaque data showing high ^{18}F-Fluoride uptake localises to areas of plaque rupture that showed greater immunostaining for markers of macrophage infiltration, cell death and active calcification when compared to areas of low uptake. Moreover, we have shown that in patients with carotid stenosis and recent neurovascular symptoms, ^{18}F PET-CT was able to discriminate between culprit and non-culprit plaques (Figure 1); the carotid ipsilateral to the affected cerebral hemisphere showed higher uptake of ^{18}F-Fluoride compared to either its contra-lateral partner or to carotids from control stroke patients. Carotid uptake of ^{18}F-Fluoride was focal, readily identifiable and quantifiable. Tracer uptake was also associated with high-risk plaque features and with predicted cardiovascular risk. Therefore, we have shown that ^{18}F-Fluoride identifies the early microscopic calcific response

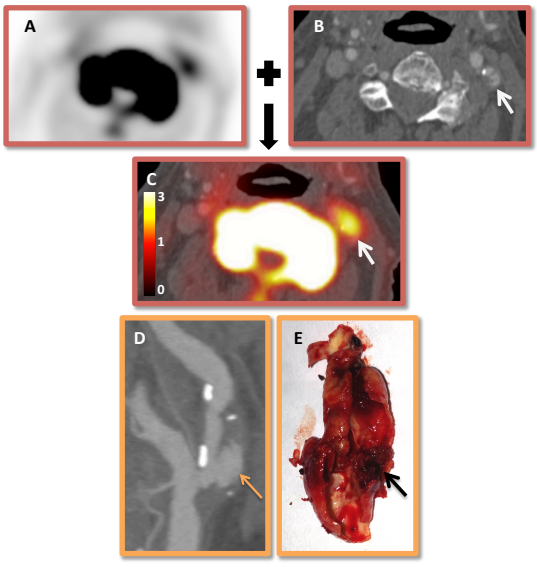

Figure 1. ^{18}F PET- CT of a recently symptomatic plaque: (A) PET image, (B, D) CT images, (C) fused image showing intense tracer uptake. (E) surgical specimen with large plaque rupture.

and may thus identify high-risk ruptured carotid plaque in patients with recent cerebrovascular events.

1.4 Hybrid Magnetic Resonance Imaging - ^{18}F-Fluoride Positron Emission Tomography

Positron Emission Tomography (PET) has traditionally been combined with computed tomography (CT) as PET-CT, but recently, novel hybrid systems combining PET and magnetic resonance imaging (MRI), have become available.[14] These systems have been developed with the specific intention of combining PET with the generic advantages that MRI holds over CT; principally improved soft tissue contrast, lack of radiation exposure, lack of requirement for iodine-based contrast media, and the potential for full motion correction of PET data. MRI offers multiple other key advantages over CT when specifically considering the carotid arteries. CT is limited by "one-dimensional" plaque segmentation (i.e. based purely on photon attenuation) and blooming artefact from dense calcification. By comparison, MRI offers superior soft tissue detail at high resolution and can better segment plaque by exploiting the varying T1/T2 properties and proton density of different lesion constituents. In particular, intra-luminal thrombus or intra-plaque haemorrhage may be identified (due to the presence of methaemoglobin, a breakdown product of haemoglobin) as regions of high signal on non-contrast T1-weighted echo gradient sequences. Such signal has been observed in the culprit plaques of patients who have suffered a recent stroke,[15-17] corresponding to acute thrombus on histology and localising to complex carotid lesions with evidence of surface rupture or intra-plaque haemorrhage.[18] A recent meta-analysis of 689 patients, has confirmed the prospective utility of this technique by demonstrating a 6-fold increase in cerebrovascular events in patients with high-intensity carotid plaques on T1-weighted imaging.[19] Figure 2 shows an example from our institution of a recently symptomatic patient scanned with both ^{18}F PET-CT and MRI. This large plaque shows both intense uptake of radiotracer and hyperintensity on T1-weighted imaging. At surgery, this lesion was ruptured with a large amount of adherent thrombus. Finally, PET-MRI also provides the exciting potential for a fully "one-stop-shop" neurovascular assessment: carotid imaging combined with a sensitive assessment of the brain parenchyma looking for acute and sub-clinical evidence of

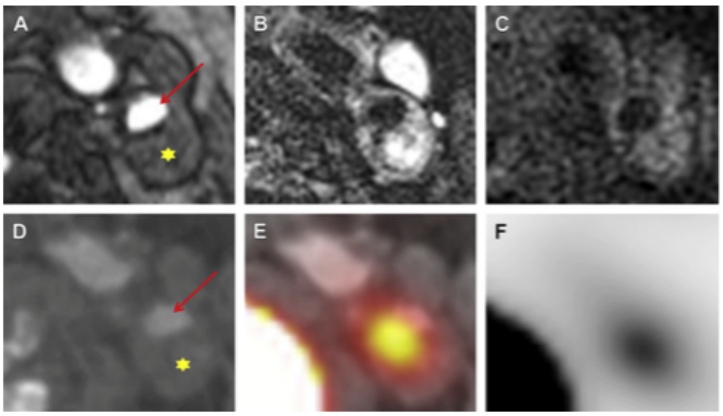

Figure 2. Symptomatic carotid plaque on MRA (3T) and ^{18}F PET-CT. The red arrow denotes the lumen of the internal carotid artery, and the yellow star denotes culprit haemorrhagic plaque with intense ^{18}F-Fluoride uptake. (A) Axial time-of-flight MRA. (B) T2-weighted image. (C) T1-weighted image. (D) CTA. (E) Fused PET-CT. (F) ^{18}F-Fluoride PET.

ischaemic cerebral injury.

We believe that combining ^{18}F-Fluoride PET with MRI, therefore, holds great promise in evaluating symptomatic carotid atherosclerosis, and we propose to assess whether this novel multimodal technique has the potential to improve risk stratification in patients at high-risk of stroke.

1.5 Magnetic Resonance Spectroscopy

Magnetic resonance spectroscopy (MRS) is a non-invasive method that combines the spatial localising of MRI with information of chemical composition from spectroscopy.[45 46] In effect, MRS identifies and quantifies various metabolites in tissues including liquid phase cholesteryl ester in *ex vivo* atherosclerotic plaques.[45 47 48] This is of particular importance since the early stages of atherosclerosis are characterised by the deposition of cholesteryl ester in the foam cell as "fatty streaks".[49 50] Furthermore, the liquid cholesteryl ester is the major class of lipids found within the atheroma lipid-rich necrotic cores associated with plaque rupture.[51] Hence, quantification of specific lipid content can provide vital information central to the pathophysiology of atherosclerosis and potentially aid in the identification of culprit carotid plaque.

Although both cholesterol and cholesteryl ester accumulate pathologically in the arteries, their imaging is challenging. MRI lacks the capacity to differentiate specific lipid plaque components. In general, lipid regions are inhomogeneous, and cholesterol crystals create a signal void in proton-density MRI.[51] Whereas, MRS detects liquid cholesteryl ester by providing a spectrum of resonances (proton spectra) from lipid-rich or poor regions.[49] MRS has been successfully validated by several studies that obtained consistent cholesteryl ester chemical composition and physical state from *ex vivo* carotid and aortic plaques specimens that have been confirmed on histology.[47-53] Moreover, plaque lipids can undergo thermotopic transitions between liquid and solid phases, and the physical state of cholesteryl ester influences enzymatic activities, lipids transport, and storage; all which are essential in atherogenesis.[50] There is no doubt that the chemical composition of plaque lipids influences the stability of a plaque as well as their potential for regression.[52] Ultimately, a better understanding of the arterial plaque lipid constituents may form the basis for future treatment strategies and provide a means of assessing response to treatment.

1.6 Transcranial Doppler

Transcranial Doppler (TCD) is a well established real-time imaging modality that detects microembolic signals (MES) in patients with atherosclerotic disease of large arteries who suffer from cerebral or retinal ischaemia.[54-57] It is a non-invasive, non-ionising, portable and safe technique that utilises an acoustic temporal bone window through which the

ultrasound beam can focus on the middle cerebral artery, which receives 80% of an ipsilateral internal carotid artery inflow.[54 58 59] Several studies have shown that the presence of MES is associated with up to a 40-fold increased risk of future neurological events.[56 60-63] Furthermore, even patients following CEA remain at greater risk of MES-induced postoperative stroke.[64 65] Moreover, MES correlates with a greater number of MRI detectable cerebral infarcts when compared with patients free from microembolism.[62 64] Interestingly, the actual number of MES appears to be equally important. This was confirmed in a study where patients with 10-30 MES per 30-min period suffered more severe neurological deficits than those with <10 MES per 30-min period.[62] Similarly, following CEA, microembolic counts >50 per hour were associated with an increased risk of neurological events.[56] Therefore, detection and prevention of embolic events may have a role in the prediction and prevention of future stroke.[57] Despite this, no centres routinely use TCD for patient triage for CEA.

Although the pathological events that lead to embolisation into the cerebral circulation have been extensively investigated, the clinical consequences are not fully understood. Emboli generated within large arteries such as the aortic arch and its major branches can cause either large disabling strokes or small subclinical events.[57] The embolic material may consist of a thrombus, calcified plaque or other plaque constituents, and is often <0.1 mm in diameter. If such microemboli pass into the small arteriolar branches, the result can be a micro-infarction of brain parenchyma.[57] However, not all microemboli are symptomatic, and some authors suggested that this phenomenon may explain frequently reported subcortical ischaemic changes on CT or MRI in elderly patients with atherosclerotic risk factors.[57] Indeed, this may reflect the accumulated impact of asymptomatic microemboli over the years leading to diffuse brain damage.[57 62] In contrast, other researchers highlight capillary dysfunction as a primary cause for the cerebral small vessel disease that manifests on MRI as small subcortical infarcts, white matter hyperintensities, lacunes, microbleeds, perivascular spaces and atrophy.[66 67]

Substantial evidence indicates that microemboli in symptomatic carotid artery stenosis are associated with an increased risk of a recurrent ipsilateral focal ischaemia.[4 56] Furthermore, MES have been detected in patients with an aortic or intracranial atherosclerotic disease.[68] Although there are only three small and heterogenous studies that reported MES originating from an aortic source, the results of a systematic review suggest that microemboli are more prevalent in patients with larger aortic plaques (>4 mm).[69] However, no study has investigated the relationship between MES and recurrence of stroke in patients with a non-carotid artery source of embolism. We believe that TCD monitoring will add valuable information regarding the correlation between MES and subsequent stroke risk in patients with unstable atherosclerotic aortic plaque. This is particularly important as the disease in these patients is often not amenable to any form of surgical revascularisation. Whether this will translate into an improved treatment strategy is yet to be established.

1.7 Silent Brain Ischemia and Intracranial Atherosclerotic Disease

More evidence is emerging about silent brain ischaemia that ultimately is responsible for a cognitive decline and future stroke risk.[67 70] Large population-based studies have found that in subjects without clinical stroke, the most common subclinical pathology found on MRI were cerebral and lacunar infarcts.[70 71] Another study showed that patients who suffered a minor stroke or TIA were diagnosed with silent early (33.7%) and late (22.1%) recurrent ischaemic lesions on diffusion-weighted imaging by MRI.[72] Even after carotid revascularisation procedures (CEA and stenting), patients develop silent new ischaemic infarcts.[73]

Over the past decade, the intracranial atherosclerotic disease has not received the same amount of research focus as the extracranial component when considering the aetiology of neurovascular events. Interestingly, the intracranial disease that involves large arteries at the base of the brain is almost as common as carotid artery stenosis.[68] More importantly, intracranial atherosclerosis is responsible for 10% of all strokes and TIAs.[68] Despite OMT, patients with severe (>70%) intracranial disease have a 25% risk of stroke at two years.[68] Although studies describe a high technical success rate with minimal complications following intracranial angioplasty, conflicting data exist regarding a post-procedural stroke rate.[68 74-76] Some authors report a low angioplasty stroke risk of between 2-4%, whereas others revealed stroke rates as high as 14% that ultimately led to a termination of a randomised trial of stenting versus OMT.[77] Addition of stenting to traditional angioplasty showed restenosis rates of between 25-32% and no difference in stroke-free survival at 2 years.[74 77] The optimal treatment of intracranial atherosclerotic disease, therefore, remains unknown.

2. Research proposal

Using a novel multimodal imaging approach, we propose to investigate a range of key pathobiological pathways (inflammation, microcalcification, necrosis with lipid-rich core and intraplaque haemorrhage) that underlie the culprit plaque rupture and acute neurovascular events. We hypothesise that ^{18}F-Fluoride PET-MRI (^{18}F PET-MRI) will identify specific pathobiological pathways that will provide an ideal translational biomarker to identify culprit ruptured plaque and to test the plaque stabilising effects of novel therapeutic interventions.

We plan to develop a “one-stop-shop” neurovascular ^{18}F PET-MRI protocol to assess the uptake of ^{18}F-Fluoride and plaque MRI characteristics in symptomatic patients with carotid artery stenosis who are scheduled to undergo carotid surgery in line with the NASCET guidelines. We will then examine plaque removed at the time of surgery for the presence or absence of plaque rupture. We will also undertake MRS of carotid plaque both *in vivo* and

ex vivo to identify lipid composition and correlate the results with ^{18}F-Fluoride uptake and MRI plaque characteristics. Finally, we will perform histopathological examination of the plaque to validate our imaging findings.

2.1 Study Hypotheses

We hypothesise that in subjects scheduled for endarterectomy, hybrid ^{18}F PET-MRI imaging will be able to differentiate clinically and surgically adjudicated culprit and non-culprit plaque. We also predict that ^{18}F-Fluoride uptake will be associated with high-risk MRI features (especially T1 detected thrombus) and histological features as well as MRS detected lipid chemical composition.

2.2 Study Outcomes

2.2.1 Primary Outcome Measure

Carotid and aortic plaque co-localisation of ^{18}F-Fluoride uptake and T1 MRI-detected thrombus.

2.2.2 Secondary Outcome Measures

We will explore a number of exploratory outcomes and specifically will compare plaque ^{18}F-Fluoride uptake and T1 MRI-detected thrombus with:

i. Microembolic signals detected by transcranial Doppler.
ii. High-risk plaque features on magnetic resonance imaging.
iii. Magnetic resonance spectroscopy quantification of *in vivo* and *ex vivo* plaque lipid composition.
iv. Histological markers of high-risk plaque characteristics.
v. Magnetic resonance imaging detected cerebral ischaemia.

3. Details of Proposed Investigation

3.1 Patient Population and Recruitment

Patients with evidence of an acute stroke, transient ischaemic attack or amaurosis fugax will be recruited as early as possible, but within 14 days of symptom onset. The diagnostic criteria will be based on the clinical symptoms and radiological evidence of infarction in line with the guidelines produced by the American Heart and Stroke Associations. The diagnosis of an acute stroke or amaurosis fugax will include clinically evident episode of an acute neurological dysfunction persisting >24 hours that is caused by the image proven focal brain or retinal ischaemia.[78] Whereas, transient ischaemic attack will be recognised when clinical

symptoms of a focal ischaemia will last <24 hours with no evidence of infarction on imaging.[78] All patients will undergo careful clinical evaluation including carotid Doppler ultrasound assessment and magnetic resonance imaging of the brain. We will recruit patients who are scheduled to undergo carotid endarterectomy for symptomatic carotid artery stenosis (≥50% by NASCET criteria for men, ≥70% for women). This cohort will be identified at the point they are referred to a vascular surgeon at Edinburgh Royal Infirmary.

After screening for eligibility by the patient's usual care team, the initial approach will be made by the PI (Mr. Jakub Kaczynski) under the supervision of the responsible Consultant Surgeon, Neurologist or Stroke Physician. This approach will be through the Vascular or TIA Clinic and stroke wards at Edinburgh Royal Infirmary or Western General Hospital either by a telephone or directly. If the patient is willing to consider participation, the PI will provide a verbal description of the study and go over the patient information sheet. Any questions that arise will be answered. The patient will be contacted at least 24 hours after the initial approach to establish their willingness to participate. Any further questions will be answered, and provisional verbal consent will be sought. Written consent will be obtained at the beginning of the first study visit.

3.1.2 Inclusion criterion

i. Cohort 1: Patients with carotid artery stenosis (>50% for men and >70% for women, by NASCET criteria).[79]

3.1.3 Exclusion criteria

i. Patients with new stroke and a modified Rankin score >3
ii. Chronic kidney disease with an estimated Glomerular Filtration Rate (eGFR) of <30 ml/min/1.73 m^2
iii. Atrial fibrillation
iv. Pregnant women
v. Prior ipsilateral carotid intervention
vi. Prior neck radiotherapy
vii. Inability to tolerate the supine position
viii. Participation in the study would result in delay to surgery
ix. Psychiatric illness/social situations that would limit compliance with study requirements
x. History of allergic reaction attributed to ^{18}F-fluoride
xi. History of allergic reaction to gadolinium contrast media
xii. Metal implants and devices including pacemakers and defibrillators

3.2 Study Design

This will be a prospective observational cohort study (See Appendix 10a for study flow chart).

3.2.1 Study Visits

For a flowchart overview of the participant's pathway, please refer to Appendix 10b. The investigated cohort is composed of patients awaiting expedited surgery, and the imaging timetable at the Edinburgh Imaging Facility Queen's Medical Research Institute (QMRI) may be challenging, therefore the timings of the various scans required as part of the study protocol will vary. A strict timetable is therefore not realistic. However, three principles will apply:

i. Patients will be put through the study protocol as quickly as possible (without delay to surgery as a result of participation).

ii. The inconvenience will be minimised (where possible, scans will be performed on the same day, and venous cannulation will be kept to an absolute minimum).

iii. A clinician (PI or delegated member of the research team) will always be present with the subject at the Edinburgh Imaging Facility QMRI.

3.2.2 Baseline Clinical Review and Written Consent

Formal written consent will be obtained prior to any study-related procedures. Demographic and clinical data (including past medical/surgical history, medications history, smoking history, etc.) will be collected through patient interview, examination and review of case records. A safety MRI questionnaire will be formally completed. A venous cannula will be inserted, and 50 mL of blood will be taken if recent blood tests results are not available (to test for a panel of inflammatory and calcific biomarkers, as well as standard haematological and biochemical variables).

3.2.3 Baseline Assessment

All participants will undergo baseline plaque, and brain assessment with ^{18}F PET-MRI with diffusion-weighted imaging and TCD. However, the brain imaging will be performed only if it was not completed already as part of an acute stroke evaluation.

3.2.4 Total Duration of Participation

Patient follow-up will continue using electronic health records data for up to 5 years after patient participation.

3.2.5 ^{18}F-Fluoride PET-MRI Protocol

The ^{18}F PET-MRI will be undertaken using a Siemens Biograph mMR hybrid scanner using dedicated head and neck coils. Upon confirmation of MRI safety, and after intravenous administration of 125 MBq ^{18}F-Fluoride, the subject will then rest in a quiet environment for 60 min to allow radiotracer uptake to occur. Subsequently, the subject will be guided to the ^{18}F PET-MRI suite where baseline imaging will be undertaken.

Protocols will incorporate:

- 3D ^{18}F-Fluoride-PET using list mode acquisitions with beds centred over the aortic arch, carotid arteries, and brain
- Dixon and UTE attenuation correction sequences
- 3D time-of-flight Magnetic Resonance Angiography
- Contrast-enhanced Magnetic Resonance angiography of the cerebral circulation including aortic arch and intracranial vessels centred on the internal carotid artery
- Coronal 3D black blood T2-SPACE of the carotid bifurcation (and other plaques of interest)
- High spatial resolution multi-contrast MRI will be performed using standard protocols. 2D-Axial black blood T1-weighted, T2-weighted and proton density-weighted stacks of the carotid bifurcation
- Cerebral diffusion weighted imaging

PET-MRI images will be reconstructed with corrections applied for attenuation, dead time, scatter and random coincidences. To estimate ^{18}F-Fluoride uptake, volumes of interest (VOI) will be drawn around the carotid bifurcations (as in our previous studies) and other areas of interest. From these VOI, mean and maximal standardised uptake values (SUV) will be derived. Tissue-to-background ratios (TBR) will also be calculated after correction for blood pool activity in the right atrium.

3.2.6 Transcranial Doppler

Transcranial Doppler (TCD) will be performed by the PI on the symptomatic (ipsilateral to an index event) Middle Cerebral Artery at the WTCRF in a quiet temperature controlled room. The Middle Cerebral Artery will be identified through the temporal window in a supine position with a flow direction towards the probe at the depth range 40-65 mm.[80] The subject will have a head frame (Marc 600 Spencer Technologies, USA) fitted to reduce motion and to secure a constant angle of the Middle Cerebral Artery (mid-point) insonation depth at 50 mm from the skull surface.[80] All recordings will be made using the ST^3 Transcranial Doppler Ultrasound System (Spencer Technologies, USA) with a 2-MHz transducer for 1 hour. Emboli will be detected by listening for their characteristic short

audible sound (range 10-100ms, intensity threshold above 7 dB) and spectral appearance using the International Consensus Group microembolus identification criteria and an automated Embolus Detection Software (Spencer Technologies, USA).[81] The recorded Doppler wave forms will be reassessed by a qualified sonographer to exclude artefact and confirm the presence of true emboli.

3.2.7 Tissue Collection and Histopathology

At the time of carotid endarterectomy, plaque tissue will be collected, and lesion integrity and geometry will be preserved as much as possible. Specimens will be photographed in detail to permit subsequent assessment by independent and blinded reviewers. Dr Maurits Jansen (Edinburgh University) who has expertise in the field of the MRI and spectroscopy will collaborate with us regarding an *ex vivo* plaque MRS. The excised tissue will be oriented and labelled in such a manner as to permit orientation in the carotid artery axis and will be transported to the Edinburgh Pre-clinical Imaging suite where 7.4 T MRS will take place. Subsequently, carotid plaque will be transported back to the QMRI where specimen will be snap frozen in liquid nitrogen. Specimens will subsequently be prepared and stained according to agreed protocols. Cellular content, macrophage infiltration, apoptosis levels, and calcification-associated molecules within the plaques will be assessed by RNA analysis immunohistochemistry and immunofluorescence using a variety of validated markers.

3.2.8 Magnetic Resonance Spectroscopy

3.2.8.1 *Ex vivo*

Specimen

Following CEA, fresh plaque will be placed in 50 mL of 0.9% saline to prevent tissue dehydration. The carotid specimen will be then transported from operating theatre to the Preclinical MRI facility at Edinburgh University, where MRS will take place. MRS will be performed on the same day at 37^{o}C and immediately after the plaque has been delivered. However, this approach may not always be feasible, because occasionally CEA may be performed on an urgent basis and giving a busy timetable at the research facility, MRS may not be achievable up to 24-48 hours after the specimen retrieval. In such scenario, we will proceed directly with the histopathological assessment of the excised carotid plaque that will be placed in 50 mL of formaldehyde fixative immediately following CEA.

Standards

Purchased lipids standards comprising cholesteryl ester, triacylglycerol and phospholipids will be used to verify acquired spectra of lipids in line with the published standards.[47 51] Cholesteryl ester will be heated to 45^{o}C to ensure complete melting (crystal-to-isotropic transition at 42^{o}C), and then permitted to cool to physiological temperature (37^{o}C), at which

temperature images and spectra will be obtained. Triglyceride standards will be heated to 37^{o}C and analysed directly.

MRI

The *ex vivo* plaque will be oriented in the carotid artery axis, and MRI will be performed at 7.4 T using a horizontal-bore Agilent MRI scanner to identify either lipid-rich or lipid-poor plaque regions. Specimens will be placed in a 26-mm diameter imaging coil and loaded into the isocenter of the magnet. The plaque will be heated by air exchange to 37^{o}C 20 min before initiation of the imaging protocol to permit thermal equilibration. High-resolution images will be acquired from 1 mm thick axial slices utilising T1-weighted (T1W), and T2-weighted (T2W) spin echo protocols.

T1W parameters will be: matrix,256 x 256; field of view (FOV), 1.5 cm; repetition time (TR), 300–500 ms; echo time (TE), 15 ms. T2W parameters were: matrix, 256 x 256; FOV, 1.5 cm; TR, 2,000 ms; TE, 30 ms. In-plane resolution was 60um (FOV/matrix). The time needed to acquire a complete set of either T1W or T2W images will bet typically between 45 to 60 min. Following image acquisition, a colourized polar map of the ratio of T1/T2 image intensity (based solely upon the signal and dependent upon T1/T2 contrast weighting) will be generated using the algebraic function of Paravision. This polar map will highlight the signal intensity differences between the T1 and T2 images and will be utilised to select regions for proton spectroscopy.

MRS

Subsequently, image-guided proton MRS will be performed from 3 mm^3 voxels using the PRESS technique (point-resolved spectroscopy) of voxel selection (Bruker sequence VSEL_SE_ SPEC). Following identification of the region of interest, a larger 5mm 3 voxel will be placed over the region to permit shimming of B_o on the water peak and optimisation of the 90^{o} and 180^{o} pulses. The water signal will be then selectively suppressed by presaturation. This procedure will be performed at the onset of experimentation for each specimen, with shimming optimisation repeated only if the region of interest moved outside the initial shimming volume. Voxel size will be then reduced to 1 mm3 and localised to the region of interest. Spectroscopy parameters will be as follows: spectral width, 10K; acquisition size, 2048; TR, 500ms; TE, 15ms; and Number of Excitations (NEX), 600. Additional spectroscopic measurements will be made with identical parameters except for TR of 2,000 ms. Spectral acquisition time is anticipated to take 5 minutes. A second spectrum from the same voxel position will be acquired without water suppression for standardisation. This technique of voxel selection and the signal acquisition will be applied to phantom samples of pure cholesteryl ester and triacylglycerol to test the sensitivity of the technique and the accuracy of voxel selection. Following the acquisition, spectra will be processed and analysed using Magnetic Resonance User Interference (MRUI) and compared with published standards to permit peak assignment. The water peak will be assigned to 4.7

ppm. Methyl and methylene resonances of fatty acyl chains will be identified in their characteristic spectral region (0.8–1.4 ppm). A lipid: water ratio will be calculated to permit semiquantitative comparison between different voxel regions by taking the integrated area subscribed by the peak methyl and methylene resonances and expressing it as a fraction of the integrated water peak without presaturation (assigned to 1.0). Ratios from a priori-identified lipid-rich and lipid-poor plaque regions will be compared statistically using an unpaired Student's t-test. Voxel-defined MRS will also be performed on standards of purified cholesteryl ester and triacylglycerol.

3.2.8.2 *In vivo*

The proposed MRS of *in vivo* carotid plaques will be optional due to the time constraints of the main ^{18}F PET-MRI protocol. Therefore, MRS (*in vivo*) will be performed only if the participant will be willing to undergo additional carotid plaque imaging.

The proton spectra of *in vivo* carotid plaques will be acquired on the Siemens Biograph mMR (3T). The location of the target plaque will be identified using structural magnetic resonance images to plan the spectroscopy acquisition. Signal will be received using the head and neck coils. The magnetic resonance spectroscopy will use a chemical shift imaging sequence that acquires spectra from multiple regions of interest surrounding and over the plaque of interest.[47] The sequence parameters will be as follows: TR/TE = 1100/30 ms, FOV = 80 mm^2, matrix = 160×160 mm, voxel dimensions = 5×5×5 mm.[47] As for the ex-vivo spectra, the water peak will be assigned to 4.7 ppm. Spectral analysis will be carried out using the Java Magnetic Resonance User Interference (JMRUI) software package for advanced analysis of magnetic resonance spectroscopy and metabolite amplitudes, including those for relevant lipids, will be reported as a ratio to the amplitude of intrinsic water.

3. Statistical Analysis and Sample Size

3.1 Statistical Analysis

Radiotracer uptake, expressed as mean and maximum SUV, will be compared between the clinically adjudicated culprit internal carotid plaque and the contralateral side. Continuous variables will be expressed as mean ± standard deviation for normally distributed data and median (interquartile range) for skewed distributions. Skewed datasets will undergo logarithmic transformation to normalise their distribution. Parametric (unpaired and paired *t*-tests) and non-parametric (Mann-Whitney U or Wilcoxon matched-pairs signed rank) tests will be used for normally distributed and skewed data respectively. Categorical data will be presented as n (%) and will be compared using Fisher's exact or Chi-squared tests. Correlation will be undertaken with either Pearson's r or Spearman's Rho subject to the normality of the variables tested. To quantify inter and intra-observer reproducibility of imaging measurements, the intra-class correlation coefficient will be calculated and Bland-

Altman analysis undertaken. Statistical significance will be taken as a two-sided P<0.05.

Cohort 1: The primary endpoint of the study is the co-localisation of ^{18}F-Fluoride uptake and T1 MRI-detected thrombus. We will assess the relative frequencies of their co-localisation and levels of agreement with surgical findings using intra-class correlation coefficient and kappa statistics. We will further explore the relative frequencies of co-localisation of ^{18}F-Fluoride uptake and T1 MRI-detected thrombus in culprit and non-culprit plaques using the chi-squared test. We will also compare microembolic signals detected on TCD with ^{18}F-Fluoride uptake and T1 MRI-detected thrombus. Associations will be determined by regression analysis using Pearson's or Spearman Rho tests depending on the normality of the distribution of the data.

Further exploratory analyses will be performed as detailed above to establish whether there are further associations between our panel of exploratory imaging, spectroscopic and histologic biomarkers.

3.2 Sample Size

Data will be analysed to address the question of whether ^{18}F-fluoride uptake can differentiate ruptured from non-ruptured carotid plaque. Based on recent data, we have a variance (standard deviation) of 0.13 for TBR_{max} with mean values of 1.88 for ^{18}F-fluoride uptake.[82] We have previously seen a difference of 0.08 between culprit and non-culprit plaques.[82] At 80% power and two-sided P<0.05, we will need 33 patients to detect a between ipsilateral and contralateral plaques. We will recruit 40 patients in each cohort to account for incomplete data, drop-outs, and multiple comparisons.

4. Ethics

This study will be carried out by the ethical principles outlined in the Research Governance Framework for Health and Community Care, Second Edition, 2006 and the World Medical Association Declaration of Helsinki Ethical Principles for Medical Research Involving Human Subjects 1964 (as amended). The study will be reviewed by an accredited independent Ethics Committee for approval.

5. Finance and Indemnity

The study is funded through the Princess Margaret Research Development Fellowship and the British Heart Foundation.

Jakub Kaczynski (PI) and Professor Newby each have a contract with NHS Lothian and the University of Edinburgh. Indemnity against legal liability for non-negligent harm caused to a research subject will, therefore, be provided through the existing NHS and University of Edinburgh schemes. Both will provide cover for such harm arising from the design, management or conduct of the research.

6. Dissemination of Results

The results will be presented at national and international meetings and will be submitted for publication in peer-reviewed journals. A lay summary of the results will also be disseminated by post to participants who wish to wish to receive it.

7. Gadolinium Contrast Safety Assessment and Related Procedures

For patients with risk factors for renal dysfunction (diabetes; heart failure; age >over 70; multiple myeloma; drug history including: aminoglycosides, diuretics, regular NSAIDs; gout; HIV infection) and no blood tests within the last 6 months, biochemical analysis of a blood sample will be performed prior to participation in the study. A history of allergy to iodine-based contrast or atopy, in general, will be directly elicited. All patients will be advised to drink water before their scan for adequate hydration.

Patients on metformin with a normal eGFR (>60 ml/min/1.73m^2) will be advised to continue taking metformin up until the scan. After the scan, they shall be advised to withhold metformin for 48 hours and will then have a blood test to check renal function. They will be informed by telephone when they are to restart the metformin following the result of this.

Patients on metformin with an eGFR 30–60 ml/min/1.73m^2 will be advised to stop metformin for 48 hours before and after the scan. They will then have a blood test to check renal function and be advised on when to restart metformin.

These safety assessments represent standard clinical care with respect to Gadolinium contrast.

8. Adverse Events

The PI will be responsible for the detection and documentation of events meeting the criteria and definitions detailed below.
Participants will be instructed to contact the PI at any time after consenting to join the trial if any symptoms develop. All adverse events (AE) that occur after participants have joined the trial and up to 7 days after their scan will be reported in detail in the Case Report Form (CRF). In the case of an AE, the PI will initiate the appropriate treatment according to his medical judgement and will be followed up until resolution of the event.

8.1 Definitions

An **adverse event** (AE) is any untoward medical occurrence in a trial participant that does not necessarily have a causal relationship with gadolinium-based contrast media or ^{18}F-Fluoride.

An **adverse reaction** (AR) is any untoward or unintended response to gadolinium-based contrast media or ^{18}F-Fluoride that is related to any dose administered to that participant.

An **unexpected adverse reaction** (UAR) is an adverse reaction that is not consistent with the applicable product information for gadolinium-based contrast media or ^{18}F-Fluoride.

A **serious adverse event** (SAE), **serious adverse reaction** (SAR) or **suspected unexpected serious adverse reaction** (SUSAR) is any AE, AR or UAR that at any dose:

- results in death
- is life threatening (i.e. the participant was at risk of death at the time of the event; it does not refer to an event which hypothetically might have caused death if it were more severe)
- requires in-patient hospitalisation
- results in persistent or significant disability or incapacity
- is a congenital anomaly or birth defect

8.2 Detecting AEs and SAEs

All AEs and SAEs will be recorded from the time a participant joins the trial until the end of their participation (the day of discharge following CEA).Participants will be asked about the occurrence of AEs/SAEs at every study visit. Open-ended and non-leading verbal questioning of the participant will be used. Participants will also be asked if they have been admitted to the hospital, had any accidents, used any new medicines or changed concomitant medications. If there is any doubt as to whether a clinical observation is an AE, the event will be recorded.

8.3 Recording AEs and SAEs

When an AE/SAE occurs, it will be the responsibility of the PI to review all documentation (e.g. hospital notes, laboratory and diagnostic reports) related to the event. The PI will then record all relevant information in the CRF and if relevant on a SAE form.

Information to be collected includes dose, type of event, onset date, PI assessment of severity and causality, date of resolution as well as treatment required, investigations needed and outcome.

8.4 Assessment of AEs and SAEs

The PI will be responsible for assessing the seriousness, causality, severity and expectedness of each AE.

The CI may not downgrade an event that has been assessed by the PI as an SAE or SUSAR but can upgrade an AE to an SAE, SAR or SUSAR if appropriate.

8.5 Assessment of Seriousness

The PI will make an assessment of seriousness as defined in Section 3.6.1.

8.6 Assessment of Causality

The PI will make an assessment of whether the AE/SAE is likely to be related to gadolinium-based contrast media or ^{18}F-Fluoride. AEs/SAEs judged as having a reasonable suspected causal relationship to gadolinium-based contrast media, or ^{18}F-fluoride will be considered as ARs/SARs.

8.7 Assessment of Severity

The PI will make an assessment of severity for each AE/SAE and record this on the CRF according to one of the following categories:

Mild: an event that is easily tolerated by the participant, causing minimal discomfort and not interfering with every day activities.

Moderate: an event that is sufficiently discomforting to interfere with normal everyday activities.

Severe: an event that prevents normal everyday activities.

8.8 Assessment of Expectedness

If an event is judged to be an AR/SAR, the evaluation of expectedness will be made based on knowledge of the reaction and the relevant product information documented in the Summary of Product Characteristics.

The event may be classed as either:

Expected: the AR is consistent with the toxicity of gadolinium-based contrast media or ^{18}F-Fluoride.

Unexpected: the AR is not consistent with the toxicity gadolinium-based contrast media or ^{18}F-Fluoride.

8.9 Reporting of SAE/SARs/SUSARs

Once the PI becomes aware that an SAE/SAR/SUSAR has occurred in a study participant, the information will be reported to the ACCORD Research Governance & QA Office **immediately or within 24 hours**. If the PI does not have all information regarding a SAE/SAR/SUSAR, they should not wait for this additional information before notifying ACCORD. The SAE/SAR/SUSAR report form can be updated when the additional information is received.

The SAE/SAR/SUSAR report will provide an assessment of causality and expectedness at the time of the initial report to ACCORD according to Sections 3.6.6, Assessment of Causality and 3.6.8, Assessment of Expectedness.

The SAE/SAR/SUSAR form will be transmitted by fax to ACCORD on **+44 (0)131 242 9447** or may be transmitted by hand to the office. All reports faxed to ACCORD, and any follow-up information will be retained by the PI in the Investigator Site File (ISF).

8.10 Regulatory Reporting Requirements

The ACCORD Research Governance & QA Office is responsible for pharmacovigilance reporting on behalf of the co-sponsors (Edinburgh University and NHS Lothian).

Although this study is not a Clinical Trial of an Investigational Medicinal Product, the ACCORD Research Governance & QA Office will notify the competent regulatory authority and relevant ethics committee (Research Ethics Committee (REC) that approved the trial) where appropriate. Fatal or life-threatening SUSARs will be reported no later than seven calendar days, and all other SUSARs will be reported no later than 15 calendar days after ACCORD is first aware of the reaction.

8.11 Follow Up Procedures

After initially recording an AE or recording and reporting an SAE, the Investigator will follow each participant until resolution or death of the participant. Follow-up information on an SAE will be reported to the ACCORD office.

AEs still present in participants at the last study visit will be monitored until resolution of the event or until no longer medically indicated.

8.12 Changes to Concomitant Medicines

Other than that addressed in section 3.5, there will be no changes to concomitant medications.

8.13 Criteria for Discontinuation

- Withdrawal of consent for whatever reason.
- At the discretion of the investigator.

8.14 Data Collection and Data Security

Demographic, clinical, laboratory and all electronic radiological data will be collected and stored in a linked-anonymous format. The Principal and Chief Investigators (Mr Jakub Kaczynski and Professor Newby) will have access to a master sheet linking the subjects' names to their unique patient identifier. This master sheet will be stored electronically on the NHS password-protected computer. A hard copy will also be kept in a locked cabinet within the NHS premises.

Clinical and demographic data will be transcribed onto a CRF – these will, in turn, be kept in the study file that shall be stored securely. CRF data will be transcribed onto electronic spreadsheets for subsequent analysis. These spreadsheets will be stored electronically on a password-protected computer (PI's University-issued laptop). Identifiable radiological/scan data will be stored on a secure hard-drive at the Edinburgh Imaging Facility QMRI. The same data in linked-anonymous format will also be transferred onto Mr Jakub Kaczynski's password-protected laptop for analysis.

9. References

1. Naylor AR. Why is the management of asymptomatic carotid disease so controversial? *The surgeon : journal of the Royal Colleges of Surgeons of Edinburgh and Ireland* 2015;13(1):34-43. doi: 10.1016/j.surge.2014.08.004
2. Vavra AK, Eskandari MK. Treatment options for symptomatic carotid stenosis: timing and approach. *The surgeon : journal of the Royal Colleges of Surgeons of Edinburgh and Ireland* 2015;13(1):44-51. doi: 10.1016/j.surge.2014.09.001
3. Cardiovascular Imaging. 1 ed: Springer International Publishing 2015.
4. Valton L, Larrue V, le Traon AP, et al. Microembolic signals and risk of early recurrence in patients with stroke or transient ischemic attack. *Stroke; a journal of cerebral circulation* 1998;29(10):2125-8.
5. Rothwell P, Slattery J, Warlow C. A systematic review of the risks of stroke and death due to endarterectomy for symptomatic carotid stenosis. *Stroke; a journal of cerebral circulation* 1996;27(2):260-65.
6. Rudarakanchana N, Halliday AW, Kamugasha D, et al. Current practice of carotid endarterectomy in the UK. *Br J Surg* 2012;99(2):209-16. doi: 10.1002/bjs.7810
7. Wu TY, Anderson NE, Barber PA. Neurological complications of carotid revascularisation. *J Neurol Neurosurg Psychiatry* 2012;83(5):543-50. doi: 10.1136/jnnp-2011-301162
8. Hill MD, Brooks W, Mackey A, et al. Stroke after carotid stenting and endarterectomy in the Carotid Revascularization Endarterectomy versus Stenting Trial (CREST). *Circulation* 2012;126(25):3054-61. doi: 10.1161/CIRCULATIONAHA.112.120030
9. Faggioli G, Pini R, Mauro R, et al. Perioperative outcome of carotid endarterectomy according to type and timing of neurologic symptoms and computed tomography findings. *Ann Vasc Surg* 2013;27(7):874-82. doi: 10.1016/j.avsg.2012.12.003
10. Ferguson GG, Eliasziw M, Barr HW, et al. The North American Symptomatic Carotid Endarterectomy Trial : surgical results in 1415 patients. *Stroke; a journal of cerebral circulation* 1999;30(9):1751-8.
11. Rerkasem K, Rothwell PM. Carotid endarterectomy for symptomatic carotid stenosis. *Cochrane Database Syst Rev* 2011(4):CD001081. doi: 10.1002/14651858.CD001081.pub2
12. Labropoulos N, Ashraf Mansour M, Kang SS, et al. Viscoelastic properties of normal and atherosclerotic carotid arteries. *European journal of vascular and endovascular surgery : the official journal of the European Society for Vascular Surgery* 2000;19(3):221-5. doi: 10.1053/ejvs.1999.1008
13. Saito D, Oka T, Kajiyama A, et al. Factors predicting compensatory vascular remodelling of the carotid artery affected by atherosclerosis. *Heart* 2002;87(2):136-9.
14. Das M, Braunschweig T, Muhlenbruch G, et al. Carotid plaque analysis: comparison of dual-source computed tomography (CT) findings and histopathological correlation. *European journal of vascular and endovascular surgery : the official journal of the European Society for Vascular Surgery* 2009;38(1):14-9. doi: 10.1016/j.ejvs.2009.03.013

15. Howard DP, van Lammeren GW, Rothwell PM, et al. Symptomatic carotid atherosclerotic disease: correlations between plaque composition and ipsilateral stroke risk. *Stroke; a journal of cerebral circulation* 2015;46(1):182-9. doi: 10.1161/STROKEAHA.114.007221
16. Libby P. Inflammation in atherosclerosis. *Arteriosclerosis, thrombosis, and vascular biology* 2012;32(9):2045-51. doi: 10.1161/ATVBAHA.108.179705
17. Ewence AE, Bootman M, Roderick HL, et al. Calcium phosphate crystals induce cell death in human vascular smooth muscle cells: a potential mechanism in atherosclerotic plaque destabilization. *Circulation research* 2008;103(5):e28-34. doi: 10.1161/CIRCRESAHA.108.181305
18. Lovett JK, Gallagher PJ, Hands LJ, et al. Histological correlates of carotid plaque surface morphology on lumen contrast imaging. *Circulation* 2004;110(15):2190-7. doi: 10.1161/01.CIR.0000144307.82502.32
19. Makris GC, Nicolaides AN, Geroulakos G. Histological analysis of the carotid plaque post-endarterectomy: a waste of time or a wasted piece of information? *European journal of vascular and endovascular surgery : the official journal of the European Society for Vascular Surgery* 2011;42(1):13-4. doi: 10.1016/j.ejvs.2011.03.028
20. Salem MK, Sayers RD, Bown MJ, et al. Features of unstable carotid plaque during and after the hyperacute period following TIA/stroke. *European journal of vascular and endovascular surgery : the official journal of the European Society for Vascular Surgery* 2013;45(2):114-20. doi: 10.1016/j.ejvs.2012.11.023
21. Redgrave JN, Lovett JK, Gallagher PJ, et al. Histological assessment of 526 symptomatic carotid plaques in relation to the nature and timing of ischemic symptoms: the Oxford plaque study. *Circulation* 2006;113(19):2320-8. doi: 10.1161/CIRCULATIONAHA.105.589044
22. Howard DP, van Lammeren GW, Redgrave JN, et al. Histological features of carotid plaque in patients with ocular ischemia versus cerebral events. *Stroke; a journal of cerebral circulation* 2013;44(3):734-9. doi: 10.1161/STROKEAHA.112.678672
23. Wardlaw JM, Chappell FM, Best JJ, et al. Non-invasive imaging compared with intra-arterial angiography in the diagnosis of symptomatic carotid stenosis: a meta-analysis. *Lancet* 2006;367(9521):1503-12. doi: 10.1016/S0140-6736(06)68650-9
24. Wardlaw JM, Stevenson MD, Chappell F, et al. Carotid artery imaging for secondary stroke prevention: both imaging modality and rapid access to imaging are important. *Stroke; a journal of cerebral circulation* 2009;40(11):3511-7. doi: 10.1161/STROKEAHA.109.557017
25. Rothwell PM, Pendlebury ST, Wardlaw J, et al. Critical appraisal of the design and reporting of studies of imaging and measurement of carotid stenosis. *Stroke; a journal of cerebral circulation* 2000;31(6):1444-50.
26. Chappell FM, Wardlaw JM, Young GR, et al. Carotid artery stenosis: accuracy of noninvasive tests--individual patient data meta-analysis. *Radiology* 2009;251(2):493-502. doi: 10.1148/radiol.2512080284
27. Wardlaw JM, Chappell FM, Stevenson M, et al. Accurate, practical and cost-effective assessment of carotid stenosis in the UK. *Health Technol Assess* 2006;10(30):iii-iv, ix-x, 1-182.
28. Veith FJ, Bell PR. How Many of You Can Read But Still Not See? A Comment on a Recent Review of Carotid Guidelines. *European journal of vascular and endovascular surgery : the official journal of the European Society for Vascular Surgery* 2016;51(4):471-2. doi: 10.1016/j.ejvs.2015.10.017
29. Karlsson L, Kangefjard E, Hermansson S, et al. Risk of Recurrent Stroke in Patients with Symptomatic Mild (20-49% NASCET) Carotid Artery Stenosis. *European journal of vascular and endovascular surgery : the official journal of the European Society for Vascular Surgery* 2016;52(3):287-94. doi: 10.1016/j.ejvs.2016.05.014
30. Oliver TB, Lammie GA, Wright AR, et al. Atherosclerotic plaque at the carotid bifurcation: CT angiographic appearance with histopathologic correlation. *AJNR American journal of neuroradiology* 1999;20(5):897-901.

31. Huibers A, de Borst GJ, Wan S, et al. Non-invasive Carotid Artery Imaging to Identify the Vulnerable Plaque: Current Status and Future Goals. *European journal of vascular and endovascular surgery : the official journal of the European Society for Vascular Surgery* 2015;50(5):563-72. doi: 10.1016/j.ejvs.2015.06.113
32. den Hartog AG, Bovens SM, Koning W, et al. Current status of clinical magnetic resonance imaging for plaque characterisation in patients with carotid artery stenosis. *European journal of vascular and endovascular surgery : the official journal of the European Society for Vascular Surgery* 2013;45(1):7-21. doi: 10.1016/j.ejvs.2012.10.022
33. Hjelmgren O, Holdfeldt P, Johansson L, et al. Identification of vascularised carotid plaques using a standardised and reproducible technique to measure ultrasound contrast uptake. *European journal of vascular and endovascular surgery : the official journal of the European Society for Vascular Surgery* 2013;46(1):21-8. doi: 10.1016/j.ejvs.2013.03.023
34. Arnold JA, Modaresi KB, Thomas N, et al. Carotid plaque characterization by duplex scanning: observer error may undermine current clinical trials. *Stroke; a journal of cerebral circulation* 1999;30(1):61-5.
35. Golledge J, Siew DA. Identifying the carotid 'high risk' plaque: is it still a riddle wrapped up in an enigma? *European journal of vascular and endovascular surgery : the official journal of the European Society for Vascular Surgery* 2008;35(1):2-8. doi: 10.1016/j.ejvs.2007.09.004
36. Lammie GA, Wardlaw J, Allan P, et al. What pathological components indicate carotid atheroma activity and can these be identified reliably using ultrasound? *Eur J Ultrasound* 2000;11(2):77-86.
37. Russell DA, Wijeyaratne SM, Gough MJ. Relationship of carotid plaque echomorphology to presenting symptom. *European journal of vascular and endovascular surgery : the official journal of the European Society for Vascular Surgery* 2010;39(2):134-8. doi: 10.1016/j.ejvs.2009.11.003
38. Devuyst G, Karapanayiotides T, Ruchat P, et al. Ultrasound measurement of the fibrous cap in symptomatic and asymptomatic atheromatous carotid plaques. *Circulation* 2005;111(21):2776-82. doi: 10.1161/CIRCULATIONAHA.104.483024
39. Giannoni MF, Vicenzini E, Citone M, et al. Contrast carotid ultrasound for the detection of unstable plaques with neoangiogenesis: a pilot study. *European journal of vascular and endovascular surgery : the official journal of the European Society for Vascular Surgery* 2009;37(6):722-7. doi: 10.1016/j.ejvs.2008.12.028
40. Gronholdt ML, Nordestgaard BG, Schroeder TV, et al. Ultrasonic echolucent carotid plaques predict future strokes. *Circulation* 2001;104(1):68-73.
41. Thapar A, Jenkins IH, Mehta A, et al. Diagnosis and management of carotid atherosclerosis. *BMJ* 2013;346:f1485. doi: 10.1136/bmj.f1485
42. Eesa M, Hill MD, Al-Khathaami A, et al. Role of CT angiographic plaque morphologic characteristics in addition to stenosis in predicting the symptomatic side in carotid artery disease. *AJNR American journal of neuroradiology* 2010;31(7):1254-60. doi: 10.3174/ajnr.A2078
43. Treiman GS, McNally JS, Kim SE, et al. Correlation of Carotid Intraplaque Hemorrhage and Stroke Using 1.5 T and 3 T MRI. *Magn Reson Insights* 2015;8(Suppl 1):1-8. doi: 10.4137/MRI.S23560
44. Yuan C, Mitsumori LM, Ferguson MS, et al. In vivo accuracy of multispectral magnetic resonance imaging for identifying lipid-rich necrotic cores and intraplaque hemorrhage in advanced human carotid plaques. *Circulation* 2001;104(17):2051-6.
45. Castillo M, Kwock L, Mukherji SK. Clinical applications of proton MR spectroscopy. *AJNR American journal of neuroradiology* 1996;17(1):1-15.
46. Vinitski S, Consigny PM, Shapiro MJ, et al. Magnetic resonance chemical shift imaging and spectroscopy of atherosclerotic plaque. *Investigative radiology* 1991;26(8):703-14.

47. Duivenvoorden R, van Wijk D, Klimas M, et al. Detection of liquid phase cholesteryl ester in carotid atherosclerosis by 1H-MR spectroscopy in humans. *JACC Cardiovasc Imaging* 2013;6(12):1277-84. doi: 10.1016/j.jcmg.2013.03.010
48. Zajicek J, Pearlman JD, Merickel MB, et al. High-resolution proton NMR spectra of human arterial plaque. *Biochemical and biophysical research communications* 1987;149(2):437-42.
49. Guyton JR. MR spectroscopy of cholesteryl ester in human atherosclerosis. *JACC Cardiovasc Imaging* 2013;6(12):1285-6. doi: 10.1016/j.jcmg.2013.04.018
50. Pearlman JD, Zajicek J, Merickel MB, et al. High-resolution 1H NMR spectral signature from human atheroma. *Magnetic resonance in medicine : official journal of the Society of Magnetic Resonance in Medicine / Society of Magnetic Resonance in Medicine* 1988;7(3):262-79.
51. Ruberg FL, Viereck J, Phinikaridou A, et al. Identification of cholesteryl esters in human carotid atherosclerosis by ex vivo image-guided proton MRS. *Journal of lipid research* 2006;47(2):310-7. doi: 10.1194/jlr.M500431-JLR200
52. Guo W, Morrisett JD, Lawrie GM, et al. Identification of different lipid phases and calcium phosphate deposits in human carotid artery plaques by MAS NMR spectroscopy. *Magnetic resonance in medicine : official journal of the Society of Magnetic Resonance in Medicine / Society of Magnetic Resonance in Medicine* 1998;39(2):184-9.
53. Moreno PR, Muller JE. Identification of high-risk atherosclerotic plaques: a survey of spectroscopic methods. *Current opinion in cardiology* 2002;17(6):638-47.
54. Markus H. Transcranial Doppler detection of circulating cerebral emboli. A review. *Stroke; a journal of cerebral circulation* 1993;24(8):1246-50.
55. Sarkar S, Ghosh S, Ghosh SK, et al. Role of transcranial Doppler ultrasonography in stroke. *Postgraduate medical journal* 2007;83(985):683-9. doi: 10.1136/pgmj.2007.058602
56. van Dellen D, Tiivas CA, Jarvi K, et al. Transcranial Doppler ultrasonography-directed intravenous glycoprotein IIb/IIIa receptor antagonist therapy to control transient cerebral microemboli before and after carotid endarterectomy. *The British journal of surgery* 2008;95(6):709-13. doi: 10.1002/bjs.6204
57. Grotta JC, Alexandrov AV. Preventing stroke: is preventing microemboli enough? *Circulation* 2001;103(19):2321-2.
58. Markus HS, Droste D, Brown MM. Ultrasonic detection of cerebral emboli in carotid stenosis. *Lancet* 1993;341(8860):1606.
59. J.D B, P.A G. Vascular and Endovascular Surgery. 4th ed. Edinburgh: Elsevier 2009.
60. Verhoeven BA, de Vries JP, Pasterkamp G, et al. Carotid atherosclerotic plaque characteristics are associated with microembolization during carotid endarterectomy and procedural outcome. *Stroke; a journal of cerebral circulation* 2005;36(8):1735-40. doi: 10.1161/01.STR.0000173153.51295.ee
61. Wolf O, Heider P, Heinz M, et al. Microembolic signals detected by transcranial Doppler sonography during carotid endarterectomy and correlation with serial diffusion-weighted imaging. *Stroke; a journal of cerebral circulation* 2004;35(11):e373-5. doi: 10.1161/01.STR.0000143184.69343.ec
62. Kimura K, Minematsu K, Koga M, et al. Microembolic signals and diffusion-weighted MR imaging abnormalities in acute ischemic stroke. *AJNR American journal of neuroradiology* 2001;22(6):1037-42.
63. Saedon M, Dilshad A, Tiivas C, et al. Prospective validation study of transorbital Doppler ultrasound imaging for the detection of transient cerebral microemboli. *The British journal of surgery* 2014;101(12):1551-5. doi: 10.1002/bjs.9634
64. Stork JL, Levi CR, Chambers BR, et al. Possible determinants of early microembolism after carotid endarterectomy. *Stroke; a journal of cerebral circulation* 2002;33(8):2082-5.
65. Abbott AL, Levi CR, Stork JL, et al. Timing of clinically significant microembolism after carotid endarterectomy. *Cerebrovasc Dis* 2007;23(5-6):362-7. doi: 10.1159/000099135

66. Valdes Hernandez Mdel C, Armitage PA, Thrippleton MJ, et al. Rationale, design and methodology of the image analysis protocol for studies of patients with cerebral small vessel disease and mild stroke. *Brain Behav* 2015;5(12):e00415. doi: 10.1002/brb3.415
67. Ostergaard L, Engedal TS, Moreton F, et al. Cerebral small vessel disease: Capillary pathways to stroke and cognitive decline. *Journal of cerebral blood flow and metabolism : official journal of the International Society of Cerebral Blood Flow and Metabolism* 2016;36(2):302-25. doi: 10.1177/0271678X15606723
68. McTaggart RA, Jayaraman MV, Haas RA, et al. Intracranial atherosclerotic disease: epidemiology, imaging and treatment. *Med Health R I* 2009;92(12):412-4.
69. Ritter MA, Dittrich R, Thoenissen N, et al. Prevalence and prognostic impact of microembolic signals in arterial sources of embolism. A systematic review of the literature. *Journal of neurology* 2008;255(7):953-61. doi: 10.1007/s00415-008-0638-8
70. Cheung N, Mosley T, Islam A, et al. Retinal microvascular abnormalities and subclinical magnetic resonance imaging brain infarct: a prospective study. *Brain : a journal of neurology* 2010;133(Pt 7):1987-93. doi: 10.1093/brain/awq127
71. Vernooij MW, Ikram MA, Tanghe HL, et al. Incidental findings on brain MRI in the general population. *The New England journal of medicine* 2007;357(18):1821-8. doi: 10.1056/NEJMoa070972
72. Kang DW, Lattimore SU, Latour LL, et al. Silent ischemic lesion recurrence on magnetic resonance imaging predicts subsequent clinical vascular events. *Archives of neurology* 2006;63(12):1730-3. doi: 10.1001/archneur.63.12.1730
73. Schnaudigel S, Groschel K, Pilgram SM, et al. New brain lesions after carotid stenting versus carotid endarterectomy: a systematic review of the literature. *Stroke; a journal of cerebral circulation* 2008;39(6):1911-9. doi: 10.1161/STROKEAHA.107.500603
74. Siddiq F, Vazquez G, Memon MZ, et al. Comparison of primary angioplasty with stent placement for treating symptomatic intracranial atherosclerotic diseases: a multicenter study. *Stroke; a journal of cerebral circulation* 2008;39(9):2505-10. doi: 10.1161/STROKEAHA.108.515361
75. Qureshi AI, Feldmann E, Gomez CR, et al. Consensus conference on intracranial atherosclerotic disease: rationale, methodology, and results. *Journal of neuroimaging : official journal of the American Society of Neuroimaging* 2009;19 Suppl 1:1S-10S. doi: 10.1111/j.1552-6569.2009.00414.x
76. Qureshi AI, Feldmann E, Gomez CR, et al. Intracranial atherosclerotic disease: an update. *Ann Neurol* 2009;66(6):730-8. doi: 10.1002/ana.21768
77. Khan M, Naqvi I, Bansari A, et al. Intracranial atherosclerotic disease. *Stroke Res Treat* 2011;2011:282845. doi: 10.4061/2011/282845
78. Sacco RL, Kasner SE, Broderick JP, et al. An updated definition of stroke for the 21st century: a statement for healthcare professionals from the American Heart Association/American Stroke Association. *Stroke* 2013;44(7):2064-89. doi: 10.1161/STR.0b013e318296aeca
79. Rothwell PM, Eliasziw M, Gutnikov SA, et al. Analysis of pooled data from the randomised controlled trials of endarterectomy for symptomatic carotid stenosis. *Lancet* 2003;361(9352):107-16.
80. Alexandrov AV, Sloan MA, Wong LK, et al. Practice standards for transcranial Doppler ultrasound: part I--test performance. *J Neuroimaging* 2007;17(1):11-8. doi: 10.1111/j.1552-6569.2006.00088.x
81. Ringelstein EB, Droste DW, Babikian VL, et al. Consensus on microembolus detection by TCD. International Consensus Group on Microembolus Detection. *Stroke; a journal of cerebral circulation* 1998;29(3):725-9.
82. Vesey AT IA, Moss A, Jenkins WSA, Sng G, Forsythe RO, Clark T, Roberts G, Fletcher A, Lucatelli C, Rudd JH, Davenport AP, Mills NL, Al-Shahi R, Dennis M, Whiteley W, van Beek EJR, Dweck MR and Newby DE. 18F-Fluoride and 18F-fluorodeoxyglucose positron emission tomography

after transient ischemic attack or minor stroke: case-control study. *Circ Cardiovasc Imaging* 2017- in press

10 Appendices

10a Appendix - Study flow chart

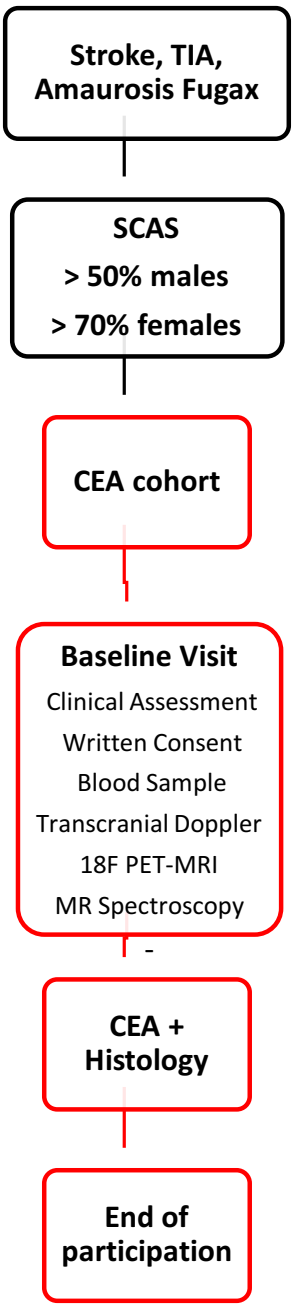

10b Appendix - Patient Flow Chart (CEA cohort)

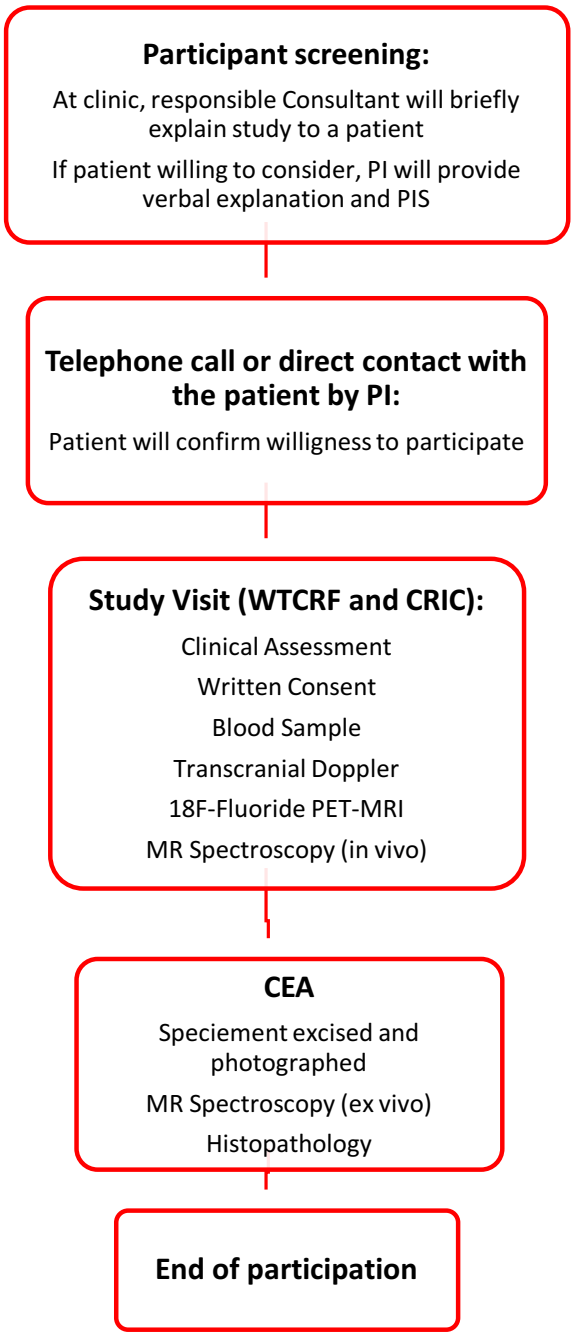

The EdinVasc *ex vivo* Imaging Study

Research Protocol v1.0

Rachael Forsythe

INTRODUCTION

The development of novel cardiovascular imaging techniques holds great potential to enhance our knowledge and influence management of patients with cardiovascular disease. Quantification of biological activity within the vasculature is possible using non-invasive cellular and molecular imaging techniques. In particular, positron emission tomography-computed tomography (PET-CT) is emerging as an important imaging modality to assess small-scale molecular events and provide functional biological information that cannot be assessed using conventional cross-sectional imaging alone. PET data (fused with structural anatomical data derived from CT) can provide regional and patient-specific information on disease activity.

We have used a number of PET tracers in clinical studies to assess disease activity in the coronary and carotid arteries, the aortic valve and in abdominal aortic aneurysm disease. The radiotracer ^{18}F-Sodium fluoride (^{18}F-NaF) detects areas of microcalcification and has been used to identify culprit lesions and high-risk plaque in both the coronary [1] and carotid arteries [2].

Recently, we have demonstrated that ^{18}F-NaF PET uptake is increased in patients with abdominal aortic aneurysm (AAA) compared to healthy controls. For the first time, we have demonstrated that increased aneurysm uptake of ^{18}F-NaF is associated with more rapid aneurysm expansion, independent of diameter and other known clinical risk factors for disease progression [data not yet published]. However, whilst this represents an exciting new potential clinical imaging biomarker for the prediction of outcomes in AAA, we now require *ex vivo* validation and histological correlation.

^{18}F-NaF has also been used in a small pilot study of patients with peripheral artery occlusive disease (PAD; n=16), which demonstrated that arterial ^{18}F-NaF uptake was inversely correlated with arterial calcification and burden of atherosclerosis [3]. No clinical follow up data or histological analysis were provided, however this proof-of-concept study suggests that ^{18}F-NaF provides

different and incremental information in the assessment of PAD over and above visible calcification on conventional imaging.

In addition, there are myriad other PET tracers that may have the potential to track disease processes implicit in aortic disease and atherosclerosis, including process-specific tracers that can identify inflammation, angiogenesis and cellular hypoxia. Some of these have been investigated in animal studies, however we propose to investigate the utility of specific PET tracers in human tissue *ex vivo.* We anticipate that the successful *ex vivo* identification of pathobiologically important processes within the vasculature could pave the way for exciting new clinical PET-CT studies that aim to characterise vascular disease activity and predict clinical outcomes.

Molecular Imaging

Molecular imaging techniques use cell-specific or process-specific probes that assess the biological function of small-scale molecular events, such as gene transcription, or identify surrogate markers for disease activity, such as inflammation and calcification. Knowledge of a relevant biological 'target' is a prerequisite. A suitable tracer needs to be able to bind to the target with high affinity and selectivity, and offer compatibility with a clinically-available imaging modality that provides appropriate spatial and tissue resolution for the disease process. Molecular imaging techniques can often define and identify evolving disease states at an earlier stage than conventional imaging.

Positron Emission Tomography-Computed Tomography

Positron emission tomography-computed tomography (PET-CT) facilitates the acquisition of images from PET and CT devices in the same session, allowing fusion of all data into a single co-registered image. CT obtains anatomic information, whereas PET, which allows evaluation of biological or metabolic activity, obtains functional information at a cellular or molecular level.

There is a wide range of PET tracers available that can target different disease processes, many of which have the potential to be used in cardiovascular disease but have not yet been extensively investigated in the clinical setting. PET has lower spatial resolution (~5 mm) when compared to MRI or CT, and on its own cannot provide optimal anatomical information for detailed evaluation. However, fusion techniques (PET-CT and PET-MRI) allow the integration of molecular information obtained through PET with anatomical detail gained from CT or MRI.

^{18}F-Sodium fluoride – imaging microcalcification in plaque

^{18}F-Sodium fluoride (^{18}F-NaF) has been used as a bone tracer for many years. After intravenous injection, ^{18}F-NaF rapidly equilibrates within the extracellular fluid, and fluorine is subsequently incorporated into hydroxyapatite crystals (a key component of bone and vascular calcification) to form fluoroapatite. Incorporation of fluorine is preferentially at sites of new mineralisation, such as that which occurs during inflammation. In the vasculature, microscopic calcification is the first aberrant event in the process of calcium dystrophy, mediated by cell death and the release of apoptotic bodies as part of the response to underlying necrotic inflammation.[4 5] Microcalcification is a precursor to the laying down of larger, established macroscopic deposits, which are considered a surrogate marker of disease burden in the coronary arteries.

In a case control study and prospective observational cohort study of patients with asymptomatic AAA (n=72), we have recently demonstrated that ^{18}F-NaF uptake is increased in aneurysmal abdominal aorta and is independently associated with future aneurysm growth and clinical outcomes such as AAA repair (Figures 1 and 2).

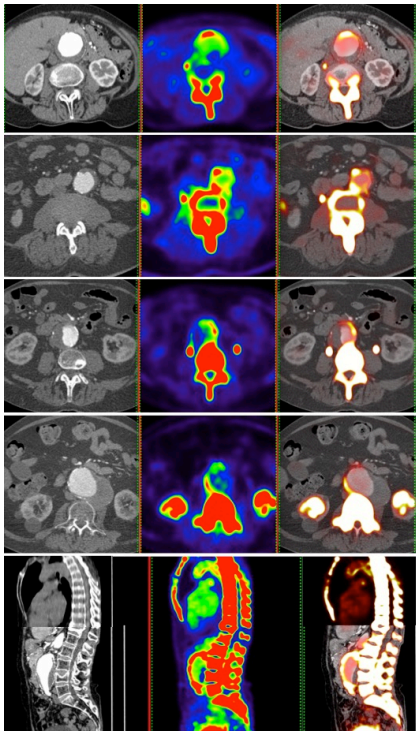

Figure 1: A) CT angiogram of the aorta; B) ^{18}F-NaF PET; C) fused PET-CT.
Areas of increased tracer activity are detected in the wall of the aneurysm, representing microcalcification and underlying necrotic inflammation.

Figure 2: Patients in the highest tertile of aneurysm ^{18}F-NaF uptake expanded 2.5 times as rapidly as those in the lowest tertile, independent of aneurysm diameter.

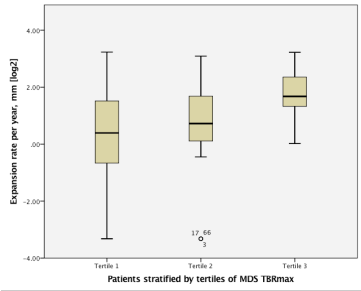

^{18}F-NOTA-RGDfK – imaging angiogenesis and fibrosis in plaque

^{18}F-NOTA-RGDfK binds to integrins and has a high affinity for $\alpha_v\beta_3$, which is expressed on endothelial cells, fibroblasts and inflammatory cells. $\alpha_v\beta_3$ integrin is a transmembrane cell surface receptor that facilitates migration, proliferation and interaction with the extra-cellular matrix (ECM). It is expressed at low levels in quiescent cells but is upregulated in states of angiogenesis, including the myocardium following myocardial infarction, and is thought to be a key player in

the coordination of repair following tissue damage. $\alpha_v\beta_3$ is also expressed in high levels by vascular macrophages [6].

The $\alpha_v\beta_3$ radiotracer, ^{18}F-fluciclatide, has been used to identify areas of functional recovery of the myocardium following infarction[7] and one autoradiography study demonstrated that ^{18}F-fluciclatide detects areas of angiogenesis in AAA *in vitro*[8]. Collagen and other proteins also express the RGD tripeptide sequence, therefore RGD peptides can also mark areas of fibrosis.

^{18}F-NOTA-RGDfK, an alternative $\alpha_v\beta_3$ radiotracer to ^{18}F-fluciclatide, has not been extensively evaluated in the aorta or peripheral arteries.

^{11}C-PK11195 – imaging inflammation in plaques

^{11}C-PK11195 selectively binds to the translocator protein (TSPO) and has been used primarily in the assessment of neuronal damage. However, TSPO are also highly expressed by macrophages. One clinical study has demonstrated the potential use of ^{11}C-PK11195 in localising vascular inflammation in atherosclerotic disease states such as symptomatic carotid artery disease and inflamed aortic plaques.[9] Neither tracer is known to have been investigated in the clinical setting of aortic disease or PAD to date.

^{18}F-NS14490 – imaging atherogenesis

The non-neuronal nicotinic cholinergic pathway contributes to the regulation of many of the pathobiological processes implicit in atherosclerosis, including inflammation, vascular smooth muscle cell (VSMC) expression, cellular proliferation, migration and neovascularisation. [10]

Non-neuronal vascular nicotinic acetylcholine receptors (nAChRs) are the most abundant cholinergic receptors in the CNS and are of increasing interest in vascular research. nAChRs are expressed in abundance in almost all cells in the vasculature, including VSMCs, aortic endothelial cells, platelets, leucocytes,

macrophages and lymphocytes. [11] They are responsible for the regulation of atherosclerosis and are know to mediate the maladaptive effects of nicotine and nitrosamine, components of tobacco smoke. The endogenous ligand for nAChRs is acetylcholine, however nicotine and nitrosamines express high affinity for the receptors, leading to the proliferation of pro-atherogenic growth factors and inflammatory mediators, migration of inflammatory cells into atherosclerotic plaques, apoptosis and thrombus formation. [10]

Smoking is the most important modifiable risk factor for aortic disease and PAD and therefore the investigation of nAChRs as a cardiovascular PET tracer holds exciting potential. ^{18}F-labelled radiotracers have been used successfully in the evaluation of neurodegenerative disorders, [12] but there have been few clinical studies in cardiovascular disease and we believe that this will be the first *ex vivo* autoradiographic study in human aortic and peripheral artery tissue.

α7-nAChRs play an important role in atherogenesis, and therefore represent a potential target for nAChRs imaging. ^{18}F-NS14490 has been used in one pre-clinical study, which demonstrated specific binding of the tracer to α7-nAChRs in the cerebral and carotid arteries in pigs. {Bucerius:2014uc}

^{3}H-NS14490 is a tritiated ligand for the α7 receptor, and we plan to investigate the use of this through autoradiography.

STUDY AIMS

The primary aim of this exploratory study is to investigate the use of PET radiotracers to identify and characterise inflammation and other pathobiological processes implicit in PAD and aortic disease.

By conducting microPET-CT and autoradiography studies on human tissue *ex vivo*, we aim to identify areas of increased biological activity using a variety of PET tracers that identify different disease processes. We will co-register these

images to investigate the spatial relationship between processes and we will then correlate this with relevant histopathological markers of disease activity.

RESEARCH QUESTIONS

We will address the following questions:

1) Is radiotracer uptake on PET-CT increased in peripheral artery specimens and aortic specimens from patients with PAD or aortic disease when compared to control artery?
2) Does increased radiotracer uptake on PET-CT co-localise with histological markers of disease activity?

STUDY DESIGN

This will be a prospective proof-of-concept case-control study using microPET-CT and autoradiography to investigate inflammation and angiogenesis in arterial specimens from patients with PAD and aortic disease, compared to control tissue from patients with sudden cardiac death.

RESEARCH POPULATION

We will prospectively recruit 10 patients with PAD and 20 patients with aortic disease (including aneurysm disease, aortic dissection and aortic occlusive disease) undergoing surgical intervention in the Department of Vascular Surgery at the Royal Infirmary of Edinburgh. Prospective patients will be identified by a member of their usual clinical team, who will confirm and record informed consent. Specimens will be obtained during surgery and limited to tissue that would otherwise be discarded.

Control tissue (10 samples of peripheral artery tissue, 10 samples of aortic tissue) will be obtained from patients with sudden cardiac death who have died in the community. The population will include those with or without a suspected

cardiac cause of death, however specimens with evidence or suspicion of PAD or aortic disease will not be included. Tissue will be collected through our collaboration with the Edinburgh Brain Bank. We will not request access to cases where there has been suspicion around the cause of death, or cases of homicide. To date the Edinburgh Brain Bank has contacted over 200 families to obtain authorization for carrying out medical research using post-mortem tissue.

INCLUSION CRITERIA

Patients with PAD / aortic disease

1) Clinical and / or radiological diagnosis of PAD or aortic disease undergoing operative intervention
2) Able to give informed consent

Control patients

1) Patients with sudden cardiac death
2) No evidence of PAD or aortic disease in resected specimen
3) Consent obtained from family

EXCLUSION CRITERIA

1) Age under 18 years
2) Suspicion around the cause of death (in control patients)

IMAGING TECHNIQUES AND HISTOLOGICAL ANALYSIS

Intact tissue will undergo microPET-CT using ^{18}F-NaF and ^{18}F-NOTA-RGDfK. Specimens will then be sectioned to facilitate autoradiography with ^{3}H-PK11195 and ^{3}H-NS14490 (Fig 3). ^{3}H-PK11195 and ^{3}H-NS14490 are the tritriated forms of the *in vivo* ligands ^{11}C-PK11195 and ^{18}F-NS14490, respectively, necessary to conduct autoradiography experiments.

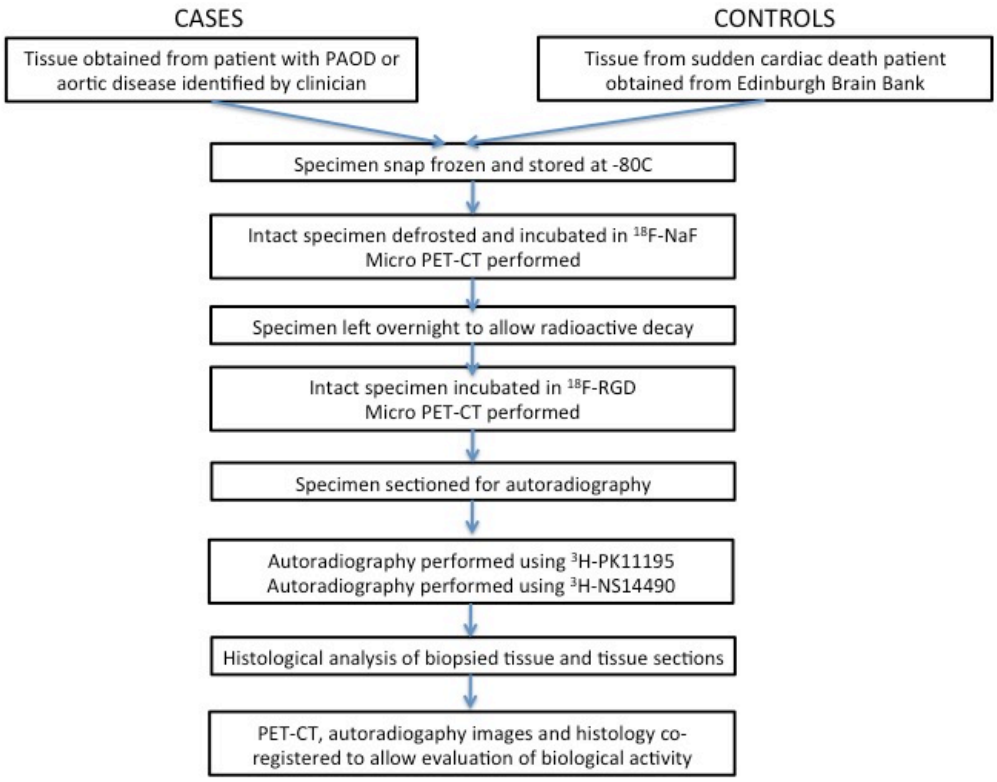

PET-CT Protocol and Reconstructions

After incubation of the intact specimen in ^{18}F-NaF for 30 minutes, PET data will be acquired using a nanoPET/CT scanner (Mediso, Hungary). A 30 min emission scan will be obtained and a CT scan will then be acquired for attenuation correction.

The specimen will be left overnight to allow complete radiotracer decay.

The intact specimen will then be incubated in ^{18}F-NOTA-RGDfK for 30 minutes and the PET protocol will be repeated as above.

PET data will be reconstructed using a 3D reconstruction algorithm, with correction for randoms, scatter and attenuation. Volumes of interest (VOIs) will be manually drawn on the images, and radioactive concentration will be measured for each radiotracer.

Specimens will subsequently be sectioned for autoradiography and histological analysis.

Autoradiography Protocol

Tissue sections will be pre-washed in cold buffer for 15 minutes, then the sections will be incubated in 1nM [^{3}H]PK11195 for 60 minutes or 2.5 nM [^{3}H]NS14490 for 120 minutes at room temperature. The reaction will be terminated by two 5 minutes washes in cold buffer and the slides will be left to dry overnight. The nonspecific binding will be determined by adding 10 μM PK11195 or 10 μM NS14490. Slices will then be left to dry overnight in a desiccator at room temperature before being exposed to a BAS TR240 tritium sensitive imaging plate for 5 to 15 days and then imaged using a FLA-5000 scanner. Tritium standards will be used for quantification of binding.

Histological Analysis

Where possible, histological analysis will be performed following the PET-CT and autoradiography protocols, focussing on the identification of markers of inflammation, angiogenesis, mineralisation and apoptosis.

POTENTIAL FUTURE APPLICATIONS

This is an exploratory study that aims to firstly validate our recent *in vivo* results demonstrating that ^{18}F-NaF uptake on PET-CT is increased in patients with abdominal aortic aneurysm and can predict AAA growth and clinical outcomes. In addition, we will explore the application of other novel PET tracers in identifying disease activity *ex vivo* in aortic disease and in peripheral artery occlusive disease.

This study will provide further insight into the pathobiology of aortic disease and PAD and will allow evaluation of potential new imaging biomarkers. Successful identification of new PET tracers that identify relevant disease processes *ex vivo* would translate into future *in vivo* studies to investigate the feasibility and efficacy of clinical PET-CT in predicting disease outcomes.

Based on the findings of this study, we intend to apply for further funding to support larger clinical studies of patients with aortic disease and PAD. In particular, if *ex vivo* characterisation of AAA tissue using ^{18}F-NaF supports the findings in our recent clinical study, we will propose a larger clinical feasibility study of ^{18}F-NaF PET-CT in predicting AAA growth. If successful, this could lead to a randomised trial evaluating early intervention in AAA disease, based on ^{18}F-NaF PET-CT findings. Taken together, this has the potential to change management of patients with AAA.

In addition, results from this study would help us to support future clinical studies using other the novel PET radiotracers described in this protocol that have not previously been investigated in aortic disease or PAD. This could lead to a number of other proof-of-concept clinical studies, and beyond.

References

1. Joshi NV, Vesey AT, Williams MC, Shah ASV, Calvert PA, Craighead FHM, Yeoh SE, Wallace W, Salter D, Fletcher AM, van Beek EJR, Flapan AD, Uren NG, Behan MWH, Cruden NLM, Mills NL, Fox KAA, Rudd JHF, Dweck MR, Newby DE. 18F-fluoride positron emission tomography for identification of ruptured and high-risk coronary atherosclerotic plaques: a prospective clinical trial. *Lancet*. 2014;383(9918):705-713. doi:10.1016/S0140-6736(13)61754-7.

2. Vesey AT, Jenkins W, Irkle A, Moss A, Sng G, Forsythe RO, Clark T, Roberts G, Fletcher AM, Lucatelli C, Rudd J, Davenport AP, Mills NL, Al-Shahi Salman R, Dennis M, Whiteley W, van Beek E, Dweck MR, Newby DE. 18F-Fluoride and 18F-Fluorodeoxyglucose Positron Emission Tomography After Transient Ischemic Attack or Minor Ischemic Stroke. Case-Control Study. *Circ Cardiovasc Imaging*. March 2017. doi:10.1161/CIRCIMAGING.116.004976.).

3. Chowdhury M, Tarkin J, Makris G, Rudd J, Coughlin P. 208 Arterial Inflammation and Calcification in Patients with Lower Limb Atherosclerosis using PET/CT Analysis: A Proof-of-Principle Study. *Heart*. 2015;101(Suppl 4):A114-A114. doi:10.1136/heartjnl-2015-308066.208.

4. Proudfoot D, Skepper JN, Hegyi L, Farzaneh-Far A, Shanahan CM, Weissberg PL. The role of apoptosis in the initiation of vascular calcification. *Z Kardiol*. 2001;90(3):43-46. doi:10.1007/s003920170041.

5. Rudd JHF, Myers KS, Bansilal S, Machac J, Woodward M, Fuster V, Farkouh ME, Fayad ZA. Relationships Among Regional Arterial Inflammation, Calcification, Risk Factors, and Biomarkers A Prospective Fluorodeoxyglucose Positron-Emission Tomography/Computed Tomography Imaging Study. *Circ Cardiovasc Imaging*. 2009;2(2):107-115. doi:10.1161/CIRCIMAGING.108.811752.

6. Antonov AS, Kolodgie FD, Munn DH, Gerrity RG. Regulation of macrophage foam cell formation by alpha V beta 3 integrin - Potential role in human atherosclerosis. *Am J Pathol*. 2004;165(1):247-258.

7. Jenkins WS, Vesey A, Neale A, Anna V, Moles C, Lucatelli C, Fletcher A, Mirsadee S, Van Beek EJ, Rudd JH, Dweck MR, Newby DE. Abstract 20055: The αvβ3 Integrin Positron Emission Tomography Radiotracer 18F-Fluciclatide is a Marker of Remodeling Following Myocardial Infarction. *Circulation*. 2015;132(Suppl 3):A20055-A20055.

8. Tegler G, Estrada S, Hall H, Wanhainen A, Björck M, Sörensen J, Antoni G. Autoradiography screening of potential positron emission tomography tracers for asymptomatic abdominal aortic aneurysms. *Ups J Med Sci*. 2014;119(3):229-235. doi:10.3109/03009734.2014.894157.

9. Gaemperli O, Shalhoub J, Owen DRJ, Lamare F, Johansson S, Fouladi N, Davies AH, Rimoldi OE, Camici PG. Imaging intraplaque inflammation in carotid atherosclerosis with 11C-PK11195 positron emission tomography/computed tomography. *Eur Heart J*. 2012;33(15):1902-1910. doi:10.1093/eurheartj/ehr367.

10. Santanam N, Thornhill BA, Lau JK, Crabtree CM, Cook CR, Brown KC, Dasgupta P. Nicotinic acetylcholine receptor signaling in atherogenesis. *Atherosclerosis*. 2012;225(2):264-273. doi:10.1016/j.atherosclerosis.2012.07.041.

11. Bauwens M, Mottaghy FM, Bucerius J. PET Imaging of the Human Nicotinic Cholinergic Pathway in Atherosclerosis. *Curr Cardiol Rep*. 2015;17(8). doi:10.1007/s11886-015-0614-8.

12. Schmaljohann J, Gündisch D, Minnerop M, Bucerius J, Joe A, Reinhardt M, Guhlke S, Biersack H-J, Wüllner U. In vitro evaluation of nicotinic acetylcholine receptors with 2-[18F]F-A85380 in Parkinson's disease. *Nucl Med Biol*. 2006;33(3):305-309. doi:10.1016/j.nucmedbio.2005.12.012.